

Fiber-optic sensor for detection of hydrogen peroxide in PEM fuel cells

by

Juan F. Botero-Cadavid

Mech.Eng., Universidad Nacional de Colombia – Sede Medellín, 2004

M.Sc., Universidad Nacional de Colombia – Sede Medellín, 2007

A Dissertation Submitted in Partial Fulfillment
of the Requirements for the Degree of

DOCTOR OF PHILOSOPHY

in the Department of Mechanical Engineering

© Juan F. Botero-Cadavid, 2014
University of Victoria

All rights reserved. This dissertation may not be reproduced in whole or in part, by photocopy or other means, without the permission of the author.

Supervisory Committee

Fiber-optic sensor for detection of hydrogen peroxide in PEM fuel cells

by

Juan F. Botero-Cadauid

Mech.Eng., Universidad Nacional de Colombia – Sede Medellín, 2004
M.Sc. Physics, Universidad Nacional de Colombia – Sede Medellín, 2007

Supervisory Committee

Dr. Nedjib Djilali, Department of Mechanical Engineering
Co-supervisor

Dr. Peter Wild, Department of Mechanical Engineering
Co-supervisor

Dr. Alexandre G. Brolo, Department of Chemistry
Outside Member

Abstract

Supervisory Committee

Dr. Nedjib Djilali, Department of Mechanical Engineering
Co-supervisor

Dr. Peter Wild, Department of Mechanical Engineering
Co-supervisor

Dr. Alexandre G. Brolo, Department of Chemistry
Outside Member

This dissertation presents chemical sensors that are based on an emerging optical fiber sensing technology for the determination of the presence and concentration of hydrogen peroxide (H_2O_2) at low concentrations. The motivation to determine hydrogen peroxide lies on the fact that this chemical species is generated as a by-product of the operation of hydrogen-based polymer electrolyte membrane fuel cells (PEMFCs), and the presence and formation of this peroxide has been associated with the chemical degradation that results in low durability of PEMFCs. Currently, there are no techniques that allow the hydrogen peroxide to be determined *in situ* in PEMFCs in a reliable manner, since the only report of this type of measurement was performed using electrochemical techniques, which can be affected by the environmental conditions and that can alter the proper operation of the PEMFCs.

The sensors presented in this dissertation are designed to detect the presence and quantify hydrogen peroxide in solution at the conditions at which PEMFCs operate. Since they are made using fused silica optical fibers and are based on a spectroscopic technique to perform the detection of H_2O_2 , they are not affected by the electromagnetic fields or the harsh chemical environment inside PEMFCs. In addition, they are able to still detect the presence of H_2O_2 at the operating temperatures.

The construction of the sensing film on the tip of an optical fiber and its small size (125 μm diameter), make the sensors here developed an ideal solution for being deployed *in situ* in PEMFCs, ensuring that they would be minimally invasive and that the operation of the fuel cell would not be compromised by the presence of the sensor.

The sensors developed in this dissertation not only present design characteristics that are applicable to PEMFCs, they are also suitable for applications in other fields such as environmental, defense, and biological processes.

Table of Contents

Supervisory Committee	ii
Abstract	iii
Table of Contents	v
List of Figures	xi
List of Tables	xvii
List of Symbols and Nomenclature.....	xviii
Acknowledgments.....	xix
Chapter 1: Introduction.....	1
1.1 Introduction.....	1
1.2 Polymer electrolyte membrane fuel cells.....	1
1.3 Membrane degradation	4
1.3.1 The role of hydrogen peroxide (H ₂ O ₂) in PEMFCs.....	5
1.3.2 The role of radicals in the PFSA membrane degradation	6
1.4 Challenges of the <i>in situ</i> detection of H ₂ O ₂ in PEMFCs	9
1.5 Techniques for detection of hydrogen peroxide in small concentrations	11
1.5.1 Electrochemical techniques	12
1.5.2 Spectroscopic techniques based on absorption.....	13
1.5.3 Spectroscopic techniques based on fluorescence.....	14
1.5.4 Spectroscopic techniques based on chemiluminescence	15
1.5.5 Optical fibers as platform for detection of chemical species using spectroscopic techniques.....	16
1.6 Scope and research questions.....	18
1.7 Organization of dissertation.....	19

Chapter 2: Design parameters of an optical fiber sensor for hydrogen peroxide detection	21
2.1 Principle of optical fibers and optical fiber sensors configurations for detection of chemical species	21
2.1.1 Multi-mode optical fibers	21
2.1.2 Fiber sensors using absorption-scattering techniques.....	23
2.2 Detection of hydrogen peroxide based on the Prussian blue – Prussian white system	25
2.3 Electrostatic self-assembly (ESA) of polyelectrolytes in a layer-by-layer (LbL) deposition.....	30
2.3.1 Immobilization of reagents using the ESA of polyelectrolytes	31
2.3.2 Tailoring the properties of polyelectrolyte multilayer structures	32
2.3.3 Immobilization of Prussian blue within polyelectrolyte multilayer films and reagents immobilization using optical fibers as a template	34
2.4 Pragmatic considerations: <i>in situ</i> detection of H ₂ O ₂ in PEM fuel cells using Prussian blue based optical fiber sensors.....	35
Chapter 3: <i>In situ</i> sensing techniques in PEMFCs: A review.....	37
3.1 Abstract.....	37
3.2 Introduction.....	37
3.3 Operating conditions.....	38
3.3.1 Temperature	38
3.3.2 Relative humidity.....	53
3.4 Performance parameters.....	57
3.4.1 Electrical current sensors	57
3.4.2 Voltage sensors	65
3.4.3 Electrical resistance	67

	vii
3.5	Contaminants and other stressors in PEMFCs..... 69
3.5.1	Carbon monoxide (CO) detectors for H ₂ gaseous fuel 70
3.5.2	Other contaminants and stressors..... 72
3.6	Remarks 75
Chapter 4: Detection of hydrogen peroxide using an optical fiber-based sensing probe . 78	
	Preamble 78
	Abstract..... 78
4.1	Introduction..... 79
4.1.1	Sensing mechanism..... 81
4.1.2	Polyelectrolyte multi-layered films..... 81
4.2	Materials and methods 84
4.2.1	Materials 84
4.2.2	Sensing film deposition..... 84
4.2.3	Test solutions preparation 85
4.2.4	Instrumentation 86
4.2.5	Test procedures 86
4.2.6	Measurement of the changes in absorbance..... 87
4.2.7	Response time evaluation 88
4.3	Results and discussion 88
4.3.1	First experiment-conditioning stage 89
4.3.2	Operational stage 92
4.3.3	Response time evaluation 94
4.4	Conclusions..... 96
	Acknowledgments..... 98

Chapter 5: Temperature response and durability characterization of an optical fiber sensor for the detection of hydrogen peroxide.....	99
Preamble	99
Abstract.....	99
5.1 Introduction.....	100
5.2 Materials and Methods.....	102
5.2.1 Sensing film deposition.....	102
5.2.2 Liquid test solutions preparation.....	103
5.2.3 Test for temperature response.....	103
5.2.4 Tests for temperature durability.....	105
5.2.5 Sample characterization after durability tests.....	106
5.3 Results and Discussion	108
5.3.1 Temperature response.....	108
5.3.2 Durability tests	112
5.4 Conclusions.....	118
Acknowledgments.....	120
Chapter 6: Fiber optic based sensor for H ₂ O ₂ detection in PEMFC's	121
Preamble	121
Abstract.....	121
6.1 Introduction.....	122
6.1.1 Sensing mechanism.....	123
6.1.2 Prussian blue immobilization on the optical fiber	123
6.2 Materials and methods	125
6.2.1 Materials	125

6.2.2	Sensing film deposition.....	125
6.2.3	Instrumentation and measurement of the changes in absorbance.....	126
6.2.4	Test procedures.....	127
6.2.5	Response time determination.....	128
6.3	Results.....	129
6.4	Discussion and conclusions.....	129
6.5	Nomenclature.....	131
	Acknowledgements.....	131
	Chapter 7: Contributions, Conclusions, and future work.....	132
7.1	Detection of hydrogen peroxide using an optical fiber-based sensing probe.....	132
7.2	Temperature response and durability characterization of an optical fiber sensor for detection of hydrogen peroxide.....	133
7.3	Fiber optic based sensor for H ₂ O ₂ detection in PEMFCs.....	134
7.4	Conclusions.....	134
7.5	Future work.....	135
	Bibliography.....	137
	Appendix A: Summary of <i>in situ</i> sensing techniques in PEMFCs.....	167
	Appendix B: Review on spectroscopic techniques for detection of hydrogen peroxide in small concentrations.....	170
	Appendix C: Practical considerations for the immobilization of Prussian blue on the tip of multimode optical fibers.....	177
C.1	Fiber cleaving.....	177
C.2	Fiber chemical cleansing.....	178
C.3	Polyelectrolyte solutions preparation.....	179
C.4	Coating process (deposition of the multilayer coating).....	180

C.5	Annealing and aging processes.....	181
Appendix D:	Detection of hydrogen peroxide in vapor phase.....	183
D.1	Introduction.....	183
D.2	Concentration of hydrogen peroxide vapor in a solution of H ₂ O-H ₂ O ₂	184
D.3	Concentration of hydrogen peroxide in vapor phase produced in an operating PEMFC	191
D.3.1	Approach using rotating ring-disc electrode experiments	191
D.3.2	Approach considering experimental detected values of <i>in situ</i> H ₂ O ₂ in an operating PEMFC	196
D.4	Materials and Methods.....	197
D.5	Results.....	200

List of Figures

Figure 1-1: a) Schematic of a single flow channel of a PEMFC illustrating the main components and operating principle; b) Schematic of close-up on the cathode side of the MEA showing the triple-phase boundary (Adapted from [3], Reproduced with permission from Elsevier).....	2
Figure 1-2: Nafion [®] simplified molecular structure.	4
Figure 1-3: Schematic of the radical formation pathways (Note that the complete pathways and their stoichiometry are not entirely presented).	8
Figure 1-4: a) Surface and b) cross-section SEM micrographs of a Nafion [®] membrane treated in 30 wt% H ₂ O ₂ /metal ions for 48 h. (From [22], Reproduced with permission from Elsevier).....	9
Figure 1-5: Stokes' shift in the spectra of absorption and emission of a fluorescent compound. (©Mikhal/Wikimedia Commons/CC-BY-SA 3.0/GFDL).....	15
Figure 1-6: Commonly used configurations for fibre optic chemical sensors: (a) unmodified; (b) declad; (c) active or doped cladding; (d) fibre bundle; (e) bifurcated; (f) U-bend; (g–i) distal end based. Reprinted with permission from Ref.[65]. Copyright 2008 American Chemical Society.	17
Figure 2-1: Schematic (not to scale) showing relevant features of multi-mode optical fiber. Inset cross section of the fiber with 225 μm cladding and 200 μm core size (to scale) showing relative sizes of core and cladding. Refractive index profile of core and cladding areas.	22
Figure 2-2: Some phenomena caused by the light-matter interaction. Adapted from Ref.[69] under CC 3.0 BY.	23
Figure 2-3: Schematic of a membrane absorption-scattering sensor. (Adapted from Ref. [41]).....	25
Figure 2-4: a) Iron(II) ion surrounded octahedrally by cyanide groups and iron(III) ions; b) Crystalline structure of hexacyanoferrate compound; c) Bottle-neck in the crystalline structure of Prussian blue (Adapted from Ref. [73]); d) Schematic of the intervalence electron charge transfer between the iron(II) and iron(III) ions,	

responsible of the blue color of the PB due to the absorption of the red wavelengths of the visible spectrum.	27
Figure 2-5: Voltammogram of PB film on a gold wire; sweep rate 1 mV/s (Adapted from Refs. [71, 81])	28
Figure 2-6: Absorption spectra of Prussian blue and Prussian white films (Adapted from Ref. [84]).....	29
Figure 2-7: Absorption spectra of PB films recorded in different buffer solutions at various pH values (Adapted from Ref. [87])	30
Figure 2-8: a) Schematic representation of the deposition of a bilayer of polyelectrolytes onto the surface of an optical fiber immobilizing Prussian blue; and b) Molecular units of the polycation Poly(allylamine hydrochloride), PAH ⁺ and the polyanion Poly(acrylic acid), PAA ⁻ (Adapted from Ref. [95]).....	32
Figure 3-1: Location of the thermocouples embedded at the anode collector plate. (Republished with permission from Electrochemical Society, Inc. from Ref. [121]; permission conveyed through Copyright Clearance Center, Inc.).....	40
Figure 3-2: Microphotograph of temperature and humidity micro-sensors (Republished from Ref. [124], ©2007 IEEE)	43
Figure 3-3: Microphotograph of a flexible temperature micro-sensor (Republished from Ref. [130], ©2010 IEEE)	44
Figure 3-4: Instrumented flow field and optical fiber ruby tip. (Republished from Ref. [134]).....	46
Figure 3-5: Diagram of sensor placement in experimental PEMFC (Republished with permission from Elsevier S.A. from Ref. [135]; permission conveyed through Copyright Clearance Center, Inc.)	47
Figure 3-6: Placement of optical fibers installed in flow channel plate (left) and Cr:YAG phosphor material applied to the outer surface of the GDL (right) (Republished with permission from Electrochemical Society, Inc. from Ref. [133]; permission conveyed through Copyright Clearance Center, Inc.)	48
Figure 3-7: Schematic of the <i>in situ</i> FBG sensor located in the bottom of the flow channel showing how the sensors were installed into the flow plate (Republished with	

permission from Electrochemical Society, Inc. from Ref. [138]; permission conveyed through Copyright Clearance Center, Inc.)	49
Figure 3-8: a) Recess in the graphite flow plate showing the sensors installation; b) Schematic of the relative position of the sensors in anode and cathode flowplates. (Republished with permission from Elsevier S.A. from Ref. [144]; permission conveyed through Copyright Clearance Center, Inc.)	52
Figure 3-9: Microphotography of a flexible humidity micro sensor (Republished from Ref. [131], ©2010 IEEE)	54
Figure 3-10: Scheme of the embedded gold-plated stainless steel strips forming a flow-field acting as current collector on a polymer substrate as described in Refs. [165, 167, 168]	60
Figure 3-11: Schema of design of fuel cell with segmented flow field and collector (Republished with permission from Elsevier S.A. from Ref. [170]; permission conveyed through Copyright Clearance Center, Inc.)	61
Figure 3-12: Schematic drawing of a current sensor with a magnetic loop and Hall sensor (Republished with permission from Kluwer Academic Publishers from Ref.[164]; permission conveyed through Copyright Clearance Center, Inc.)	62
Figure 3-13 Schematic of the measurement principle, the potential drop over flow-field plate and GDL provides information on the current distribution (Republished with permission from the Electrochemical Society, Inc. from Ref. [176]; permission conveyed through Copyright Clearance Center, Inc.)	64
Figure 3-14: Ideal voltage transient in a PEMFC after current interruption at t_0 (Republished with permission from Elsevier S.A. from Ref. [185]; permission conveyed through Copyright Clearance Center, Inc.)	68
Figure 4-1: Scheme of hydrogen peroxide sensing using the Prussian blue/Prussian white system in a layer-by-layer electrostatic self-assembled structure coating the tip of the optical fiber probe.	83
Figure 4-2: Experimental setup to measure the reflected light from the Prussian blue coated tip	86
Figure 4-3: Response of the sensing probe during the first experiment to solutions with increasing concentration of H_2O_2	89

Figure 4-4: Intensity response to the increase in the concentration of H ₂ O ₂ solutions; (a) linear scale, (b) logarithmic scale. This behavior was only observed in the first experiment, and could not be used for calibration or measurements purposes.	90
Figure 4-5: Response of the sensing probe to immersion in solutions with increasing and decreasing H ₂ O ₂ concentration.	92
Figure 4-6: Response of the sensing probe to immersion in solutions with decreasing and increasing H ₂ O ₂ concentration.	93
Figure 4-7: Response of the sensing probe to immersion in 100 μmol L ⁻¹ H ₂ O ₂ solutions.	94
Figure 4-8: Time response to reach 63% of the maximum intensity for the different concentrations tested.	95
Figure 5-1: Experimental setup to measure the response in the Prussian blue/Prussian white sensitive coating under temperature changes.	104
Figure 5-2: Temperature (top) and Intensity of the reflected light from the sensing probe (bottom) during the H ₂ O ₂ detection tests at different temperatures. Brackets indicate the setpoint temperature in the environmental chamber, arrows indicate the instant at which setpoints are modified	109
Figure 5-3: Amplitude of each test vs. temperature.	112
Figure 5-4: Extended Raman spectrum of the sensing coating on Fiber A. Spectrum obtained after an exposure time of 10 sec. and a single accumulation.	113
Figure 5-5: Raman spectra obtained from fibers A, B, C, and D	114
Figure 5-6: Scanning electron microscope images at 18,000X (left side) and 45,000X (right side) of fiber A (a), (b); fiber B (c), (d); fiber C (e), (f); and fiber D (g), (h)	117
Figure 5-7: Weight percentage content of Fe in fibers A, B, C, and D	118
Figure 6-1: Scheme of PB/PW system immobilized on the tip of the optical fiber illustrating the sensing mechanism of the H ₂ O ₂ and the recovery stage in ascorbic acid [244]	124
Figure 6-2: Experimental setup to measure the absorbance response from the Prussian blue coated tip of the optical fiber	127
Figure 6-3: Embedded optical fiber sensing device within the Nafion [®] membrane.	128

Figure 6-4: Reflected intensity to different concentrations of H ₂ O ₂ solutions (a) Sensing fiber without Nafion [®] and (b) Sensing fiber embedded in Nafion [®]	129
Figure 6-5: Response time for the sensing probe without and within the Nafion [®] membrane.....	130
Figure 7-1: Insertion technique of an optical fiber sensor for <i>in situ</i> detection of H ₂ O ₂ in a PEMFC	136
Figure C-1: Optical fiber immobilized for the cleansing and coating processes.....	178
Figure C-2: Schematic of the deposition of immobilizing bilayers on the tip of an optical fiber by the electrostatic self-assembly (ESA) of polyelectrolytes (Adapted from Ref. [95]).....	181
Figure C-3: Coated optical fiber.	182
Figure D-1: Piecewise B ₀ function	189
Figure D-2: Rates of H ₂ O ₂ formation in the cathode side of the PEMFC as function of relative humidity and temperature. Local potential ~0.6 V, which translates as an overpotential of 0.095 V in the H ₂ O ₂ formation (Adapted from Ref.[18]).....	193
Figure D-3: Estimated rates of H ₂ O ₂ formation in the cathode side of a PEMFC with different catalysts as a function of relative humidity at 75 °C. Local potential ~0.6 V, (overpotential of 0.095 V in the H ₂ O ₂ formation) (Adapted from Ref. [267]) ..	195
Figure D-4: Estimation of H ₂ O ₂ concentration in fuel cells with different membrane thickness. (Adapted from Ref. [23])	197
Figure D-5: Schematic of the experimental setup for the detection of H ₂ O ₂ in vapor phase	199
Figure D-6: Reflected intensity of the sensor to H ₂ O ₂ in vapor phase from liquid solutions at 30, 25, 20, 15, 10 wt%	200
Figure D-7: Rise time vs. Concentration for a sensor in vapor phase. Liquid solutions at 30, 25, 20, 15, and 10 wt% H ₂ O ₂	201
Figure D-8: Reflected intensity of the sensor to dry N ₂ and H ₂ O ₂ vapor from liquid solutions with 0, 1, 2, 3, 4, 5, 10, 15, 20, 25, and 30 H ₂ O ₂ wt%	202
Figure D-9: Rise time versus concentration for a sensor in vapor phase. Liquid solutions at 1, 2, 3, 4, 5, 10, 15, 20, 25, and 30 wt% H ₂ O ₂	203

Figure D-10: a) Intensity vs. time response observed during a complete experiment in vapor phase; b) Response of the sensor to vapor at 6.1 ppm H ₂ O ₂ ; c) Response of the sensor to water vapor.	204
Figure D-11: Response of the optical fiber sensor to various concentrations of H ₂ O ₂ in vapor phase: a) 0.429 ppm; b) 3.99 ppm; c) 6.10 ppm; d) 9.47 ppm; e) 7.62 ppm; and f) 17.3 ppm.....	205
Figure D-12: Rise time versus concentration for a sensor in vapor phase for tests showed in Figure D-11.....	206

List of Tables

Table 3-1: Summary of the <i>in situ</i> techniques for measuring temperature in PEMFCs...	52
Table 3-2: Summary of the <i>in situ</i> techniques for measuring humidity in PEMFCs.....	57
Table 3-3 : Merits and drawbacks of the <i>in situ</i> techniques for measuring current in PEMFC	65
Table A-1: Summary of the <i>in situ</i> techniques for measuring temperature in PEMFCs	168
Table A-2: Summary of the <i>in situ</i> techniques for measuring humidity in PEMFCs.....	168
Table A-3 : Merits and drawbacks of the <i>in situ</i> techniques for measuring current in PEMFC	169
Table D-1: Concentrations in liquid and gas phase for sensing experiment 2.....	201

List of Symbols and Nomenclature

Symbol or Acronym	Meaning	Units, Value, or Comments
HOR	Hydrogen oxidation reaction	
OCV	Open cell voltage	
ORR	Oxygen reduction reaction	
PEMFC	Polymer electrolyte membrane fuel cell	
PFSA	Perfluorosulfonated acid	
PTFE	Polytetrafluoroethylene	Commercially known as Teflon [®]
SHE	Standard hydrogen electrode	Reference electrode for voltage values in electrochemistry. Equivalent to 0.0 Volts
GDL	Gas diffusion layer	
CL	Catalyst layer	
MEA	Membrane electrode assembly	
GDE	Gas diffusion electrode	
RTD	Resistance temperature detector	

Acknowledgments

Firstly, I would like to thank Dr. Ned Djilali for all the provided professional and personal guidance throughout all the stages of my studies. A big thanks from the bottom of my heart. I also want to extend my gratitude to Dr. Peter Wild for his valuable advice and direction as co-supervisor of this dissertation.

I don't want to let this opportunity pass without acknowledging all the people that played an important role during my time at UVic, encouraged me academically and also gave me their friendship. I would specially like to thank to Dorothy in the Mechanical engineering department, and to Sue and Peggy in IESVic; they were always ready to provide help and advice whenever I needed it. Also, I would like to thank to my classmates, my colleagues in the lab, and my other friends at UVic. Thanks to all of you for your help and for making this stage of my life more enjoyable. Dr. Chris Denisson, Dr. Nigel David, Dave Singlehurst, Chris Bueley, Devan Bouchard, Arash Ash, Dr. Hui Zhang, Dr. Wei Ye, Hamed Akbari Khorami, Victor Keller, Dr. Armando Tura, and of course, special thanks to my Colombian friend Dr. Norha Villegas.

Of course, I cannot forget to thank those that I left back in Colombia and that are my support network in the distance, my family and friends. Thanks to my parents for all the love and emotional support, I would have never come this far without them. Same goes to my friends Felipe, Martín, Milena, Paula, Wilmer, thank you guys for being there all the time.

I would like to acknowledge financial support from the Universidad Nacional de Colombia - Sede Medellín and from the Departamento Administrativo de Ciencias, Tecnología e Innovación – Colciencias from Colombia, as well as the support from the Natural Sciences and Engineering Research Council of Canada (NSERC).

Finally, there are no words that can describe the immense gratitude that I want to express to my beloved Andrea for all her support, care, and incommensurable love. Without her, this dissertation would have not been possible and these words would have never been written. I love you my pandita loca!

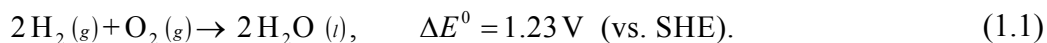
Chapter 1: Introduction

1.1 Introduction

The formation and presence of hydrogen peroxide in PEM fuel cells is associated with one of the main chemical degradation mechanisms affecting lifetime and durability. This dissertation describes the optical and chemical design, characterization, and thermal response of optical fiber-based sensors for the detection of hydrogen peroxide in polymer electrolyte membrane fuel cells. The work spans the disciplines of optics, chemistry, and material science. To put the motivation and objectives of this dissertation into context, the next two sections provide an overview of polymer electrolyte membrane fuel cells, the mechanisms of formation and membrane degradation associated with hydrogen peroxide, and of the role played by hydrogen peroxide in the production of radicals. The challenges for *in situ* detection of H₂O₂ in PEMFCs are discussed in Section 1.4, followed, in Section 1.5, by a detailed review and assessment of techniques proposed to date in the literature. This background sets the stage for the scope of the dissertation in Section 1.6 in terms of sensor operating principle, design, construction, modeling, characterization, and validation.

1.2 Polymer electrolyte membrane fuel cells

Polymer electrolyte membrane fuel cells (PEMFCs) are electrochemical devices that convert chemical energy directly into electricity via the overall fuel cell reaction between hydrogen and oxygen given by:



This energy conversion process is highly efficient and generates power with low environmental impact [1].

PEMFCs have the potential to replace existing power sources in multiple applications; there is particular interest in transportation systems. For this specific

purpose, high power density, fast start-up, high efficiency, and durability are required in order to allow PEMFCs be competitive with internal combustion engines [2].

The primary component of the PEMFC is the polymer electrolyte membrane, located in the middle of the membrane electrode assembly (MEA) (Figure 1-1a). This membrane has a thickness of about 50 μm or less in the state-of-the-art in fuel cells. The most popular electrolyte is an ionomer called Nafion[®], a composite of sulfonated fluoropolymers. This polymer electrolyte has the ability to conduct ions (H^+) when it is hydrated, while remaining an insulator for the conduction of electrons (e^-).

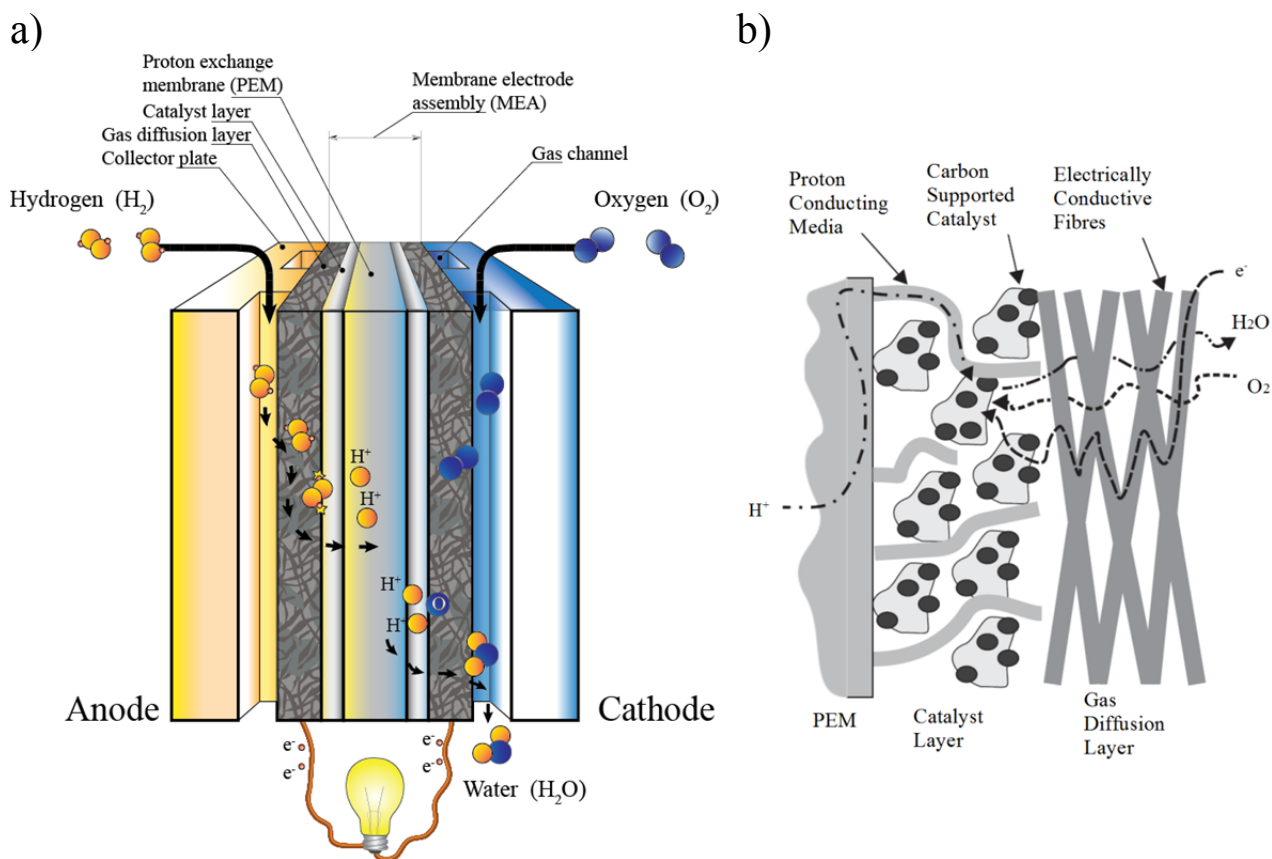


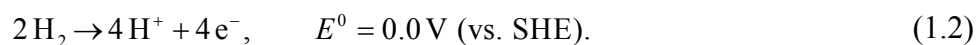
Figure 1-1: a) Schematic of a single flow channel of a PEMFC illustrating the main components and operating principle; b) Schematic of close-up on the cathode side of the MEA showing the triple-phase boundary (Adapted from [3], Reproduced with permission from Elsevier).

In a typical configuration, the active area of the membrane is coated with a layer of catalyst, which is usually comprised of platinum particles supported on carbon particles.

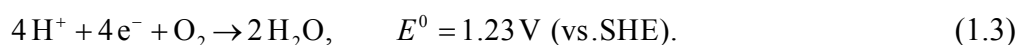
PTFE-coated carbon paper, acting as a gas diffusion layer (GDL) and current conductor, sandwich the catalyst coated membrane, completing the MEA structure (Figure 1-1b).

On either side of the MEA, collector plates with flow channels distribute the fuel and the oxidant to the electrodes. The collector plates also provide structural support to the cell and conduct the heat generated during the reaction. Most importantly, however, the plates perform the function of conducting the electrons to the adjacent cell [2] –via the land areas that separates the flow channels.

The operation of a fuel cell involves the supply of hydrogen and oxygen through the anode and cathode flow channels respectively, and the connection of a suitable external load completes the circuit. Hydrogen (H_2) in gaseous phase diffuses through the GDL on the anode side of the cell. The H_2 molecules reach the catalyst sites being ionized via the hydrogen oxidation reaction (HOR); this reaction is catalyzed by the platinum particles. The HOR can be expressed as:



H^+ ions are transported across the hydrated electrolytic membrane. Electrons meanwhile, unable to travel through the electrolyte, are conducted by the GDL fibers to the anodic collector plate and the external load en route for the cathode side. At the cathodic triple-phase boundary, the electrons and the H^+ ions combine in another elementary reaction, the oxygen reduction reaction (ORR), involving four electrons to reduce one mole of oxygen (O_2) and producing water molecules and heat as by-products. The ORR can be expressed as:



1.3 Membrane degradation

The molecular structure of Nafion[®] consists of a fluorocarbon backbone (Teflon[®]) with side chains containing sulfonic acid structures at their ends (Figure 1-2). This compound is part of the family of polymers known as perfluorinated sulfonic acids (PFSA).

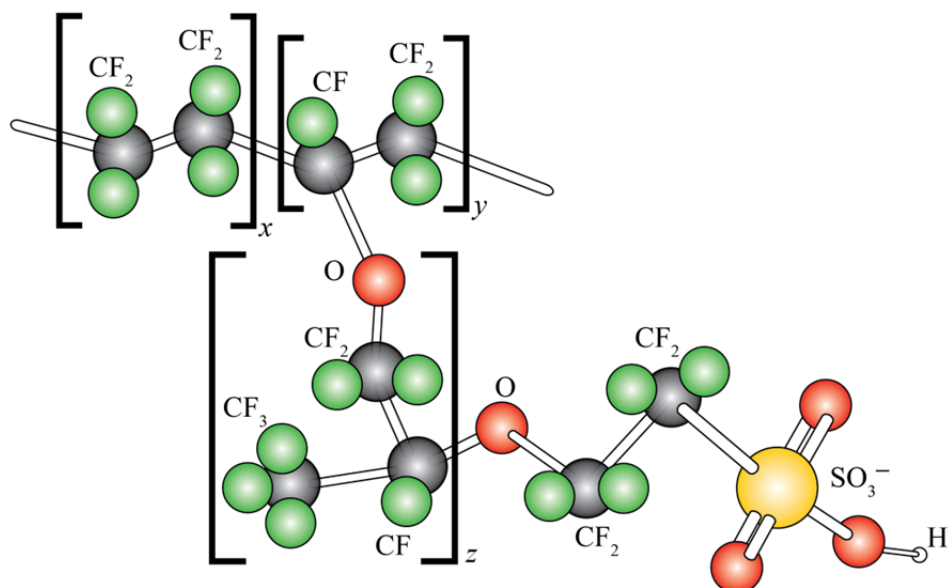


Figure 1-2: Nafion[®] simplified molecular structure.

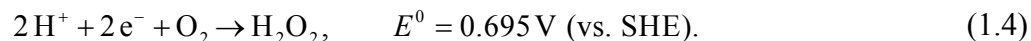
Generally, PFSA membranes are mechanically, thermally, and chemically stable [4]. However, multiple physical and chemical phenomena can result in membrane degradation and, consequently, reduce lifetime. In particular, the polymer membrane can suffer damage due to flooding, dry-out, excessive pressure from the collector plates, delamination of the catalyst layer, particle intrusion, and pinholes due to thermal stresses and hot spots, among other causes [2].

There are also numerous mechanisms of chemical damage. Impurities and undesirable compounds can cause poisoning of the catalyst layer and reduce the conductivity of the ionomer [5]. Furthermore, these factors can trigger degradation of the electrolyte itself, causing the loss of mass with the consequent thinning of the membrane and increased susceptibility to pinholes and gas crossover [2].

Chemical degradation of PFSA membranes is commonly inferred from the measurements of fluoride ion (F^-) release rate (FRR) in effluent condensates at the anode and cathode sides [6]. The FRR quantifies the fluoride ions liberated from the backbone and the side chains of the electrolyte. An additional indicator of the degradation of PFSA membranes is the presence of sulfate (SO_4^{2-}) and sulfite (SO_3^{2-}) ions, which indicate the degradation of the side chains [7, 8].

1.3.1 The role of hydrogen peroxide (H_2O_2) in PEMFCs

One of the chemical compounds that is believed to affect the electrolyte membrane is hydrogen peroxide (H_2O_2). Hydrogen peroxide can be produced in a PEMFC as a by-product of the reaction between hydrogen and oxygen via a 2-electron reduction step [9]. In acidic media, there are two overall pathways for the oxygen reduction, the one involving four electrons shown in reaction (1.3), and the pathway given by [10]:



The standard potential for this oxygen reduction indicates that the formation of H_2O_2 at the cathode side of the fuel cell is not viable at open cell voltage (OCV) conditions, when the electrical potential is higher than 900 mV. However, O_2 migrating through the membrane from the cathode towards the anode can reach lower potentials, and indeed this has been proposed as a mechanism of H_2O_2 formation in PEMFCs [11].

The presence of H_2O_2 in PEMFCs has been confirmed indirectly by condensing the exhaust gases [12], and in the drain water from the cathode [6]. Also, H_2O_2 was found *in situ* using electrochemical techniques in the electrolyte membrane [13]. However, one of the open questions is whether the initial formation of H_2O_2 occurs in the liquid or gaseous phase. Arguments favoring the liquid phase formation include a higher boiling temperature than water in the range of operating pressures in the PEMFC (1-3 atm) [14,

15]. Thus, while the water produced stays in vapor phase under well controlled water and temperature management conditions, the formed H_2O_2 could remain in the liquid phase. On the other hand, others consider that because of the rate of decomposition of H_2O_2 at high temperatures increases [16, 17], part of the H_2O_2 produced will dissociate into oxygen and water.

The production of H_2O_2 is highly dependent on the relative humidity and the temperature, and has been estimated [18] to reach a maximum rate of $0.35 \times 10^{-9} \text{ mol cm}^{-2} \text{ s}^{-1}$ (95 °C and 50% RH) at the anode, whereas in the cathode the production is three order of magnitude larger, reaching $0.70 \times 10^{-6} \text{ mol cm}^{-2} \text{ s}^{-1}$ (95 °C and 0% RH). However, these production rates were not determined in an operating PEMFC but using the electrochemical technique of rotating-ring/disc electrode [18].

The PFSA membrane, despite its high chemical stability, is not completely stable against H_2O_2 , and fluoride (F^-) and sulfate (SO_4^{2-}) ions are released when Nafion[®] membranes are immersed in H_2O_2 solutions [7].

1.3.2 The role of radicals in the PFSA membrane degradation

Radicals are defined as a sole atom or group of atoms with an unpaired electron [19]; i.e. they are readily available to create bonds. Radicals are considered one of the main cause of polymer degradation. Hydrogen peroxide because of its low strength bonds, lower than those of water for example, can convert into radicals. The radicals formed from H_2O_2 exhibit the unpaired electron depending on the location of the broken bond. These radicals are called: hydrogen ($\text{H}\cdot$), hydroxyl ($\text{HO}\cdot$), and hydroperoxy ($\text{HO}_2\cdot$) radicals.

Since PFSA membranes require certain levels of hydration to conduct protons, there are other proposed mechanisms for radical formation. These mechanisms are a consequence of the presence of water which, in addition to enhancing ionic conductivity,

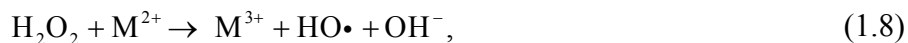
also allows some hydrogen and oxygen crossover. LaConti et al. proposed a mechanism for the formation of hydroperoxy radical and H_2O_2 following these steps [11]:



and



Upon the formation of H_2O_2 via the 2–electron ORR (1.4), or the crossover pathway in reaction (1.7), other mechanisms of radical formation are triggered. Some of these onset mechanisms occur as an effect of the presence of metal cations such as Fe^{2+} , Cu^{2+} , Ca^{2+} , Na^{2+} , due to corrosion of electrical contacts or other ancillary components in the fuel cell stack, as well as from impurities in the inlet gases. These trace metals bring about the formation of hydroxyl radicals following these pathways [11]:



where M represents any of the aforementioned contaminant metals; for the particular case of Fe^{2+} the above reaction is known as *Fenton's reaction* [20].

The aforementioned pathways for the formation of radicals are shown schematically in Figure 1-3, and contribute to a chain reaction that is sustained as long as metal cations and hydrogen radicals are available.

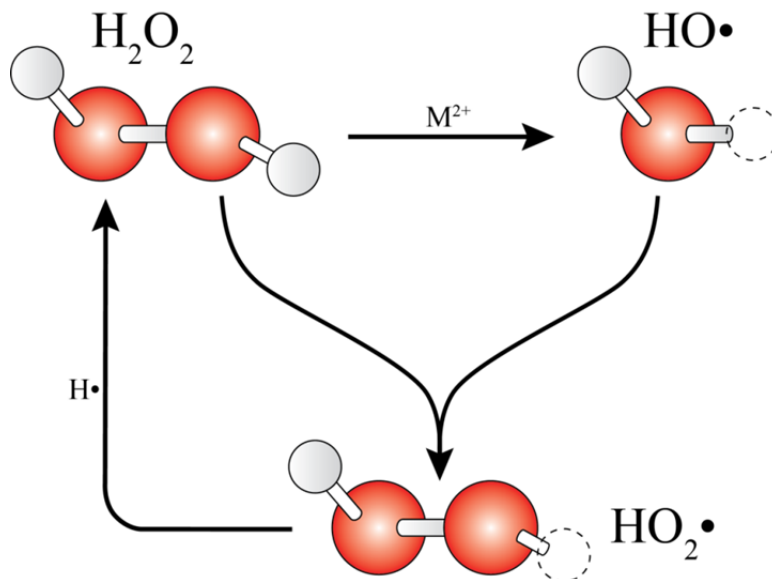


Figure 1-3: Schematic of the radical formation pathways (Note that the complete pathways and their stoichiometry are not entirely presented).

In this context, degradation of PFSA membrane occurs not only in the presence of contaminant metal cations, which reduce the conductivity because of their better affinity than H^+ with sulfonic acid ends [21], but also due to the existence of radicals which attack the side chains or the main backbone of the polymeric structure [13].

Studies performed on Nafion[®] membranes immersed in H_2O_2 solutions have shown accelerated degradation when traces of metal cations such as Fe^{2+} and Cu^{2+} were added [7]. Furthermore, investigations using scanning electron microscopy (SEM) put in evidence the formation of voids, pinholes, and the overall thinning of the membrane when it was exposed to H_2O_2 solutions and metal cations [22].

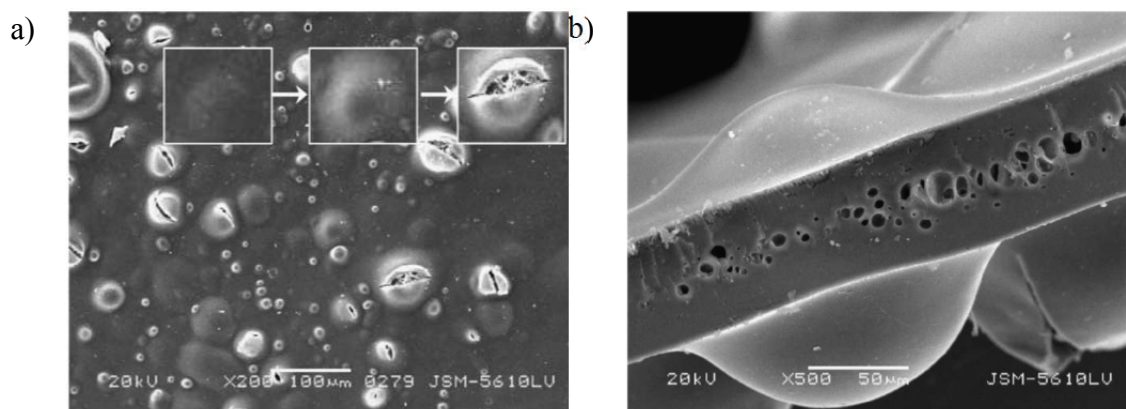


Figure 1-4: a) Surface and b) cross-section SEM micrographs of a Nafion[®] membrane treated in 30 wt% H₂O₂/metal ions for 48 h. (From [22], Reproduced with permission from Elsevier)

1.4 Challenges of the *in situ* detection of H₂O₂ in PEMFCs

Detecting the chemical species that cause the degradation (or the precursors of these chemical species) is one of the ways to improve the durability of PEMFCs, in particular the lifetime of the electrolyte membrane. This detection in PEMFCs, however, involves challenges that reduce the range of possible sensing techniques for chemical detection to just a handful.

Some of the challenges for *in situ* measurement of chemical species in PEMFCs, in particular H₂O₂, include: the low concentration of the produced hydrogen peroxide in the PEMFC operation; the small size of the flow channels and thickness of the MEA in PEMFCs; the insertion of the sensing device in the cell; and the electrochemical environment inside a PEMFC.

Reported values of hydrogen peroxide determined *in situ* in operating PEM fuel cells range from 90 to 700 $\mu\text{mole L}^{-1}$ (3-25 ppm) [23]. It seems then reasonable, for this type of application, that a sensor developed for the detection of hydrogen peroxide is aimed to detection limits lower than 90 $\mu\text{mole L}^{-1}$ and a dynamic range that covers at least the maximum detected concentration, this is over 700 $\mu\text{mole L}^{-1}$.

As noted in Section 1.3.1, the rate of production of H₂O₂ is highly dependent on the relative humidity and temperature of the fuel cell, and under typical operating conditions

these lead to very low concentrations of peroxide. This represents a major challenge for *in situ* detection of H_2O_2 in PEMFCs, and requires the use of a highly sensitive and selective technique of detection, which minimizes the possibility of interferences from other chemical species present, while providing the adequate detection limit required for the application.

Another consideration is the fact that PEMFCs are closed systems, usually involving a series of channels (sometimes smaller than submillimetric range) through which fuel and oxidant are transported. The deployment of an *in situ* sensor for the detection of H_2O_2 needs to be minimally invasive, and allow the reagents involved in the normal operation of the PEMFC to be transported to the catalyst layer, and the products of the reaction to be removed with ease. The insertion of the sensor in the PEMFC has to be performed in the least disruptive manner, without compromising the sealing of the reagent gases and allowing the measuring signal to be acquired remotely.

The electrochemical environment inside PEMFCs also brings key challenges to the *in situ* detection of H_2O_2 in PEMFCs. The highly acidic electrolyte used may cause corrosion of the materials of which the sensor is made. Thus, the materials and reagents used for the fabrication of the sensor should not be susceptible to degradation inside the PEMFC nor affect the chemical processes that take place in it.

Another constraint is the need to avoid the use of platinum as part of the sensing device. Pt is commonly required in PEMFCs as the catalyzer of the main electrochemical reactions, and its presence in an acidic environment can trigger an alternative path for the oxygen reduction reaction (ORR) with 2 electrons involved. As noted in reaction (1.4), the product of this 2-electron ORR is indeed H_2O_2 [9, 24]. Thus the use of Pt may induce the formation of H_2O_2 in addition to the one that forms naturally at the operating conditions.

Finally, high current densities in PEMFCs can be a potential source of electromagnetic (e.m.) noise interfering with electric and electronic devices, especially sensing systems that rely on small currents. This e.m. noise could be manifested as

induced currents on the conductor wires of a sensor due to Faraday's law of induction, and result in erroneous measurements.

Based on a comprehensive literature review of the techniques for *in situ* sensing in PEMFCs (see Chapter 3:), it is apparent that the state-of-the-art in sensing technologies for fuel cells is mostly focused on the measurement of temperature, relative humidity, and current. It is also apparent that there is a lack of *in-situ* detection methods for chemical species in PEMFCs.

To date, the only reported *in situ* detection of H₂O₂ in a PEMFC was by Liu and Zuckerbrod [23]. Their measurements, which were based on an electrochemical technique, determined the presence of H₂O₂ but were not reliable in quantifying the amount produced or the concentration.

1.5 Techniques for detection of hydrogen peroxide in small concentrations

Multiple techniques have been described in the literature for determining the presence and quantifying the concentration of H₂O₂ in applications not related to fuel cells. These techniques include titrimetric, colorimetric, gasometric, electrochemical, and spectroscopic techniques. Titrimetric techniques, which were among the first shown to provide H₂O₂ quantification, rely on the oxidation or reduction of H₂O₂ using chemicals such as potassium permanganate (KMnO₄) and acid potassium iodine (KI) [25, 26]. Colorimetric techniques are based on a reaction with hydrogen peroxide that produces a colored compound. Gasometric techniques measure the amount of a gas produced, generally oxygen, when hydrogen peroxide reacts with a chemical compound [27]. None of these techniques can address the challenges of the *in situ* detection of H₂O₂ in PEMFCs since some are sensitive to interference from other chemical species, some require a sample extraction defeating the purpose of the *in situ* measurement, and finally, in some cases these techniques cannot determine the concentration of H₂O₂ at the micromolarity level, which is the expected concentration in PEMFCs [28].

This leaves two main groups of techniques suitable to perform this detection: electrochemical and spectroscopic techniques capable of detecting micro/submicromolarity concentrations of H_2O_2 . A brief discussion of electrochemical techniques is presented in Section 1.5.1. Sections 1.5.2 to 1.5.4 present an overview of the three main categories of spectroscopic techniques: absorptive, fluorescent, and chemiluminescent techniques [29]. Finally, Section 1.5.5 introduces optical fibers as a platform for the development of spectroscopic techniques that combines the accuracy of these techniques with the versatility of optical fibers.

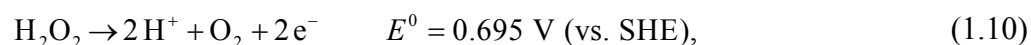
The discussion presented in the following subsections is a distillation of a comprehensive review of spectroscopic techniques suitable for the detection of hydrogen peroxide, particularly at low concentration levels which can be found in Appendix B.

1.5.1 Electrochemical techniques

Using the measurement of potential, charge, or current, electrochemistry provides diverse analytical techniques to determine an analyte concentration or to characterize the chemical reactivity of a substance. Some of the commonly used electrochemical techniques for the determination of chemical substances comprise: voltammetry, potentiometry, and amperometry. Voltammetric techniques apply a time-dependent potential to an electrochemical cell and measure the resulting current as a function of that potential. The result is a plot of the current versus applied potential or voltammogram. In potentiometric techniques, the potential of an electrochemical cell is measured under static conditions (i.e. without the presence of a current). Since there is no current through the electrochemical cell, the composition of the reagents remains unchanged. These two techniques, however, are not practical for the detection of hydrogen peroxide in small concentrations since they require complex instrumentation with high quality reference electrodes, and provide a very low signal-to-noise ratio. For the case of the potentiometric techniques, the environment inside PEMFCs is not free of currents [30].

Thus, only amperometric techniques could be candidates for the detection of H_2O_2 in small concentrations in a practical manner. The amperometric measurement consists of

measuring the current produced when a constant potential is applied between a working and a reference electrode. The current produced by the redox reactions is proportional to the concentration of the analyte at the electrode surface. In the determination of H_2O_2 , the sensing electrode at the anode is made of Pt and poised to +500 to +800 mV, relative to a reference electrode (Ag|AgCl). With this potential, Pt oxidizes H_2O_2 by the reaction:



while at the cathode, the reaction is:



and the overall reaction for the electrochemical cell in detection can be written as:



This detection, however, does not account for the fact that the use of a Pt electrode (as required by this technique) may influence the formation of additional H_2O_2 in the 2-electron ORR as discussed earlier, and also that electrodes and conductor wires may be susceptible to e.m. interference. Detection of H_2O_2 in PEMFCs may therefore be ambiguous, and other alternatives may be more adequate for the detection of *in situ* H_2O_2 in PEMFCs.

1.5.2 Spectroscopic techniques based on absorption

One of the simplest optical detection systems to determine the presence of chemical substances relies on the measurement of absorption. The sensing scheme works by passing light through the sample and measuring the amount absorbed. The physical mechanism of absorption can be expressed as a function of the energy absorbed by an atom or a molecule. This energy can be expressed in terms of the concentration of a certain analyte by the Lambert-Beer law:

$$I = I_0 \exp(-\varepsilon C \Delta x) \quad (1.13)$$

where I represents the intensity of the light measured after the interaction with the sample; I_0 , the intensity of the incident light; ε , the extinction coefficient; C , the concentration of the absorption analyte; and Δx , the thickness or length of the absorption medium [31]. Since the absorption is wavelength dependent, changes in the absorbance in the visible spectrum can be observed as changes in the color of the compound.

Hydrogen peroxide-water solutions do not obey the Lambert-Beer law. Furthermore, due to their similar optical properties, it is not easy to quantify low concentrations of hydrogen peroxide in water solutions based merely in the changes of the refractive index [32]. Nonetheless, it is possible to employ reagents, in solution or immobilized in polymeric matrices, that act as indicators of hydrogen peroxide by observing a change in their spectrum of absorbance [29, 33-40].

The advantages of absorption based techniques include the low cost of the required instrumentation and the wide availability of indicators that may be used for a specific target analyte. Whereas within the possible disadvantages there is the fact that if the measurement is solely based on light intensity changes, the light source and the losses due to connections become a critical factor that may affect the measurement.

1.5.3 Spectroscopic techniques based on fluorescence

Fluorescence is a phenomenon that occurs when molecules absorb light at a certain wavelength (excitation), followed by the re-emission of light at a longer wavelength. Frequently, these excitation and emission wavelengths are unique fingerprints of certain substances called fluorophores, which makes possible their use in sensing. Two main detection principles can be used to determine the presence of the analyte: the first is correlation of the concentration of the analyte with the intensity of the emitted light, which can be either increasing or being dimmed; and the second is measurement of the lifetime of the fluorescence. The latter relies on the determination of the time that the

fluorophore stays in an excited state after the photon absorption, which follows a time-dependent exponential decay [31].

The difference in peak wavelength among the excitation and the emission spectra is known as Stokes' shift [41], and it is illustrated in Figure 1-5.

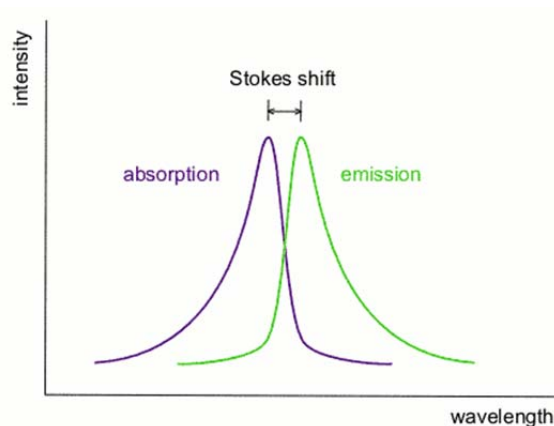


Figure 1-5: Stokes' shift in the spectra of absorption and emission of a fluorescent compound. (©Mikhal/Wikimedia Commons/CC-BY-SA 3.0/GFDL)

In the detection of H_2O_2 using fluorescence based techniques, multiple fluorophores, with diverse excitation and emission wavelengths have been reported [42-52].

One of the advantages attributed to fluoroscopic techniques is the fact that the emitted spectrum is a unique fingerprint of the targeted analyte. However, it is a detection technique that requires a complex instrumentation, which includes specialized light sources and detectors, as well as techniques to resolve possible overlaps on the excitation and the emission spectra.

1.5.4 Spectroscopic techniques based on chemiluminescence

Chemiluminescence is a phenomenon related to fluorescence in the sense that there is a characteristic wavelength of light emission. However, the excitation energy absorbed by the molecules comes from a chemical reaction instead of from light of a shorter wavelength [31]. The H_2O_2 sensing principle relies on the oxidation of a chemical compound, usually requiring the catalyzing effect of enzymes of the peroxidase group [53-55].

Most chemiluminescent techniques used to detect hydrogen peroxide are based on luminol (3-aminophthalhydrazide), whose oxidation by H_2O_2 is catalyzed by the aforementioned peroxidases [56]. Luminol can be used in solution or immobilized in polymeric or sol-gel matrices [57-59]. However, this mechanism of detection is highly dependent on the pH of the medium, and exhibits a maximum of intensity of emitted light in the 8.5 to 9.0 pH range while having a very low response in acidic media.

Other chemiluminescent systems using indicators based on peroxalate esters encapsulated with a fluorescent dye in polymeric nanocapsules have been recently reported. In this case, the chemical reaction excites the luminescence and the emitted light in turn acts as the excitation source of a fluorescent molecule. This system has only been proven in physiological environments to detect H_2O_2 produced by cell cultures [60, 61].

The high specificity and low detection limit are some of the pros associated with chemiluminescent techniques. However, as mentioned above, most of these techniques are suitable for physiological pHs and temperatures, which may not be the case for PEM fuel cells.

1.5.5 Optical fibers as platform for detection of chemical species using spectroscopic techniques

Spectroscopic techniques usually require a clear path or a line-of-sight through which the optical signal can travel, this is called free-space detection. However, optical waveguides made of a suitable material can be used and produce the same results as detection performed in free-space. Of particular interest are optical fibers, which are cylindrical waveguides that carry the optical signal by confining the light within a medium of refractive index slightly higher than the surroundings.

Optical fibers are also an adequate platform to perform remote detection since light can be carried long distances with minimal losses. The reduced size of the fibers makes them a suitable candidate for sensing physical variables in a minimally invasive way. The most commonly used material in the fabrication of optical fibers is fused silica (SiO_2),

which exhibits a high chemical inertness and is thermally stable. The material, combined with the fact that the carried signal is in the visible spectrum, make optical fibers immune to electromagnetic interference.

Optical electrodes, also known as optrodes, have been adapted for the detection of chemical species in multiple applications [62-64]. The most common scheme in these optrodes involves the use of reagents that are sensitive to the presence of the target analyte, and which exhibit changes in their optical properties such as absorbance, refractive index, or that display spectroscopic phenomena such as fluorescence and chemiluminescence.

Multiple configurations have been proposed using the optical fibre as both active and passive medium. In the active configurations, fibres can be coated with indicators for fluorescence-, chemiluminescence-, or absorbance-based techniques; while in the passive configurations, fibres are only used to carry light to and/or collect light from the detection site [65]. Some common configurations used for chemical sensing in optical fibres are shown in Figure 1-6.

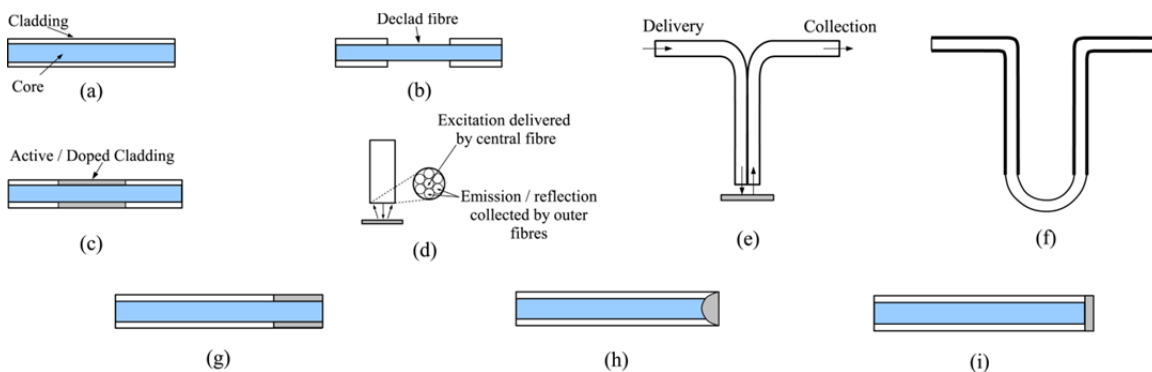


Figure 1-6: Commonly used configurations for fibre optic chemical sensors: (a) unmodified; (b) declad; (c) active or doped cladding; (d) fibre bundle; (e) bifurcated; (f) U-bend; (g-i) distal end based. Reprinted with permission from Ref.[65]. Copyright 2008

American Chemical Society.

1.6 Scope and research questions

Polymer electrolyte membranes fuel cells are electrochemical devices that can create electromagnetic and chemical conditions that may be adverse to the signals and materials involved in sensing techniques for detection of chemical species. In addition, small size of channels and thin electrolyte membranes require of a minimally invasive sensor that does not interfere with the flow of reactants and products. Finally, the production of small concentrations of hydrogen peroxide under normal operating conditions of PEMFCs requires the use of highly sensitive and selective techniques of detection.

Based on the thorough assessment of available detection mechanisms, it appears that a suitable sensor to perform *in situ* detection of H₂O₂ in PEMFCs can be developed by combining a highly selective and sensitive spectroscopic technique of detection with the features of optical fibers such as: small size, ability to perform remote detection, and immunity to electromagnetic fields.

The focus of this research is therefore the development of an optical fiber sensor based on a spectroscopic technique for the detection of the generated hydrogen peroxide. The optical fiber serves as the platform onto which a suitable reagent will be immobilized.

In this order of ideas, the overarching objective of this work is to develop an optical fiber sensing device able to determine the presence and quantify the concentration of hydrogen peroxide produced under normal operating conditions in a PEMFC. This sensor ideally would achieve detection limits lower than 90 $\mu\text{mole L}^{-1}$ H₂O₂, and be able to detect and quantify the produced peroxide to concentrations over 700 $\mu\text{mole L}^{-1}$ H₂O₂. The work is organized into three sub-objectives that are structured to systematically progress toward fulfilling the overall objective.

The first sub-objective is to validate the design of an optical fiber sensing device that is able to detect the presence and quantify the concentration of hydrogen peroxide in liquid phase in an *ex situ* environment. This validation is crucial since the most important design considerations have to be incorporated at this stage. These considerations are: the

spectroscopic technique to use, the chemistry involved that leads to the choice of the reagents for the detection to be used, the immobilization technique that will be used to attach those reagents to the sensing surface, the instrumentation required to perform the recording of the detected signals, and the analysis and post processing required to obtain the adequate measurement.

The second sub-objective is to validate, also in an *ex situ* manner, the temperature response of the sensing device developed in the previous stage. Since the typical operating temperatures of PEMFCs are within 60 °C to 90 °C, the sensing device must be able to detect H₂O₂ at these temperatures.

The third sub-objective involves evaluating the sensor response when it is embedded in a layer of Nafion[®]. Considering that one of the possible alternatives of embodiment of the optical fiber *in situ* sensor is to embed it directly into the Nafion[®] membrane, it is important to understand how this type of installation would affect the sensing properties of the device. Principally, since adding an extra layer could possibly increase the response time and can certainly prevent hydrogen peroxide from reaching the sites of reaction that lead to detection from the optical fiber sensor.

Additionally, the possibility of using the optical fiber sensor to detect and quantify the concentration of H₂O₂ in a gaseous phase is an important feature that requires evaluation.

1.7 Organization of dissertation

This dissertation comprises two *introductory* chapters followed by chapters that present the contributions in the form of *manuscripts* that are in preparation or that have been published in scientific journals and presented at international conferences.

Chapter 1, describes the motivations for the detection of hydrogen peroxide in PEMFCs, as well as the current state of its detection in small concentrations. The design parameters including the optics, and the principle of operation of the sensing mechanism and reagents immobilization onto the surface of an optical fiber are presented in

Chapter 2, which concludes with a short discussion of the pragmatic considerations in choosing the design parameters in the development of the optical fiber sensor.

In Chapter 3, a comprehensive literature review of the state-of-the-art on *in situ* sensing techniques developed for the monitoring, as well as detection of contaminants that decrease the performance and durability of PEMFC is presented.

Chapter 4 presents the contribution on *ex situ* sensors for the detection of hydrogen peroxide in liquid solutions. The thermal response of these sensors and the durability to temperature is presented in the submitted manuscript that is the core of Chapter 5.

Finally, Chapter 6 presents the response of a sensor embedded into a Nafion[®] membrane. A summary of contributions, conclusions, and recommendations for future work is presented in Chapter 7.

Four appendices complete this dissertation: Appendix A, which summarizes the *in situ* sensing techniques for PEMFCs; Appendix B includes a compendium of the multiple sensing techniques found in the literature for the detection of small quantities of hydrogen peroxide; Appendix C, presents a detailed procedure of the fabrication and assembly of the optical fiber sensors developed as part of the research in this dissertation; and Appendix D, which explores the detection of vapor phase of hydrogen peroxide and presents a theoretical and practical approach for the estimation of the production of this chemical species in an operating PEMFC. This appendix also documents the experimental methods and results of the first attempts towards developing a purely optical fiber based sensor for the detection of hydrogen peroxide in vapor phase.

Chapter 2: Design parameters of an optical fiber sensor for hydrogen peroxide detection

This chapter provides background information on optical fibers, detection of chemical species employing optical fibers, as well as in the selected absorptive technique and the immobilization of the reagents that allows the detection of hydrogen peroxide. This information provides a basis for the design of the optical fiber based sensor.

2.1 Principle of optical fibers and optical fiber sensors configurations for detection of chemical species

Optical fibers have become one of the most common platforms to perform optical sensing of chemical substances. This approach has been so successful that the term “optrodes” has been coined from “optical electrodes” [31, 65].

Maxwell’s equations for electromagnetic propagation in cylindrical waveguides provide the theoretical foundation required to describe the total internal reflection and the guided modes theory in optical fibers [66, 67]. The discussion in this chapter focuses on a description of the physico-chemical aspects of the fiber operation and the integration with absorptive based techniques.

2.1.1 Multi-mode optical fibers

In this work, conventional silica/silica multi-mode optical fibers (hereafter referred to as the optical fibers or MMOF) were used in the fabrication of the optical fibers sensor for the detection of H_2O_2 . These optical fibers present a simple coaxial geometry where a fused silica (SiO_2) cladding surrounds a fused silica core doped with Germanium, Boron, and other elements. This difference in chemical composition causes the refractive index of the core to be slightly higher than the refractive index of the cladding, and allows the optical fiber to be a waveguide for light within certain range of wavelengths (Figure 2-1).

The dimensions of core and cladding vary depending on the manufacturer and the application. Multimode optical fibers SFS105/125Y and SFS200/225Y with high OH,

and suitable for a spectral range that spans from ultraviolet (UV) to near-infrared (NIR) from Thorlabs (Newton, NJ) were used in this dissertation. These fibers have cladding diameters of 125 and 225 μm (two of the most common cladding diameters), and core sizes of 105 and 200 μm , respectively.

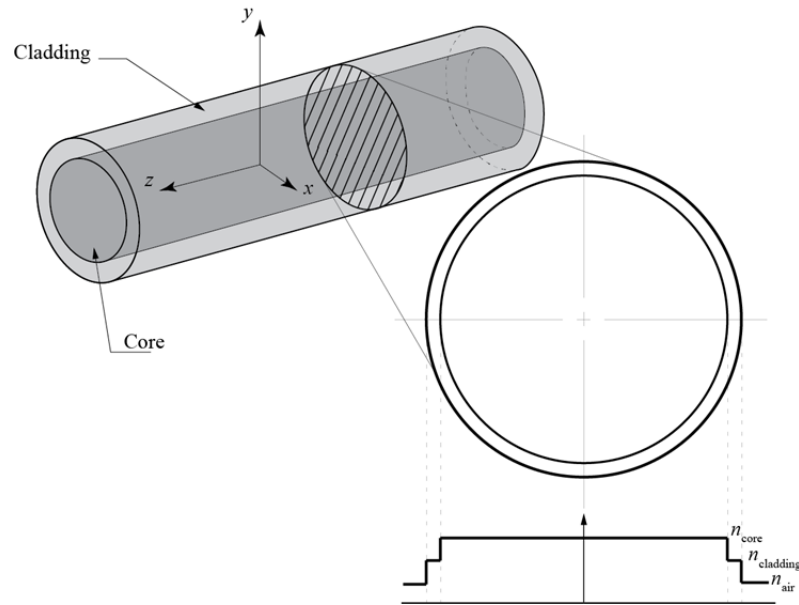


Figure 2-1: Schematic (not to scale) showing relevant features of multi-mode optical fiber. Inset cross section of the fiber with 225 μm cladding and 200 μm core size (to scale) showing relative sizes of core and cladding. Refractive index profile of core and cladding areas.

Total internal reflection of the light that propagates within the fiber core occurs when the refractive index, n , of the core exceeds the refractive index of the cladding in an optical fiber. This difference in refractive indices, the core and cladding diameters, and the wavelength of the light, dictate the number of *modes* propagating through an optical fiber.

Each mode is a unique solution of the electromagnetic wave equation for light propagation along the fiber. Some fibers are designed to transmit a single mode, whereas others can carry multiple modes and are referred to as multi-mode optical fibers (MMOFs) [66].

Some of the advantages of MMOFs in sensing devices are: (1) inexpensive operation; (2) using the multiple modes within the fiber for multiple sensing parameters; (3) sensing spectral changes over a wide range of wavelengths; and (4) easy integration with inexpensive light sources and detectors [68].

2.1.2 Fiber sensors using absorption-scattering techniques

Some of the phenomena where light interacts with matter do not cause the energy levels of the atoms or molecules to change; these are known as elastic interactions. In some other cases, the energy levels of the atoms or molecules change as a consequence of the interaction with the incident light; these are known as inelastic interactions. These interactions cause the electrons to move from a ground state to an excited state. In the former case, there is no induced change in the wavelength of the light. Thus, the light is reflected, absorbed, scattered, or transmitted at the same wavelength as the incident light. During the latter case (i.e. inelastic interactions) in which electrons modify their energy levels, this additional energy is radiated and the electrons return to an energetic ground state. Since some energy is consumed as vibrational energy, light emitted as radiation has a lower energy and, therefore, longer wavelength than the light used for excitation [69] (Figure 2-2).

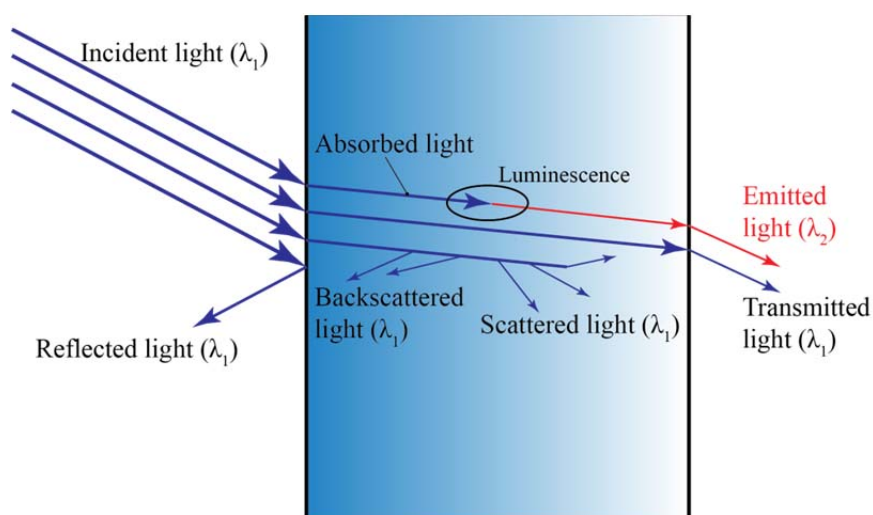


Figure 2-2: Some phenomena caused by the light-matter interaction. Adapted from Ref.[69] under CC 3.0 BY.

Opto-chemical sensors rely on quantifying the changes of the optical properties of a material as they change due to the presence of a chemical analyte. In many cases, these types of sensors can be combined with an optical fiber platform, obtaining an optical fiber sensor, as in one of the multiple configurations presented in Section 1.5.5.

Optical fiber sensors may be divided in two main categories: extrinsic sensors, in which the sensing element is external to the fiber itself, and intrinsic sensors in which changes in the characteristics of the optical fiber are the basis of the measurement [70]. In the case of extrinsic sensors, the optical fiber simply acts as a carrier guiding the exciting light from the source to the sensing area, and the emitting light, from the sensing element to the detection system [69].

The simplest optical phenomenon with practical applications for detection of chemical species using optical fibers is the absorption of radiation at a specific wavelength. Absorption is used primarily with extrinsic sensors, using a fiber or a bundle of fibers to carry the light to and from the sensing area. The degree of absorption is a function of the absorption cross-section of the transducing molecule, the optical path length, and the illumination wavelength. The intensity of the light that penetrates to a distance Δx into an absorbing medium with absorption coefficient εC , as shown in Equation (1.13) is given by:

$$I = I_0 \exp(-\varepsilon C \Delta x). \quad (2.1)$$

Conventional measurements of absorption require monitoring of the signal transmitted through the absorbing material, which makes the integration with optical fibers difficult. However, this drawback can be mitigated by using a reflective material or by employing a medium that backscatters the partially absorbed light from the end of the fiber [41]. As Figure 2-2 illustrates, a component of the absorbed light in the media scatters in the opposite direction of the incident light, providing information on the changes suffered by the absorbing material.

The simplest arrangement employs a membrane material affixed to the end of the fiber in which the reagent is immobilized (Figure 2-3). The light scatters not only from the fiber-membrane interface but also from within the membrane; the amount of backscattered light is modified by changes in the optical absorption of the reagent immobilized within the membrane.

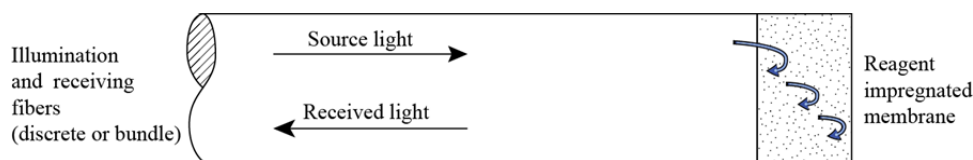


Figure 2-3: Schematic of a membrane absorption-scattering sensor. (Adapted from Ref. [41])

The material chosen to immobilize the reagents within this membrane requires certain characteristics [41]:

1. The membrane should not interfere with the sensing properties of the immobilized reagent, and any alteration must be minimal;
2. The membrane should allow the chemical species to diffuse within the desired response time;
3. The light reflected from the membrane should not have spectral changes as a result of the interaction with the material of the membrane to prevent interference with the measurand.

2.2 Detection of hydrogen peroxide based on the Prussian blue – Prussian white system

Prussian blue¹ ($\text{Fe}^{\text{III}}\text{Fe}^{\text{II}}[\text{CN}]_6$) is an organometallic compound, commonly used as a dye, with a molecular structure of ions of iron(II) and iron(III) bridged by cyanide groups. In this configuration, the carbon atoms of the cyanide groups surround octahedrally the iron(II) ions, while iron(III) ions are linked to the nitrogen end of the cyanides (Figure 2-4 a) [71]. The crystalline structure of Prussian blue (PB) forms a cubic

¹ IUPAC name: Iron(II,III) hexacyanoferrate(II,III)

cell of a size that is determined by the length of the cyanide complex ($-\text{C} \equiv \text{N}-$) that lays between each pair of iron ions; thus the cubic structure of the Prussian blue has a lattice parameter of 0.51×10^{-9} m (510 pm) (Figure 2-4 b). This particular arrangement creates a microporous network that allows the migration of ions and small molecules, the pore-size of 3.5 Å of this porous network allows the easy migration of small molecules and cations –including for example H_2O and H_2O_2 (Figure 2-4 c) [71-73].

The blue color of the pigment is a result of an intense intervalence-transfer charge between the iron ions that absorbs light in the 700 nm range (Figure 2-4 d). In order to balance the charge of the unit cell, some of the interstitial spaces are filled with either potassium ions (K^+) or ferric ions (Fe^{III}) leading to two different stoichiometries of the Prussian blue compound. In the former case, Prussian blue is called “soluble” ($\text{KFe}^{\text{III}}\text{Fe}^{\text{II}}[\text{CN}]_6$), and for the latter case, it is known as “insoluble” ($\text{Fe}^{\text{III}}_4(\text{Fe}^{\text{II}}[\text{CN}]_6)_3$). Both compounds present low solubility in water [71].

Prussian blue has been studied due to its electrochemical and spectroscopical properties. It has been used as a catalyst and employed in analytical sensors and biosensors in the form of films [71, 74-80]. Electrochemically, a cyclic voltammogram of Prussian blue films reveals two sets of peaks, one indicating the transitions to and from Prussian white (PW), and the other one the transitions to and from Prussian Green (Figure 2-5).

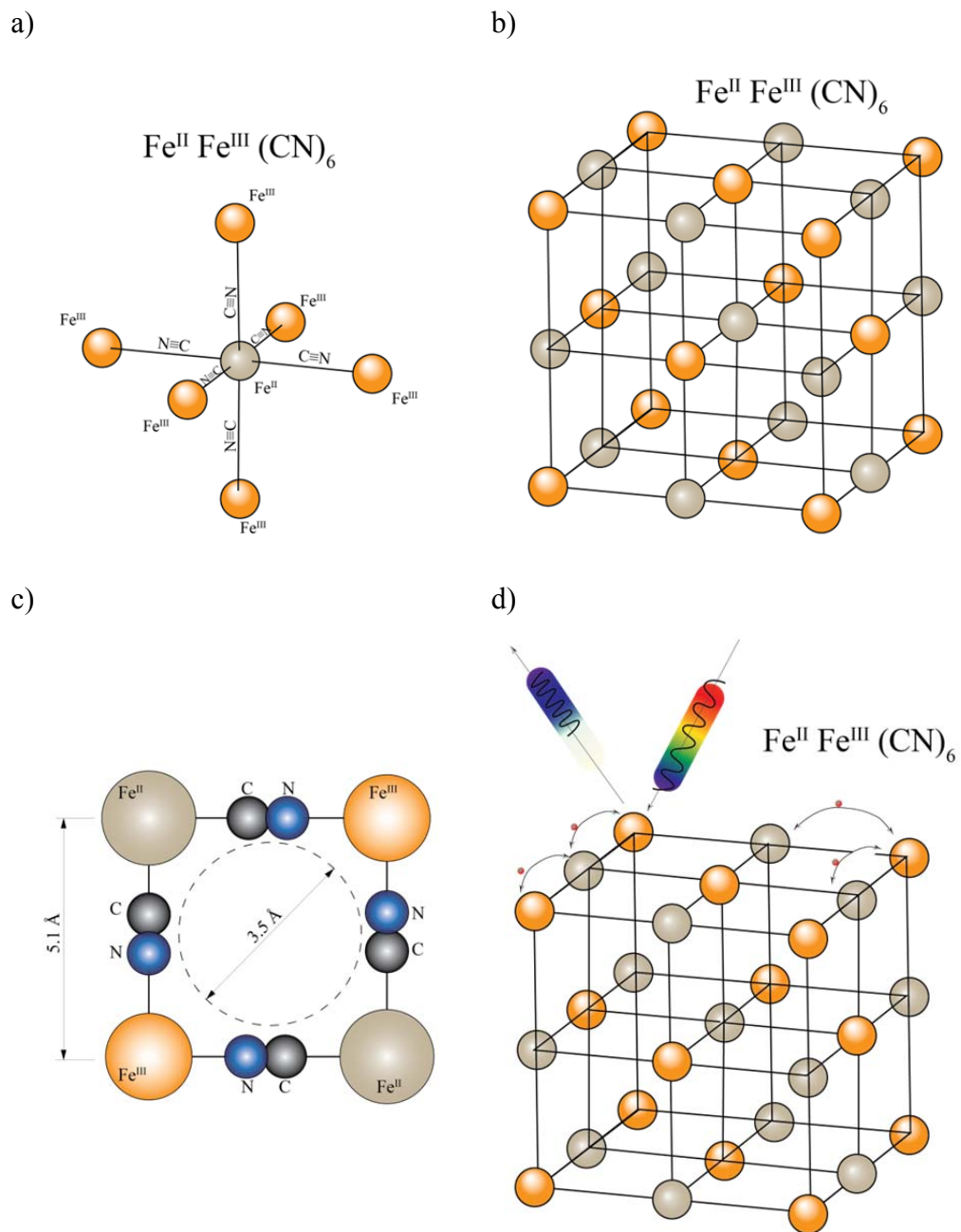


Figure 2-4: a) Iron(II) ion surrounded octahedrally by cyanide groups and iron(III) ions; b) Crystalline structure of hexacyanoferrate compound; c) Bottle-neck in the crystalline structure of Prussian blue (Adapted from Ref. [73]); d) Schematic of the intervalence electron charge transfer between the iron(II) and iron(III) ions, responsible of the blue color of the PB due to the absorption of the red wavelengths of the visible spectrum.

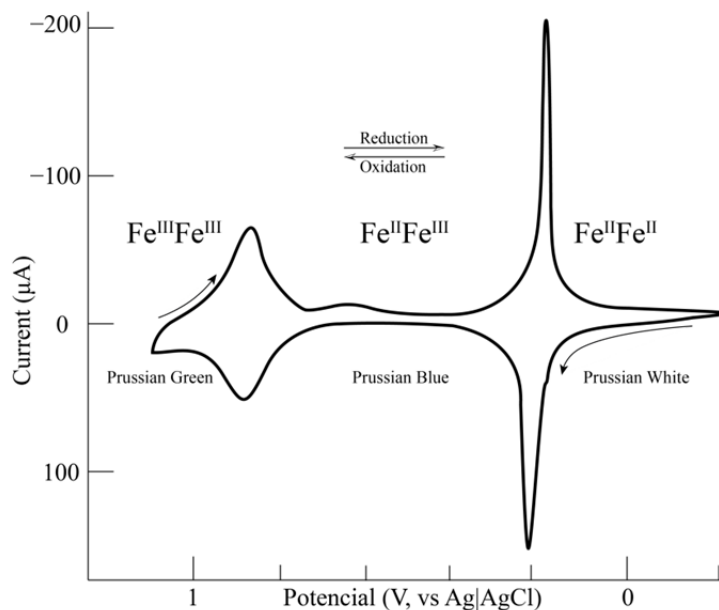
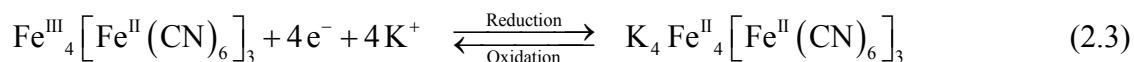
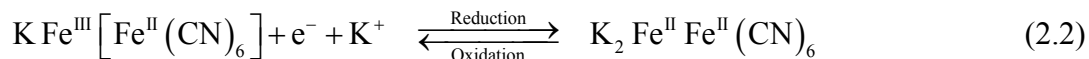


Figure 2-5: Voltammogram of PB film on a gold wire; sweep rate 1 mV/s (Adapted from Refs. [71, 81])

The reduction reactions leading PB to PW for both formulas “soluble” and “insoluble” of PB are formulated as follows [71]:



These processes of PB reduction to PW, and PW oxidation to PB have also been achieved by exposing PB films to chemical reducing agents such as *L*-Ascorbic acid and oxidants like hydrogen peroxide, respectively [38, 40, 82, 83].

The optical properties of these two states of the Prussian compound, PB and PW, exhibit rather different optical properties. In the PB case, the intervalence charge-transfer mechanism with an intense absorbance in the 700 nm, produces a deep blue color. PW instead, has a minimal absorbance in the visible range, making the compound essentially transparent (Figure 2-6).

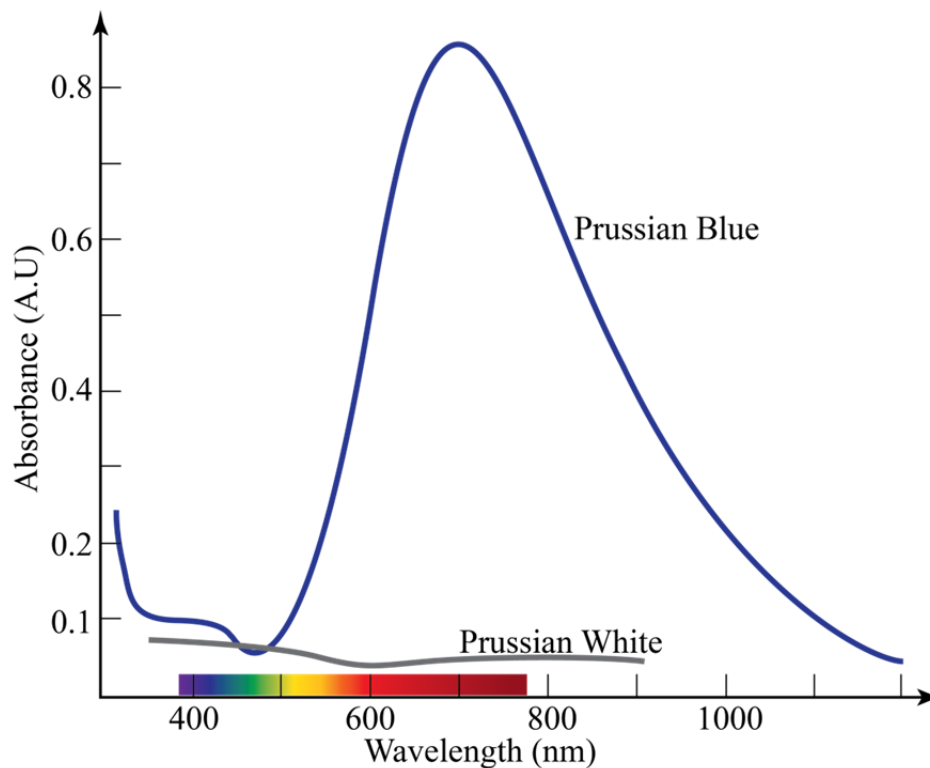


Figure 2-6: Absorption spectra of Prussian blue and Prussian white films (Adapted from Ref. [84])

These unique optical properties have been used in the fabrication of opto-chemical sensors where PB plays a role as an indicator for diverse analytes such as hydrogen peroxide, ascorbic acid, and some mercaptocompounds [85-87]. Furthermore, the range of maximum absorbance showed by the system is compatible with inexpensive sensors and light sources in the near-infrared band of the spectrum [71].

Another crucial feature of the PB/PW is the response of the absorption spectra to changes in pH of the media. The observed response of the peak of absorbance at 700 nm in the PB compound increases its intensity with low values of pH (Figure 2-7), making the PB/PW system suitable for detection of H_2O_2 in acidic media such as those present in PEMFCs. At high pH values, in alkaline media, the PB exhibit irreversible hydrolysis and its absorbance in the visible range disappears [87].

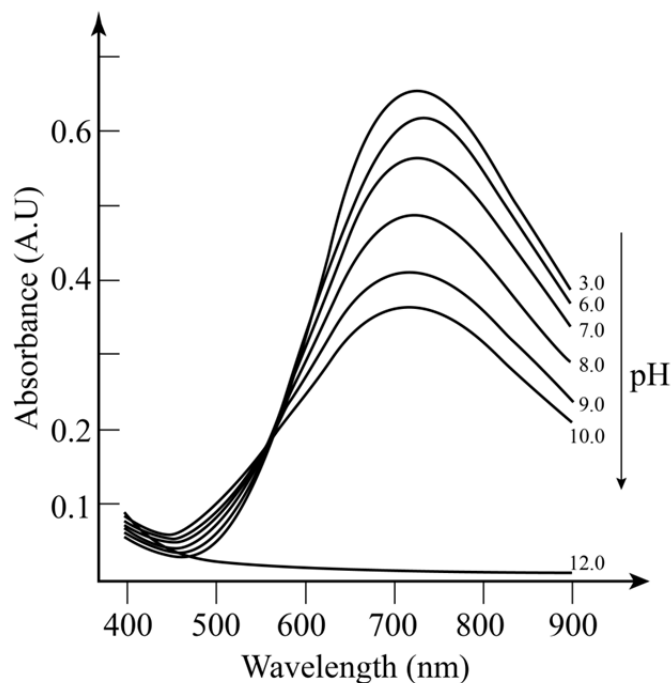


Figure 2-7: Absorption spectra of PB films recorded in different buffer solutions at various pH values (Adapted from Ref. [87])

The selectivity of the PB/PW system also makes it a good choice as an indicator for the presence of H_2O_2 . The optical response of the PB films is insensitive to a variety of chemical compounds including: chloride, bromide, iodide, sulfites, and cyanides, among others. Only ascorbic acid and some mercaptocompounds are able to produce the reduction of PB to PW. The oxidation of PW to PB occurs in the presence of permanganate, chlorine, bromine, iodine, in addition to hydrogen peroxide [71]. However, among all these substances, only hydrogen peroxide is likely to be present during the operation of hydrogen-fuelled PEMFCs.

2.3 Electrostatic self-assembly (ESA) of polyelectrolytes in a layer-by-layer (LbL) deposition

The field of chemical sensing has advanced with the incorporation of indicators on optical fibers to allow the detection, and, in some cases, quantification of diverse analytes in environments where only optical fibers can be employed. Such indicators react and enhance or modify the response of the guided light in the presence of the analyte.

Using this principle, it is important for the design of the H_2O_2 sensor to ensure that the reagents are adequately immobilized on the surface of the optical fiber. In order for the sensor to produce reliable and consistent results, requires proper control of the optical properties and the thickness of the immobilizing film [88]. It is also important to ensure that the reagent diffusion is not affected by the selected materials of the immobilizing film so that the response time of the sensor is not hindered and remains within the time scale of the events to be monitored [89].

Electrostatic Self-Assembly (ESA) of polyelectrolytes in a Layer-by-Layer (LbL) deposition technique is one of several techniques for reagents immobilization onto surfaces that has been intensively studied for the last two decades. The LbL deposition technique is independent of the geometry, and is suitable for application onto planar, spherical, cylindrical or other irregular shapes [90, 91]. This type of deposition allows the immobilization of multiple types of materials in a multi-layered structure [92].

2.3.1 Immobilization of reagents using the ESA of polyelectrolytes

The properties of the film deposited onto a surface depend on the materials that are immobilized within the structure. This technique allows the substrates to be coated with indicators or reactants such as proteins, dyes, oxides, or metallic nanoparticles. These indicators or reactants tailor material properties such as the mechanical, thermal, optical, among others, and make them suitable for optochemical and biochemical sensing devices [88, 93].

The process of immobilization of reagents such as Prussian blue onto the surface of an optical fiber (Figure 2-8a) begins with obtaining an electrostatically charged surface onto the distal end of an optical fiber. This electrostatically charged surface is placed in contact with a solution of Prussian blue mixed with a polyelectrolyte with electrostatic charges of the opposite sign. An adsorption process by electrostatic attraction occurs at the surface to neutralize the original charge in the surface. After a few minutes of immersion (usually more than 10 minutes are required to ensure a homogeneous layer [94]), a layer of material is adsorbed onto the surface.

The process continues with rinsing with a solvent (e.g. distilled water) that removes the non-adsorbed material leaving the outermost surface charged with the new electrostatic charge. The process is completed by exposing the surface to a second polyelectrolyte of the opposite charge. Once again electrostatic adsorption holds in place a new layer of this second material. This procedure creates a single bilayer. This sequence is repeated to fabricate a polyelectrolyte multi-layered (PEMU) structure [92, 95].

Further details about this deposition process can be found in Appendix C.

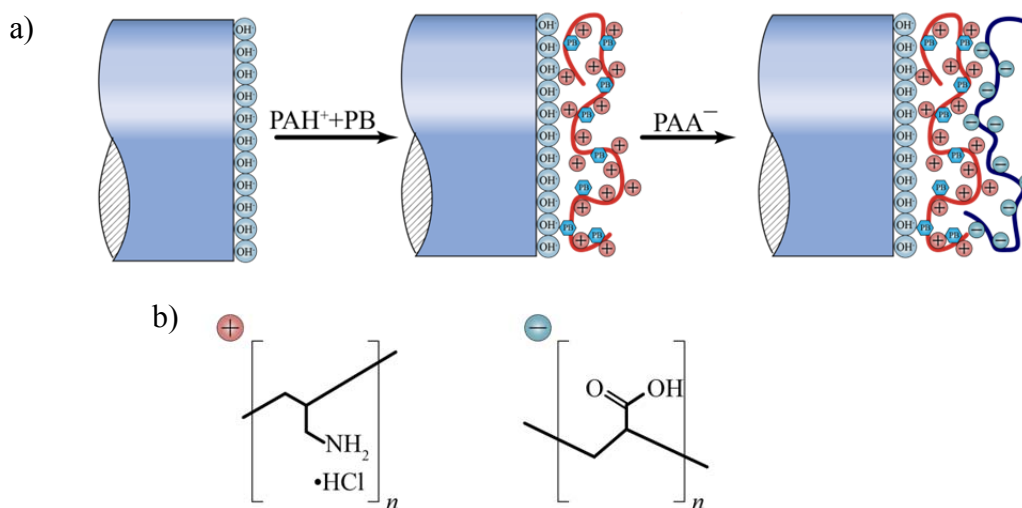


Figure 2-8: a) Schematic representation of the deposition of a bilayer of polyelectrolytes onto the surface of an optical fiber immobilizing Prussian blue; and b) Molecular units of the polycation Poly(allylamine hydrochloride), PAH^+ and the polyanion Poly(acrylic acid), PAA^- (Adapted from Ref. [95])

2.3.2 Tailoring the properties of polyelectrolyte multilayer structures

Multiple polyelectrolytes can be used in the fabrication of PEMUs. The most commonly found polyelectrolytes in the literature are the polycations Poly(allylamine hydrochloride) or PAH^+ , and Polyethyleneimine hydrochloride or PEI^+ . Likewise, the most used polyanions are Poly(acrylic acid) or PAA^- , and Poly(styrene sulfonate) or PSS^- . Figure 2-8b presents the molecular units of PAH^+ and PAA^- .

The use of PEMUs to immobilize reagents for optochemical sensors requires the tuning of the properties of the multi-layered structure or film. In this way, the film allows

species diffusion, as well as maintains its optical properties without interfering with those of the reagents.

The diffusivity of species through a film made of polyelectrolytes can be controlled during the fabrication of the multilayered structure. Normally, the diffusion coefficient of different species in a film made of polyelectrolyte is on the order of $10^{-15} \text{ cm}^2 \text{ s}^{-1}$ [96]. However, a lower value in the ionic strength of the precursor solutions causes more tightly packed structures. This allows only small particles to penetrate the polymeric network of the film structure and can modify the diffusion coefficient by one or two orders of magnitude [96].

Hydrogen peroxide, like water, is a small molecule, with dimensions well below 250 pm, which allows it to be rapidly diffused in the PEMU structure. In particular, films made of PAH^+ have been proven to allow the diffusion of H_2O_2 while restricting the diffusion of species of higher molecular weight. The selectivity mechanism in this case is based on the size exclusion throughout the molecular density of the polyelectrolyte [97].

A high diffusivity, however, can lead to a situation where the immobilized reagent is able to diffuse away from the restraining matrix. This property is used in the fabrication of PEMU microcapsules that can provide a dosage of the immobilized material in a controlled manner such as in long release medication [98]. Clearly, this effect needs to be avoided in the fabrication of long lasting sensors, which require the immobilized reagent to remain within the multilayer structure for its entire lifetime. To achieve this, capping bilayers of slightly higher pH have been applied followed by annealing at temperatures of approximately 80 °C [38, 40, 92, 99].

The optical behavior of the immobilizing film requires both dimensional and mechanical stability. These two parameters are related to the thickness and swelling of the deposited films, which have been shown to depend on the pH of the precursor solutions and the pH of the testing solutions. The thickness of each monolayer can be tailored from 5 to 80 Å by varying the pH value of the precursors [100]. Additionally, excessive swelling of the film can lead to dimensional changes and alteration of the light

pathway, and irreversible morphological changes in the structure of PEMUs when they are tested in solutions with large pH differences to the one set during the fabrication have been observed [101, 102].

2.3.3 Immobilization of Prussian blue within polyelectrolyte multilayer films and reagents immobilization using optical fibers as a template

The chemical synthesis of Prussian blue onto electrodes or optically transparent materials has been reported in the literature. The optoelectrochemical properties of Prussian blue, described in Section 2.2, make it a widely accepted indicator in the detection of H_2O_2 using amperometric or optical techniques [75-77, 82, 87, 103-109].

The first report of immobilization of Prussian blue using PEMUs was published in 2003. The authors coated glass, quartz, Indium Tin Oxide (ITO), and other materials by alternately dipping the substrates in solutions of PEI^+ and PSS^- [110]. The immobilization of Prussian blue onto an ITO coated electrode using a PEMU of PAH^+ has also been reported [78].

Optical fibers can also be used as a template for the PEMU fabrication and great advances in the development of chemicals sensors have been made immobilizing dyes, gold nanoparticles, and other indicators. One of the first developed sensors was by researchers of the Universidad Pública de Navarra (Spain), where gold nanoparticles were immobilized in a PEMU of Poly(diallyldimethyl ammonium chloride) and PSS^- ; this multilayered structure was sensitive to humidity [111, 112].

Researchers from the same group later presented a hydrogen peroxide sensor based on the immobilization of the dye Meldola's blue Hemin onto an optical fiber using PAH^+ and PAA^- multilayers. In this approach, Hemin acts as a surrogate peroxidase enzyme to catalyze the colorimetric oxidation of Meldola's blue in the presence of H_2O_2 [29, 39]. This sensor proved to be unstable and dependent on the pH and temperature conditions.

Last, and most significantly in the context of this work, Del Villar and co-workers developed a sensor that immobilizes Prussian blue and that is sensitive to the presence of

H₂O₂ [38, 40]. Once again, the immobilization of the reagent is obtained by the multilayer structure of PAH⁺ and PAA⁻, and the detection mechanism is the same as presented in Section 2.2. These sensors are the starting point in the development of the sensor for *in situ* detection of H₂O₂ in PEM fuel cells that is presented in this dissertation.

2.4 Pragmatic considerations: *in situ* detection of H₂O₂ in PEM fuel cells using Prussian blue based optical fiber sensors

In the context of application to *in situ* detection of H₂O₂ in PEM fuel cells, optical fiber sensors with immobilized Prussian blue possess key characteristics that will allow these sensors to be deployed into the PEM fuel cell while avoiding some of the limitations of other electrochemical sensors:

1. *Small size*: optical fibers are inherently small. Fibers that can carry light at visible wavelengths, where the Prussian blue/Prussian white system presents the maximum contrast in absorbance, are on the order of 125 μm in diameter. This small size along with the remote measurement capabilities of the optical fibers should allow the sensor to be placed *in situ* in a PEM fuel cell, either along the flow field channels or embedded inside the polymer electrolyte membrane without causing great disturbance to the normal operation.
2. *Materials compatibility*: Unlike platinum-based electrodes used in electrochemical techniques of H₂O₂ detection and which can catalyze the production of H₂O₂, optical fibers are constructed with fused silica that is chemically inert. This is a major advantage in the use of optical fiber sensors since the environment inside a fuel cell is chemically harsh with high levels of acidity due to the polymeric electrolyte membrane.
3. *Electromagnetic noise immunity*: The optical signals carried by optical fibers are not affected by, nor do they interfere with the electromagnetic fields and currents that arise in the normal operation of the PEM fuel cell.
4. *Detection reagents*: the Prussian blue/Prussian white system is an adequate reagent to perform the detection of H₂O₂. The Prussian blue reagent can be used

off-the-shelf or synthesized from readily available precursors. The optical properties of the compounds allow an adequate contrast between the oxidized and reduced states of the indicator that make possible a simple sensor configuration comprised of an absorption-scattering sensor deposited onto the distal end of an optical fiber. The spectral properties of the detection system also allow the use of inexpensive light sources and detectors.

Furthermore, the PB/PW system shows its highest absorbance in media at low pH [87], which is compatible with the acidic environment observed in PEMFCs. Finally, the crystalline structure of the PB/PW system creates a microporous network that is inherently selective and allows only small size molecules, such as H_2O_2 , to diffuse and produce the oxidation necessary to perform the peroxide detection.

5. *Reagent immobilization technique:* the polyelectrolyte multilayer structure was selected as the technique to immobilize the reagents because it allows reagent immobilization onto diverse geometries. This type of immobilization technique has been shown to exhibit the optical and mechanical characteristics required for the detection of H_2O_2 using optical fibers.

The diffusion properties and the thickness of the multi-layered structure can be tuned by controlling the pH of the precursor solutions during its fabrication. Exploiting this characteristic, however, is beyond the scope of this dissertation.

Chapter 3: *In situ* sensing techniques in PEMFCs: A review

(Manuscript in preparation for submission to the International Journal of Hydrogen Energy)

To provide the context for the development of a hydrogen peroxide sensor in PEMFCs, the state-of-the-art for the measurement of parameters of interest for monitoring PEMFC performance and degradation is reviewed in this Chapter. This review is in the form of a self-contained manuscript.

3.1 Abstract

Optimal performance and lifetime of Polymer Electrolyte Membrane Fuel Cells (PEMFCs) relies to a large extent on cell and stack system controls that require measurement and monitoring of operational and performance parameters. Numerous experimental techniques have been used to measure these parameters both *in situ* and *ex situ*. Some of these techniques, however, are only suitable for use under controlled laboratory conditions.

This manuscript provides a review of *in situ* techniques for the measurement of operational parameters in PEMFCs, including temperature, relative humidity, and electric current distribution, as well as for the detection of chemical species in which there has been growing interest for the purpose of monitoring and mitigation of degradation. The importance of each of these measurements and how they affect the performance and lifetime of PEMFCs are discussed.

3.2 Introduction

Basic monitoring of fuel cell performance is commonly done by recording the average cell current as a function of the cell potential. The graph obtained by plotting these two parameters is known as a polarization curve [113]. Polarization curves, however, provide no information regarding local conditions within a fuel cell stack.

Optimal performance of a Polymer Electrolyte Membrane Fuel Cell (PEMFC) requires monitoring and control of the operating parameters and environmental conditions. The

monitoring and control are typically achieved *globally*, because *local* measurements which are very desirable remain also very challenging. Physical parameters that are commonly measured in a PEMFC include: temperature, relative humidity, electrical current density, voltage, and pressure of the fuel and oxidant gases [2]. This review focuses on *in situ* techniques that allow *localized* measurements. Prior to presenting a critical assessment of the techniques demonstrated to date, the importance of specific parameters of interest and how they impact the operation of fuel cells are discussed.

3.3 Operating conditions

3.3.1 Temperature

The importance of monitoring temperature during the operation of a PEMFC lies in the multiple effects that it has on performance [114-116]. Thermodynamically, increasing the temperature lead to reductions in the reversible electric potential [1], but of more significance, temperature has also a strong effect on kinetics of the electrodes, hydration of the polymeric membrane, mass transfer, and heat management [117]. Because of the higher kinetic energy of the molecules in the reactants, high temperature reduces the activation energy; which in turn minimizes the voltage loss required to initiate the catalytic reactions [2]. Temperature in PEMFCs is also strongly coupled to changes in the *relative humidity*, because *saturation pressure* is solely a function of temperature [2]. Furthermore, in-plane variations of temperature can lead to the formation of hot spots and potential damage of the membrane electrode assembly (MEA) [118].

In situ techniques for the local determination of temperature frequently involve the simultaneous determination of other performance parameters, particularly electric current and relative humidity which are discussed later in this review.

Temperature sensors can be classified under contact and contactless devices [119], and due to the nature of the *in situ* measurements in a PEMFC, contact sensors are the most commonly used. The wide range of devices tested in PEMFCs includes: thermocouples

[117, 118, 120-122], resistance temperature detectors (RTDs) [123-132], optical fibers [133-138], absorption spectroscopy [139-143], and solid state sensors [144]

3.3.1.1 Thermocouples

Thermocouples are the most conventional and widely used type of device for the measurement of local temperature. They have the advantage of fast dynamic response, easy configuration, ability to operate remotely, and broad measurement range [117]. The operating principle of a thermocouple is based on the relatively straight-forward *Seebeck effect*, whereby a voltage is produced when two electrical conductors of dissimilar metals are joined at the end of a circuit. A thermocouple has a “hot” (or measurement) junction, and a “cold” (or reference) junction. When these two junctions are subjected to different temperatures, an electrical current proportional to their thermal gradient will flow through the wires [119].

Some considerations need to be taken into account in order to perform *in situ* measurement of temperature in an MEA. The thermocouple should be close to the electrodes, but avoid interference with the electrons that take part in the electrochemical reactions; its size must be small enough not to disturb the PEMFC normal operation, or compromise sealing that would result in gas leakage [117].

Mench et al. [120] placed an array of eight R-type[†] thermocouples hot pressed between two 25 μm thick Nafion[®] sheets in a 50 cm^2 active area. This type of thermocouple was chosen to sustain the temperature and acidic environment inside the electrolyte. The thermocouples were placed uncoated along the centerline of the membrane, and evenly distributed between the inlet and the outlet ports on the flow-field plates. The area screened by each sensor and the area masked by the wires was approximately 0.02% of the total active area. Only three thermocouples resisted the assembly process. With the remaining

[†] The electrodes in the R-type thermocouple are made of Platinum-13% Rhodium vs. Platinum

ones, the authors observed temperature variations as big as 15 °C when the operating current density was increased from 0 to 1 A cm⁻².

Wilkinson et al. [121] presented an approach for measuring *in situ* current distribution based on temperature (the correlation of current with temperature is discussed in Section 3.4.1). Nineteen (19) K-type[‡] thermocouples were placed in the graphite collector plates of a Ballard Mk V fuel cell with an active area of 280 cm². The arrangement required drilling the back of the collector plates, directly under the land area of the serpentine channel to allow the 0.25-mm diameter thermocouples to be placed in direct contact with the gas diffusion layer (GDL). Figure 3-1 shows the distribution of the thermocouples in the anode plate.

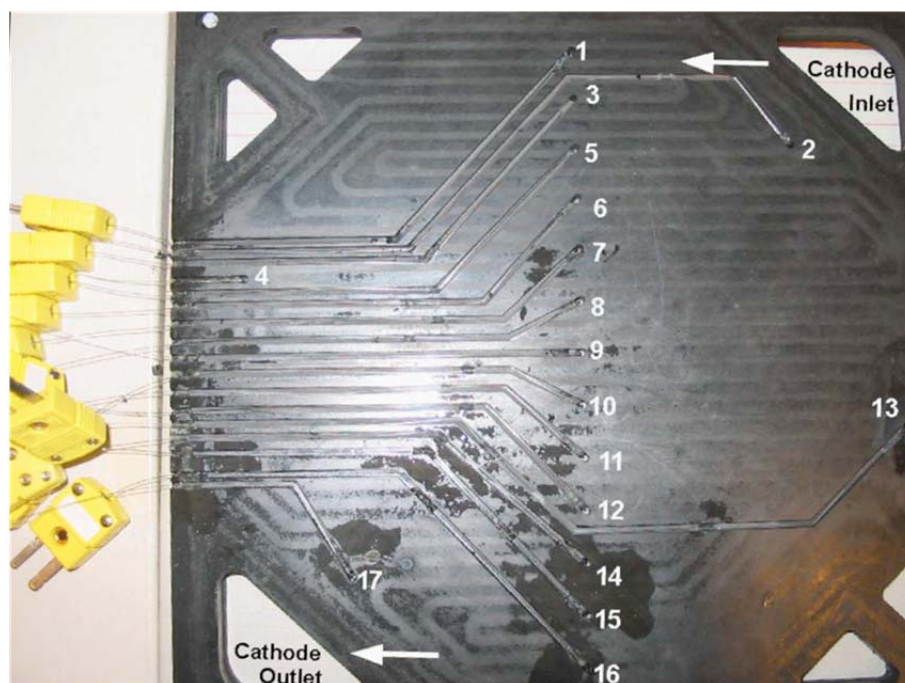


Figure 3-1: Location of the thermocouples embedded at the anode collector plate. (Republished with permission from Electrochemical Society, Inc. from Ref. [121]; permission conveyed through Copyright Clearance Center, Inc.)

[‡] The electrodes in the K-type thermocouple are made of Nickel-Chromium (Chromel) vs. Nickel-Aluminum (Alumel)

Seventeen thermocouples were placed on the anode-side and two on the cathode-side. This difference in the number of sensors was due to the lack of space on the cathode-side plate which incorporated the coolant channels on its back. After the assembly process, only ten thermocouples remained operational. The temporal temperature differences observed in this study were of up to 30 °C when the current density was increased to 1 Amp cm⁻². In addition, spatial differences as large as 6 °C were observed at the same current density.

Using a similar approach, Lebak et al. [118] embedded T-type[§] thermocouples in the back of the land areas on the flow-field plates of a PEMFC. The insertion holes were not drilled through the whole plate up to the GDL but just 0.7 mm away from it. This allowed the fuel cell to keep its original sealing. The electrolyte of this fuel cell was polybenzimidazole, which can operate at higher temperatures than Nafion[®]. Twelve thermocouples (4 in the anode- and 8 in the cathode-side) were placed in the flow fields. Only two thermocouples failed after the assembly. Tests under varying conditions showed that the array of sensors can determine variations in temperature along the flow path and potentially identify hot spot areas of the MEA. Although this approach was less invasive since the thermocouples were not in contact with the GDL, better performance for the instrumented flow field was reported and attributed to a lower ohmic resistance.

Zhang et al. [122] placed ten T-type thermocouples between the catalyst layer (CL) on the cathode side and the GDL, with an additional thermocouple in the center of the cathode endplate. The ten thermocouples were placed along the center of the channel of a serpentine flow-field. The measurements showed an evolution of the temperature along the channel and its dependency on the current. Moreover, the temperatures in the channel were approximately 5 °C higher than registered by the sensor on the endplate.

Thermocouples are inexpensive, technically mature and widely used in many applications. However their *in situ* use for PEMFCs presents some drawbacks: (1) the difficult insertion in the flow-field plates [118, 121]; (2) a trade-off between robustness and

[§] The electrodes in the T-type thermocouple are made of Copper vs. Copper-Nickel

size that may cause the sensors to break during installation [120]; and (3) the requirement of having two pair of wires per each single sensor which makes cumbersome the instrumentation of even a single cell.

3.3.1.2 Resistance temperature detectors (RTDs)

RTDs are based on the relationship between electrical resistance of metals and temperature. Platinum (Pt) is often used for RTDs as it is stable and inert, even at high temperatures [145]. Lower cost alternatives include nickel (Ni), copper (Cu), and certain alloys, but as shown in Section 1.3.2, metal cations can trigger the formation of radicals that promote the degradation of the polymer electrolyte in PEMFCs. Avoiding this source of contamination would require the enclosing of the RTD device within a membrane acting as a barrier but that also may interfere with the species transport.

He et al. [123] presented a technique for embedding deposited Cr–Au RTDs inside the Nafion[®] membrane. The alloy was enclosed in a polymeric film fabricated using chemical vapor deposition (parylene). The resulting RTD had a sensitivity of $3.0 \times 10^{-3} \text{ }^\circ\text{C}^{-1}$ in the 20–100 $^\circ\text{C}$ range. The temperatures measured with this device matched those of a thermocouple placed in the back of the endplate of a PEMFC under transient operation. However, the performance observed in generated power of the cell with the sensors was only 50% of the performance of the cell without sensors. The authors attribute this to the reduction of the active area since 1/3 of the active area of the cell was masked by the films in which the sensors are embedded.

Lee and his research group [124-132] have developed numerous *in situ* sensors employing techniques to produce micro-electro-mechanical-systems (MEMS). The most remarkable characteristic of these sensors is their small size, which for some of the reported sensors is as small as $100 \times 100 \text{ } \mu\text{m}$ [124, 125]. Their initial work consisted on depositing an array of temperature and humidity sensors on the land areas of a parallel-serpentine flow field in a stainless steel plate. The reported sensitivity was $3.91 \times 10^{-3} \text{ }^\circ\text{C}^{-1}$, with an accuracy of less than 0.5 $^\circ\text{C}$. Figure 3-2 presents a microphotograph of these sensors.

A later work by the same authors [127] describes a microsensor on a film of parylene. These sensors were placed directly in the MEA. The dimensions, sensitivity, and accuracy of this temperature sensor are $180 \times 180 \mu\text{m}$, $2.3 \times 10^{-3} \text{ }^\circ\text{C}$, and $0.5 \text{ }^\circ\text{C}$, respectively. Another work by Lee's team [128], presented the fabrication of temperature and humidity sensors on a parylene film using MEMS technology. These $2 \mu\text{m}$ thickness sensors were embedded in the MEA and exhibited a thermal sensitivity of $4.81 \times 10^{-3} \text{ }^\circ\text{C}^{-1}$. The thermal gradient observed between the outer surface of the bipolar plate and the *in situ* sensor was $5.7 \text{ }^\circ\text{C}$. In 2010, Lee et al. [129] presented a microthermal sensor on the GDL of a micro fuel cell. The sensitivity of this device was $1.805 \times 10^{-3} \text{ }^\circ\text{C}^{-1}$.

This same year, Lee's team also presented temperature microsensors made of gold on flexible substrates [130, 131]. The thermal sensitivity of these sensors is $2.7 \times 10^{-3} \text{ }^\circ\text{C}^{-1}$. Figure 3-3 shows the substantial improvement with respect to the sensors showed in Figure 3-2 on the refinement level observed in the fabrication of these sensors.

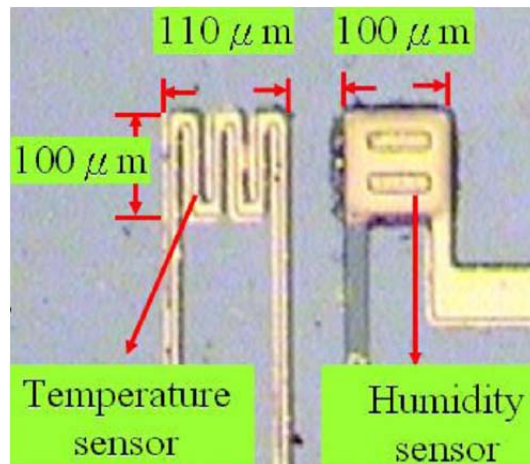


Figure 3-2: Microphotograph of temperature and humidity micro-sensors (Republished from Ref. [124], ©2007 IEEE)

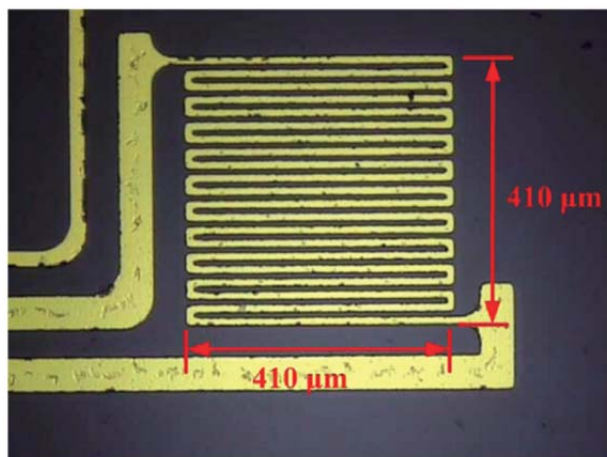


Figure 3-3: Microphotograph of a flexible temperature micro-sensor (Republished from Ref. [130], ©2010 IEEE)

The latest approach in this type of devices also comes from Lee's group [132] in the form of flexible temperature micro sensors on a stainless steel foil substrate coated with gold. This time the reported sensitivity is $2.4 \times 10^{-3} \text{ } ^\circ\text{C}^{-1}$. Although this sensitivity is lower than what they have reported earlier; the technique is intended for mass production, with low cost, and the possibility to place the sensor anywhere across the membrane. However, the performance reported with the sensors placed was reduced up to 14%, and the clamping pressure had to be reduced 50% in order not to damage the sensors.

RTD devices have showed a high development in their adaptation to *in situ* measurements of the temperature in PEMFCs. The most recent advances have been mainly focused on designs that allow mass production and positioning within the fuel cell requiring minimal alterations of the PEMFC geometry [132]. The use of the well-known MEMS fabrication techniques has greatly helped with miniaturization. Drawbacks include: reduced performance due to masking of the active area, contamination produced by metal cations, corrosion of the sensor due to the tough chemical environment, and the possible electromagnetic interference that may affect the reliability of the measurement.

3.3.1.3 Optical fiber approaches

Optical fibers have been employed for sensing multiple physical parameters like temperature, pressure, and chemical detection [146]. The versatility of optical fibers to be

used as sensors in tough environments comes from features such as being: made of electrical insulation materials, chemically inert, immune to electromagnetic fields. In addition, optical fibers are able to perform remote sensing, and due to their inherent reduced size can be inserted within the measured system in a minimally intrusive way. Although there are multiple physical principles related to optical fibers that could be used for sensing parameters, only spectral techniques have been successfully used in PEMFCs. Such techniques include *phosphorescence thermometry* [133-135], *fluorescence* [136], and *Diffraction gratings* [137, 138].

Phosphorescence thermometry with optical fibers

Phosphorescence is the emission of light from a substance that has been stimulated to a higher level with an external energy source. Thermometry by phosphorescence is based on a decay method, which consists of observing the emitted light when the stimulation is removed. The time-dependent emission has a radiative component (light) and a non-radiative component (vibrational relaxation, quenching, etc.). Of which the latter are temperature-dependent. As there is a correlation between the two components of emission, measuring the intensity of the light emitted, as it decays with the time, serves as an indicator of the temperature [135].

McIntyre et al. [134] at the Oak Ridge National Laboratory of the U. S. Department of Energy (DOE), developed guidelines of expected performance for optical fiber sensors for PEMFCs in automotive applications for the 2005 Annual Meeting Review of the *Hydrogen, Fuel Cells, and Infrastructure Technologies*. These guidelines include:

- Operating range: -40 to 150 °C
- Response time: -40 to 100 °C, < 0.5 seconds, with 1.5% accuracy
- Response time: 100 to 150 °C, < 1.0 seconds, with 2.0% accuracy
- Gas environment: High humidity reformer or partial oxidation with compositions H_2 (30–75%), CO_2 , N_2 , H_2O at 1–3 atm. total pressure
- Insensitive to flow velocity

Based on these guidelines, McIntyre describes advances achieved in partnership with companies and institutions such as General Motors, United Technologies, and the Oregon State University. These advances, however, could not be found in the academic or patent literature.

Nonetheless, observing the slides presented in that report [134], it is possible to elucidate that their approach in using optical fibers were focused on the insertion of the optical fibers in the flow channels, as shown in Figure 3-4. These fibers have a spherical ruby tip that serves as a transducer for luminescence-based sensors. In the absence of condensation, temperature profiles along the flow channels remained flat, but when condensation occurred, localized cooling areas were created.

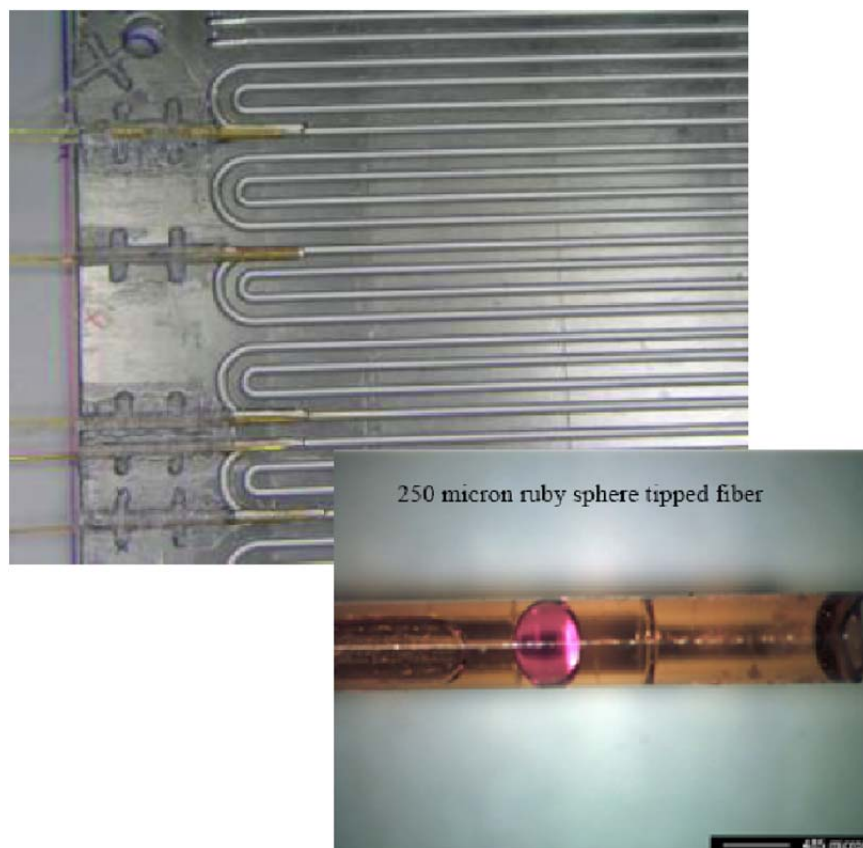


Figure 3-4: Instrumented flow field and optical fiber ruby tip. (Republished from Ref. [134])

Inman et al. [135] presented a similar approach using ruby (Chromium-doped Aluminum oxide 0.5% Cr:Al₂O₃) on the tip of an optical fiber. This material exhibits an

emission peak at 694 nm when it is excited with light at 550 nm. The sensors were placed in the GDL through a hole drilled in the cathode flow-field, as can be schematically seen in Figure 3-5. The accuracy reported was ± 0.6 °C.

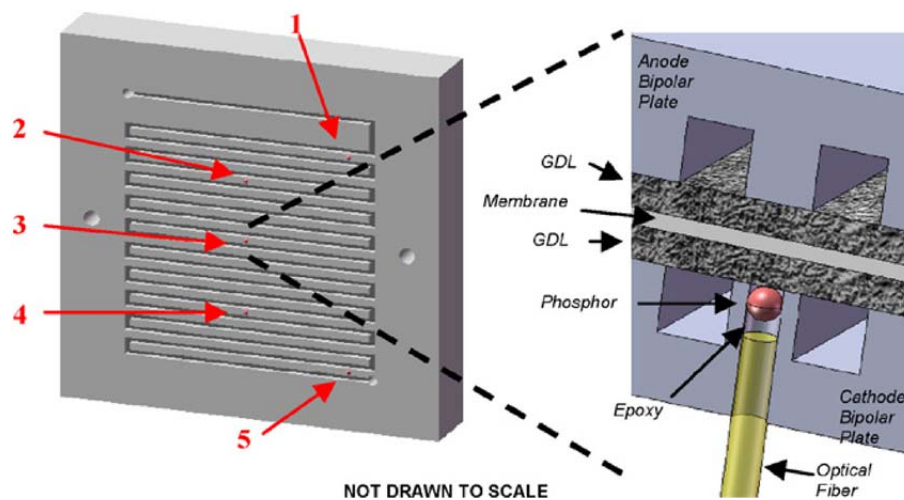


Figure 3-5: Diagram of sensor placement in experimental PEMFC (Republished with permission from Elsevier S.A. from Ref. [135]; permission conveyed through Copyright Clearance Center, Inc.)

A recent refinement in the *in situ* measurement of temperature in a PEMFC using phosphorescence thermometry was developed by Inman and Wang [133]. The approach consisted of applying a coating of Cr:YAG, a phosphorescent material, to a small region of the outer surface of a GDL. Optical fibers embedded perpendicular to the flow field delivered the excitation light and collected the phosphorescent emission from the GDL (Figure 3-6). This technique allowed the authors to determine the temperature inside the PEMFC to within 0.11 °C of the temperature recorded by a high accuracy RTD device.

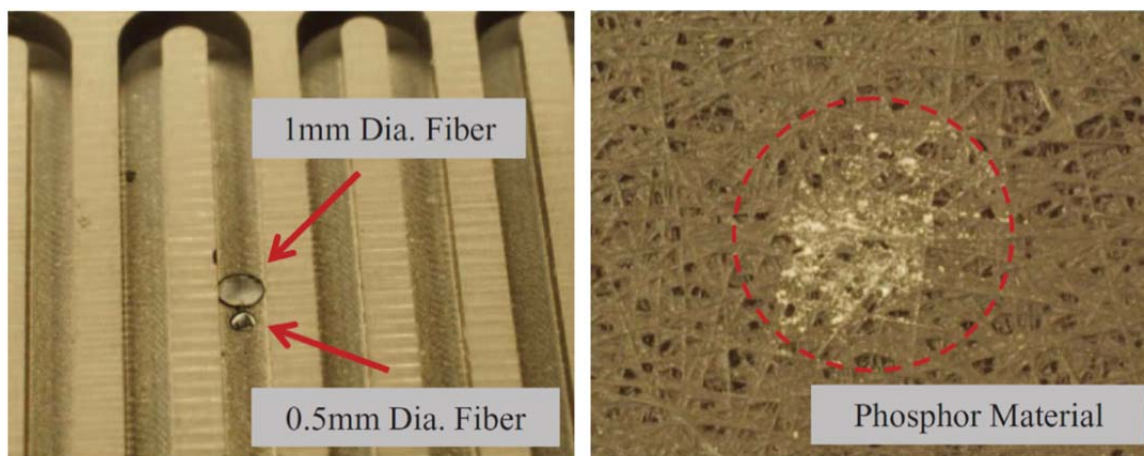


Figure 3-6: Placement of optical fibers installed in flow channel plate (left) and Cr:YAG phosphor material applied to the outer surface of the GDL (right) (Republished with permission from Electrochemical Society, Inc. from Ref. [133]; permission conveyed through Copyright Clearance Center, Inc.)

Fluorescence thermometry

Fluorescence is the emission of light from a substance that is stimulated from an external source of energy. It differs from the phosphorescence in the quantum mechanism that leads to variations in the decay times. In fluorescence, the decay time is around three to six orders of magnitude faster than in phosphorescence. In spite of the time frame, the spectral behaviors of these phenomena emitting light at a specific wavelength when it is stimulated with a shorter wavelength. Furthermore, the intensity of the peak of fluorescent emission of some substances exhibits dependence on temperature [147].

Tao et al. [136] used this principle to develop an optical fiber thermometer that was used to measure the temperature inside a fuel cell. The thermometer consists of two optical fibers whose distal ends were fixed together in a small glass capillary tube. At the tip of this device, a layer of epoxy resin and a reflective coating of gold were deposited. The epoxy resin contains PAHs, a group of aromatic compounds, which emit light in the UV and visible wavelength region when they are stimulated with a UV source of light. In this case, the stimulation and emitted wavelengths were 470 and 580 nm. A later work by Tao and Jayaprakash [148] revealed that the specific wavelengths and sensitivity to temperature

can be modified by using different epoxy glues. This work reported stimulation and emission wavelengths at 410 and 505 nm, and a range of measurement from 25 to 100 °C.

Diffraction gratings

Another fiber optic technique that allows measurements of physical magnitudes are diffractive gratings called in-fiber Bragg gratings (FBG). FBGs are periodical modulations in the refractive index of the optical fiber core. The reflected power spectrum of an FBG exhibits a peak centered at a wavelength known as Bragg's wavelength λ_B , which is given by: $\lambda_B = 2 n_{eff} \Lambda$, where n_{eff} is the refractive index of the optical fiber core, and Λ is the grating pitch. Sensing with FBGs relies on the fact that the spectral position of λ_B changes with thermal and mechanical stresses. Comprehensive reviews of the use of FBGs as sensors can be found in the literature [149, 150].

The *in situ* measurement of the temperature in PEMFCs was first presented by David et al. [137]. Their approach consisted of a 10-mm length FBG inserted in machined channels on the flow-field graphite plate. The reported accuracies were less than 0.2 °C under dynamic cycling of the PEMFC (Figure 3-7).

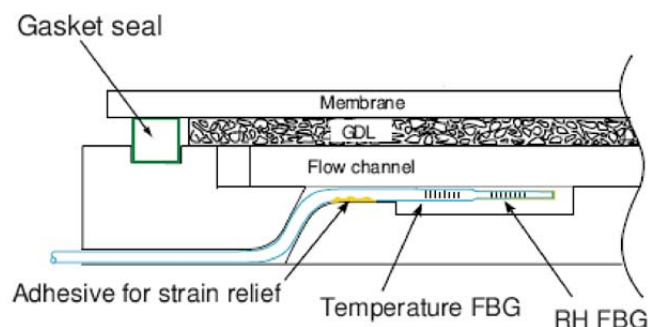


Figure 3-7: Schematic of the *in situ* FBG sensor located in the bottom of the flow channel showing how the sensors were installed into the flow plate (Republished with permission from Electrochemical Society, Inc. from Ref. [138]; permission conveyed through Copyright Clearance Center, Inc.)

FBGs are immune to some of the problems associated with electrical-based sensors; in particular, they are not affected by electromagnetic interference and the ability to operate in adverse chemical environments without degrading or contaminating the measured system.

Additional capabilities can be achieved by multiplexing FBGs at different wavelengths in the same optical fiber. Since the spectral position of the reflected light from an FBG is a function of the period of the grating, then varying this parameter changes the wavelength position of the reflected peak of light. Also, by reducing the length of the FBG to sub-millimetric dimensions, it is possible to enhance the spatial resolution of the technique [137, 138].

3.3.1.4 Absorption spectroscopy

Tunable Diode Laser Absorption Spectroscopy (TDLAS) has been reported by Basu et al. [139-141] and Sur et al. [143] as a suitable technique for *in situ* measurement of temperature in a PEMFC. This technique, patented by Cetegen et al. in 2008 [142], relies on a laser beam from a tunable diode that passes through the gas contained in a chamber of known length L . The laser's spectrum is then tuned on a resonant vibration mode of the molecules of the target substance. When this stage is reached, some of the incident radiation will be absorbed. The amount of energy absorbed is given by the Beer's Law as:

$$I = I_0 \exp\left(-\int_0^L \kappa \cdot P_s \, dx\right), \quad (3.1)$$

where I_0 and I are the intensities of the light emitted and received, $\kappa = (\text{atm}^{-1} \text{cm}^{-1})$ is a constant parameter depending on the wavelength and temperature, and P_s (atm) is the partial pressure of the gas. In this case the gas is H_2O in gaseous phase. By comparing the intensity absorbed with a reference signal, the temperature and partial pressure of the water can be determined [139]. By employing a more refined signal processing the reference signal can be unnecessary [143]. The accuracies reported by using this technique are in the order of ± 3 °C for the *in situ* measurement of the temperature in PEMFCs [139, 143].

The absorption-spectrum related techniques have the great advantage of being selective. They can be used to measure not only the temperature and partial pressure of water vapor but also, when the diode laser is tuned to a wavelength related to another species, can detect its presence in the fuel cell. However, this method requires a

line-of-sight between the diode laser and the photodiode, which calls for the alteration of the fuel cell to insert these components. Another drawback is the low accuracy of the temperature determination when compared to other techniques, and the impossibility of measuring the properties in the presence of liquid water.

3.3.1.5 Solid state sensors

Semiconductor diodes have voltage-current characteristics that are temperature sensitive. The silicon or germanium p-n diode band gap increases with the temperature causing a larger voltage drop across the junction. By measuring this voltage drop, the temperature can be determined [151].

Hinds et al. and Bell et al. [144, 152] measured temperature *in situ* in PEMFCs using a commercial silicon-bandgap temperature detector (Sensirion SHT75). This unit is capable of performing measurements of temperature and relative humidity simultaneously. The sensors were embedded around the edges of the flow-field plates in pockets machined directly on the graphite, each pocket connected through channels to the nearest flow channel (Figure 3-8). The size of these pockets was $\approx 16 \times 23$ mm and 4 mm depth. The sensor datasheet reports response times around 8 seconds, and accuracies of ± 1.2 °C in temperature. However, the authors reported calibration accuracies of ± 0.3 °C. This approach to *in situ* temperature measurements is of limited application due to the significant modifications that must be made to the flow-field plates.

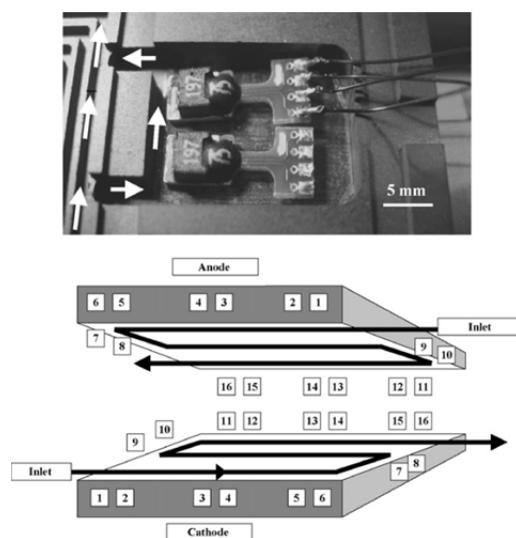


Figure 3-8: a) Recess in the graphite flow plate showing the sensors installation; b) Schematic of the relative position of the sensors in anode and cathode flowplates. (Republished with permission from Elsevier S.A. from Ref. [144]; permission conveyed through Copyright Clearance Center, Inc.)

Table 3-1 summarizes the state-of-the-art of the different techniques employed for *in situ* measurement of the temperature in a PEM fuel cell discussed in this paper.

Table 3-1: Summary of the *in situ* techniques for measuring temperature in PEMFCs

	Spatial resolution	Temporal resolution	Best accuracy	Cost	Merits	Drawbacks
Thermocouples	0.25 mm [121]	Good	± 0.19 °C	Low	Well-known technology. Widespread.	Difficult insertion on stack. Two wires per sensor. Trade-off robustness-size. May be affected by e. m. noise.
RTDs	110 μm [124]	Good	± 0.3 °C [132]	Medium	Small size. Easy to mass produce. Easy placement in fuel cell.	2 wires per sensor. Substrate masks active area.
Optical fibers	700 μm (phosph). [136] 10 mm (FBG) [137]	Good	± 0.2 °C [138]	High (interrogation system)	Multiple sensors on a fiber (FBG). Immune to e.m. noise. Chemically inert.	Brittle. May disturb gas flow. Difficult insertion.
Absorption Spectroscopy	Low (average over channel length)	4 s [141]	$\pm 2\%$ in 80-100 °C [141]	High	Allows species detection. Does not disturb fuel cell operation.	Cannot be used if water condensates. Complex optical alignment and signal processing. Requires straight line-of-sight. Average temperatures
Solid state	Low (average over diverted channel)	8 s [144]	± 1.2 °C [144]	Low	Commercial. Easy to instrument.	Requires machining big pockets on flow-field plates. Mainstream gases do not flow through diverted channels.

3.3.2 Relative humidity

Relative humidity also plays an important role in PEMFC performance. Since the ionic conductivity of Nafion[®] depends strongly on the water content, high levels of hydration are needed to function well as an ionic conductor. On the other hand, excess water may lead to condensation in the gas diffusion layers and flow channels which can prevent the reactants from reaching the catalyst layer and removal of the products of the reaction. Water management is, therefore, critical to fuel cell operation.

However, water content is not easily measured in an operating fuel cell, typically requiring complex techniques, such as those presented by Bazylak [153]. Relative humidity of the gases in the flow channel is more easily measured and can be correlated to water content of the membrane.

The state-of-the-art for *in situ* techniques to measure relative humidity in PEMFCs includes devices and technologies such as: capacitors [124, 125, 127, 128, 131], optical fibers [136, 138], absorption spectroscopy [139-143], gas chromatography [154], solid state sensors [144, 152], and fluorescent dyes [155, 156].

3.3.2.1 Capacitive sensors

In a capacitor, the capacitance, C , can be expressed in terms of geometrical parameters, such as; plate area, A , distance between plates, d , and dielectric parameters, such as, the vacuum permittivity constant, ϵ_0 , and the relative permittivity, ϵ_r , as shown in Equation (3.2)

$$C = \epsilon_0 \epsilon_r A d^{-1} \quad (3.2)$$

Since the relative permittivity of certain dielectric materials changes with humidity, changes in the capacitance can be used to measure the relative humidity. Capacitive humidity sensors for PEMFCs have been developed using MEMS fabrication techniques [124, 125, 127, 128, 131]. These designs are based on an interdigitated pattern where the deposited electrodes are insulated by a polyimide film. A first approach by Lee et al. [124,

125] is presented in Figure 3-2 (right). The dimensions and sensitivity of this device are $100 \times 100 \mu\text{m}$ and $0.51 \text{ pF } \%RH^{-1}$, respectively, with an accuracy of $\pm 0.25 \%RH$. In later approaches by the same researchers, the sensors were embedded in flexible substrates. For example, Lee et al. developed a sensor which dimensions are $740 \times 730 \mu\text{m}$ made on a flexible stainless steel foil [131]. As observed in

Figure 3-9, the level of detail on the fabrication was greatly enhanced with respect to earlier stages such as those shown in Figure 3-2. However, no information about the performance of this sensor was provided.

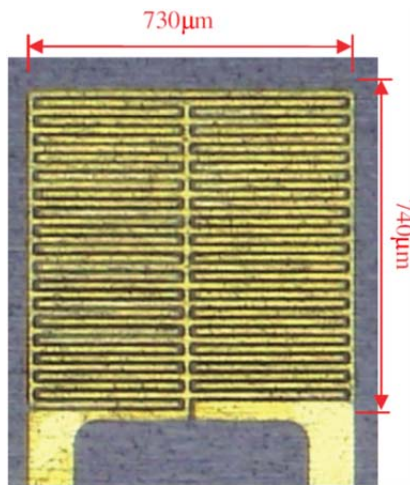


Figure 3-9: Microphotography of a flexible humidity micro sensor (Republished from Ref. [131], ©2010 IEEE)

3.3.2.2 Optical fiber methods

Relative humidity in PEMFCs has been measured using fiber optic devices that sense the effect of humidity on evanescent field interactions [136] and on strain in hygroscopic coatings [138].

Evanescent field interaction

The evanescent wave in an optical waveguide, such as an optical fiber, is the portion of the electromagnetic wave that propagates in the medium that surrounds the waveguide. This wave, which decays exponentially with radial distance from the fiber, is present when the guided light interacts with a dielectric boundary and, occurs as a consequence of the

continuity of the electromagnetic field across this boundary [66]. The intensity and penetration depth of the evanescent field in the surrounding medium depends on the dielectric properties of the media on both sides of the boundary. If the surrounding medium changes its properties, the intensity of the guided light in the waveguide will be modified.

Using a bent optical fiber coated with a silica-gel solution, a material that changes its dielectric properties with moisture content, Tao et al. [136] developed a sensor in which the intensity of the transmitted light changes with relative humidity. The reported range of measurement and response time at 90% of the total signal of this sensor were 4-95 %RH and 3 minutes, respectively. This sensor was not tested in an operating fuel cell but tested in an *ex situ* manner and proposed for its use in PEMFCs.

Fiber Bragg gratings

As noted in Section 3.3.1.3, an FBG exhibits a wavelength shift when it is subjected to mechanical strain. David et al. [138] developed a sensor that measures temperature and relative humidity based on two FBGs written in the same fiber, where each FBG has a distinct, λ_B . The fiber cladding of the distal FBG was chemically etched and covered with a polyimide coating, that swells in the presence of water. Thus, changes in RH generate axial strains in the FBG that lead to shifts in the spectral position of the Bragg wavelength. The reported accuracies were ± 2 %RH with a response time in the order of 10 seconds. The schematic of this application is presented in Figure 3-7.

3.3.2.3 Absorption spectroscopy

The operating principle of this approach is presented in Section 3.3.1.3. TDLAS has been used to measure the partial pressure of water in a fuel cell by Baki Cetegen's group at the University of Connecticut [139-141, 143]. Their initial work reported accuracies of ± 5 %RH. This measurement was only possible up to a maximum of 80 % RH due to condensation problems [139]. In a later work, using a different vibrational state, the measurement range was extended (40-90 %RH) with an accuracy of ± 5 %RH, and response times less than 10 s. By modulating the signal of the laser and bifurcating the

laser light over two channels in the flow field, the technique can have better accuracies, avoid the need for a reference signal, and reduce the response times [141, 143].

3.3.2.4 Other approaches

Gas chromatography

Mench et al. [154] extracted gases from the flow channels of a PEMFC using glass capillaries. Samples of these gases were conducted to and analyzed in a gas chromatograph to perform the direct measurement of molar content of water. Determining the relative humidity in the fuel cell in this way required up to two minutes per sample, with accuracies between 2 and 5% mole fraction.

Solid state sensors

Nishikawa et al. [157] drilled 1 mm diameter holes at six positions along the flow channel of the cathode side in a PEMFC. The diverted gases were conducted to the probe of a commercial humidity sensor (HMI41 with HMP42 probe, Vaisala, Finland). The reported time responses and accuracies from the sensor's manufacturer catalogue were 90 s and 2 %RH [158].

Hinds et al. [144] placed the Sensirion sensor SHT75 in the pockets machined in the graphite plates, as shown in Figure 3-5. The reported time responses and accuracies from the sensor's manufacturer were 8 s to a 63 % response and ± 1.8 %RH [159].

Fluorescent dyes

A physical principle used to directly measure the water content of the membrane in a PEMFC was presented by Patil et al. [155] and granted a patent in 2010 [156]. The technique uses the fluorophore, Rhodamine-6G. A 400 μm thick membrane is cast from a mixture of Nafion[®] solution with Rhodamine. During the casting, a 300 μm diameter optical fiber is embedded in the membrane. In operation, light propagating in the optical fiber stimulates the fluorescence of the Rhodamine. The ratio between two wavelengths in the fluorescence spectra vary according to the water content in the membrane. This effect is

due to the formation of a complex between the Rhodamine and the protonated Nafion[®]. This complex has a different fluorescent spectrum than the original reagent, which modifies the fluorescent spectrum collected by the optical fiber. The casting of membranes with fluorescent dyes, although being a novel approach and determine the water content directly in the membrane, implies the alteration of the membrane to thicknesses that are at least ten fold bigger than the commercial applications.

Table 3-2 presents a summary of techniques employed for the *in situ* measurement of the relative humidity in PEMFCs, as discussed in this review.

Table 3-2: Summary of the *in situ* techniques for measuring humidity in PEMFCs

	Spatial resolution	Temporal resolution	Best accuracy	Cost	Merits	Drawbacks
Capacitors	100 μm [124]		0.25 %RH [124]	Medium	Small size. Easy to mass produce. Easy placement inside the fuel cell	2 wires per sensor. Substrate masks active area. May be affected by e.m. noise
Optical fibers	10 mm (length of FBG) [138]	10 s (90% full height) [138]	± 2 %RH [138]	High (interrogation system)	Small size. Multiple sensors on a fiber. Immune to e.m. noise. Chemically inert.	Brittle. May disturb gas flow. Difficult insertion.
Absorption Spectroscopy	Low (average over channel length)	4 s [141]	± 2.5 %RH [143]	Medium	Does not interfere with PEMFC operation	Cannot be used if water condensates. Complex optical alignment and signal processing. Requires straight line-of-sight. Average temperatures. Limited range (40-90 %RH)
Gas chromatography	Medium (limited by proximity of extraction ports)	2 min [154]	$\pm 5\%$ [154]	High (Instrument)		High cost associated with equipment. Not feasible for commercial applications.
Solid state	Medium (limited by proximity of ports of sensor insertion)	90 s [157]	± 1.8 %RH [144]	Low	Commercial. Easy to instrument.	Requires altering graphite plates. Not feasible for stacks.
Fluorescent dyes	Medium (limited by placement of optical fiber)			Low	Only technique that measures water content in membrane	Requires custom membrane. Membrane thicker than commercial membranes.

3.4 Performance parameters

3.4.1 Electrical current sensors

Electrical current distributions in fuel cells have been intensively studied. A uniform distribution of current density across the active area corresponds to optimal performance of the PEMFC. Conversely, uneven distributions of current density are associated with low

performance. Non-uniform current densities also cause reduced utilization of the reactants and the catalysts, limited energy, and decreased lifetime [121, 160].

Small cells may exhibit relatively uniform current distributions, while larger cells may have gradients leading to local variations of humidity, flooding, and concentration of species, among other effects [2]. Current also correlates to operating parameters such as voltage –through Ohm’s Law–, and temperature. The correlation with temperature may be understood by considering localized increases in the current density that will reduce voltage and efficiency, and create excessive waste heat [154].

A comprehensive review of the literature reveals that only three physical principles have been used to quantify the *in situ* electrical current in PEMFCs: *Ohm's law*, *Hall Effect*, and *extrapolated methods from theoretical relationships*. On the other hand, there is a multiplicity of techniques reported for acquisition of current data from the fuel cell and to map its distribution. These techniques include:

- Masking portions of the active area of the fuel cell or selectively deposit catalyst in certain regions of the electrodes in the fuel cell [161]
- Isolating small regions creating subcells [161]
- Adding an array of resistors to the assembly [161, 162]
- Segmenting components of the fuel cell: Flow-field [163-172], current collectors [163, 165-168, 170-174], GDL [163, 166, 174], and the Catalyst layer [163, 166], either in one or both sides.
- Placing a printed circuit board (PCB) to draw the current out of the cell [122, 163, 166-168, 171, 173-175]
- Inserting commercial current sensors [157]
- Using an array of voltage probes [176]

Due to the impractical amount of possible combinations reported this review will present each physical principle and then describe the approaches found in the state-of-the-art for *in situ* measurement of the current in PEMFCs.

3.4.1.1 Electrical current measurement using Ohm's law

In PEMFCs, mapping of the current using Ohm's law has been performed by placing individual resistors perpendicular to the electrode surface between the flow-field and the current collector plate. The current distribution is obtained by measuring the voltage drop across these resistors [2].

The first *in situ* approach to the measurement of the current in a PEMFC is presented by Cleghorn et al. [163]. In this approach, the flow-field, GDL, and catalyst layer were segmented in a 9×2 array. The flow field was directly machined onto a double-sided printed circuit board (PCB) with vias configured so that one conductive layer is used as the current collector while the other conducts the current to the measuring instrument.

Stumper et al. [161] reported three different approaches to current distribution measurement. In the first approach, MEAs partially coated with catalyst material were used. In the second approach, small regions in different locations of the flow-field were electrically isolated as sub-cells. Each sub-cell was tested independently, and then in conjunction with the main cell. This allowed the performance for specific areas of the fuel cell to be determined. In the third approach, a network of isolated graphite blocks was placed between the flow-field and the current collector. The current was determined by measuring the voltage drop across each graphite block.

Brett et al. [173] used a single channel PEMFC in which the current collector was a segmented PCB. Each segment (2×4 mm) was wired to allow independent current measurement and, thereby, a complete mapping of the current.

Noponen et al. [165] measured the current distribution in an air-breathing PEMFC by arranging flat pieces of gold-plated stainless steel perpendicular to an electrically insulated material. These pieces were arranged so that they formed a parallel segmented flow-field and current collector. The back of the insulating plate each segment was wired to a resistor unit to measure the current.

Mench and Wang [167], and later Mench et al. [168], evaluated the current distribution in PEMFCs with an electrically isolated serpentine flow-field in both the anode and cathode in direct contact with the GDL. 48 sheets of gold-plated stainless steel were arranged as the ribs of the flow-field. The electrical insulation was obtained by embedding the pieces in a polycarbonate matrix 0.89 mm apart. The current was drawn by cables affixed to the back of the ribs, and a constant voltage was kept while the current of each segment was being determined.

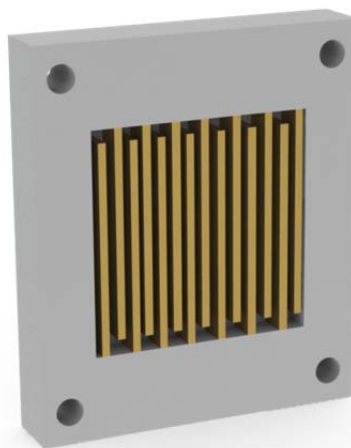


Figure 3-10: Scheme of the embedded gold-plated stainless steel strips forming a flow-field acting as current collector on a polymer substrate as described in Refs. [165, 167, 168]

Noponen et al. [174] segmented the anode current collector into a 4×8 array with segment areas of 1.7 cm^2 . The gaps between segments were filled with an epoxy resin. The total current in the fuel cell was controlled with an electronic load interfaced to a potentiostat. The current was determined by measuring the voltage drop from each segment with respect to a copper back plate in the cathode side.

Hakenjos et al. [170] presented an approach in which the anode side is segmented into a 7×7 array with $5 \text{ mm} \times 5 \text{ mm}$ steel blocks embedded in a polymeric substrate. The novelty in this approach, schematized in Figure 3-11, is that the flow-field is directly machined into the polymer substrate (the red block in the figure) with the embedded segments. Since the polymer substrate is held by a frame on the anode side, the clamping pressure can be

modified. This allows the study of the contact resistance vs. the clamping pressure. The current distribution is mapped by measuring the current of each individual segment.

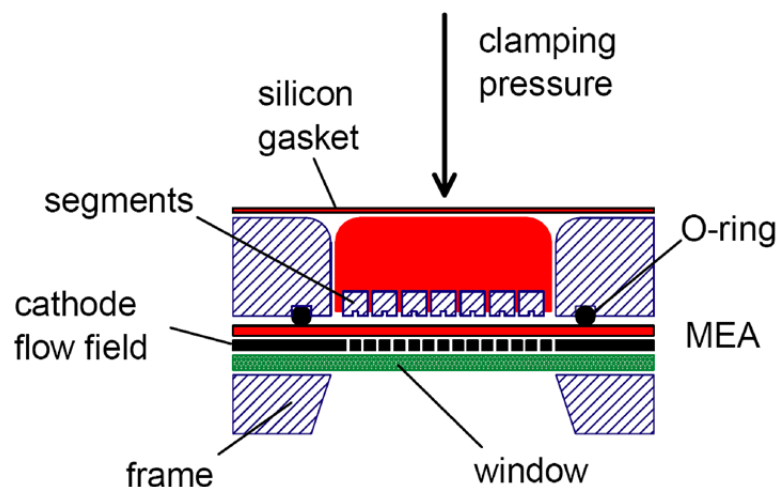


Figure 3-11: Schema of design of fuel cell with segmented flow field and collector (Republished with permission from Elsevier S.A. from Ref. [170]; permission conveyed through Copyright Clearance Center, Inc.)

Ghosh et al. [162] following a similar approach to Stumper et al. [161], placed a segmented network of resistors between the GDL and the current collector on the cathode side of a PEMFC. The resistors are created by the partial segmentation of a graphite plate. Each segment is individually wired but still in electrical contact with the adjacent segments. To determine the current flowing from a segment to another, the in-plane and through-plane resistances were measured. As the in-plane resistance was ~ 1000 times higher than the through-plane resistance, it can be assumed that all of the current travels in the through-plane direction. A major advantage of this technique is that it can be integrated to a commercial stack without further modifications on the stack design.

Nishikawa et al. [157] placed three insulated conductor rods in the lands of a parallel serpentine flow-field in the cathode side of a PEMFC. These rods acting as current collectors allowed the current to be drawn from the fuel cell and measured by the voltage drop on a shunt resistor.

Sun et al. [175] placed a PCB made of gold-plated copper foil strips on the cathode side of a PEMFC. The electrically insulated foil strips were arranged to match the land areas in

the flow-field ensuring the current collection at the GDL. Thus, the mapping of the current is performed along the flow-field on each land.

3.4.1.2 Electrical current measurement using Hall Effect

In a semiconductor, the Hall Effect occurs when an induction magnetic field \vec{B} moves perpendicular to the current produced by an electric field $\vec{\xi}_x$. As a consequence of the *Lorentz force*, electrons are deflected in a direction mutually orthogonal to the magnetic field and the electric field, creating a voltage V_H that is proportional to \vec{B} .

In PEMFCs, measurement of current using the Hall Effect requires conversion of current into a magnetic induction field \vec{B} . This can be accomplished by placing an annular ferrite around the conductor that carries the current. Thus, the magnetic field \vec{H} becomes into a magnetic induction field \vec{B} inside the ferrite ring. The Hall Effect sensor can then be placed in a slit on the annular material (Figure 3-12) [169].

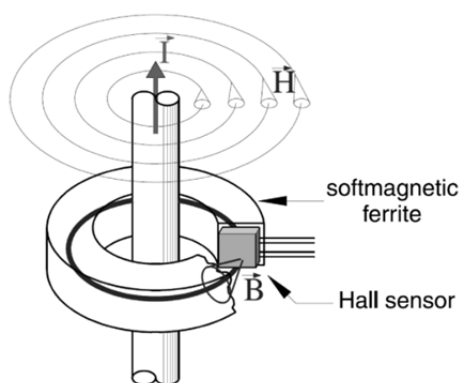


Figure 3-12: Schematic drawing of a current sensor with a magnetic loop and Hall sensor (Republished with permission from Kluwer Academic Publishers from Ref.[164]; permission conveyed through Copyright Clearance Center, Inc.)

The first reported approach for measuring the current in a PEMFC using Hall Effect sensors was by Wieser et al. [164]. The flow plate was segmented in a 5×8 segments array. Each segment was made with a cylindrical protrusion on its back. Ferrite rings with the Hall Effect sensors in machined slits were placed around these protrusions to quantify the current. The temporal resolutions were less than 3 seconds.

Bender et al. [166] segmented the entire anode components (flow-fields, GDL, catalyst layer) in a PEMFC, machining the flow field after embedding graphite blocks in a polymeric substrate. The current was drawn out the cell and measured in an external bank of Hall Effects sensors to avoid thermal drifts.

3.4.1.3 Indirect determination of electrical currents

On some situations, theoretical approaches can be used to evaluate physical magnitudes that have technical challenges to be directly measured. In the case of PEMFCs, the electrical current has been determined by theoretical correlations to temperature and voltage.

A first method to indirectly determine the current distribution is based on a thermodynamic approach. Wilkinson et al. [121] developed a method in which, under adiabatic conditions, the heat rejected locally can be considered as the difference between the ideal and the real power. In this method, temperature distribution is measured with an array of thermocouples. From these measurements, as well as cell voltage, the local power loss is calculated and the local electrical current is inferred.

A second method to indirectly determine the current distribution, based on Laplace's equation for electric potential, is presented by Freunberger et al. [176]. A parallel array of 25 μm diameter gold wires is placed in the current collector and the catalyst layer on the anode side. Each wire acts as a potential probe, enabling measurement of the potential difference between the catalyst layer and the current collector. The current density is obtained by solving the Laplace's equation with the potentials at the current collector and the catalyst layer as boundary conditions. A schematic of this approach is presented in Figure 3-13.

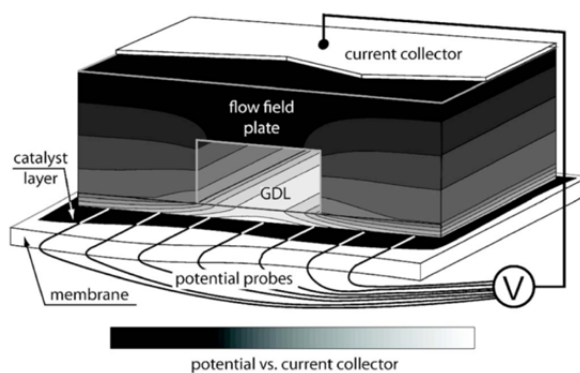


Figure 3-13 Schematic of the measurement principle, the potential drop over flow-field plate and GDL provides information on the current distribution (Republished with permission from the Electrochemical Society, Inc. from Ref. [176]; permission conveyed through Copyright Clearance Center, Inc.)

Table 3-3 presents the merits and drawbacks of the techniques used in the measurement of current.

Table 3-3 : Merits and drawbacks of the *in situ* techniques for measuring current in PEMFC

Technique	Merits	Drawbacks	Remarkable approaches
Partial catalyst	Spatial resolution customizable according to the catalyzed area.	Requires special MEA fabrication process	Stumper et al. [161]
Subcells	Performance isolated from main cell. Good for localized information.	Complex alignment during assembly. Requires special MEA fabrication process	Stumper et al. [161]
Segment current collector	Medium spatial resolution. Can be improved reducing size of segments.	Complex manufacture. MEA placed in the spacers between segments is not covered.	Bender et al. [166]
Segment GDL	Medium spatial resolution. Can be improved reducing size of segments.	Complex manufacture. Incomplete MEA utilization.	Hakenjos et al. [170]
Segment catalyst layer	Increased spatial resolution.	Complex manufacture.	Bender et al. [166]
Flow field lands as current collector	Reduced contact resistance. Customizable design.	Complex manufacture.	Mench and Yang [167]
Resistor network	Low alterations to fuel cell components. It could be integrated into a stack. Low cost. Spatial resolution dependent on number of segments.	It has not been tested in a stack yet.	Ghosh et al. [162]
Current collector embedded in polymeric flow field	Flow field easily machined. Multiple geometries of flow field can be studied.	Matching thermal expansion of material is required. Complex manufacturing.	Bender et al. [166] Hakenjos et al. [170]
Printed circuit board (PCB)	Easy to mass produce. Well-known technique	May increase contact resistance. It is not a complete <i>in situ</i> measurement	Sun et al. [175]
Theoretical approaches	Current can be determined by measuring another parameter. Good spatial resolution.	Based in adiabatic assumptions.	Freunberger et al. [176]
Insertion of commercial sensor	Off the shell application	Highly intrusive.	Nishikawa et al. [157]

3.4.2 Voltage sensors

3.4.2.1 Commercial applications

The electric potential between electrodes in a single cell is one of the parameters that can be used to monitor the PEMFC operation. Changes in system-level operating parameters, such as humidity and temperature, will often be reflected in cell voltage changes [177].

In commercial applications; however, cells are usually stacked to increase the current and/or voltage supplied. Depending on conditions such as: catalyst homogeneity, current density distribution, poisoning, and other factors, each cell in the stack may exhibit a unique voltage and rate of degradation. For this reason, controls based on measurement of the system-level parameters only cannot ensure optimal operation of a stack. Thus, the measurement of the voltage across individual cells or small groups of cells can be an important aspect of fuel cell operation.

In 2005 Ballard Power Systems, Inc. was granted with a patent for a system based on optical isolators that monitored the voltage in a fuel cell stack. Whenever the voltage of any of the cells drops under a certain threshold level, a transistor based circuit produced a signal indicating this undesirable condition [178].

General Motors was granted in 2010 with a patent to measure the voltage in a PEMFC stack [179]. The system was based on a surface mounted device such as a light emitting diode (LED) for each single cell. The intensity of each LED was an indicator of the voltage of the particular cell.

3.4.2.2 Research applications

The measurement of the *in situ* voltage in PEMFCs has been also used as an evaluation and diagnostic method in fuel cell research.

Han et al. [180] embedded a 50 μm diameter gold wire, which served as a potential probe in the Nafion[®] electrolyte membrane. The voltage measurements were performed between the gold wire and the anode and cathode back plates. This approach was used to measure the effect of the CO poisoning on the PEMFC voltage.

Herrera et al. [181] performed a similar diagnostic technique with a less invasive approach. In this approach, Pt wires were placed through the gaskets into the fuel inlet and outlet ports. The voltage measured was not directly the one produced by the fuel cell but just between these two points. It however, allowed them to diagnose the performance under flooding, membrane dehydration, poisoning, and low reactant supply.

3.4.3 Electrical resistance

Since the ohmic losses are a function of the resistivity of the elements in the fuel cell, as well as of the contact resistance between them, some authors have focused on techniques that enable measurement of resistivity. As in many of the presented parameters, resistivity exhibits interdependence with other parameters. In the electrolytic membrane, for example, the resistivity is dependent on parameters such as temperature and membrane hydration [182].

3.4.3.1 Measurement of resistivity/resistance

There are several methods to measure the resistance of MEA components. These include: DC contact Kelvin probe (also known as 4-point probe), the AC resistance method, and the current interruption technique. These techniques impose changes in the electrical conditions of the cell that are evaluated by measuring the current and/or voltage resulting from these alterations [183].

The 4-point probe consists of two probes measuring the current while the voltage is measured by another pair of probes. This method is suitable for low resistivity measurements and can be applied when the geometry of the fuel cell allows insertion of the probes [182, 184].

In the AC resistance method an AC signal of a high frequency (~ 1 kHz) is applied on the DC voltage from the cell and the magnitude of the impedance at that frequency is measured. At high frequencies the electrochemical capacitances of the components will reduce to zero and the measurement is purely ohmic. Since the resistance is not directly proportional to the output voltage signal, it is necessary to determine simultaneous phase and amplitude of this output signal [2, 183].

The current interruption technique is based on the faster decay rate of ohmic losses relative to the decay rate of electrochemical overpotentials when the current is interrupted. The ideal shape of voltage response is shown in Figure 3-14. Here, the fuel cell is operated at a fixed current until t_0 , where the current interruption causes the ohmic losses to vanish

immediately, and the electrochemical overpotentials start to decay and the cell voltage trends asymptotically toward the open-cell voltage [185].

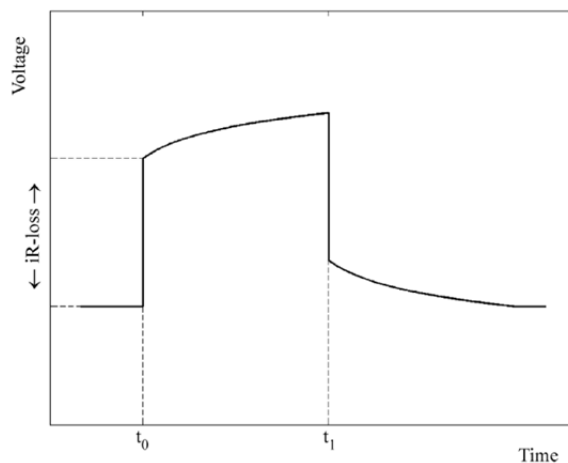


Figure 3-14: Ideal voltage transient in a PEMFC after current interruption at t_0 (Republished with permission from Elsevier S.A. from Ref. [185]; permission conveyed through Copyright Clearance Center, Inc.)

This technique can also be applied without interruptions in the stack or cell current by superimposing an auxiliary pulsed current on the cell through an external circuit. This approach was applied to perform the *in situ* measurement of MEA resistance by Buchi et al. [182], and Mennola et al. [185].

Stumper et al. [186] using a similar technique, isolated the cathode compartment by closing both inlet and outlet supplies, while H_2 was still fed in the anode and the load was switched on. The immediate reaction was a drop in the voltage from the open cell voltage. As time evolved the confined oxygen was depleted, leading to a voltage drop. This experiment was performed at different current densities, with the initial voltage dropping at different values. From these voltages and current densities a transient polarization curve was plotted and extrapolated to obtain the values of the internal resistance [187].

3.4.3.2 Measurement of the contact resistance

Some authors have estimated contact electrical resistance and its dependence on the clamping force using numerical models and simulations based on the method of the finite elements [188-191]. Other authors have performed *ex situ* measurements of contact

resistance [192-195]. As these approaches were not *in situ* measurements, they will not be discussed in detail in this review.

In situ determination of the contact resistance in PEMFCs has been performed exclusively by measuring voltage drop using specialty low resistance probes made of noble metals.

Makkus et al. [196] placed a pair of gold wires, one at each side of the MEA. By measuring the voltage drop against each back plate during the fuel cell operation allowed them to determine the contact resistance and its relationship with the clamping pressure.

Ihonen et al. [197] remarked that the results in [196] included also the force required to compress the seals, and therefore, were not very accurate. In their experimental setup they used a PEMFC in which they placed a Pt foil strip (20 $\mu\text{m} \times 2 \text{ mm}$) in contact with the GDL. The contact pressure was controlled through a spring screw with a known spring constant. The contact resistance as a function of the clamping pressure was determined within $\pm 1 \text{ m}\Omega \text{ cm}^2$.

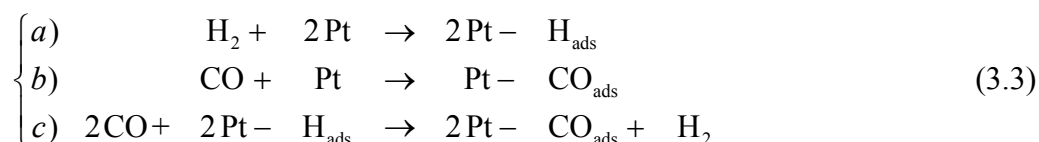
3.5 Contaminants and other stressors in PEMFCs

In situ measurements have also been made of harmful chemical substances that are a potential threat to the lifetime and durability. Some compounds (e.g. carbon monoxide, hydrogen sulphide, and ammonia) are known to cause poisoning of the catalyst layer by reducing the amount of platinum (Pt) available to perform the reaction, which leads to reduced performance [5]. Other compounds (e.g. hydrogen peroxide and reactive oxygen species) can cause the degradation of the electrolytic membrane and reduce the lifetime of PEMFCs.

Substances that act as contaminants can find a way to enter into the system through the fuel or the oxidant, particularly if the fuel is derived from reformed hydrocarbons and/or the oxidant is atmospheric air. In addition, materials from the sealing systems, or trace metals from electrical contacts can also cause degradation to the cell.

3.5.1 Carbon monoxide (CO) detectors for H₂ gaseous fuel

For the case of H₂-based PEMFC, the presence of carbon monoxide (CO) is mainly due to the use of reformed hydrocarbons. A typical composition of dry gases after the reforming process can be: 40% H₂, 43% N₂, 17% CO₂, and CO traces [198]. Poisoning of PEMFCs with CO is by far the most extensively studied and well documented of all the contaminants [5]. CO binds to Pt sites in the catalyst layers reducing availability of these surfaces to perform H₂ adsorption. In this way, the hydrogen oxidation reaction (HOR) reduces its effectiveness. CO poisoning follows the reactions shown below:



In reaction (3.3)a) the adsorption of H₂ in the catalyst layer in the HOR, requires two adjacent locations of Pt. Conversely, reaction (3.3)b), which is the adsorption of CO onto the Pt surface, only requires one Pt location, being a faster reaction. In addition, as reaction (3.3)c) shows, CO has the ability to remove the adsorbed H₂ from the Pt surface and replace its position.

Several detection approaches for CO have been developed. These approaches can be categorized into two groups: (1) systems in which CO is chemically adsorbed onto a material's surface altering its electrical properties, and (2) systems that use a small electrochemical device whose response is monitored to determine the CO presence.

3.5.1.1 CO detection system using chemical adsorption

The operation of these sensors is based on changes in the resistance that some materials exhibit when CO is adsorbed onto their surface. One approach uses semiconductor oxides such as SnO₂, which exhibits changes in resistivity. However, these devices require O₂ to oxidate CO into CO₂ [199]. As there is no O₂ into the fuel gases, this technique is not useful in the anode side. Instead, Holt et al. [199] used a CuCl based sensor, made by

depositing a film onto an interdigitated structure of gold electrodes. The sensor was able to detect a CO concentration of 5,000 ppm within a range of 50 to 60 °C. However, it also showed cross sensitivity to water and loss of response above 75 °C.

Pijolat et al. [200] developed a sensor based on Samarium doped Ceria (SDC) that showed response to CO traces to as low as 50 ppm, but that saturated above 400 ppm. This device however, suffered from reduced performance when condensation occurs.

3.5.1.2 CO detection systems based on small electrochemical cells

Another approach to determine CO concentration in PEMFCs, particularly in stacks, is to use a small single fuel cell or another type of electrochemical cell operating on the same feed gases as the main fuel cell and whose electrical parameters change in the presence of CO. This technique can be used by directly monitoring the voltage output on the small cell or using dedicated software that performs pattern recognition on the changes of the electrical signals occurring as consequence of known CO concentrations. The state-of-the-art presents studies of the effect of CO on these small-size cells rather than describe its implementation on a fuel cell stack.

Hashimoto et al. [201] tested a SDC solid oxide fuel cell with reformed gases at 300 °C. The current produced by this fuel cell dropped by 11% with respect to its baseline when the concentration level of CO rose by 50 ppm. Additional increments in the CO concentration did not cause further reductions in current.

Kirby et al. [202] reduced the catalyst load of a small PEMFC to 5-10 $\mu\text{g cm}^{-2}$ to reduce the response time in the CO detection. The device showed a drop in the generated current in less than 2 seconds after 50 ppm of CO was added to the fuel stream. A cycle of 0.5 seconds in clean air allowed the response to be recovered to the initial level.

Planje et al. [203] placed an electrochemical cell with Nafion[®] as an electrolyte. The electrodes are loaded with Pt. 1-10 $\mu\text{g cm}^{-2}$ and 1-10 mg cm^{-2} for anode and cathode, respectively. The difference in catalyst loading makes cathode side more sensitive towards CO than the anode. By cycling the voltage on this electrochemical device, the reactions on

each electrode change. The authors found that CO concentrations from 1 to 500 ppm modify the voltage response within 5 to 20 seconds. Another approach using an electrochemical device was presented by Mukundan et al. [204]. In this case, the low sensitivity toward CO is achieved covering one electrode with Pt-Ru. The response time of this device was around 2 minutes to 50 ppm CO.

Bhambare et al. [205] developed a CO sensor to be used in fuel cell stacks, whose operating principle is based on filtering and performing pattern recognition of the voltage and current generated by a small PEMFC. This process is performed by a statistical comparison with an internal database of the current response when the small PEMFC was operating at different concentration levels of CO. The system is able to detect CO concentrations in a range of 0-100 ppm, with a response time within a few minutes.

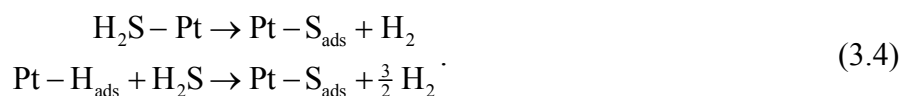
3.5.2 Other contaminants and stressors

Carbon monoxide (CO) is not the only contaminant that affects fuel cell performance. Other species such as sulfurs and halogens, as well as reactive oxygen species (ROS) such as hydrogen peroxide (H₂O₂), hydroxyl (HO•) and hydroperoxyl (HOO•) radicals may cause irreversible damage [1, 11, 22, 206].

To date, the research has focused more on reporting the effects of contaminants in the performance of PEMFCs, and comprehensive reviews are available in the literature [5, 21], rather than in developing *in situ* sensors to determine contaminants presence in these systems.

3.5.2.1 Hydrogen sulphide (H₂S)

H₂S is a more severe contaminant than CO [5] causing voltage drops at concentrations as low as 0.1 ppm. The poisoning effect of H₂S can be explained through the following reactions [207]:



As occurs with CO poisoning, H₂S has a strong affinity with Pt and causes desorption of the previously adsorbed hydrogen from the Pt sites

Pijolat et al. [200] showed that their SDC-based sensor is responsive to H₂S. This device is the only one reported in the literature that is intended for being used in PEMFCs. This system is responsive to H₂S concentrations as low as 0.5 ppm and proportional until reach 1.5 ppm.

3.5.2.2 Ammonia (NH₃)

Ammonia is susceptible to interactions with membrane protons, causing a decrease in the membrane conductivity. After diffusing into the membrane, ammonia binds to the protons producing an ammonium ion (NH₄⁺). Several authors reported the effect of the presence of ammonia in PEMFCs but no sensors have been reported for detecting this contaminant in these systems [208-211].

3.5.2.3 Radicals, trace metals, and hydrogen peroxide

As presented in Section 1.3, the degradation mechanisms of Nafion[®] are believed to be caused by a variety of chemical substances. In PEMFCs the perfluorinated membrane requires hydration to enable proton mobility. However, this water also provides a path for molecular hydrogen and oxygen to crossover the membrane, bringing together the ingredients for the formation of radicals [11].

Radicals attack the main backbone or decouple the side chains from the molecular structure of Nafion[®] causing the loss of the mechanical integrity, and the reduction in the proton conductivity required for the proper operation of PEMFCs [21, 212].

Radicals hydrogen(H•), hydroxyl(HO•), and hydroperoxy(HO₂•), can be formed as a result of gas crossover or hydrogen peroxide (H₂O₂) decomposition, after its formation in the membrane by the mechanisms described in Sections 1.3.1 and 1.3.2. Crossover of H₂ through the membrane is more likely to occur than crossover of O₂ due to its smaller molecular size. Once this happens, H₂ can be catalyzed onto the cathode side of the MEA,

where more Pt sites are available, and form hydrogen radicals ($\text{H}\cdot$). The hydrogen radicals can form hydroperoxy radicals ($\text{HO}_2\cdot$) when they come into contact with the available O_2 in the cathode. From here, a first path for the formation of hydrogen peroxide (H_2O_2) is paved when ($\text{HO}_2\cdot$) combines with an additional ($\text{H}\cdot$). Hydrogen peroxide also decomposes in the presence of metal cations to form new radicals, making worse the situation for the durability of the membrane [11, 20].

A second path that leads to the formation of hydrogen peroxide in PEMFCs is the oxygen reduction reaction with a 2-electron mechanism [10]. This path can occur when O_2 diffuses into the membrane and reaches a lower level of potential.

In spite of a large body of research on degradation mechanisms, little research has been done to develop *in situ* sensors to detect the presence of H_2O_2 in operating PEMFCs. To date, one electrochemical approach, and two optical fiber *ex situ* methods (one of which results from the work described in this dissertation), are the only studies found in the literature that deal with H_2O_2 sensors for PEMFCs.

In the electrochemical approach of Liu and Zuckerbrod [23], a pair of Pt wires acts as electrodes inside an MEA to perform a cyclic voltammetry test. The obtained voltammogram revealed the characteristic peaks of H_2O_2 . This was the first reported experimental detection of H_2O_2 *in situ* in an operating PEMFC.

From the optical fiber perspective, two operating principles have been proposed to perform the detection of H_2O_2 in PEMFCs, yet none of these has been tested *in situ*. The first approach is based on changes in absorbance that a compound of Titanium(IV), suspended in Nafion[®], has in the presence of H_2O_2 . Tao et al. [136] coated a U-shaped plastic optical fiber to perform the measurement of H_2O_2 in solution at concentrations from 8.8×10^{-6} to 88×10^{-6} mole L^{-1} . With the same type of coating and configuration, Hu and Tao [213] were able to perform the detection of H_2O_2 in solution at concentrations ranging 0.88×10^{-6} up to 1.8×10^{-3} mole L^{-1} .

The second optical fiber approach reported in the literature use the Prussian blue/Prussian white to determine the presence of H_2O_2 was by Khorami et al. [214], where Prussian blue was chemically synthesized on the tip of an optical fiber. The range of detection of H_2O_2 of this sensor ranged from 10 to 400 $\mu\text{mole L}^{-1}$.

3.6 Remarks

This review presents the state-of-the-art of the *in situ* techniques reported in the literature to measure the parameters that can describe the performance of PEMFCs. The importance of measuring parameters such as temperature, relative humidity, current, voltage, and detecting the presence of contaminants lies in obtaining the information that assure an optimal performance and protect the fuel cell from inadequate operating conditions.

The techniques for measuring temperature *in situ* in PEMFCs showed a wide variety of alternatives that can be applied depending on the specific purposes of the application. Thermocouples are one of the standard techniques for measuring temperature in scientific applications; they are widely available. However, their use in PEMFCs has been reported to be complex, especially during the installation stage. Also, they can be susceptible to electromagnetic interference, which may reduce their accuracy. Resistive temperature devices (RTDs), due to their small size, have the best spatial resolution within the techniques reported, and can be fabricated using mass production processes. However, RTDs may suffer similar drawbacks to those experienced by thermocouples. Within the optical fiber approaches, FBGs are a technique with great potential, not just because of the immunity of the optical fiber to the environmental conditions inside a PEMFC, but also because they can be multiplexed on the same fiber. The insertion of the optical fiber in the PEMFC, however, presents technical challenges. Finally, regardless of its low resolution in determining the temperature in a PEMFC and its difficult implementation, laser absorption spectroscopy has the unique advantage of being able to perform the detection of species in gaseous form; which still makes it interesting from a research perspective.

Capacitive sensors have been successfully used for *in situ* measurement of RH in PEMFCs, and indirectly determine the water content of the membrane. These sensors, however, have similar drawbacks to those experienced by thermocouples, including the susceptibility to electromagnetic interference. In a similar way, approaches using optical fibers with FBGs coated to determine RH present the same issues as its counterpart in the temperature determination, such as the fragility of the optical fiber material and difficult insertion in the PEMFC.

Techniques for the measurement of the current distribution in PEMFCs include resistor networks, printed circuit boards, and segmented collector plates. Each of these has advantages and disadvantages, as summarized in Table 3-3. These devices have been almost exclusively used in research rather than commercial applications.

In situ measurement of voltage has been identified as one of the simplest methods to monitor the performance in PEMFCs. The cell voltage changes faster than other operating parameters such as temperature or relative humidity when the operating conditions drive away from the optimal. There are numerous techniques that allow the voltage of individual cells to be monitored in a PEMFC stack.

Electrical resistance sensors aim to minimize ohmic losses. Their implementation usually requires complex techniques and equipment, which keeps them away from being used in commercial devices. These systems are mostly used as a diagnostic and optimization tool in research.

Finally, the literature in sensors for *in situ* detection of contaminants is dominated by devices to prevent CO poisoning. These systems are usually electrochemical devices which voltage or current responses are affected by the presence of CO. The use in PEMFCs of sensors for other gaseous species is almost irrelevant.

Hydrogen peroxide, which may form as part of the operation of the PEMFC or as a result of the gases crossover, has been detected *in situ* by electrochemical techniques. This method of detection, however, can be affected by the electromagnetic noise inside a PEMFC. In addition, the use of Pt electrodes may catalyze the production of H₂O₂ inside

the PEMFC. Therefore, it would not be possible to determine if the presence of this contaminant was due to the production in the cell operation or self-induced by the sensing element. The approaches with optical fibers still have not been proven under *in situ* conditions but they are promising due to their good performance in *ex situ* conditions.

Chapter 4: Detection of hydrogen peroxide using an optical fiber-based sensing probe

(Sensors and Actuators B: Chemical, volume **185**, 2013, 166–173)

Reproduced with permission from Elsevier.

Preamble

The first step in the development of the *in situ* optical fiber sensors for the detection of hydrogen peroxide is the fabrication and testing of a sensing prototype using the reagents required for the sensing mechanism, as well as ensuring the proper immobilization of the active films onto the surface of the tip of an optical fiber.

This chapter presents the techniques and tests that validate the proof of concept of the sensing device. A model is also presented that for the first time represents the physical principles on which the detection technique relies.

The body of this Chapter was published in the journal *Sensors and Actuators B: Chemical*.

Abstract

A sensing probe for hydrogen peroxide (H_2O_2) in solution at low concentrations has been developed by deposition of Prussian blue dye in a multi-layer structure of polyelectrolytes onto the tip of a multi-mode optical fiber. The sensing mechanism of this optrode (optical electrode) relies on the oxidation of Prussian white (reduced form of Prussian blue) in the presence of hydrogen peroxide. The sensing capabilities of the probe can be recovered by *ex situ* reduction of Prussian blue to Prussian white using ascorbic acid. A first set of experiments yielded a linear-log relationship between the peak intensity of the reflected light and the concentration of hydrogen peroxide. The intensity of the light, relative to the intensity at immersion, showed an inverse exponential dependency on the time required to reach the saturation for each H_2O_2 solution tested. Subsequent experiments in which the sensing probe was exposed to H_2O_2 solutions with different concentrations, showed that only the time-dependent behavior of the intensity of the light remained.

Furthermore, the response time for the intensity to reach 63% of its peak value was found to be linearly dependent on the concentration of the H_2O_2 in a log–log scale. Reproducible results were for H_2O_2 concentrations ranging from $10 \mu\text{mol L}^{-1}$ up to the maximum concentration tested of 1 mmol L^{-1} . This range of concentrations makes this sensing probe suitable for the remote detection of H_2O_2 as a by-product of biological reactions and electrochemical reactions in polymer electrolyte membrane fuel cells.

Keywords: Optical fiber sensor; Optrode; Hydrogen peroxide; Prussian blue; Membrane degradation; Electrostatic self-assembly of polyelectrolytes; Fuel cell; PEMFC

4.1 Introduction

Hydrogen peroxide (H_2O_2) is a highly reactive oxidant that plays an essential role in many chemical, industrial, medical, environmental, and biological processes. It is used as a disinfectant due to its antimicrobial properties, and in bleaching of textiles, paper pulp, hair, and teeth [215, 216].

H_2O_2 also plays an important role in biological and environmental processes. In biological processes, H_2O_2 is often the intermediate product of enzymatic reactions and its monitoring allows the control of bioreactions [30, 216, 217]. H_2O_2 is also one of the by-products of cellular processes such as phagocytosis [43], which are used in medical diagnosis of pulmonary illnesses including asthma [218]. Finally, H_2O_2 is also found in rain water [34], causing acidity, which can alter the equilibrium of an ecosystem [219].

H_2O_2 can be produced as part of the electrochemical reactions in a Polymer Electrolyte Membrane Fuel Cell (PEMFC) [220]. Localized measurements of H_2O_2 concentrations in PEMFCs have not been possible to date, but it has been detected in the exhaust gases [12], in the drain water from the cathode [6], and by *in-situ* electrochemical techniques in the ionomeric membrane [23]. The role played by H_2O_2 in PEMFCs has been extensively investigated since it is believed to be a precursor of hydroxyl ($\text{HO}\cdot$) and hydroperoxyl ($\text{HO}_2\cdot$) radicals, which have been linked to the accelerated chemical degradation of Nafion[®] –the proton conductive membrane used in many PEMFCs [7, 13, 20, 22, 221-226].

Conventional techniques for detection of H_2O_2 include titration, colorimetry, and gasometry [27, 216, 227]. Although these methods are used in many applications, they are not well suited to the detection of small concentrations of H_2O_2 such as those occurring in a PEMFC. The rate of production of H_2O_2 in a PEMFC has been estimated to reach values of up to $0.7 \times 10^{-6} \text{ mol cm}^{-2} \text{ s}^{-1}$ on the cathode side. This rate of production is highly dependent on operating conditions such as relative humidity and temperature [18].

Electrochemical techniques are well suited determining small concentrations of H_2O_2 [29], but can suffer interference from other reactive oxygen species [77, 228]. Furthermore, these techniques are susceptible to electromagnetic interference (EMI) in environments such as a PEMFC.

Spectroscopic techniques including chemiluminescence [56, 229, 230], fluorescence [43, 44, 46, 231, 232], and absorptive techniques [29, 33-40] can also be used for detection of H_2O_2 at low concentrations. These techniques have been integrated with optical fibers, making possible the development of sensors with high sensitivity and many of the advantages of optical fibers, such as small size, high selectivity, and immunity to EMI [29, 38-40, 56, 62, 63, 213, 233]. In addition, some absorptive-based approaches involve the use of low-cost reagents, which because of their absorbance in the visible and near infrared region of the light spectrum allows the use of readily available light sources and detectors [38, 40].

The use of optical fiber sensors has been successfully demonstrated for the measurement of temperature and relative humidity in PEMFCs using fluorescent and phosphorescent methods [135, 136], and fiber Bragg gratings [138]. In the present work, an optical fiber sensing probe for H_2O_2 was developed. The reagents employed in this absorptive-based technique, as well as the proposed technique of immobilization are compatible for use in PEMFCs.

4.1.1 Sensing mechanism

The mechanism of detection of H_2O_2 relies on the metallic hexacyanoferrate compound Prussian blue (PB). PB ($\text{Fe}_4(\text{Fe}(\text{CN})_6)_3$) has a cubic crystalline structure in which C atoms of cyanide ions surround Fe(II) ions while the N atoms surround Fe(III) ions [71]. PB can be reduced electrically or chemically to Prussian white (PW), by applying a voltage of 0.2 V vs. SCE [234] or in the presence of strong reducing agents such as ascorbic acid [85]. In a similar way, the chemical oxidation of PW can be achieved by exposing it to H_2O_2 which makes it revert back to the PB form.

The spectrum of absorption of PB spans part of the visible and near infrared and has its maximum at 720 nm. Conversely, the absorbance of PW is almost negligible and appears transparent to the visible light [71, 104, 235]. Thus, the oxidation of PW to PB increases absorbance the 400–900 nm range. Moreover, the intensity of the absorbance reaches a maximum at low pH and decreases with increasing pH [87].

The absorbance properties of the PB/PW system have been used in optical biosensors [87, 104, 235]. In this work the scheme of detection of H_2O_2 follows the one illustrated in Figure 4-1.

4.1.2 Polyelectrolyte multi-layered films

Nano-sized multi-layer films fabricated by the electrostatic self-assembly (ESA) of polyelectrolytes, in a layer-by-layer (LbL) deposition technique, have been the subject of a number of studies because of their simplicity, low-cost, and flexibility in applying multiple substrates regardless of the material and geometry [95, 99, 236, 237]. LbL ESA deposition is based on the immersion of a substrate whose surface is electrostatically charged into a solution of a polyelectrolyte with the opposite electric charge. Due to the effect of electrostatic forces, the polyelectrolyte is adsorbed onto the surface until the charge is neutralized, creating a layer where the outermost surface has the opposite charge. The excess non-adsorbed material is rinsed away using a proper solvent, which is followed by the immersion into a solution with a counter polyelectrolyte. This procedure is repeated to fabricate a multi-layered structure.

LbL ESA deposition allows a variety of materials to be immobilized within the multi-layered structure. By immobilizing gold colloids, dyes and enzymes, and fluorophores, the LbL ESA deposition of polyelectrolytes has allowed the fabrication of biosensors and filters among others devices [29, 90, 111, 238]. By modifying the template of deposition it is also possible to fabricate microcapsules that allow drugs to be released in a controlled manner [98]. It is also possible to tailor the permeability properties of the multi-layers. This is achievable by modifying parameters during the deposition of the layers such as concentration, pH and ionic strength of the precursor solutions, and also by applying thermal treatments and capping layers at different pH to the multi-layer structure [98]. In this manner it is possible to alter features such as the thickness of each layer (ranging in values from 5 to 80 Å), the smoothness and porosity of the surface, and the interaction between opposite charges creating a looser structure [38, 99, 239]. An approach to H₂O₂ detection using an optical fiber probe, whose distal end was coated with an LbL ESA structure of polyelectrolytes immobilizing PB, has been previously presented by Del Villar et al. [38, 40] and served as a starting point for the developments presented here. Del Villar et al. reported a time-dependent relationship between the concentration of H₂O₂ solutions and the change in intensity of the reflected light due to the oxidation of PW. The ratio between the difference of two intensities, 10 and 90% of the maximum value, and the elapsed time within these intensities was found to increase with H₂O₂ concentration.

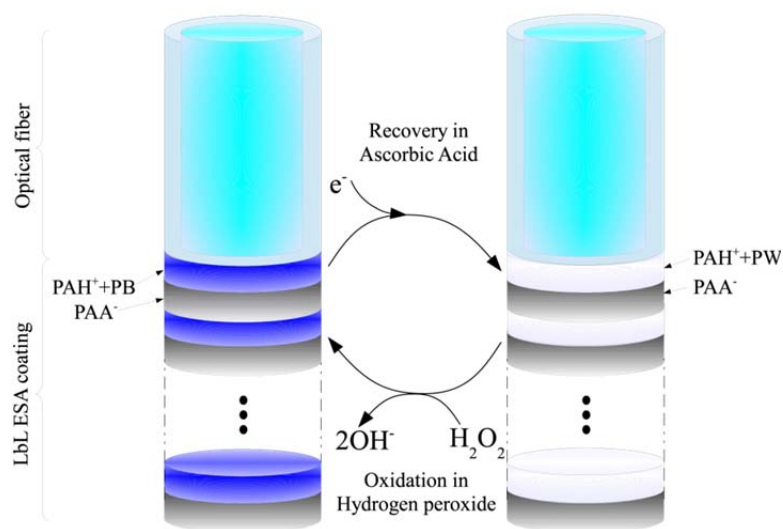


Figure 4-1: Scheme of hydrogen peroxide sensing using the Prussian blue/Prussian white system in a layer-by-layer electrostatic self-assembled structure coating the tip of the optical fiber probe.

While this linearization of the response fits the experimental data and allows the concentration to be quantified, it does not correlate with the phenomenology of the change in absorbance. To build on this initial proof of concept, measurement and response as function of concentration need to be established, and the impact and possible dependence on the intensity of the light source investigated.

The current work presents an optical fiber based sensing probe for H₂O₂ immobilizing PB in a multi-layered structure of polyelectrolytes by LbL ESA deposition. Multiple experiments were performed to determine the response of the probe as a function of intensity of the reflected light and H₂O₂ concentration, as well as to establish a better phenomenological understanding of its operation. The role of the ESA multi-layer structure immobilizing the PB/PW reagent in limiting the underlying transport processes is also clarified.

4.2 Materials and methods

4.2.1 Materials

Poly(allilamine hydrochloride) (PAH^+ , $M_w \approx 15,000$, product number 283215), Poly(acrylic acid) (PAA^- , $M_w \approx 100,000$, product number 523925), and Prussian blue soluble (Product number 03899) from Sigma-Aldrich (Oakville, ON, Canada), were used as the polycation, polyanion, and sensing dye, respectively, in the LbL ESA process.

L-ascorbic acid from Aldrich, (catalog number 25,556-4), was used as the reducing agent for the Prussian blue to Prussian white reaction. Glacial acetic acid from Anachemia and Sodium acetate trihydrate from ACP Chemicals were used to prepare an acetate buffer solution (ABS) at pH 4.0 in which the H_2O_2 solutions and ascorbic acid were prepared. The reducing solution was prepared in ABS with 0.04 mol L^{-1} of *L*-ascorbic acid. H_2O_2 (30 wt.%) from ACP Chemicals was used to prepare the oxidizing solutions at different concentrations in ABS. Sodium hydroxyde (NaOH) and Hydrochloric acid (HCl) at concentrations of 0.1 mol L^{-1} were used to adjust the pH of the solutions to the desired values. Sulfuric acid (H_2SO_4) (EMD Chemicals, Gibbstown, NJ) with a concentration (>98%) was used for preparing the initial cleansing solution.

All chemicals were used as received with no further purification. The water used in the experiments was purified with a four-cartridge system of purification (Super-Q Plus, Millipore, Billerica, MA) and had a resistivity of $18.2 \text{ M}\Omega \text{ cm}$.

The optical fiber was a multi-mode optical fiber SFS105/125Y from Thorlabs (Newton, NJ), with core and cladding diameters of $105 \mu\text{m}$ and $125 \mu\text{m}$, respectively.

4.2.2 Sensing film deposition

LbL ESA of polyelectrolytes using the optical fiber as a substrate was employed. The optical fiber was cleaved and thoroughly cleansed by immersion in a 3:1 solution of H_2SO_4 (>98%) and H_2O_2 (30 wt%) for 30 minutes. This surface treatment also hydroxylates the tip of the fiber conferring it a negative charge.

PAH⁺ and PB were mixed in solution with concentrations of 2.0 and 2.5 mg mL⁻¹, respectively. PAA⁻ was also prepared in solution with a concentration of 2.0 mg mL⁻¹. The pH values of these polyelectrolyte solutions were adjusted to 4.0. The negatively charged tip of the optical fiber was immersed in the {PAH⁺+PB} solution until the intensity reached the saturation. Intensity was determined by measuring the reflected light from the probe as described in Section 4.2.6. After this, the fiber was rinsed with distilled water to remove the non-adsorbed polyelectrolyte and immersed into the PAA⁻ solution until the signal of the reflected light reached saturation. The fiber was then rinsed again using distilled water. This process results in a bilayer of PAH⁺+PB and PAA⁻. After Del Villar et al. [39], 17 bilayers of PAH⁺+PB/PAA⁻ at pH 4.0 were deposited onto the tip of the optical fiber.

Two capping bilayers were adsorbed onto the surface of the structure by immersing it in solutions of PAH⁺ (without PB) and then PAA⁻ with the same concentrations as before. The pH of these capping solutions was adjusted to 5.5. This difference of pHs between the sensing structure and the capping films reduces the leaching of the dye [39, 98].

The prepared probe with the multi-layered structure was finally annealed for 2 h at 100 °C [99] and stored at room temperature and ambient humidity for a week before using it in the experiments.

4.2.3 Test solutions preparation

Test H₂O₂ solutions prepared in ABS with a pH of 4.0 ± 0.1 were used. The pH was the same as the one used in the LbL ESA to ensure that there were no morphological changes in the polyelectrolyte structure, which occur when this is subjected to a change in pH [100, 102].

L-ascorbic acid in solution was used as a reducing agent in all the performed tests. This solution was prepared at a concentration of 0.04 mol L⁻¹ using ABS as solvent and adjusting its pH to 4.0 ± 0.1.

4.2.4 Instrumentation

The absorbance measurements of the Prussian blue/Prussian white system were performed using the experimental setup illustrated in Figure 4-2. The white light lamp (LS-1, OceanOptics, Dunedin, FL) was connected to the arm 1 of a bifurcated optical fiber (BIF200-UV-Vis, OceanOptics), which carries the light to the common arm. The end of the common arm was connected to the fiber probe with the sensing structure that contacts the test solutions. Light was reflected from the sensing structure and guided back through the common arm and the arm 2 of the bifurcated fiber to an optical fiber spectrometer (USB2000, OceanOptics), which measured the intensity of the light in a wavelength range of 370 to 1048 nm.

The pH measurements of all the prepared solutions were performed using a digital pH-meter (AR25 accumet[®], Fisher Scientific, Hampton, NH) using an Ag|AgCl electrode.

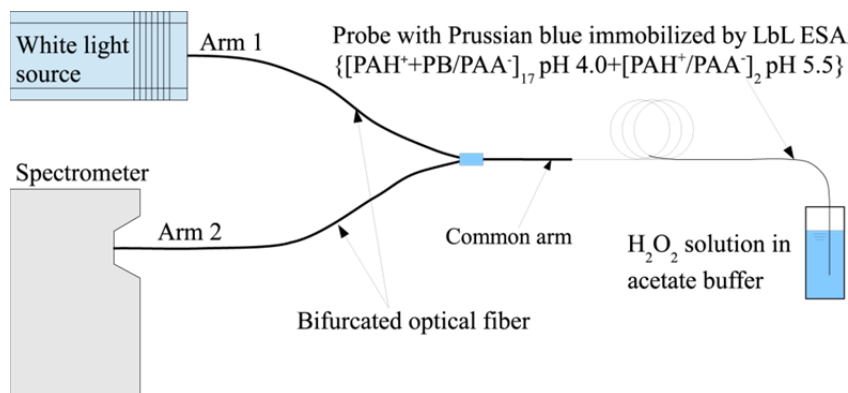


Figure 4-2: Experimental setup to measure the reflected light from the Prussian blue coated tip.

4.2.5 Test procedures

Each test was conducted by alternating steps of recovery and oxidation of the PB/PW sensing coating in ascorbic acid and H₂O₂ solutions, respectively. For the recovery steps, glass vials were filled with 3.0 mL of fresh ascorbic acid solution. The optical fiber sensing probe was mounted in a vertical position above the vial. The glass vial was then raised using a lab scissor jack to ensure a consistent depth of immersion of the fiber tip. For the oxidation steps, the lab scissor jack was lowered to remove the fiber from the immersion in the ascorbic acid solution. Immediately after, a glass vial filled with 3.0 mL of fresh ABS

and the proper aliquot of diluted H_2O_2 was placed onto the jack and raised up to immerse the fiber to the same depth.

The *first experiment* consisted of subjecting the fiber with a virgin coating to tests in which the H_2O_2 concentration in solutions for the oxidation stages was steadily increased from 2 up to $1000 \mu\text{mol L}^{-1}$. The first step consisted of the initial reduction of the fresh multi-layer coating in a solution of ascorbic acid, which caused the reduction of PB to PW. When the signal observed by the trend light was close to saturation, the probe was immersed in ABS without H_2O_2 for 15 minutes. The fiber was then subjected to oxidation-reduction tests with 15-minute intervals for each reaction step.

Each fiber was subjected to the first test described above prior to subsequent experiments comprising: (a) increasing then decreasing concentration tests from $2 \mu\text{mol L}^{-1}$ to $500 \mu\text{mol L}^{-1}$ and then to $20 \mu\text{mol L}^{-1}$, hereinafter called *increasing-decreasing experiment*; (b) tests decreasing the H_2O_2 concentration from 1mmol L^{-1} to $2 \mu\text{mol L}^{-1}$ and then increasing it back, hereinafter called *decreasing-increasing experiment*; and (c) tests where the sensing probe was immersed in fixed concentration solutions four to five times, with H_2O_2 concentrations of: 1000, 500, 200, 100, 50, 20, and $10 \mu\text{mol L}^{-1}$.

For all the experiments performed after the first experiment the completion of each reduction or oxidation reaction step was determined by visually monitoring the trend line of intensity until it plateaued. At this point, the fiber was removed from the ascorbic acid solution and placed into the H_2O_2 solution, or vice versa.

All three different sensing probes fabricated and used in the experiments were subjected to similar first experiments with steady increase of concentration. However, not all of them were subjected to the same subsequent experiments. Nonetheless, the overall behavior remains consistent for all fiber probes.

4.2.6 Measurement of the changes in absorbance

Measurements of the absorbance from the sensing probe were performed by sampling the reflected spectrum from the distal end of the fiber using the software SpectraSuite

(OceanOptics, Dunedin, FL). The spectrum was sampled at a frequency rate of 1 Hz. Changes in intensity of the signal as a result of the interaction of the immobilized PB/PW with the oxidizing or reducing solutions were assessed based on *total intensity*. Total intensity was calculated as the integral of intensity over the full range of the spectrometer (i.e. 370 to 1048 nm). Results are presented as this total intensity versus time. The computational suite used also allowed to reckon a trend line of the total intensity. This trend line allowed the saturation of the processes of adsorbance of layers, detection of H₂O₂, and reduction in ascorbic acid to be determined.

4.2.7 Response time evaluation

The time dependent response was fitted with an inverse exponential curve of the form:

$$I(t) = I_0 + A \left[1 - \exp\left(-\frac{t}{\tau}\right) \right]$$

where: $I(t)$ is the intensity at the time t ; I_0 is the intensity level at the moment of immersion of the sensing probe in the H₂O₂ solutions; τ represents the time elapsed for the signal to reach 63% (i.e. $[1 - 1/e]$) of the intensity at saturation, I_{sat} , and is the parameter used to evaluate the time response of the sensing probe; and A ($\equiv I_{sat} - I_0$) is a constant that depends on the geometry of the sensing probe, the diffusion conditions through the multilayered structure, and the chemical reaction of oxidation of PW to PB. The time axis for each fit was set to zero at the moment of probe immersion in each H₂O₂ solution.

4.3 Results and discussion

Data analysis showed distinct behaviors between the first (conditioning) and second (operational) set of experiments. These are consequently discussed separately. The uncertainties in determining the two key parameters, concentration and response time, were estimated for the two extreme concentrations and the maximum uncertainties are $\pm 5.2\%$ for concentration and $\pm 17.8\%$ for the response time.

4.3.1 First experiment-conditioning stage

The time evolution intensity of the reflected light from the sensing probe during the first experiment is presented in Figure 4-3. As shown, the intensity of the reflected light following each immersion of the sensing probe in the H_2O_2 solutions, increases as PB is oxidized to PW. Furthermore, the maximum intensity in each successive test at a higher H_2O_2 concentration reached a higher value than in the previous test. The spikes in the figure are a consequence of the light collected from the surroundings when the fiber is removed from one vial and placed in the next one.

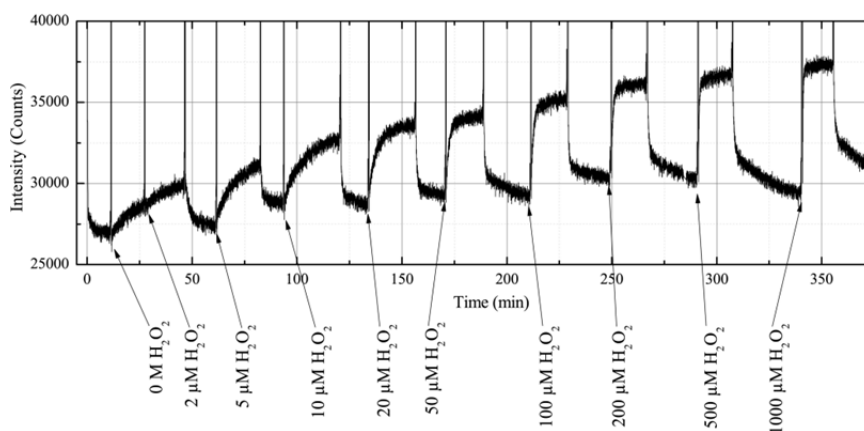


Figure 4-3: Response of the sensing probe during the first experiment to solutions with increasing concentration of H_2O_2 .

Performing the inverse-exponential fits described in Section 4.2.7 to the intensity response of each individual test allowed the determination of I_{sat} as a function of H_2O_2 concentration plotted in Figure 4-4 using linear and logarithmic scales. The reflected intensities at saturation are linearly related to the logarithm of the concentration of H_2O_2 .

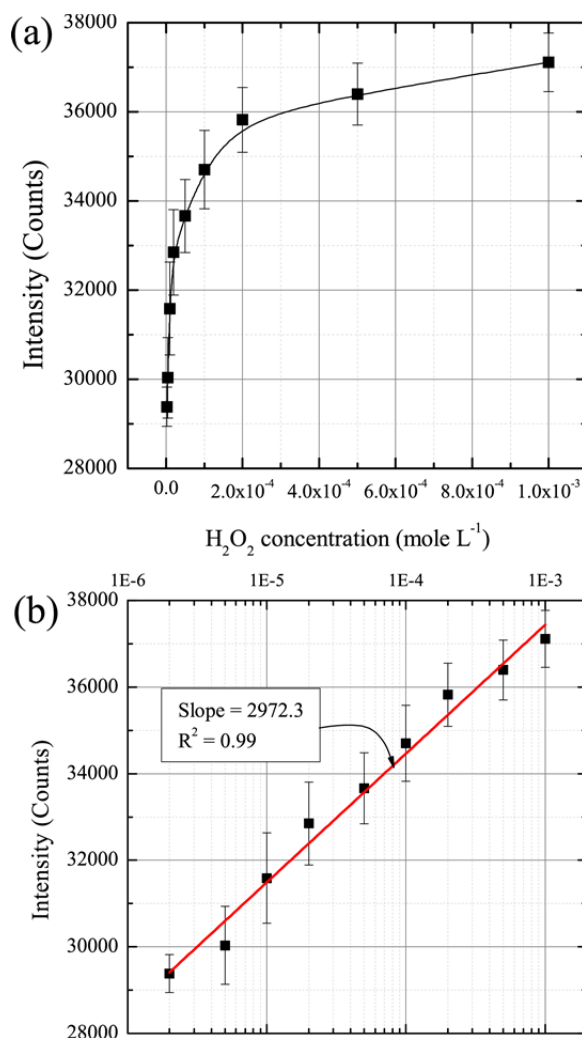


Figure 4-4: Intensity response to the increase in the concentration of H_2O_2 solutions; (a) linear scale, (b) logarithmic scale. This behavior was only observed in the first experiment, and could not be used for calibration or measurements purposes.

The response of the reflected intensity to the increase in the concentration of the tested solutions shows what can be considered as an initial stage or conditioning of the sensing probe. The increase in the concentration of H_2O_2 at every new immersion of the probe promotes what may be interpreted as an "activation" phase of the immobilized molecules. In this phase, oxidation can occur to a greater extent as the higher concentration of H_2O_2 in the bulk solution increases the rate of diffusion into the multi-layer coating, thus propitiating more immobilized molecules of PW to become PB. Since PW appears transparent to light in the visible range, less light is reflected from the tip of the fiber when

the molecules are in this state. The oxidation of the immobilized molecules towards the more opaque PB reduces the component of light transmitted through the multi-layer structure, and consequently increases the intensity of the reflected light from the multi-layer sensitive coating.

The process of diffusion happens as a result of the permeability of the polyelectrolyte layers that allow chemical species to migrate towards the immobilized PB/PW molecules when it is in a hydrated stage. Since the LbL ESA process of fabrication of the multi-layer sensing structure was performed using distilled water during the rinsing stage instead of a solvent with a higher ionic concentration, the multi-layer structure will exhibit a porous structure that allows H_2O_2 molecules to reach the immobilized PB/PW sites [98].

In addition, in both PB and PW the cyanide and iron ions form a cubic structure that acts as a porous network with a lattice of 5.1\AA , through which only small molecules ($\leq 3.2\text{\AA}$) can diffuse rapidly [71, 72]. H_2O_2 molecular dimensions are within this order of magnitude and reach the PB/PW sites with ease.

Furthermore, the PB/PW system has an enhanced response in acidic media where it exhibits a higher peak of absorbance [71], which makes it suitable for deployment in environments such as those in the PTFE membrane and the catalyst layers in a PEMFC. At this point, it should also be noted that the dielectric nature of the immobilizing layers would avoid electrons from the reactions in a fuel cell to cause the reduction of the PB/PW system. This reduction reaction only happens as a result of the chemical reaction with the ascorbic acid and it is insensitive to other chemical interferences as shown by Koncki et al. [235].

The inverse-exponential fit also indicates that the time for the reflected light to reach the saturation appears to also be correlated with the H_2O_2 concentration. This temporal dependence will be further discussed in Section 4.3.3.

The behavior exhibited during this first experiment was also seen in other fibers tested using a similar procedure to the one described in Section 4.2.5. This correspondence does not imply that this is the only valid method to perform the activation of the sensing probe

and different results could be obtained if the first experiment was performed in a distinct manner. However, this issue is not pursued any further here, as the approach used satisfied the objectives of this work.

4.3.2 Operational stage

This section presents the results of the sensing probe response in the subsequent experiments performed after the first experiment. The response of the reflected signal in the increasing-decreasing experiment is presented in Figure 4-5. The intensity after the immersion in the solutions of H_2O_2 rises as a consequence of the oxidation of PW to PW₂, and decreases when the fiber is placed back in the recovering solution of ascorbic acid that returns the PB to PW; in a similar manner to what happened in the first experiment. A first observation is that the intensity during the first recovery step does not diminish as much as in the other recovery steps. This is possibly due to the hydration of the layered structure since the fiber is dry in the initial immersion on each experiment. The second observation is that, unlike the first experiment, the intensity reached after immersion of the fiber in the H_2O_2 solutions remains essentially constant for all concentrations. The rising time of the reflected intensity remains nonetheless correlated to the H_2O_2 concentration for each test. This effect will also be discussed in Section 4.3.3.

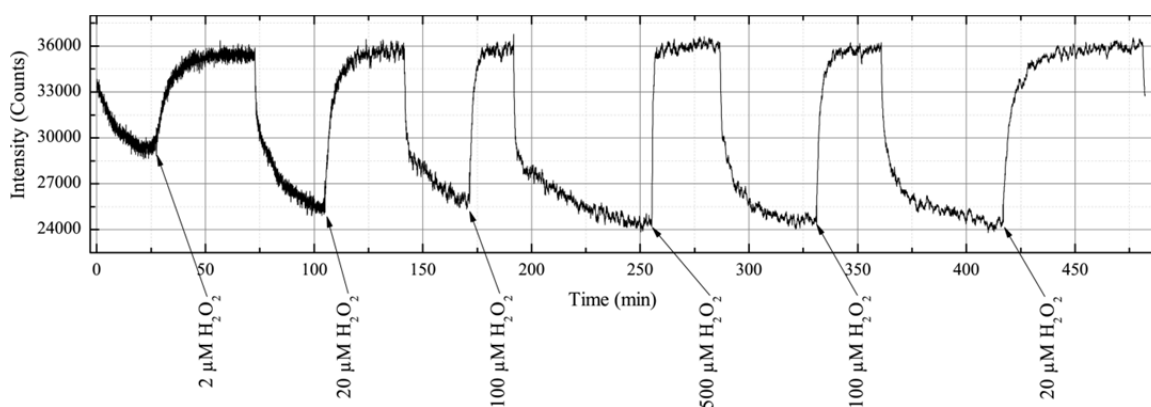


Figure 4-5: Response of the sensing probe to immersion in solutions with increasing and decreasing H_2O_2 concentration.

The response of the reflected signal for the decreasing-increasing experiment is shown in Figure 4-6. Once again, the response during the oxidation and recovery steps for each test remain consistent, increasing and decreasing the amount of light reflected as a consequence of the different absorbances of PB and PW within the visible spectrum. This experiment also illustrates more clearly the impact of H_2O_2 concentration on the rising time required for the signal to reach the saturation. At this point, an inverse relationship between the H_2O_2 concentration and the response time can be presumed.

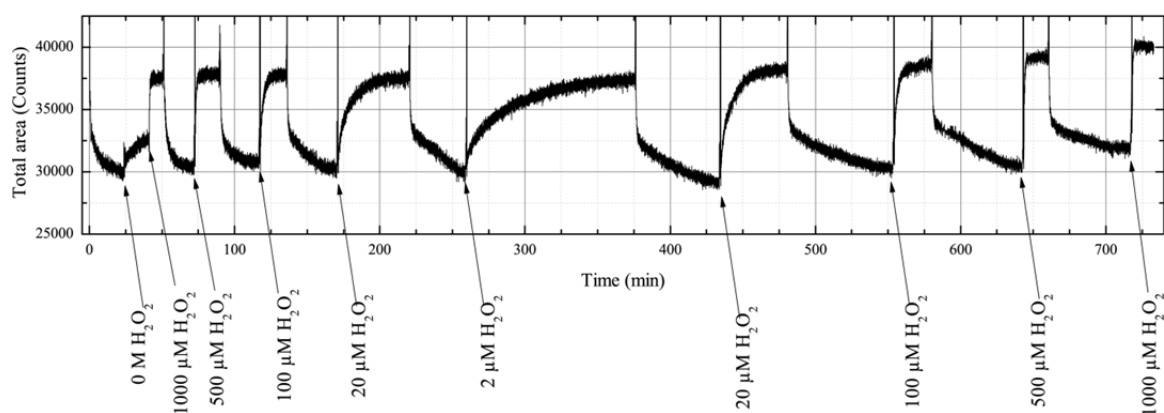


Figure 4-6: Response of the sensing probe to immersion in solutions with decreasing and increasing H_2O_2 concentration.

Multiple experiments were performed in the sensing probe subjecting it to tests in solutions with the same H_2O_2 concentration. A typical response for tests at a single concentration is shown in Figure 4-7, that presents the results of an experiment where the sensing probe was immersed six times in solutions at a H_2O_2 concentration of $100 \mu\text{mol L}^{-1}$. Once more, the oxidation and recovery steps show a consistent response, increasing and decreasing the intensity of the reflected light, respectively. In addition to this, the first recovery step performed to the fiber does not diminish the intensity to the minimum value of the entire experiment, similarly to the experiment in Figure 4-6. Despite this, the rising times to reach the saturation remain within similar values, as expected since the tests were performed at the same concentration.

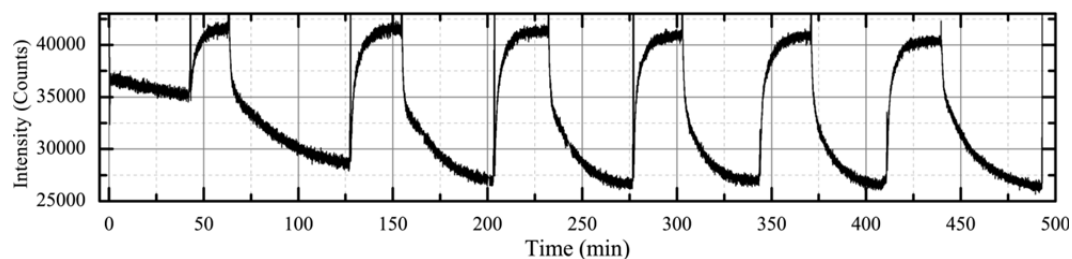


Figure 4-7: Response of the sensing probe to immersion in $100 \mu\text{mol L}^{-1} \text{H}_2\text{O}_2$ solutions.

Figure 4-7 also shows that the maximum intensity presents a slight decrease in its value as the tests proceed. A similar behavior can be seen between the overall intensity levels reached by the tests in the decreasing-increasing experiment illustrated by Figure 4-6, and the one in the increasing-decreasing experiment of Figure 4-5, since the latest was performed after three weeks of multiple other tests on the same sensing probe.

The small and gradual reduction in the intensity peaks in Figure 4-7 (about 3% overall) might be the result of leaching of the immobilized dye in the polyionic structure on the tip of the fiber. Such leaching would be in accordance with the desorptive process of the polyelectrolyte layers whereby approximately one bilayer is lost after 12-hour immersion of the sensing probe in an aqueous environment [39]. In spite of the possible leaching, the sensing probe was found to remain functional for an extended period of time and multiple tests. Moreover, the possibility of recovering the sensing capabilities of the probe using ascorbic acid after the detection of H_2O_2 makes it suitable for multiple detections with a low associated cost.

4.3.3 Response time evaluation

As previously stated, a dependence on concentration can be seen in the rising time that the signal response reached the saturation level. This behavior was consistently observed in all the experiments to which the sensing probes were subjected.

In the current work, an inverse-exponential fit was performed to the response of intensity for each test described in Section 4.2.7. This inverse-exponential behavior is

consistent with the diffusion mechanisms underlying the operating principle of the sensing probe.

The characteristic response time τ , in which the signal reached $\approx 63\%$ of the saturation intensity is plotted against the H_2O_2 concentration in Figure 4-8, with the first experiment plotted shown with the open circles. Similarly, the τ values for the subsequent experiments, also obtained through the inverse-exponential fits during the oxidation steps, are shown in Figure 4-8 as filled circles.

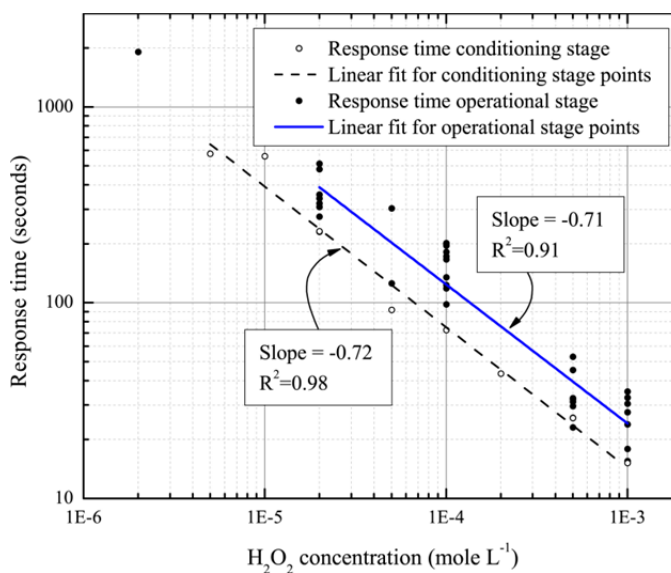


Figure 4-8: Time response to reach 63% of the maximum intensity for the different concentrations tested.

A linear dependency of the response time on the H_2O_2 concentration is observed when plotted in a log-log scale. Figure 4-8 also shows the linear fits of the response times in the conditioning and the operational stage. The slopes of the linear fits in both stages are similar, suggesting that a calibration of the sensing probe during the conditioning stage can be used to provide a measurement of the H_2O_2 concentration during the operational stage for the same sensing probe by measuring the response time.

The response time is the parameter used in this work to quantify H_2O_2 concentration. The error analysis showed that the time t is the most sensitive measurement parameter, and the results exhibit lower scatter for higher concentrations. This can be explained by the fact that at higher concentrations the reflected light are close to or at saturation.

A time dependent response of the reflected intensity from a sensing probe was earlier presented by Del Villar et al. [39]. In their work, a linearization of the light intensity response was made by defining *slope* as the ratio between the difference of intensities of the light at 90 and 10 % of the intensity at saturation and the elapsed time between these two intensities. They found the slope to be linearly dependent on the logarithm of the H₂O₂ concentration. Furthermore, whereas Del Villar's approach requires the saturation level to be reached, the present formulation of the response in terms of an inverse-exponential (diffusion mechanism) behavior circumvents the need to run experiments till saturation of the reflected light, and saturation values can simply be extrapolated from available data. For instance, extrapolated saturations based on the first half of a response curve yield saturations within 2% of the full response curve value.

The results presented here show a sensing probe that can be used not only to detect, but also to quantify the concentration of H₂O₂.

4.4 Conclusions

The development of a H₂O₂ sensing probe on the tip of an optical fiber, at concentrations ranging 10 to 1000 $\mu\text{mol L}^{-1}$, was demonstrated. A layer-by-layer electrostatic self-assembled structure of polyelectrolytes fabricated on the tip of a multi-mode optical fiber was used to immobilize Prussian blue molecules that served as indicators of the presence and concentration of H₂O₂. The sensing probe was successfully tested in solutions at pH 4.0, exhibiting an increase in the intensity of the reflected light as reduced Prussian white was oxidized back to Prussian blue due to the interaction with H₂O₂. The experiments to the optical fiber sensing probes allowed two separate regimes to be identified in the response to the interaction with the H₂O₂ solutions. The first experiment, where the sensing probes were tested in solutions steadily increasing the concentration of H₂O₂, showed a first regime in which the maximum intensity reached after each immersion increased, in what can be interpreted as an activation stage of the sensing probe. The subsequent experiments performed did not exhibit a similar behavior and can be considered as part of a second, or operational, regime.

Both regimes share an inverse-exponential dependence of the intensity of the light on the time elapsed, and the response times are linearly dependent on the H_2O_2 concentration in a log-log scale. The behavior is consistent with the underlying diffusion processes that drive the probe operation. A dependence of the response time on H_2O_2 concentration has been previously reported, but the phenomenology agrees to a better extent in the present work. A key aspect of the signal processing technique presented here is the physically consistent correlation of the light intensity response and the possibility this allows to make measurements without necessarily attaining saturation.

Although an increase in the intensity with concentration was consistently observed in multiple tests of optical fibers subjected to similar first experiments, there are no conclusive results to determine if the maximum intensity observed in the subsequent experiments would have been the same under different initial tests. Additional experiments will be required to address this in the next phase of development of this sensing device.

Several attributes open the possibility for this sensing device to be employed for *in-situ* detection of H_2O_2 generated as a by-product in PEMFC's, where it could help improve understanding of the operating conditions that promote its formation and mitigation of the membrane degradation. These comprise: the selectivity of the PB/PW system to H_2O_2 , the increased absorbance of PB in low pH environments, the microporous structure formed by the PB allowing only small molecules to reach the reaction sites, the LbL ESA of polyelectrolytes structure that not only immobilizes the PB/PW molecules, but also creates a diffusive barrier for the H_2O_2 solutions to react with the PB/PW sites, among others factors.

Other possible applications of this sensing probe include the detection and quantification of H_2O_2 in rainwater, and applications where minimal invasiveness is key as for example in the medical diagnosis of pulmonary diseases.

The results presented here were obtained over a period of approximately two months after the fabrication and first test of the sensing probe and showed a consistent and reproducible behavior; although this is a good indication of the probe stability, additional

tests over longer periods are required to systematically determine the robustness, reliability, and lifetime prior to routine use. The measured uncertainty is large for some of the tested concentrations, and though acceptable for most intended applications, the uncertainties can be reduced with improving the probe signal to noise ratio and by low-pass filtering of the reflected light.

Acknowledgments

J.F.B-C. acknowledges the financial support provided by the Universidad Nacional de Colombia-Medellín campus. The authors also acknowledge Ms. Koh-Yiin Hong for her guidance in the chemical procedures involved in this work. This work was funded by the Natural Sciences and Engineering Research Council (NSERC) of Canada through the Strategic Grants program and supported by Ballard Power Systems.

Chapter 5: Temperature response and durability characterization of an optical fiber sensor for the detection of hydrogen peroxide

(*Electrochimica Acta*, volume **129**, 2014, 416–424)

Reproduced with permission from Elsevier.

Preamble

The previous Chapter presented the development of an optical fiber-based sensor for the detection of hydrogen peroxide in small concentrations in a liquid solution under ambient conditions. PEMFCs operate typically at temperatures that range from 60 to 90 °C, characterization of the temperature response and stability of the sensor is investigated in this Chapter.

The body of this Chapter was published in the *Electrochimica Acta* Journal.

Abstract

Hydrogen peroxide is a precursor to damage mechanisms in numerous applications; its monitoring is important and challenging. The effect of temperature on the performance and durability of a recently developed optical fiber sensors sensitive to the presence of hydrogen peroxide in low concentrations is investigated. The sensors are fabricated by immobilizing Prussian blue within a multilayer of electrostatically self-assembled polyelectrolytes. The sensing principle of this optical electrode relies on the change in the intensity of the reflected light when Prussian white is oxidized back to the blue state due to the presence of hydrogen peroxide. The amplitude of the intensity of the reflected light is found to vary with temperature in a quadratic fashion, but the characteristic response time which correlates with concentration remains constant. Thus the sensing device retains its abilities to determine and quantify the concentration of hydrogen peroxide in a liquid solution. Additionally, the degradation of these fiber sensors when subjected to high temperature is examined. Four optical fiber sensing devices were subjected to different testing conditions and a characterization protocol that included: measurement of the intensity of the cyanide stretch (2150 cm^{-1}) via Raman micro spectroscopy; imaging with scanning electron microscopy; and

measurement of the presence of iron ions using energy dispersive X-ray spectroscopy. The results show a gradual degradation of the sensing device as a result of progressive desorption of the polyelectrolyte multilayer structure that leads to leaching of the Prussian reagent. This degradation mechanism does not compromise the functionality of the device which is found sufficiently robust for multiple tests at high temperature. The simplicity of this sensing system combined with its relative robustness and reusability make it a good candidate for minimally intrusive and localized monitoring of hydrogen peroxide formation in operating PEMFCs.

Keywords: Hydrogen peroxide; Optical fiber sensor; Temperature; Prussian blue; Polymer Electrolyte Membrane Fuel Cell (PEMFC) degradation

5.1 Introduction

Hydrogen peroxide (H_2O_2) is generated as a by-product in the electrochemical reactions occurring in polymer electrolyte membrane fuel cells (PEMFC) [18], and has been linked to chemical degradation that causes premature failure in PEMFCs. Reactive oxygen species (ROS) such as hydroxyl ($\text{HO}\cdot$) and hydroperoxyl ($\text{HOO}\cdot$) radicals can be formed upon the decomposition of H_2O_2 , and the rate of this decomposition increases in the presence of cations like Fe^{2+} due to the Fenton reaction [11, 206]. These ROS induce degradation of polymers due to their high reactivity [240]. In the case of PEMFCs, degradation is associated with the attack of the C-F bonds in the side chains and the main backbone of the perfluorosulfonated polymer, and results in low ionic conductivity and thinning of the membrane [7]. The quantification of this degradation mode has typically been done by measuring the released fluorine ions (F^-) in the condensates at the exhaust of PEMFCs [241].

It should be noted that there is some debate on the role that H_2O_2 plays in the chemical degradation of PEMFCs, and other mechanisms that promote radical formation have been proposed [224, 242]. Regardless of possible alternative mechanisms, multiple *ex situ* and *in situ* tests have shown an increase in F^- ions release as a consequence of the presence of H_2O_2 [7, 9, 225, 241, 243].

The presence of H_2O_2 in PEMFCs has been detected using methods based on *ex situ* measurements in membranes that have been removed from operational fuel cells [22] and in fuel cells exhaust gases [6, 226] using techniques such as ion chromatography, Fourier transform infrared spectroscopy (FTIR), and nuclear magnetic resonance (NMR).

In addition to the exhaust gas and membrane methods, *in situ* detection of H_2O_2 in PEMFCs has been achieved using electrochemical techniques. Liu and Zuckerbrod reported the presence of H_2O_2 inside PEMFC membranes while in operation using an electrochemical amperometric measurement, consisting of a measurement of the current between a working and a reference electrode at constant potential. The H_2O_2 detected in the PEMFC ranged from 3 to 25 ppm ($\approx 90\text{--}735 \mu\text{mole L}^{-1}$) [23]. This technique, although having the advantage of better signal-to-noise ratio and simpler instrumentation required compared to other electrochemical techniques such as potentiometric and conductometric techniques [30], can still be affected by the electromagnetic fields (EMF) generated by the electrical currents in a PEMFC. Furthermore, in an acidic environment such as the catalyst layer of a PEMFC, Pt can catalyze the formation of H_2O_2 [10, 24]. Thus, the Pt wire used as a working electrode could itself be inducing the formation of H_2O_2 rather than simply detecting the by-product of the operating PEMFC.

The use of optical fiber sensors for the detection and quantification of H_2O_2 has recently been demonstrated [244]. These sensors are well-suited to the detection of H_2O_2 by-products in PEMFCs because: (1) optical signals are immune to interference due to electric currents in a PEMFC; (2) silica glass fibres are not adversely affected by the electrochemical reactions that take place in the PEMFC; (3) optical fibers are relatively small, which enable minimally invasive distributed measurements, and; (4) immobilization techniques for chemical reagents that are sensitive to H_2O_2 , using the electrostatic self-assembly (ESA) of polyelectrolytes, have been demonstrated on optical fibers allowing H_2O_2 to be detected in acidic media. These techniques use the Prussian blue/Prussian white (PB/PW) system, where the organometallic compound PB is chemically reduced to PW by the immersion of the fiber in ascorbic acid, and is oxidized back to PB by the action of

H₂O₂. Fiber optic devices based on this system provide reusable sensing systems for the detection of H₂O₂ [40, 214, 244].

The PB/PW fiber optics sensors presented in [244] were demonstrated at room temperature. Heat transfer and temperature variations play a key role in the operation and durability of PEMFCs [114, 116] which typically operate at temperatures that range from 60 °C to 90 °C. It is therefore essential that *in situ* sensors for this application operate reliably across this range. The focus of this work is, therefore, to characterize the performance of PB/PW-based fibre optic sensors for H₂O₂ over this temperature range. The key performance parameters that are assessed in this study are: (1) verification of the ability of the PB/PW system to detect H₂O₂ at typical operational temperatures of a PEMFC; (2) characterization of the response of the sensing device to changes in the temperature, and (3) quantification of the degradation experienced by the sensitive coating, which limits the lifetime of the sensing device in continuous operation.

5.2 Materials and Methods

5.2.1 Sensing film deposition

The fabrication of a multilayer structure for immobilizing PB on the tip of an optical fiber using the layer-by-layer (LbL) ESA of polyelectrolytes follows the procedure described in [244]. Briefly, pigtailed multimode optical fibers SFS105/125Y and SFS200/225Y from Thorlabs (Newton, NJ) are cleaved, and then cleansed using a 3:1 solution of H₂SO₄ (>98%) and H₂O₂ (30 wt%) for 30 min. This promotes the attachment of hydroxide anions (OH⁻) onto the fiber surface. The fibers are then dried at 80 °C for 60 min. to ensure that the surfaces remained negatively charged [93, 245].

The fibers are then immersed for 20 min. in a polycation solution of poly(allylamine hydrochloride) (PAH⁺, $M_w \approx 15,000$, product number 283215) and Prussian blue soluble (product number 03899) with concentrations of 2.0 mg mL⁻¹ and 2.5 mg mL⁻¹, respectively. A thin film of this positively charged polyelectrolyte is adsorbed by the glass surface and held by electrostatic forces. The non-adsorbed excess material is removed by

three consecutive immersions in distilled water, each for 1 min. The first bilayer is completed by immersing the fibers for 20 min. in a polyanion solution of poly(acrylic acid) (PAA^- , $M_w \approx 100,000$, product number 523925) with a concentration of 2.0 mg mL^{-1} . A total of 17 bilayers were deposited with these solutions at pH 4.0, and finally two capping bilayers of similar solutions at pH 5.5 but without PB were deposited onto the multilayered structure. The fibers were finally annealed for 2h at $100 \text{ }^\circ\text{C}$ and stored at room temperature for one week before the initial tests.

All solutions were prepared using acetate buffer solution (ABS) at pH 4.0 as solvent and the pH values were adjusted using aliquots of aqueous solutions of NaOH and HCl as required. All products were from Sigma-Aldrich (Oakville, ON, Canada), used without further purification.

5.2.2 Liquid test solutions preparation

A pH 4.0 solution of 0.04 mol L^{-1} of *L*-ascorbic acid (Product number 283215, Sigma-Aldrich) using ABS as solvent was used as reducing agent for the sensing film. The oxidative stages of the redox reactions were performed using solutions of $100 \times 10^{-6} \text{ mole L}^{-1} \text{ H}_2\text{O}_2$, prepared by adding $30 \text{ } \mu\text{L}$ of $0.01 \text{ mM H}_2\text{O}_2$ to 3 mL of ABS at pH 4.0. Each H_2O_2 test solution was prepared immediately before immersing the optical fiber with the multilayered sensing structure in it regardless of the temperature of the test.

5.2.3 Test for temperature response

The systematic testing of the sensor involving both changes in temperature and concentration was experimentally impractical at this stage of development, but prior to the temperature response experiments, the fiber response to concentration was checked and a log-linear behavior was obtained consisted with the results reported in [244].

The experimental setup to perform the tests of the response of the sensing devices at various temperatures is shown in Figure 5-1. The white light source (HL-2000-FHSA, OceanOptics, Dunedin, FL) was connected to the arm 1 of a bifurcated optical fiber (BIF200-UV-VIS, OceanOptics). Light was carried to the common arm that is connected to

the sensing probe in one of the optical fibers SFS105/125Y. The reflected light was carried back through the common arm and into arm 2, where the spectrum was measured using an optical fiber spectrometer (USB2000, OceanOptics). Spectra from the sensing probe were recorded at a sampling rate of 0.5 Hz using the software SpectraSuite (OceanOptics). The software was set to display the intensity at each wavelength in counts per second (cps) at a sweeping rate of 500 ms, and to present the trendline of light intensity, determined by integrating the cps over a range of wavelengths from 370 to 1050 nm.

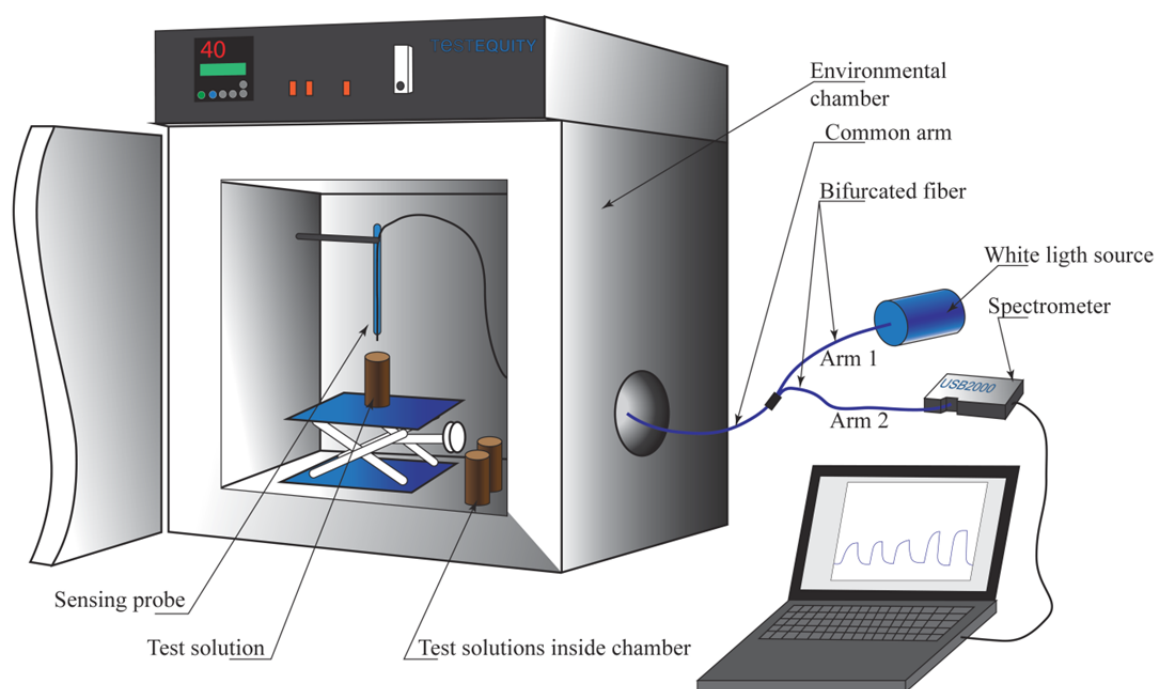


Figure 5-1: Experimental setup to measure the response in the Prussian blue/Prussian white sensitive coating under temperature changes

The temperature at which the tests were performed was controlled by placing the sensing probe inside an environmental chamber (TestEquity, Model 123H, Moorpark, CA). High density polyethylene (HDPE) containers were filled with either 3.0 mL of ABS at a pH 4.0 or 3.0 mL of ascorbic acid solution at pH 4.0 and placed inside the environmental chamber. The temperature of the solutions was monitored with a K-type thermocouple in a control bottle with 3.0 mL of ABS. Measurements were made at the time of the immersion of the probe. The uncertainty in these measurements is ± 0.1 °C. Figure 5-1 also shows how the

sensing probe is held in a vertical position, and how the immersion in the liquid reagents is performed by raising a lab scissor jack stage.

The experiment consisted of a series of cycles with an oxidation stage and a reduction stage. During each oxidation stage PW becomes PB after immersion of the sensor in solutions of 100 μM H_2O_2 . The reduction stage was induced by immersing the sensor in ascorbic acid, which reduces PB back to PW. The effect of temperature on the light response was observed by modifying the temperature setpoint of the environmental chamber. The length of the immersion in either oxidation or reduction stages was controlled by observing the plateauing of the reflected light intensity monitored using the spectrometer software. Each stage lasted approximately 10 to 15 min.

For each oxidation stage, the oxidizing solution was prepared immediately before the immersion of the sensor. An aliquot of H_2O_2 was injected in one of the bottles with ABS inside the chamber. A lab scissor jack was used to immerse the fiber in the bottle. The instant of immersion into the solutions coincided with the time at which the intensity of the optical signal plateaued and the temperature of the bottle stayed within ± 0.2 $^\circ\text{C}$ of the setpoint. The temperature was maintained constant within 2 $^\circ\text{C}$ during the procedure of exchange solutions.

Five redox tests were performed at a setpoint temperature of 25 $^\circ\text{C}$. At the beginning of the following oxidation stage, the setpoint temperature of the chamber was increased to 40 $^\circ\text{C}$. Once the control bottle reached the new setpoint temperature a reduction stage was performed and followed by four redox tests at the same temperature. The same procedure was followed at temperatures of 55, 70, and 85 $^\circ\text{C}$. After the fourth redox test and reduction at 85 $^\circ\text{C}$, the setpoint was lowered to 70, 55, 40, and 25 $^\circ\text{C}$, and two redox tests were performed again at each new temperature.

5.2.4 Tests for temperature durability

To study the effect of increasing temperature on the durability of the sensing devices, four identical SFS200/225Y multimode optical fibers with core and cladding diameters of 200

and 225 μm , respectively (fibers A, B, C, and D), were coated in the same batch as the fibers in the previous tests following the procedure described in Section 5.2.1. Fiber A was kept untested and used as a reference of the amount of PB immobilized onto the surface of the fibers in the coating stage. Fibers B, C, and D were tested with similar procedures to the one described in Section 5.2.3 for temperature response. Each of the tested fibers were subjected to three redox tests at 25 $^{\circ}\text{C}$, after which the temperature was raised and three redox tests were performed at that higher temperature. These higher temperatures were 55, 70, and 85 $^{\circ}\text{C}$ for fibers B, C, and D, respectively.

5.2.5 Sample characterization after durability tests

The characterization procedure for fibers A, B, C, and D comprised: Raman micro spectroscopy (RMS), scanning electron microscope (SEM) imaging, and energy dispersive X-ray spectroscopy (EDS). The RMS and the EDS characterization are performed to assess the impact of temperature on the chemical composition of the multilayered structure, as well as the presence of the immobilized Prussian reagent on the tip of the optical fiber, while SEM imaging is used to observe morphological changes to the surface of the coating.

5.2.5.1 Raman micro spectroscopy

The RMS spectrum produces a spectrum with a unique ‘fingerprint’ of the composition on the sensing coating of the optical fiber. One of the particular peaks in this coating is found at 2150 cm^{-1} and it is associated with a stretch of the cyanide (CN) compound. The CN stretch presence in the spectrum is due to the presence of PB or PW compounds which exhibit a cubic structure of Fe ions where the lattices are formed by CN groups [72, 246, 247].

The RMS characterization of the fibers was performed in a Renishaw inVia Raman microscope (Gloucestershire, UK). Initially, an extended Raman spectrum on a single point on the surface of the coating, ranging wavenumbers from 100 to 3200 cm^{-1} , was recorded from fiber A, the untested fiber. The spectrum was measured on the cylindrical surface close to the distal end of fiber on an area coated with the sensing film. This

spectrum allowed identification of the stretches of the compound on the surface of the fiber.

The initial Raman spectrum from fiber A was collected after focusing the light of a 785 nm high power laser (Renishaw) onto the cylindrical surface near the distal end of the optical fiber with a 50X objective. The exposure time and power of the laser were set to 10 s and 10%, respectively, and the spectrum was recorded after one accumulation of the signal reflected from the surface. To enhance the contrast of the image, the optical fiber was placed onto a gold slide.

From the spectrum, the cyanide (CN) stretch at 2150 cm^{-1} was selected to characterize the degradation of optical fibers A to D. For this purpose, a mapping of the Raman spectrum from the cylindrical surfaces close to the distal end of the fibers, at wavenumbers from 1950 to 2250 cm^{-1} was performed. Mapping was performed on areas of approximately $30\times 20\text{ }\mu\text{m}$, in steps of $1\text{ }\mu\text{m}$, using the same parameters used in the single point spectrum, but with the exposure time reduced to 1 s. No changes in the power of the laser, or the accumulations were done to avoid damage of the sensing coating due to ablation with the laser.

5.2.5.2 SEM imaging – EDS characterization

Following the RMS characterization, the tips of fibers A to D were coated with a conductive layer of graphite and SEM imaging was performed using a Hitachi S-4800 field emission scanning electron microscope (Tokyo, Japan).

The EDS characterization of the samples was performed using a Bruker Quantax EDS system for SEM (Billerica, MA, US). This characterization consisted of a multipoint analysis of the planar face on the distal end of fibers A to D. The analysis was focused on the detection of iron (Fe), which exists as iron(II) and iron(III) ions on the vertices of the cubic structure of the Prussian compounds [72].

The parameters set for the EDS analysis were held constant for all fibers to allow the tested fibers to be compared with the control fiber. A multipoint analysis was carried out on the

planar face of the tip of the fiber on a circular area with the same size as the entire planar face (225 μm in diameter), collecting a total of 400,000 counts, after which the quantification of Fe occurs. Since the target element was Fe, which is only present in the Prussian compound, the energy of the beam was set to 13 keV, doubling the energy of the spectral line $K\alpha$ for iron [248].

5.3 Results and Discussion

5.3.1 Temperature response

5.3.1.1 Changes of intensity with the temperature

The response of the sensing optical fiber probe is presented in Figure 5-2. The figure shows the reflected intensity from the tip of the optical fiber when it was subjected to the experiment described in Section 5.2.3. The most noticeable characteristic is that the reflected intensity from the sensing device increases with temperature. This is attributed to the combined effect of thermal expansion of the multilayer structure of polyelectrolytes and the increase of the activity of the chemical reaction. Thermal expansion could lead to a less dense polyelectrolyte structure in which H_2O_2 would contact more sites with immobilized PW, which would then be oxidized to PB. The increase in the activity of the reaction could cause more PW molecules to be oxidized to PB. In both cases the effect is an increase in the absorbance of the immobilized compound, so that more light is backscattered into the optical fiber and thus the intensity registered by the spectrometer is higher.

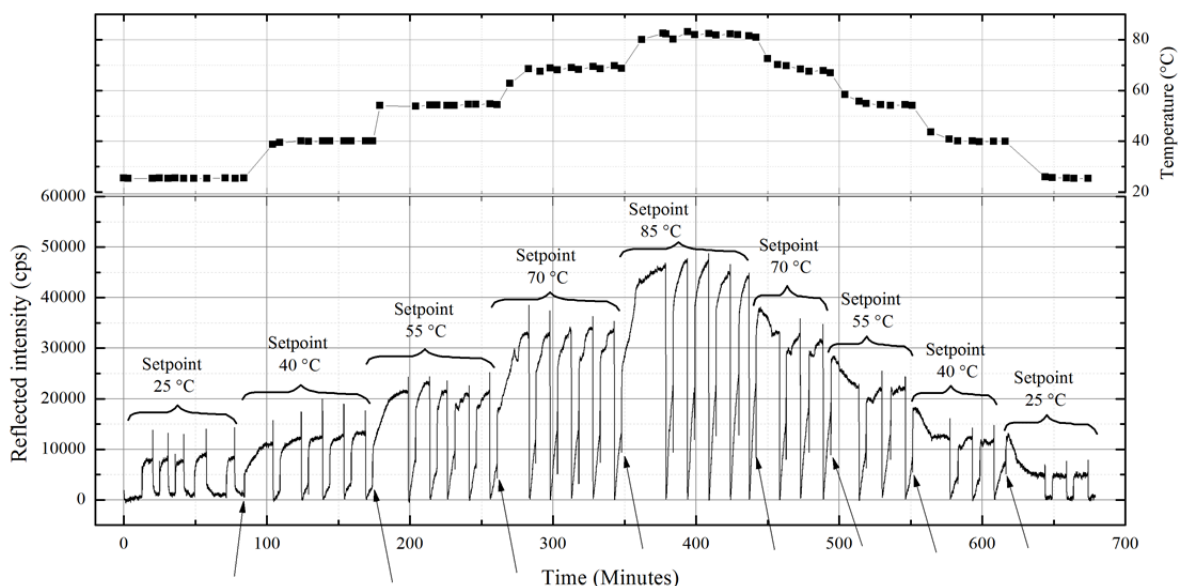


Figure 5-2: Temperature (top) and Intensity of the reflected light from the sensing probe (bottom) during the H_2O_2 detection tests at different temperatures. Brackets indicate the setpoint temperature in the environmental chamber, arrows indicate the instant at which setpoints are modified

The effects of high temperatures on the spectral properties of Prussian blue are not fully described in the literature. It has been reported, however, that at temperatures over $100\text{ }^\circ\text{C}$, PB undergoes a mass reduction. This reduction is as a consequence of water removal from the crystalline structure of PB in an inert atmosphere. The same study reported no degradation of PB below $262\text{ }^\circ\text{C}$ [249]. In wet environments some PB degradation is observed in alkaline media causing the release of cyanide, but no significant degradation is reported at $4 < \text{pH} < 10$ up to $140\text{ }^\circ\text{C}$ [250]. Consequently, it is unlikely that the immobilized PB is altered in our experiments, leaving the aforementioned changes in the polyelectrolyte structure and the increase in the activity of the reaction as the most probable causes of the increase in intensity of the reflected signal with the temperature.

The response of the sensing device during each of the oxidation stages presented in Figure 5-2 follows an inverse exponential behavior, as it was shown in our previous study [244]. Analysis of the data shows that reflected intensity increases quadratically with increasing temperature, the response time of the sensing device, which is the basis for concentration measurements, remains unaffected by temperature. The response time is the time at which

the signal of the reflected light –following the inverse exponential behavior– reaches $(1 - 1/e) \approx 63\%$ of its maximum intensity. The response times for the experiment presented here averaged 85 s. with a standard deviation of 40%. This is in agreement with the values reported for tests in solutions at concentrations of $100 \times 10^{-6} \text{ mol L}^{-1} \text{ H}_2\text{O}_2$ [244].

The reduction stages, however, exhibited temperature sensitivity. When the tests were performed at room temperature, the ascorbic acid showed an exponential decay behavior, similar to that previously reported [38, 244]. However, at 40 °C and higher, the stages of reduction after the immersion in ascorbic acid showed a sudden drop in the reflected intensity reaching a minimum value, followed by an increase and eventual stabilization of the reading. This behavior may be due to the fact that ascorbic acid undergoes complex mechanisms of decomposition when it is subjected to diverse conditions such as combined changes in temperature, pH, and oxygen content. The products of such degradation have different chemical reduction properties and cause variations in the PB/PW system behavior [251].

In spite of the possible decomposition of ascorbic acid during the initial phase of reduction, when the signal reaches a stable value and the fiber is immersed in a H_2O_2 solution to start the next test, the sensing device shows the expected increase of the intensity of the reflected light (i.e. an inverse exponential). It is important to note that the last set of tests was performed with fresh solutions of ascorbic acid and, therefore, these did not experience degradation.

As indicated in Section 5.2.3, the changes in the setpoints occurred at the beginning of some of the oxidation stages. These transition oxidation stages are shown in Figure 5-2 by the arrows indicating the moment at which the temperature setpoints were modified. Since the reduction stage did not start until the control bottle reached the setpoint temperature, these transition stages lasted longer than those in which the temperature was set constant.

Figure 5-2 also shows that tests performed when the setpoint temperature was 85 °C exhibit a gradual reduction of the reflected intensity. The reflected intensity in the fourth redox test at 85 °C is 8% lower than in the first test at the same setpoint temperature. This effect may

be caused by the progressive desorption of the ESA structure of polyelectrolytes leading to the leaching of the immobilized PB. As will be shown later, the sensing device suffers degradation after repeated tests at high temperatures.

Figure 5-2 also shows that the reflected intensities in the tests performed were also slightly affected by the direction in which the setpoint temperatures was changed. When the setpoint temperature was increased (transitions 1 and 4 in Figure 5-2, from 40 to 55 °C and from 70 to 85 °C), the reflected intensities were on average 4% higher than when temperature was decreased over the same range (transitions 8 and 5). At 40-25 °C, the intensities are only 68% of the intensities observed during the initial transition, 25-40 °C. This reinforces the hypothesis of PB leaching and gradual damage to the sensing device. Nonetheless, it should be emphasized that the sensing device remains operational after 37 redox tests and is still able to detect the presence of H₂O₂ in solution.

5.3.1.2 Intensity amplitude

The intensity amplitude is defined here as the difference between the maximum value of the recorded intensity at the oxidation stage and the minimum value during the reduction stage within a single redox test. Referring to Figure 5-2, there is a dependency of the intensity amplitude on temperature. Figure 5-3 presents the intensity amplitude of each redox test plotted against the temperature. The non-linear behavior follows a parabolic fit.

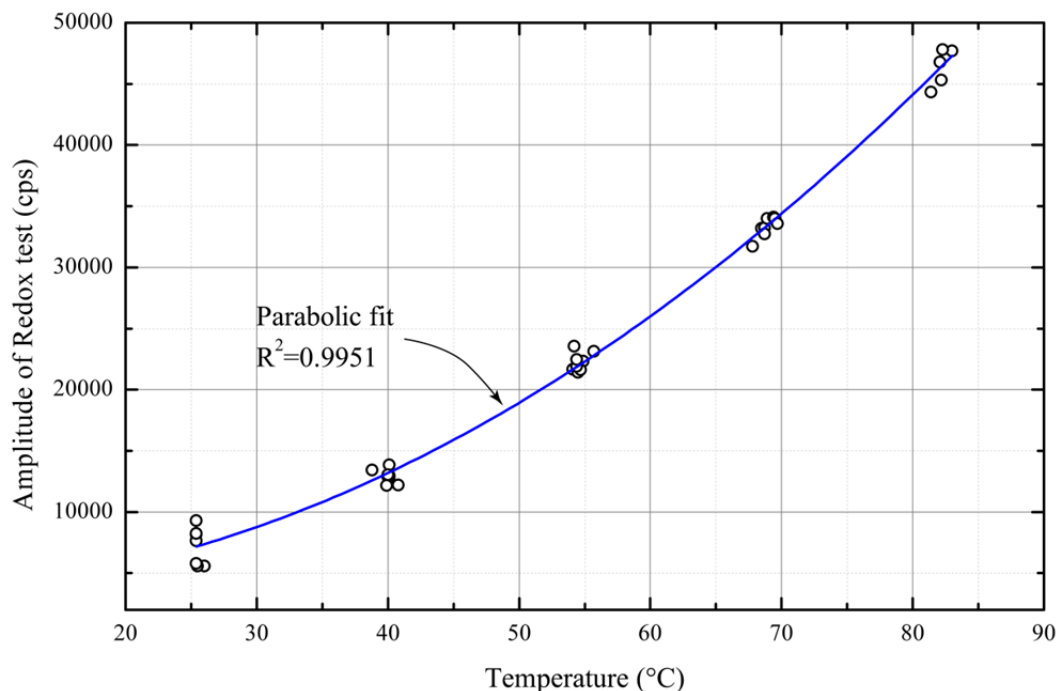


Figure 5-3: Amplitude of each test vs. temperature

5.3.2 Durability tests

5.3.2.1 Raman micro spectroscopy

The extended Raman spectrum of a single point on the cylindrical surface near the distal end of fiber A, the reference fiber, is shown in Figure 5-4. The most intense peaks are centered at 277, 529, 2090, and 2150 cm^{-1} . The first two peaks belong to iron-cyanide bending vibrations, while the last two are due to stretching vibrations of the cyanide ($\text{C}\equiv\text{N}$) groups [247]. The peak at 2150 cm^{-1} is only present in the cyanide group of the immobilized Prussian blue or white and belongs neither to the SiO_2 in the optical fiber nor to the polyelectrolytes. Therefore, this stretch is adopted as an indicator of the presence of Prussian compound in the structure.

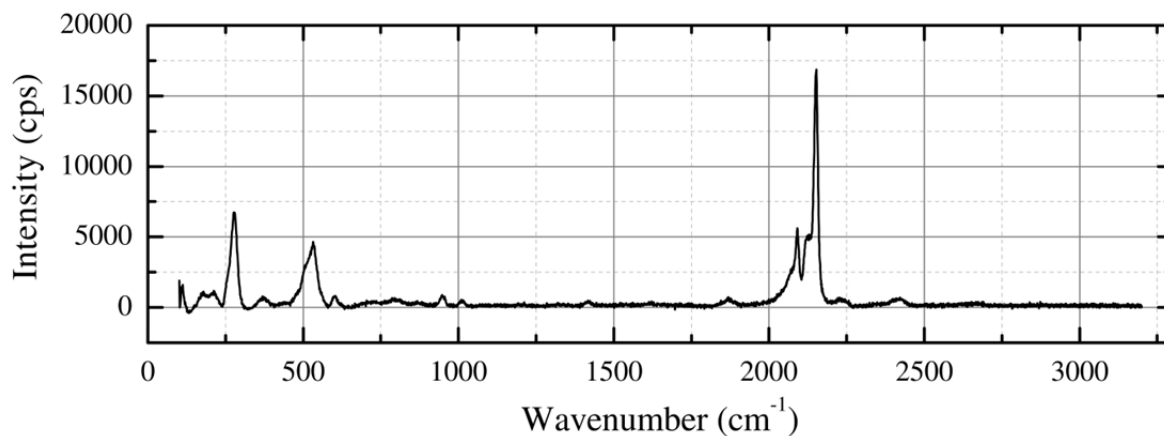


Figure 5-4: Extended Raman spectrum of the sensing coating on Fiber A. Spectrum obtained after an exposure time of 10 sec. and a single accumulation.

Spectra obtained from fibers A to D are presented in Figure 5-5. The spectrum of fiber A has a maximum intensity of approximately 1,500 counts per second (cps) for the stretch at 2150 cm^{-1} . The same peak in the extended Raman spectrum presented in Figure 5-4 reached over 15,000 cps. In Figure 5-4, the spectrum was taken with an exposure time of 10 s for the single point, whereas in the mapping of the Raman spectra in fibers A to D shown in Figure 5-5, the exposure times were only 1 s and, therefore, the lower intensity registered at the same stretch.

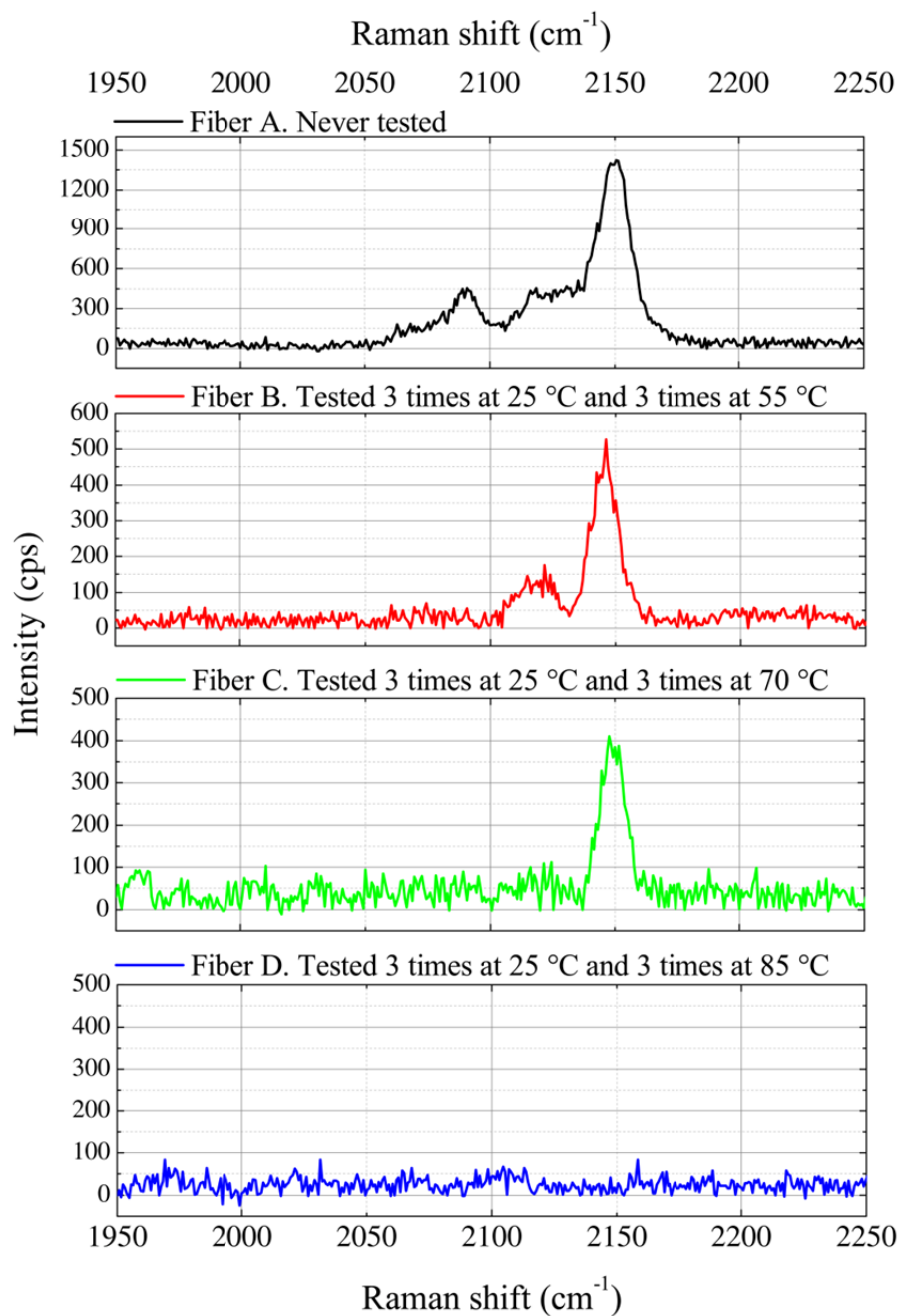


Figure 5-5: Raman spectra obtained from fibers A, B, C, and D

The intensity of the CN stretch drops from approximately 1,500 cps for fiber A to 500 cps for fiber B, tested up to 55 °C, and then to 400 cps for fiber C, tested up to 70 °C. For the case of fiber D, tested at 85 °C, the CN stretch is not visible. A gradual desorption of the polyelectrolyte multilayer structure that causes leaching of the immobilized reagent can

explain this reduction in intensity. This hypothesis is consistent with the reduction in the reflected intensity registered by the spectrometer after the sensing device was tested multiple times in the experiment presented in Section 5.3.1.1 (Figure 5-2). Equivalent mappings were performed in other areas on the surface of fiber D with similar results.

The absence of the stretch at 2150 cm^{-1} in the spectrum for fiber D indicates that the remaining concentration of reagent is below the sensitivity threshold for the Raman spectrometer under these test conditions. However, the temperature test results presented in Figure 5-2 show that even after more extreme testing (i.e. more than 35 redox tests, some of which were performed at temperatures that exceeded $80\text{ }^{\circ}\text{C}$) than in the RMS experiments, the sensing device is still operational. This suggests, at the completion of the Raman tests, small concentrations of reagent remain in the structure.

A subtle effect is observed in the spectral position of the CN stretch when comparing the spectra from fibers A, B, and C. Fiber B shows peaks at slightly lower wavenumbers than the other fibers. This could be caused by the shift in the electron density as a result of subjecting the structure to the tests [252]. In addition, random alignment of the structure of the polyelectrolytes during the coating fabrication can lead to subtle differences between specimens [38].

Another observation in the spectrum from fiber B, is the disappearance of the peak at 2090 cm^{-1} and the shoulder within 2124 and 2131 cm^{-1} that is present for fiber A. This could be a consequence of the fact that the tests of fibers B and C ended in a reduction stage, which converted the PB to PW. As reported by Samain et al. [247], the stretching at 2090 cm^{-1} and the shoulder stretching in Prussian white (also known as Berlin white) have lower intensities than those in the PB state.

5.3.2.2 SEM imaging – EDS characterization

Figure 5-6 presents the SEM images of fibers A (fiber never tested), and from fibers B, C, and D after testing, taken at magnifications of $18,000\times$ (left column) and $45,000\times$ (right column). Fiber A shows a dense distribution of agglomerated nodules ranging sizes from

200 to 500 nm, separated by 200 nm to 1 μm . Figure 5-6(b) shows an ‘orange-peel’ type of structure on fiber A, covering completely all the nodules of the immobilized PB. This ‘orange-peel’ structure is associated to the capping bilayers applied at the end of the coating process. The images of fiber B, shown in Figure 5-6(c) and (d), show fewer agglomerate nodules with spacings similar to that of fiber A. However, in Figure 5-6(c) the capping bilayers are absent. The surface of fiber B is smooth but the immobilized material remains covered. Fiber C (Figure 5-6(e) and (f)) shows evidence of desorption of the immobilized agglomerates. Figure 5-6(e) shows fewer particles held within the multilayered structure. The sizes of the nodules are comparable to those observed in the previous SEM images, but the spacings among them are on the order of 1 μm . Finally, fiber D (Figure 5-6(g) and (h)) shows that the surface is rough, with only a few particles still immobilized, suggesting a deterioration of the coating.

These findings are consistent with the prolonged immersion of the sensing device in aqueous solutions leading to progressive desorption of the polyelectrolyte layers, which causes leaching of the immobilized PB [38]. This phenomenon appears to be exacerbated by higher temperatures.

The EDS analysis measured the content (i.e. weight percentage) of Fe in the coatings of fibers A to D. The histogram shown in Figure 5-7 presents the Fe content found in these fibers. This histogram shows that the Fe content in fiber B is lower than that in fiber A indicating an initial leach of the Prussian reagent. Fe content in fiber C follows the decreasing trend at a low magnitude slope. For fiber D, tested at 85 $^{\circ}\text{C}$, the drop in Fe content is dramatic. These results confirm the progressive loss of Fe from the multilayered structure, which is characteristic of the leaching of the immobilized Prussian reagent.

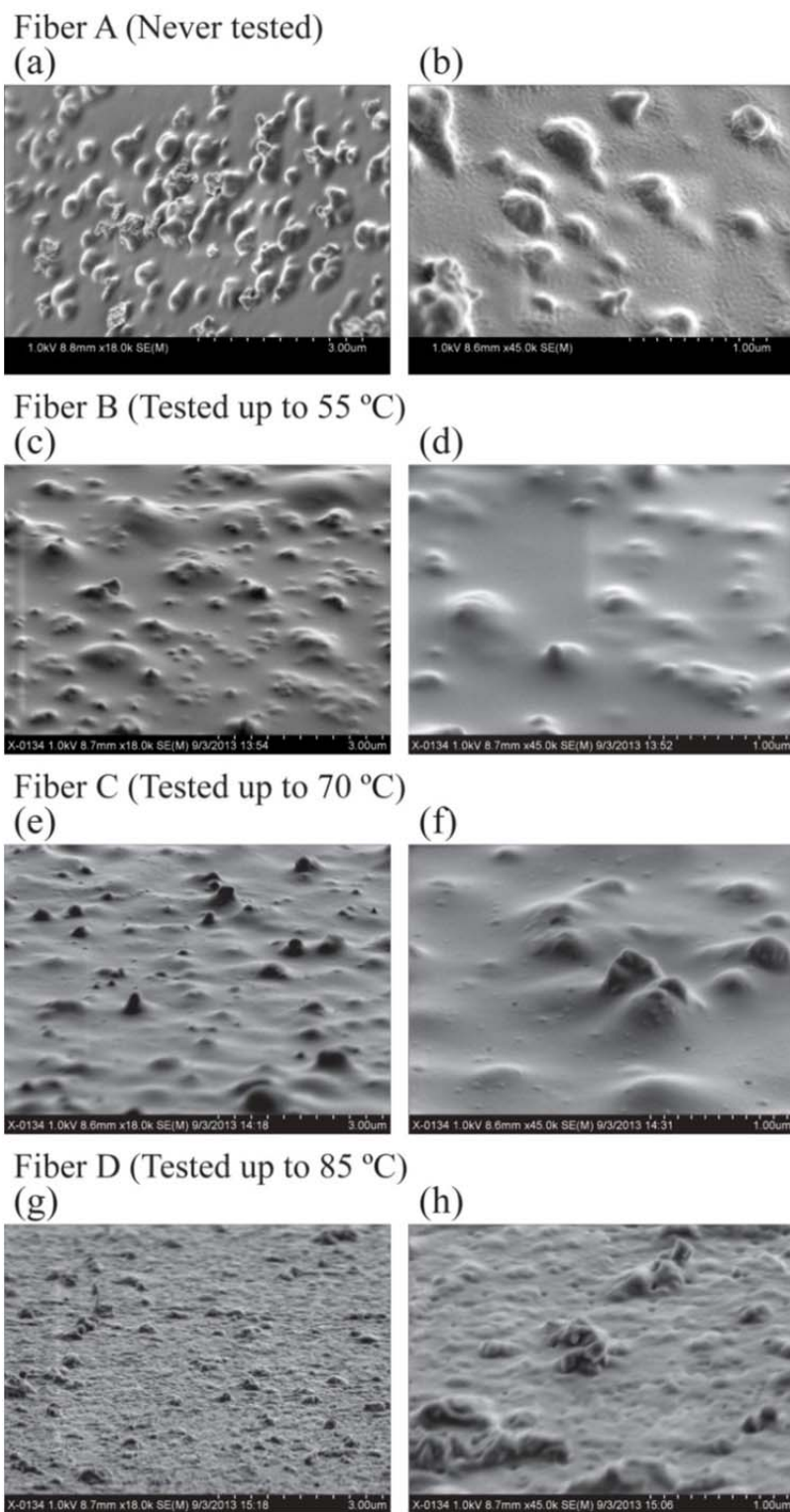


Figure 5-6: Scanning electron microscope images at 18,000X (left side) and 45,000X (right side) of fiber A (a), (b); fiber B (c), (d); fiber C (e), (f); and fiber D (g), (h)

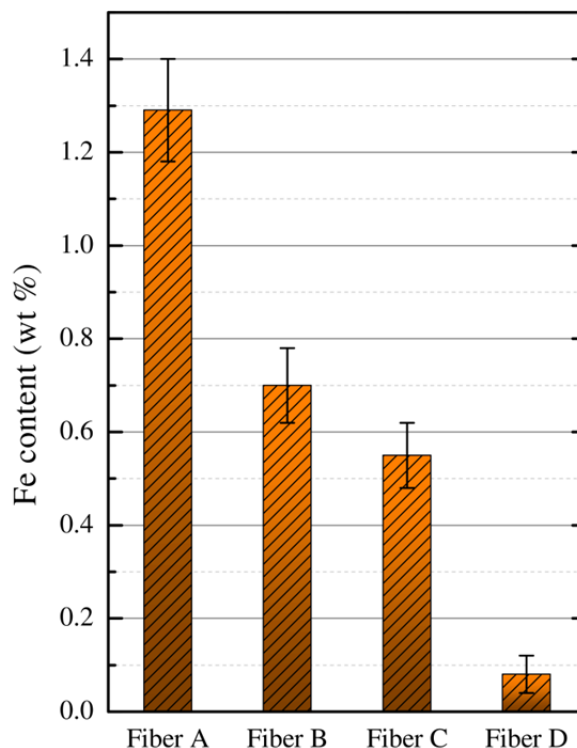


Figure 5-7: Weight percentage content of Fe in fibers A, B, C, and D

5.4 Conclusions

The thermal response of an optical fiber-based sensing device for the detection of hydrogen peroxide was investigated in terms of response and robustness. The sensing principle of this optical electrode relies on the change in intensity of the reflected light when Prussian white is oxidized back to the blue state due to the presence of hydrogen peroxide. The amplitude of the intensity of the reflected light is found to vary with the temperature. Nevertheless, the variability of the response times remains within the bounds expected for a solution at the tested concentration. In this case, the response time for solutions at a concentration of $100 \mu\text{M H}_2\text{O}_2$ (which is close to the detection limit of the electrochemical *in situ* technique) averaged 85 seconds with a standard deviation of 40%. The sensing device thus retains its capability for detecting and measuring H_2O_2 in liquid solutions at typical operating temperatures in PEMFCs.

Characterization of the sensing devices to determine damage that exposure to higher temperatures may cause to the coating was undertaken using a combination of Raman micro-spectroscopy, SEM imaging, and EDS analysis. The Raman spectroscopic analysis of the fibers showed a progressive reduction in the intensity of the cyanide stretching at 2150 cm^{-1} suggesting a progressive loss of the immobilized Prussian reagent. The SEM images revealed that for fibers that were subjected to tests at higher temperatures, the nodules of immobilized material within the multilayered structure become smaller and less densely distributed onto the surface of the optical fiber. Additionally, gradual roughening of the surface of the coating and the desorption of the deposited layers was observed. This was corroborated by EDS spectroscopy, that shows a small reduction in the weight percentage of Fe for the fiber subjected to tests at $55\text{ }^{\circ}\text{C}$, and a drastic reduction for the fiber tested at up to $85\text{ }^{\circ}\text{C}$.

The fiber tested at temperatures of up to $85\text{ }^{\circ}\text{C}$ showed degradation of the polyelectrolyte multilayer structure and the lowest wt% content of Fe, which indicates that the sensing device would not be suitable for continuous operation at this temperature. Nevertheless, the functionality of the sensing device still remain after multiple tests, even at high temperature, as demonstrated by the results of 40 redox cycles. The results suggest that sensor functionality is not impaired by PB leaching as long as a critical amount of PB remains actively bonded to the tip. Systematic characterization using larger batches of sensors will be required to fully assess the dependence of the signal-to-noise ratio of the reflected light to the morphology of the inner layer of the polyelectrolyte. The simplicity of this sensing system combined with its relative robustness and reusability make it a good candidate for minimally intrusive in-situ monitoring of hydrogen peroxide formation in operating PEMFCs. One drawback of this system is for continuous use in a PEMFC system is the redox nature of the sensor, which would require for instance the injection of the reductive agent to the sensing tip of the fiber, or the removal and replacement of the sensor. The low cost associated with the optical fiber and the reagents used would make the latter a feasible alternative, at least for laboratory studies.

Acknowledgments

This work was funded by the Natural Sciences and Engineering Research Council (NSERC) of Canada through the Strategic Grants program and supported by Ballard Power Systems. Thanks are due to Dr. Alexandre G. Brolo and his students Ms. Koh-Yiin Wang and Mr. Regivaldo Sobral-Filho from the Chemistry Department at the University of Victoria, for access to laboratory facilities and assistance with sample characterization. SEM images and EDS analysis were taken at the Advanced Microscopy Facility of the University of Victoria. Mr. Botero-Cadauid acknowledges the financial support provided by the Universidad Nacional de Colombia-Medellín campus and Colciencias Scholarship 466 of 2008.

Chapter 6: Fiber optic based sensor for H₂O₂ detection in PEMFC's

(Proceedings FDFC 2013, 5th International Conference Fundamentals & Development of Fuel Cells, Karlsruhe, Germany, April 16th-18th, 2013)

Preamble

Having demonstrated *ex situ* the capabilities of the sensor and characterized its response to temperature, in this chapter, as a first step toward *in situ* deployment in an operating PEMFC, we investigate the performance of the sensor when it is embedded in PFSA (Nafion) films, and discuss various *in situ* installation issues.

The body of this Chapter was published in the proceedings of FDFC 2013, the 5th International Conference on Fundamentals and Developments of Fuel Cells, Karlsruhe, Germany.

Abstract

Hydrogen peroxide (H₂O₂) is deemed to be a precursor of chemical degradation of perfluorosulfonic membranes in polymer electrolyte membrane fuel cells (PEMFCs) where it can decompose into radicals. The role and extent of radical peroxide attacks is poorly understood partly because of the difficulties in monitoring H₂O₂ *in situ*. We present an optical fiber sensor that relies on an absorptive optical technique for the detection of H₂O₂. The performance of the sensor is demonstrated by embedding it in a membrane. Processing of the sensor response is based on the rate of change of the reflected intensity, and *ex situ* experiments are presented showing the response time correlates log-linearly with concentration for both free and membrane-embedded sensor. The small diameter of the optical sensor makes it suitable for embedding in a membrane-electrode assembly or the gas channels of an operating PEMFC, eventually allowing minimally invasive *in situ* measurements and investigation of H₂O₂ formation.

6.1 Introduction

Hydrogen peroxide (H_2O_2) is a chemical compound with a high reactivity that plays an essential role in many chemical, industrial, medical, biological, and environmental processes [215]. H_2O_2 can occur as a by-product of the electrochemical reactions in a Polymer Electrolyte Membrane Fuel Cell (PEMFC) [220]. The production sites of H_2O_2 in a PEMFC have not been well determined yet, but its presence has been confirmed in the exhaust gases, the drain water, and the ionomeric membrane through electrochemical techniques [6, 12, 23].

The role that H_2O_2 plays in the degradation of Nafion[®] membranes has been extensively studied; particularly, since it is believed that H_2O_2 promotes the formation of the radicals hydroxyl ($\text{HO}\cdot$) and hydroperoxyl ($\text{HOO}\cdot$), both linked to the accelerated chemical degradation of Nafion[®] [7, 13, 20, 22, 221, 224-226].

Because the rate of production of H_2O_2 in a PEMFC is estimated to reach values of only up to 0.7×10^{-6} moles $\text{cm}^{-2} \text{s}^{-1}$ [18]—leading to very low concentrations in the exhaust water—, colorimetry, titration, and other conventional techniques are not suitable to perform its detection. Electrochemical techniques, though well suited to determining small concentrations of H_2O_2 , can be susceptible to electromagnetic interference in environments such as those found in the electrolyte and electrodes of a PEMFC. Furthermore, conductive materials could interfere with the operating conditions of the fuel cell itself.

Alternatively, optical spectroscopic techniques such as chemiluminescence, fluorescence, and absorptive techniques, can also be used for detecting low concentrations of H_2O_2 [29]. One of the main features of these optical techniques lies on the possibility of being mounted on platforms such as optical fibers, which minimize the size of the sensing system, are immune to electromagnetic interferences, and allow remote detection in a minimally intrusive way.

6.1.1 Sensing mechanism

In this work, the mechanism of detection of H_2O_2 relies on the changes of absorbance of the metallic hexacyanoferrate compound Prussian blue (PB). PB can be chemically reduced to a compound named Prussian white (PW) in the presence of strong reducing agents such as ascorbic acid [85]. In a similar manner, the chemical oxidation of PW can be achieved by exposing it to H_2O_2 which makes it revert back to PB.

This redox reaction is the key on the detection of H_2O_2 , and due to its absorbance properties it has been used in optical biosensors [85, 87, 104, 235]. The spectrum of absorbance of PW in the visible range of wavelengths is practically negligible, and conversely, PB has a strong absorbance in the 400–900 nm range of the spectrum with a maximum of absorbance at 720 nm. Furthermore, the absorbance of PB enhances in media with lower pH values [87]. This last feature suggests its possible use in PEMFCs, where the electrolyte is often an acidic medium.

6.1.2 Prussian blue immobilization on the optical fiber

The deposition of polyelectrolytes by electrostatic self-assembly (ESA) in a layer-by-layer (LbL) technique allows the fabrication of nano-sized films. This technique of deposition is based on the immersion of an electrostatically charged surface on a solution of a polyelectrolyte with the opposite electrical charge. Due to the interaction of electrostatic forces, the polyelectrolyte is adsorbed onto the surface until the charge is neutralized, creating an externally charged layer onto the new surface. By immersing the material into a solution with a counter polyelectrolyte a new film is adsorbed. Iterating this procedure leads to the fabrication of a multi-layer structure [95].

The simplicity of the ESA LbL deposition makes it possible to apply multi-layered structures to complex geometries regardless of their size; by adding compounds to the polyelectrolyte solutions it is possible to achieve the immobilization of those compounds within the built structure [29, 90, 111, 238].

Employing the ESA LbL technique, Del Villar and co-workers [38, 40] deposited a multi-layered structure immobilizing PB onto the tip of an optical fiber and proved the feasibility of an optical fiber sensor for H_2O_2 . The authors of the present work recently presented a sensing device based on the immobilization of PB onto the tip of an optical fiber following Del Villar's procedures. We obtained more reproducible results, and found an exponential behavior indicating that the detection of H_2O_2 occurs in a diffusive nature, and showed on that basis that it is possible to determine the concentration of the H_2O_2 [244]. Figure 6-1 illustrates the sensing mechanism of H_2O_2 immobilized onto the tip of the optical fiber in the multi-layered structured of ESA LbL polyelectrolytes.

In this work, the previously developed optical fiber sensing probe was embedded within a 50- μm thickness Nafion[®] membrane to determine whether or not the sensing capabilities of the PB/PW system remain after the embedding process. Understanding this is crucial for the development of H_2O_2 sensors suitable for *in-situ* deployment in PEMFC's. These experiments also allow analysis of the diffusive processes and the conditions involved in the production of H_2O_2 in these devices.

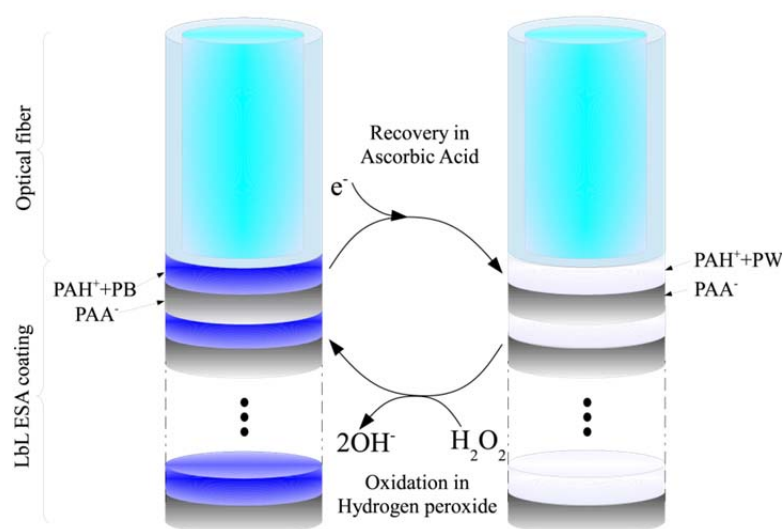


Figure 6-1: Scheme of PB/PW system immobilized on the tip of the optical fiber illustrating the sensing mechanism of the H_2O_2 and the recovery stage in ascorbic acid [244]

6.2 Materials and methods

6.2.1 Materials

The ESA LbL process used Poly(allilamine hydrochloride) (PAH⁺, $M_w \approx 15000$, product No. 283215) and Poly(styrene sulfonate) (PSS⁻, $M_w \approx 70000$, product No. 24305-1) as the cationic and anionic polyelectrolytes, and Prussian blue soluble (product No. 03899) as the sensing dye. All purchased from Sigma-Aldrich (Oakville, ON, Canada). Hydrogen Peroxide, 30 wt% (ACP Chemicals) was used to prepare the H₂O₂ solutions at different concentrations, as well as to prepare the cleansing solution by mixing it in a 1:3 ratio with Sulfuric Acid, 98 wt% (H₂SO₄) (EMD Chemicals, Gibbstown, NJ).

Glacial Acetic Acid (Anachemia) and Sodium Acetate Tryhydrate (ACP Chemicals) were employed to prepare an acetate buffer solution at pH 4.0. This buffer solution was used as the solvent to prepare both the H₂O₂ solutions at different concentrations and the recovery solution at a concentration of 0.04 mol L⁻¹ of *L*-Ascorbic Acid (Aldrich, product No. 25,556-4). All chemicals were used as received without further purification. The water in the experiments was purified with a four-cartridge system of purification (Super-Q Plus, Millipore, Billerica, MA) and had a resistivity of 18.2 MΩ.

The optical fiber employed was a multi-mode optical fiber SFS105/125Y from Thorlabs (Newton, NJ), made of silica, with core and cladding sizes of 105 and 125 μm, respectively. Nafion untreated membranes N-212 with a thickness of 50 μm used for embed the optical fiber sensing probe were from Fuel Cell Store, Inc. (Boulder, CO).

6.2.2 Sensing film deposition

The optical fiber tip was coated in a multi-layered structure of polyelectrolytes after being cleaved and thoroughly cleansed for 30 min in a solution of 1:3 ratio of H₂O₂ and H₂SO₄. This solution is commonly known as piranha. Besides the cleansing action, this solution produces a negatively charged surface due to the activation of hydroxyl groups (OH⁻) on the silica. PAH⁺ and PB were mixed in solution with a concentration of 2.0 and 2.5 mg mL⁻¹, PSS⁻ was prepared with a concentration of 2.0 mg mL⁻¹. The pH values of

these solutions were adjusted to 4.0 using Hydrochloric acid (HCl) and Sodium Hydroxide (NaOH) solutions as required.

The deposition of the multi-layered film proceeded by immersing the negatively charged surface into the PAH⁺+PB solution for ca. 15 min, followed by the rinsing of the excess of material in distilled water, and the immersion in the PSS⁻ solution for a similar amount of time. After Del Villar et al. [39], 17 bilayers of PAH⁺+PB and PSS⁻ were deposited followed by two capping bilayers of polyelectrolytes in solution with the same concentration but with a pH of 5.5 and with no mixing of PB. The use of capping bilayers reduces the leaching of the dye [39, 98].

The multi-layered structure was annealed at 100 °C for two hours and stored at room temperature for at least one week prior to testing.

6.2.3 Instrumentation and measurement of the changes in absorbance

The absorbance measurements of the PB/PW system immobilized on the tip of the fiber were performed using the experimental setup illustrated in Figure 6-2. The output of the white light source (LS-1, OceanOptics, Dunedin, FL) was connected to the arm 1 of the bifurcated optical fiber (BIF200-UV-Vis, OceanOptics), carrying the light to the common arm and to the multi-layered structure on the optical fiber sensing probe. Depending on the performed test, the optical fiber is either free or embedded within the Nafion[®] membrane. The reflected light is also carried back by the common arm to the arm 2 of the bifurcated optical fiber, and is collected and measured by the optical fiber spectrometer (USB2000, OceanOptics). The intensity of this reflected light is measured over the 370-950 nm range and integrated in the same range using the SpectraSuite software (OceanOptics) at a rate of 500 ms.

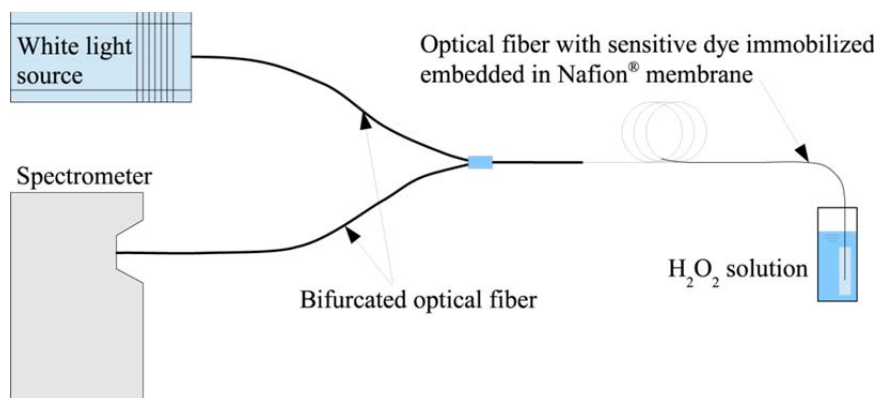


Figure 6-2: Experimental setup to measure the absorbance response from the Prussian blue coated tip of the optical fiber

6.2.4 Test procedures

Two different situations were tested. The optical fiber with the multi-layered structure and immobilized PB was subjected to alternative stages of recovery and oxidation in ascorbic acid and H₂O₂ solutions, respectively. The sensor was initially subjected to a recovery stage in ascorbic acid allowing the PB to be reduced to PW. The optical fiber was maintained immersed in this reducing solution until the intensity plateaued. The fiber was then placed in a vial with a solution of H₂O₂ at a known concentration and kept immersed again until the signal reached a stable level. Different concentrations of H₂O₂ solutions were tested ranging from 50×10^{-6} to 1.5×10^{-3} mol L⁻¹.

After performing the initial detection test, the fiber was embedded within two pieces of 2×2 cm of N-212 Nafion® membrane. The embedding procedure was performed using a bench top heated press (Carver, Wabash, IN). The optical fiber probe was placed within two pieces of the Nafion® membrane and externally protected by two pieces of Teflon® sheet with a thickness of .018" (0.46 mm). A pressure of 0.5 MPa, with hot plates temperatures of 150 °C was applied to this sandwich for 45 seconds. Figure 6-3 illustrates the embedded optical fiber within the Nafion® membrane.



Figure 6-3: Embedded optical fiber sensing device within the Nafion[®] membrane.

A second set of tests were performed to the optical fiber after the embedding in the Nafion[®]. The membrane was immersed in ascorbic acid and H₂O₂ solutions, and the intensity of the reflected light was recorded.

6.2.5 Response time determination

The reflected intensities from the tests performed in each H₂O₂ solution were fitted to an inverse exponential curve of the form:

$$I(t) = I_0 + I_{\text{sat}} - A \exp\left(-\frac{t}{\tau}\right), \quad (6.1)$$

where $I(t)$ is the reflected intensity at the time t ; I_0 is the initial intensity at immersion in the H₂O₂ solution; I_{sat} is the intensity at saturation; A is a constant that depends on the geometry and the diffusion parameters; and τ is the time constant corresponding to the signal reaching $\approx 63\%$ of I_{sat} . In order to perform this exponential fit, the time axis was zeroed at the immersion of the sensing probe in the H₂O₂ solution.

6.3 Results

Figure 6-4 presents the normalized reflected intensity from the optical fiber probe for three different concentrations of H_2O_2 solutions in both tests, before and after embedding in the Nafion[®] membrane. The maximum intensity is reached at different time scales for each concentration, with faster response as the concentration increases in both test cases. Furthermore, Figure 6-4(a) shows that the fiber without Nafion[®] exhibits a rapid increase in the reflected intensity within the first few seconds of immersion, followed by a gradually slower increase till saturation. In the case of the embedded sensor, Figure 6-4(b) the rate of increase is markedly lower for the lower concentrations.

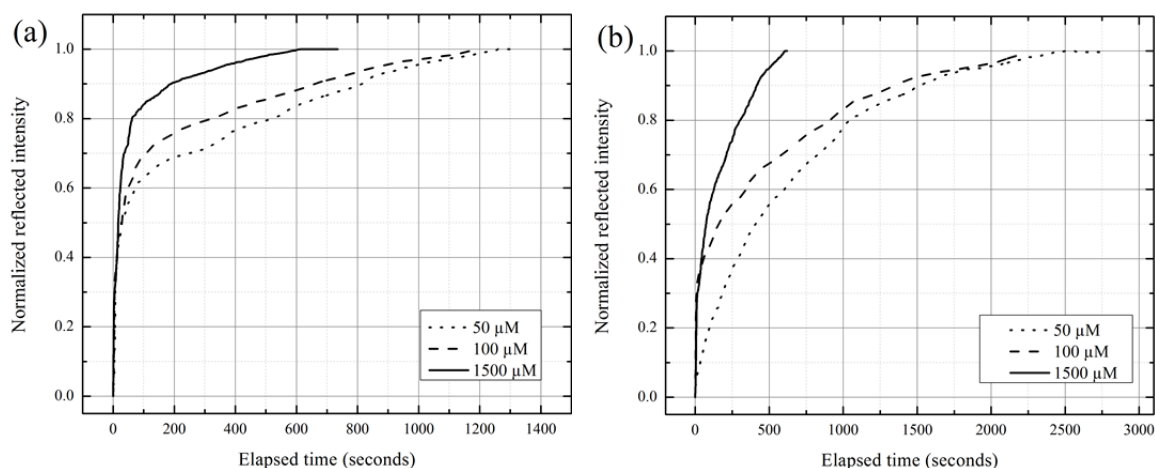


Figure 6-4: Reflected intensity to different concentrations of H_2O_2 solutions (a) Sensing fiber without Nafion[®] and (b) Sensing fiber embedded in Nafion[®]

The response time deduced from the exponential is shown in Figure 6-5 on a log–log scale; the slopes and correlation coefficient are presented in the figure for both test cases.

6.4 Discussion and conclusions

The responses for the reflected intensities in both test cases show an inverse exponential behavior to reach the saturation as seen in Figure 6-4. A reduction in the required time for the intensity to reach the saturation was observed when the concentration of the H_2O_2 solution increases. This behavior indicates that the phenomenology of the

process involved in the detection of H_2O_2 is of a diffusive nature. The diffusion occurs solely within the multi-layer structure of polyelectrolytes in the free fibre case, and through the Nafion[®] membrane and the polyelectrolyte structure for the second case.

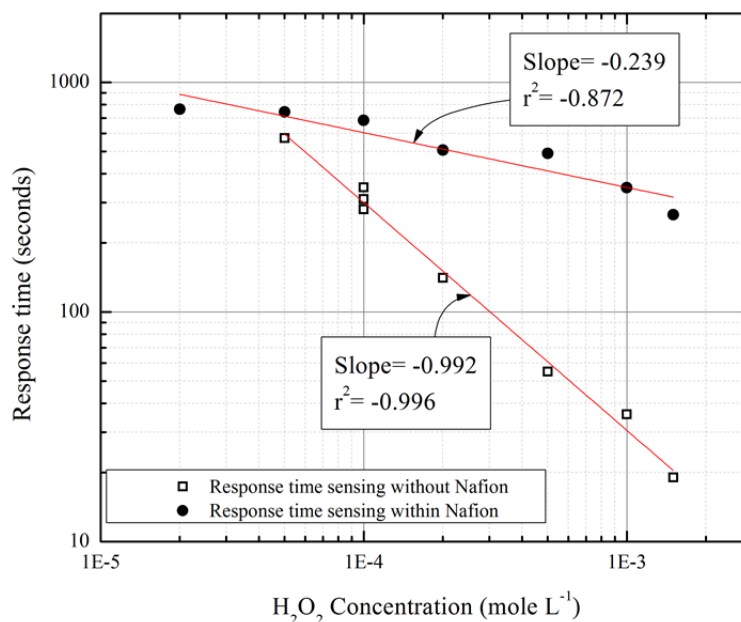


Figure 6-5: Response time for the sensing probe without and within the Nafion[®] membrane

For the case of the fiber without the membrane, a linear correlation between the concentration of the H_2O_2 solution and the response time for the intensity to reach 63% of its saturation value was determined from log-log plots, corroborating the exponential nature of the response characteristic of diffusive processes. For the fiber embedded in Nafion[®] membrane, the linear trend persists, however, the changes in the response time vary much more gradually with higher concentrations, but similar response times were observed for solutions with low concentrations.

The technique of immobilization of the PB/PW system and the tests presented here demonstrate the functionality of the H_2O_2 optical sensors for embedded measurements. Furthermore, the results showed that the embedding process in the Nafion[®] using the hot

pressing does not compromise the sensing capabilities of the optical fiber probe, or damage the Prussian blue coating as observed in Figure 6-3; rather, the response time increases due to the additional diffusive barrier. The *ex-situ* tests presented here pave the way for *in-situ* deployment in PEMFCs planned next to allow better understanding of the mechanisms that promote the H₂O₂ formation, and the eventual use of such sensors as a diagnostic tool in fuel cells.

6.5 Nomenclature

I	Intensity of reflected light	(counts)	Subscripts	
A	Geometric and diffusion constant	(counts)	0	initial
τ	Constant time	(seconds)	sat	saturation

Acknowledgements

This research work was funded by the Natural Sciences and Engineering Research Council (NSERC) of Canada through the Strategic grants program and supported by Ballard Power Systems. J.F. B-C acknowledges the financial support of Universidad Nacional de Colombia–Medellín campus, to pursue his Ph.D. studies.

Chapter 7: Contributions, Conclusions, and future work

The overarching objective of this dissertation was to design and develop optical fiber sensors capable of detecting hydrogen peroxide in small quantities such as those produced in polymer electrolyte membrane fuel cells (PEMFCs).

The results of three completed studies were presented in the form of manuscripts included as Chapters 4 to 6, and preliminary results documenting an initial approach to the detection of hydrogen peroxide in vapor phase are presented in Appendix D. This chapter provides a synopsis of the methods, key results, and links between the components of the work of this dissertation, and closes with the conclusions and recommendations for future work in the development of the optical fiber sensors for detection *in situ* of hydrogen peroxide in PEMFCs.

7.1 Detection of hydrogen peroxide using an optical fiber-based sensing probe

The primary objective of this study was to develop and demonstrate an optochemical technique for detection of hydrogen peroxide, its integration in an optical fiber as supporting platform, and the characterization and validation of the prototype sensors. This characterization and validation was a critical first step in the proof-of-concept and demonstration of the technique of reagents immobilization and of the protocol for measurement and determination of the concentration of hydrogen peroxide in solution.

Prior to this work, there was only one report of optical fiber sensors for detecting hydrogen peroxide at the levels of concentrations and pH that are relevant to PEMFCs [38, 40]. That work, however, did not completely resolve the phenomenology of detection mechanisms and consequently suffered from inaccuracy in determining the concentration of hydrogen peroxide in solution.

The experimental work presented in the thesis was focused initially on the development of an adequate technique to immobilize the reagents on the tip of the optical fibers. Appendix C: describes the detailed procedure for immobilization of Prussian blue on the tip of optical fibers to create a sensing film.

Once the immobilization of the reagents was successful, the experimental work focused on using this sensing film to detect small concentrations of hydrogen peroxide in solution based on the analysis of the reflected light intensity. As part of this work, a model of the reflected intensity as a function of the elapsed time since immersion of the sensor was presented. The functional relationship follows an inverse exponential behavior, which is consistent with the diffusivity mechanism of transport of hydrogen peroxide through the sensing film.

A key finding of this work was the linear relationship in a log-log scale between the concentration of hydrogen peroxide in the solution and the response time of each test performed (the time for the signal to reach 63% of its maximum intensity). This result makes it possible not only to detect, but also to measure the concentration of hydrogen peroxide in solution.

7.2 Temperature response and durability characterization of an optical fiber sensor for detection of hydrogen peroxide

Following the proof of concept and initial characterization, the work next examined the response of the optical fiber sensors to temperature.

Temperature is a key operating parameter that greatly influences the performance of PEMFCs. The experimental work therefore focused on reproducing the environmental conditions relevant to an operating PEMFC, and testing how changes in temperature affected the response of the sensor to hydrogen peroxide in solution.

To gain insight in the sensor durability, characterization was performed using scanning electron microscopy (SEM) imaging, energy dispersive X-ray spectroscopy (EDS), and Raman micro spectroscopy (RMS). To investigate the extent of temperature related degradation, optical fiber sensors were tested at various temperatures and measurement of the content of the sensing reagent (in this case Prussian blue) were performed.

The key findings of this study were: 1) the amplitude of the reflected intensity varies quadratically with temperature; 2) degradation of the sensing film increases with

temperature, as indicated by a reduction of the content of iron in the coating and the disappearance of the cyanide peaks in the Raman spectrum; both phenomena associated with the desorption of the Prussian blue from the optical fiber surface; 3) the sensor retains its sensing properties regardless of temperature and in spite of the sensing film degradation; and 4) the sensor remains operational after nearly 40 redox cycles at various temperatures.

7.3 Fiber optic based sensor for H₂O₂ detection in PEMFCs

The objective of this part of the work, presented in Chapter 6: , was to determine the response of the optical fiber sensor once it is embedded in a film of PFSA membrane (Nafion) typically used in the core of PEMFC membrane-electrode assembly. The importance of this study rests on determining the viability of placing the sensors of hydrogen peroxide directly in the media in which this chemical species is believed to be formed in the operating PEMFC.

The experiments were focused first on determining the proper parameters with the hot pressing technique (temperature, pressure, and time) to achieve homogeneous embedding of the optical fiber sensor within the Nafion membrane; and second, to test the response of the sensor to solutions of hydrogen peroxide at different concentrations and compare the results with those obtained in *ex situ* tests.

It was found that the fabricated optical fiber sensors can withstand the embedding process. In addition, it was observed that the diffusion processes that take place in the detection of hydrogen peroxide are slower as a consequence of the additional layer of membrane material that the species have to diffuse through to reach the reaction sites. The work also allowed verification that the log-log linear behavior between hydrogen peroxide concentration and the response time remains in the embedded sensors.

7.4 Conclusions

The general objective of this dissertation was to develop sensors to detect and quantify hydrogen peroxide in concentrations and conditions that are relevant to operating polymer electrolyte membrane fuel cells (PEMFCs), and to provide a basis for eventually deploying

such sensor *in situ* in combination with other sensors (e.g. for temperature and relative humidity) to provide researchers and fuel cell manufacturers with information about the conditions, mechanisms and rates that promote degradation, and specifically hydrogen peroxide formation rates in PEMFCs. Such insights will help improve the durability of these devices.

The work in this dissertation spanned optics, chemistry, design, material science, and required to a thorough understanding of the operation of PEMFCs. Sensors were designed and built using operating principles and immobilization techniques that are fully compatible with the environmental conditions found in PEMFCs. In addition, the use of optical fibers avoids undesired interferences with the operation of a fuel cell.

In the broader context of understanding the degradation mechanisms that affect the durability of PEMFCs, the sensors presented in this dissertation could be used to answer open questions that cannot be answered through exhaust stream measurements of hydrogen peroxide or by using electrochemical techniques. Because the sensors are built on the tip of an optical fiber, they can be deployed in a minimally invasive manner in a PEMFC to provide *localized* measurements.

The characteristics of the developed sensor are also desirable for other applications in fields such as environmental, defense, and biological processes.

7.5 Future work

A number of research avenues should be explored to eventually allow *in situ* deployment of the sensors in an operating PEMFC. These include:

- Additional parametric studies to fully establish the durability of the developed sensors. These studies could include experiments with fibers prepared under the same conditions and tested at multiple isothermal conditions to determine the number of redox tests that each fiber can undergo until its failure.
- The Prussian blue/Prussian white system proved to provide a reliable detection mechanism for hydrogen peroxide in small concentrations. However, the

immobilization technique yields films that lack robustness at high temperature. Alternative methods that may include sol-gel and other film deposition techniques should be explored to improve the durability of the sensors.

- Integration of the sensors in a PEMFC to perform *in situ* detection of hydrogen peroxide. This can be achieved with minimal modification of the PEMFC flow field plates and gaskets as illustrated in Figure 7-1.

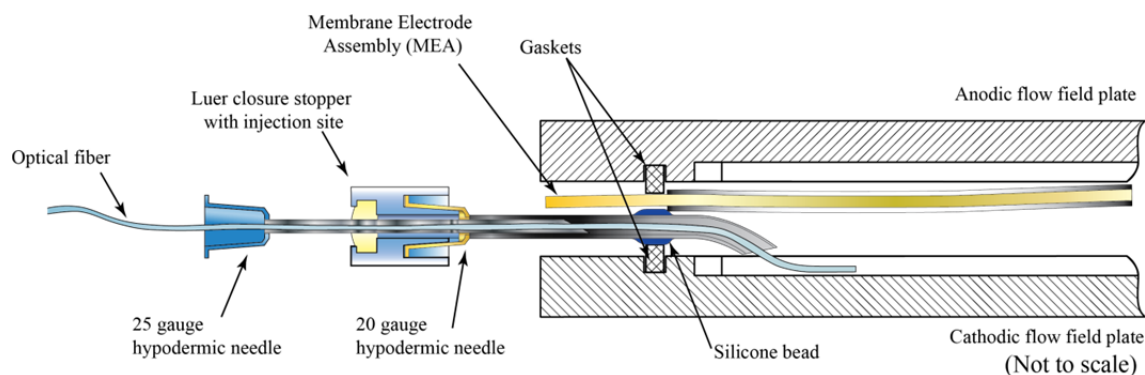


Figure 7-1: Insertion technique of an optical fiber sensor for *in situ* detection of H_2O_2 in a PEMFC

This insertion method can be adjusted to the dimensions of an optical fiber sensor developed in a 125 μm diameter multimode optical fiber. The anodic and cathodic flow field plates would require a recessing channel that allows the needle to be placed within the two plates without affecting the spacing and the clamping pressure on the MEA. In the case of a 20 gauge hypodermic needle as displayed in the figure, these recessing channels could be semi cylinders with a diameter slightly over 0.908 mm (external diameter of the needle size). To ensure adequate sealing, a pliable material can be used around the needle. Additionally, after the fiber insertion, the interior needle could be retracted beyond the Luer stopper providing sealing at this stage.

Bibliography

- [1] I. EG & G Technical Services, *Fuel Cell Handbook*, 7th ed. U.S. Department of Energy, 2004.
- [2] M. M. Mench, *Fuel cell engines*. John Wiley & Sons, 2008.
- [3] N. Djilali, “Computational modelling of polymer electrolyte membrane (PEM) fuel cells: Challenges and opportunities,” *Energy*, vol. 32, no. 4, pp. 269 – 280, 2007, eCOS 05. 18th International Conference on Efficiency, Cost, Optimization, Simulation, and Environmental Impact of Energy Systems - ECOS 05.
- [4] M. Inaba, “Chemical degradation of perfluorinated sulfonic acid membranes,” in *Polymer Electrolyte Fuel Cell Durability*, F. N. Büchi, M. Inaba, and T. J. Schmidt, Eds. Springer New York, 2009, pp. 57–69.
- [5] X. Cheng, Z. Shi, N. Glass, L. Zhang, J. Zhang, D. Song, Z.-S. Liu, H. Wang, and J. Shen, “A review of PEM hydrogen fuel cell contamination: Impacts, mechanisms, and mitigation,” *Journal of Power Sources*, vol. 165, pp. 739–756, 2007.
- [6] M. Inaba, T. Kinumoto, M. Kiriake, R. Umebayashi, A. Tasaka, and Z. Ogumi, “Gas crossover and membrane degradation in polymer electrolyte fuel cells,” *Electrochimica Acta*, vol. 51, pp. 5746–5753, 2006.
- [7] T. Kinumoto, M. Inaba, Y. Nakayama, K. Ogata, R. Umebayashi, A. Tasaka, Y. Iriyama, T. Abe, and Z. Ogumi, “Durability of perfluorinated ionomer membrane against hydrogen peroxide,” *Journal of Power Sources*, vol. 158, pp. 1222–1228, 2006.
- [8] X. Fang, P. K. Shen, S. Song, V. Stergiopoulos, and P. Tsiakaras, “Degradation of perfluorinated sulfonic acid films: An *in-situ* infrared spectro-electrochemical study,” *Polymer Degradation and Stability*, vol. 94, pp. 1707–1713, 2009.
- [9] M. Inaba, H. Yamada, J. Tokunaga, R. Umebayashi, K. Maytzuzawa, A. Hatnaka, and A. Tasaka, “Hydrogen peroxide formation as a degradation factor of polymer eletrolyte fuel cells,” in *Proton conducting membrane fuel cells, 208th ECS meeting*, M. Murthy,

K. Ota, J. W. Van Zee, S. R. Narayanan, and E. S. Takeuchi, Eds., vol. 21. ElectroChemical Society, 2004, pp. 370–379.

[10] E. Yeager, “Electrocatalysts for O₂ reduction,” *Electrochimica Acta*, vol. 29, no. 11, pp. 1527–1537, 1984.

[11] A. B. LaConti, M. Hamdan, and R. C. McDonald, “Mechanisms of membrane degradation,” in *Handbook of fuel cells: Fundamentals, technology, and applications*. Wiley, 2003, vol. 5, ch. 49, pp. 647–662.

[12] K. Teranishi, K. K. S. Tsushima, and S. Hirai, “Degradation mechanism of PEMFC under open circuit operation,” *Electrochemical and Solid-State Letters*, vol. 9, no. 10, pp. A475–A477, 2006.

[13] H. Liu, H. A. Gasteiger, A. Laconti, and J. Zhang, “Factors impacting chemical degradation of perfluorinated sulfonic acid ionomers,” *ECS Transactions*, vol. 1, no. 8, pp. 283–293, 2006.

[14] G. Scatchard, G. M. Kavanagh, and L. B. Ticknor, “Vapor-Liquid equilibrium. VIII. Hydrogen peroxide - Water mixtures,” *Journal of the American Chemical Society*, vol. 74, no. 15, pp. 3715–3720, 1952.

[15] H. Hwang and P. K. Dasgupta, “Thermodynamics of the hydrogen peroxide - water system,” *Environmental Science & Technology*, vol. 19, no. 3, pp. 255–258, 1985.

[16] J. Takagi and K. Ishigure, “Thermal decomposition of hydrogen peroxide and its effect on reactor water monitoring of boiling water reactors,” *Nuclear Science and Engineering*, vol. 89, no. 2, pp. 177–186, 1985.

[17] W. C. Schumb, “Stability of concentrated hydrogen peroxide solutions,” *Industrial and Engineering Chemistry*, vol. 41, no. 5, pp. 992–1003, 1949.

[18] V. A. Sethuraman, J. W. Weidner, A. T. Haug, S. Motupally, and L. V. Protsailo, “Hydrogen peroxide formation rates in a PEMFC anode and cathode,” *Journal of The Electrochemical Society*, vol. 155, no. 1, pp. B50–B57, 2008.

- [19] W. A. Pryor, *Free radicals*, ser. Series in Advanced Chemistry. McGraw-Hill, 1966.
- [20] V. O. Mittal, H. R. Kunz, and J. M. Fenton, "Is H_2O_2 involved in the membrane degradation mechanism in PEMFC?" *Electrochemical and Solid-State Letters*, vol. 9, no. 6, pp. A299–A302, 2006.
- [21] A. Collier, H. Wang, X. Z. Yuan, J. Zhang, and D. P. Wilkinson, "Degradation of polymer electrolyte membranes," *International Journal of Hydrogen Energy*, vol. 31, pp. 1838–1854, 2006.
- [22] H. Tang, S. Peikang, S. P. Jiang, F. Wang, and M. Pan, "A degradation study of Nafion proton exchange membrane of PEM fuel cells," *Journal of Power Sources*, vol. 170, pp. 85–92, 2007.
- [23] W. Liu and D. Zuckerbrod, "*In situ* detection of hydrogen peroxide in PEM fuel cells," *Journal of The Electrochemical Society*, vol. 152, no. 6, pp. A1165–A1170, 2005.
- [24] A. B. Anderson and T. V. Albu, "Catalytic effect of platinum on oxygen reduction. An *ab initio* model including electrode potential dependence," *Journal of The Electrochemical Society*, vol. 147, no. 11, pp. 4229–4238, 2000.
- [25] C. T. Kingzett, "Report on the atmospheric oxidation of phosphorus and some reactions of ozone and hydric peroxide," *Journal of the Chemical Society, Transactions*, vol. 37, pp. 792–807, 1880.
- [26] —, "On the estimation of peroxide of hydrogen," *Analyst*, vol. 13, pp. 62–63, 1888.
- [27] W. M. Dehn, "A gasometric method for the determination of hydrogen peroxide," *Journal of the American Chemical Society*, vol. 29, no. 9, pp. 1315–1319, 1907.
- [28] A. J. Guwy, F. R. Hawkes, S. R. Martin, D. L. Hawkes, and P. Cunnah, "A technique for monitoring hydrogen peroxide concentration off-line and on-line," *Water Research*, vol. 34, no. 8, pp. 2191–2198, 2000.

- [29] I. Del Villar, I. R. Matías, F. J. Arregui, and R. O. Claus, “ESA based fiber-optic sensor for continuous detection of hydrogen peroxide concentration,” in *Sensors, 2003. Proceedings of IEEE*, vol. 1, October 22-24 2003, pp. 393–396.
- [30] J. H. T. Luong, A. L. Nguyen, and G. G. Guilbault, “The principle and technology of hydrogen peroxide based biosensors,” in *Advances in Biochemical Engineering / Biotechnology*, A. Fietcher, Ed. Berlin / Heidelberg: Springer, 1993, vol. 50, pp. 85–115.
- [31] S. Yin, C. Zhan, and P. B. Ruffin, “Fiber optic bio and chemical sensors,” in *Fiber optic sensors*, 2nd ed., S. Yin, P. B. Ruffin, and F. T. Yu, Eds. CRC Press, 2008.
- [32] P. A. Giguère and P. Geoffrion, “Refractive index of hydrogen peroxide solutions. A revision,” *Canadian Journal of Research*, vol. 27, no. Sec. B, pp. 168–173, 1949.
- [33] E. Pick and Y. Keisari, “A simple colorimetric method for the measurement of hydrogen peroxide produced by cells in culture,” *Journal of Immunological Methods*, vol. 38, pp. 161–170, 1980.
- [34] P. Tanner and A. Wong, “Spectrophotometric determination of hydrogen peroxide in rainwater,” *Analytica Chimica Acta*, vol. 370, pp. 279–287, 1998.
- [35] M. Mizoguchi, M. Ishiyama, M. Shiga, and K. Sasamoto, “Water-soluble chromogenic reagent for colorimetric detection of hydrogen peroxide—an alternative to 4-aminoantipyrine working at a long wavelength,” *Analytical Communications*, vol. 35, pp. 71–73, 1998.
- [36] C. Gay and J. M. Gebicki, “A critical evaluation of the effect of sorbitol on the ferric-xylenol orange hydroperoxide assay,” *Analytical Biochemistry*, vol. 284, pp. 217–220, 2000.
- [37] A. Lobnik and M. Cajlakovic, “Sól-gel based optical sensor for continuous determination of dissolved hydrogen peroxide,” *Sensors and Actuators B Chemical*, vol. 74, no. 1-3, pp. 194 – 199, 2001, proceedings of the 5th European Conference on Optical Chemical Sensors and Biosensors.

- [38] I. Del Villar, I. R. Matías, F. J. Arregui, and R. O. Claus, "ESA-based in-fiber nanocavity for hydrogen-peroxide detection," *IEEE Transactions on Nanotechnology*, vol. 4, no. 2, pp. 187–193, Mar. 2005.
- [39] ———, "Fiber-optic hydrogen peroxide nanosensor," *IEEE Sensors Journal*, vol. 5, no. 3, pp. 365–371, 2005.
- [40] I. Del Villar, I. R. Matías, F. J. Arregui, J. Echeverría, and R. O. Claus, "Strategies for fabrication of hydrogen peroxide sensors based on electrostatic self-assembly (ESA) method," *Sensors and Actuators B Chemical*, vol. 108, pp. 751–757, 2005.
- [41] A. M. Smith, "Materials Interactions in Optical Fiber Sensors," in *Optical Fiber Sensors*, J. Dakin and B. Culshaw, Eds. Artech House, 1988, vol. 1: Principles and Components, ch. 6, pp. 189–208.
- [42] M. Zhou, Z. Diwu, N. Panchuk-Voloshina, and R. P. Haugland, "A stable nonfluorescent derivative of resorufin for the fluorometric determination of trace hydrogen peroxide: Applications in detecting the activity of phagocyte NADPH oxidase and other oxidases," *Analytical Biochemistry*, vol. 253, pp. 162–168, 1997.
- [43] R. K. Root, J. Metcalf, N. Oshino, and B. Chance, "H₂O₂ release from human granulocytes during phagocytosis. I. Documentation, quantitation, and some regulating factors," *Journal of Clinical Investigation*, vol. 55, pp. 945–955, 1975.
- [44] W. Ruch, P. H. Cooper, and M. Baggiolini, "Assay of H₂O₂ production by macrophages and neutrophils with homovanillic acid and horse-radish peroxidase," *Journal of Immunological Methods*, vol. 63, pp. 347–357, 1983.
- [45] J. A. Royall and H. Ischiropoulos, "Evaluation of 2',7'-dichlorofluorescein and dihydrorhodamine 123 as fluorescent probes for intracellular H₂O₂ in cultured endothelial cells," *Archives of Biochemistry and Biophysics*, vol. 302, no. 2, pp. 348–355, 1993.
- [46] F. Wang, F. Schubert, and H. Rinneberg, "A fluorometric rate assay of hydrogen peroxide using immobilized peroxidase with a fibre-optic detector," *Sensors and Actuators B Chemical*, vol. 28, pp. 3–7, 1995.

- [47] N. Jie, J. Yang, X. Huang, R. Zhang, and Z. Song, "Fluorometric determination of hydrogen peroxide in water using acetaminophen," *Talanta*, vol. 42, pp. 1575–1579, 1995.
- [48] H. Maeda, Y. Fukuyasu, S. Yoshida, M. Fukuda, K. Saeki, H. Matsuno, Y. Yamauchi, K. Yoshida, K. Hirata, and K. Miyamoto, "Fluorescent probes for hydrogen peroxide based on a non-oxidative mechanism," *Angewandte Chemie, International Edition*, vol. 43, pp. 2389–2391, 2004.
- [49] M. C. Y. Chang, A. Pralle, E. Y. Isacoff, and C. J. Chang, "A selective, cell-permeable optical probe for hydrogen peroxide in living cells," *Journal of the American Chemical Society*, vol. 126, no. 47, pp. 15392–15393, 2004.
- [50] E. W. Miller, A. E. Albers, A. Pralle, E. Y. Isacoff, and C. J. Chang, "Boronate-based fluorescent probes for imaging cellular hydrogen peroxide," *Journal of the American Chemical Society*, vol. 127, no. 47, pp. 16652–16659, 2005.
- [51] K. Xu, B. Tang, H. Huang, G. Yang, Z. Chen, P. Li, and L. An, "Strong red fluorescent probes suitable for detecting hydrogen peroxide generated by mice peritoneal macrophages," *Chemical Communications*, no. 48, pp. 5974–5976, 2005.
- [52] E. W. Miller and C. J. Chang, "Fluorescent probes for nitric oxide and hydrogen peroxide in cell signaling," *Current Opinion in Chemical Biology*, vol. 11, pp. 620–625, 2007.
- [53] E. H. White, O. Zafiriou, H. H. Kägi, and J. H. M. Hill, "Chemiluminescence of luminol: The chemical reaction," *Journal of the American Chemical Society*, vol. 86, no. 5, pp. 940–941, 1964.
- [54] F. Brabec, "Oxidation of Luminol catalyzed by stabilized solution of Haemine," *Collection of Czechoslovak Chemical Communications*, vol. 37, pp. 1605–1606, 1972.
- [55] E. L. Bastos, P. Romoff, C. R. Eckert, and W. J. Baader, "Evaluation of antiradical capacity by H₂O₂-Hemin-induced Luminol chemiluminescence," *Journal of Agricultural and Food Chemistry*, vol. 51, pp. 7481–7488, 2003.

- [56] T. M. Freeman and W. R. Seitz, "Chemiluminescence fiber optic probe for hydrogen peroxide based on the Luminol reaction," *Analytical Chemistry*, vol. 50, no. 9, pp. 1242–1246, 1978.
- [57] A. Navas Díaz, M. C. Ramos Peinado, and M. C. Torijas, Minguéz, "Sol-gel horseradish peroxidase biosensor for hydrogen peroxide detection by chemiluminescence," *Analytica Chimica Acta*, vol. 363, pp. 221–227, 1998.
- [58] K.-M. Wang, J. Li, X. hai Yang, F. lin Shen, and X. Wang, "A chemiluminescent H₂O₂ sensor based on horseradish peroxidase immobilized by sol-gel method," *Sensors and Actuators B Chemical*, vol. 65, pp. 239–240, 2000.
- [59] B. Li, Z. Zhang, and Y. Jin, "Chemiluminescence flow biosensors for hydrogen peroxide with immobilized reagents," *Sensors and Actuators B Chemical*, vol. 72, pp. 115–119, 2001.
- [60] D. Lee, S. Khaja, J. C. Velasquez-Castaño, M. Dasari, C. Sun, J. Petros, W. R. Taylor, and N. Murt, "In vivo imaging of hydrogen peroxide with chemiluminescent nanoparticles," *Nature Materials*, vol. 6, pp. 765–769, 2007.
- [61] D. Lee, V. R. Erigala, M. Dasari, J. Yu, R. M. Dickson, and N. Murthy, "Detection of hydrogen peroxide with chemiluminescent micelles," *International Journal of Nanomedicine*, vol. 3, no. 4, pp. 471–476, 2008.
- [62] O. S. Wolfbeis, "Fiber-optic chemical sensors and biosensors," *Analytical Chemistry*, vol. 72, pp. 81R–89R, 2000.
- [63] ———, "Fiber-optic chemical sensors and biosensors," *Analytical Chemistry*, vol. 80, pp. 4269–4283, June 15 2008.
- [64] X.-D. Wang and O. S. Wolfbeis, "Fiber-optic chemical sensors and biosensors," *Analytical Chemistry*, vol. 85, no. 2, pp. 487–508, 2013.
- [65] C. McDonagh, C. S. Burke, and B. D. MacCraith, "Optical chemical sensors," *Chemical Reviews*, vol. 108, no. 2, pp. 400–422, 2008.

- [66] D. Marcuse, *Light transmission optics*, 2nd ed., ser. Computer science and engineering series, S. Mitra, Ed. New York, NY: Van Nostrand Reinhold Company, 1982.
- [67] G. P. Agrawal, *Fiber-optic communication systems*, 4th ed., ser. Wiley series in microwave and optical engineering. Wiley, 2010.
- [68] G. R. Jones, R. E. Jones, and R. Jones, "Multimode optical fiber sensors," in *Optical Fiber Sensor Technology: Advanced Applications – Bragg Gratings And Distributed Sensors*, K. T. V. Grattan. and B. T. Meggitt, Eds. Boston, MA: Kluwer Academic Publishers, 2000.
- [69] M. A. Pérez, O. González, and J. R. Arias, "Optical Fiber Sensors for Chemical and Biological Measurements," in *Current Developments in Optical Fiber Technology*, S. W. Harun, Ed., 2013, ch. 10. [Online]. Available: <http://www.intechopen.com/books/current-developments-in-optical-fiber-technology/optical-fiber-sensors-for-chemical-and-biological-measurements>
- [70] W. R. Seitz, "Chemical sensors based on immobilized indicators and fiber optics," *Critical Reviews in Analytical Chemistry*, vol. 19, no. 2, pp. 135–173, 1988.
- [71] R. Koncki, "Chemical sensors and biosensors based on Prussian blue," *Critical Reviews in Analytical Chemistry*, vol. 32, no. 1, pp. 79–96, 2002.
- [72] J. F. Keggin and F. D. Miles, "Structures and formulæ of the Prussian blues and related compounds," *Nature*, vol. 137, pp. 577–278, 1936.
- [73] K. Itaya, K. Shibayama, S. Toshima, T. Ataka, and K. Iwasa, "Electrochromic Display Device," European Patent EP0068635A1, Jan 5, 1983.
- [74] A. A. Karyakin, E. A. Puganova, I. A. Budashov, I. N. Kurochkin, E. E. Karyakina, V. A. Levchenko, V. N. Matveyenko, and S. D. Varfolomeyev, "Prussian blue based nanoelectrode array for H₂O₂ detection," *Analytical Chemistry*, vol. 76, no. 2, pp. 474–478, 2004.

- [75] A. A. Karyakin, E. E. Karyakina, and L. Gorton, "Amperometric biosensor for glutamate using Prussian Blue-based "artificial peroxidase" as a transducer for hydrogen peroxide," *Analytical Chemistry*, vol. 72, no. 7, pp. 1720–1723, 2000.
- [76] I. L. de Mattos, L. V. Lukachova, L. Gorton, T. Laurell, and A. A. Karyakin, "Evaluation of glucose biosensors based on Prussian Blue and lyophilised, crystalline and cross-linked glucose oxidases (CLEC)," *Talanta*, vol. 54, pp. 963–974, 2001.
- [77] K.-S. Tseng, L.-C. Chen, and K.-C. Ho, "Amperometric detection of hydrogen peroxide at a Prussian blue-modified FTO electrode," *Sensors and Actuators B*, vol. 108, pp. 738–745, 2005.
- [78] P. A. Fiorito, V. R. Goncales, E. A. Ponzio, and S. I. Córdoba de Torresi, "Synthesis, Characterization and immobilization of Prussian blue nanoparticles. A potential tool for biosensing devices," *Chemical Communications*, no. 3, pp. 366–368, 2005.
- [79] D. Lu, A. Cagan, R. A. Munoz, T. Tangkuaram, and J. Wang, "Highly sensitive electrochemical detection of trace liquid peroxide explosives at a Prussian-blue 'artificial-peroxidase' modified electrode," *Analyst*, vol. 131, no. 12, pp. 1279–1281, 2006.
- [80] J. Li, S. Wang, I. M. Ayoub, and C. F. Yang, "A TiO₂-sol-gel derived Prussian blue nanoparticles-based glucose biosensor," in *Sensors Applications Symposium, 2007. SAS '07. IEEE*, San Diego, CA, USA, 6–8 Feb. 2007.
- [81] K. Itaya, I. Uchida, and V. D. Neff, "Electrochemistry of polynuclear transition metal cyanides: Prussian blue and its analogues," *Accounts of Chemical Research*, vol. 19, pp. 162–168, 1986.
- [82] R. Koncki, T. Lenarczuk, A. Radomska, and S. Gab, "Optical biosensors based on Prussian blue films," *Analyst*, vol. 126, pp. 1080–1085, 2001.
- [83] T. Lenarczuk, S. Gab, and R. Koncki, "Application of Prussian blue-based optical sensor in pharmaceutical analysis," *Journal of Pharmaceutical and Biomedical Analysis*, vol. 26, pp. 163–169, 2001.

- [84] K. Itaya, T. Ataka, and S. Toshima, "Spectroelectrochemistry and electrochemical preparation method of Prussian blue modified electrodes," *Journal of the American Chemical Society*, vol. 104, pp. 4767–4772, 1982.
- [85] T. Lenarczuk, D. Wencel, S. Gab, and R. Koncki, "Prussian blue-based optical glucose biosensor in flow-injection analysis," *Analytica Chimica Acta*, vol. 447, pp. 23–32, 2001.
- [86] T. Lenarczuk, I. Roszczyk, and R. Koncki, "Quick cuvette test for thiol compounds," *Analytical Letters*, vol. 33, pp. 137–144, 2000.
- [87] R. Koncki and O. S. Wolfbeis, "Composite films of Prussian blue and N-substituted polypyrroles: Fabrication and application to optical determination of pH," *Analytical Chemistry*, vol. 70, pp. 2544–2550, 1998.
- [88] M. Smietana, W. J. Bock, J. Szmids, and G. R. Pickrell, "Nanocoating enhanced optical fiber sensors," in *Advances in Materials Science for Environmental and Nuclear Technology*, ser. Ceramic Transactions. Wiley, 2010, vol. 222, pp. 275–286.
- [89] M. M. Collinson, "Sol-gel strategies for the preparation of selective materials for chemical analysis," *Critical Reviews in Analytical Chemistry*, vol. 29, no. 4, pp. 289–311, 1999.
- [90] P. S. Grant and M. J. McShane, "Development of multilayer fluorescent thin film chemical sensors using electrostatic self-assembly," *IEEE Sensors Journal*, vol. 3, pp. 139–146, 2003.
- [91] F. Davis and S. P. J. Higson, "Structured thin films as functional components within biosensors," *Biosensors & Bioelectronics*, vol. 21, pp. 1–20, 2005.
- [92] G. Decher and J. B. Schlenoff, Eds., *Multilayer thin films: Sequential assembly of nanocomposite materials*. Wiley-VCH, 2002.
- [93] S. W. James and R. P. Tatam, "Fibre optic sensors with nano-structured coatings," *Journal of Optics A: Pure Applied Optics*, vol. 8, pp. S430–S444, 2006.

- [94] V. V. Tsukruk, V. N. Bliznyuk, D. Visser, A. L. . Campbell, T. J. Bunning, and W. W. Adams, "Electrostatic deposition of polyionic monolayers on charged surfaces," *Macromolecules*, vol. 30, pp. 6615–6625, 1997.
- [95] G. Decher, "Fuzzy nanoassemblies: Toward layered polymeric multicomposites," *Science*, vol. 277, pp. 1232–1237, 1997.
- [96] R. von Klitzing and H. Möhwald, "A realistic diffusion model for ultrathin polyelectrolyte films," *Macromolecules*, vol. 29, pp. 6901–6906, 1996.
- [97] T. Hoshi, H. Saiki, S. Kuwazawa, C. Tsuchiya, Q. Chen, and J. ichi Anzai, "Selective permeation of hydrogen peroxide through polyelectrolyte multilayer films and its use for amperometric biosensors," *Analytical Chemistry*, vol. 73, pp. 5310–5315, 2001.
- [98] C. S. Peyratout and L. Dähne, "Tailor-made polyelectrolyte microcapsules: From multilayers to smart containers," *Angewandte Chemie International Edition*, vol. 43, no. 29, pp. 3762–3783, 2004.
- [99] G. Ibarz, L. Dähne, E. Donath, and H. Möhwald, "Controlled permeability of polyelectrolyte capsules via defined annealing," *Chemistry of Materials*, vol. 14, no. 10, pp. 4059–4062, 2002.
- [100] S. S. Shiratori and M. F. Rubner, "pH-dependent thickness behavior of sequentially adsorbed layers of weak polyelectrolytes," *Macromolecules*, vol. 33, pp. 4213–4219, 2000.
- [101] K. Itano, J. Choi, and M. F. Rubner, "Mechanism of the pH-induced discontinuous swelling/deswelling transitions of poly(allylamine hydrochloride)-containing polyelectrolyte multilayer films," *Macromolecules*, vol. 38, pp. 3450–3460, 2005.
- [102] J. D. Mendelsohn, C. J. Barrett, V. V. Chan, A. J. Pal, A. M. Mayes, and M. F. Rubner, "Fabrication of microporous thin films from polyelectrolyte multilayers," *Langmuir*, vol. 16, pp. 5017–5023, 2000.
- [103] A. A. Karyakin, E. E. Karyakina, and L. Gorton, "Prussian-Blue-based amperometric biosensors in flow-injection analysis," *Talanta*, vol. 43, no. 9, pp. 1597–1606, 1996.

- [104] R. Koncki and O. S. Wolfbeis, "Optical chemical sensing based on thin films of Prussian blue," *Sensors and Actuators B Chemical*, vol. 51, pp. 355–358, 1998.
- [105] Z.-X. Guo, H.-X. Shen, and L. Li, "Spectrophotometric determination of hydrogen peroxide and glucose based on hemin peroxidase-like catalyzed oxidation of bromopyrogallol red," *Mikrochimica Acta*, vol. 131, pp. 171–176, 1999.
- [106] A. A. Karyakin, E. E. Karyakina, and L. Gorton, "On the mechanism of H₂O₂ reduction at Prussian blue modified electrodes," *Electrochemistry Communications*, vol. 1, pp. 78–82, 1999.
- [107] A. A. Karyakin and E. E. Karyakina, "Prussian blue-based 'artificial peroxidase' as a transducer for hydrogen peroxide detection. Application to biosensors," *Sensors and Actuators B Chemical*, vol. 57, no. 1-3, pp. 268–273, 1999.
- [108] I. L. de Mattos, L. Gorton, T. Ruzgas, and A. A. Karyakin, "Sensor for hydrogen peroxide based on Prussian blue modified electrode: Improvement of the operational stability," *Analytical Sciences*, vol. 16, pp. 795–798, 2000.
- [109] S.-Q. Liu, J.-J. Xu, and H.-Y. Chen, "Electrochemical behavior of nanosized Prussian blue self-assembled on Au electrode surface," *Electrochemistry Communications*, vol. 4, no. 5, pp. 421–425, 2002.
- [110] A. Jaiswal, J. Colins, B. Agricole, P. Delhaes, and S. Ravaine, "Layer-by-layer self-assembly of Prussian blue colloids," *Journal of Colloid and Interface Science*, vol. 261, pp. 330–335, 2003.
- [111] F. J. Arregui, Y. Liu, I. R. Matias, and R. O. Claus, "Optical fiber humidity sensor using a nano Fabry-Pèrot cavity formed by the ionic self-assembly method," *Sensors and Actuators B Chemical*, vol. 59, pp. 54–59, 1999.
- [112] F. J. Arregui, K. L. Cooper, Y. Liu, I. R. Matias, and R. O. Claus, "Optical fiber humidity sensor with a fast response time using the ionic self-assembly method," *IEICE Transactions on Electronics*, vol. E83-C, no. 3, pp. 360–365, 2000.

- [113] J. Wu, X. Z. Yuan, H. Wang, M. Blanco, J. J. Martin, and J. Zhang, “Diagnostic tools in PEM fuel cell research: Part I Electrochemical techniques,” *International Journal of Hydrogen Energy*, vol. 33, pp. 1735–1746, 2008.
- [114] N. Djilali and D. Lu, “Influence of heat transfer on gas and water transport in fuel cells,” *International Journal of Thermal Sciences*, vol. 41, pp. 29–40, 2002.
- [115] A. M. Abdullah, T. Okajima, A. M. Mohammad, F. Kitamura, and T. Ohsaka, “Temperature gradients measurements within a segmented H₂/air PEM fuel cell,” *Journal of Power Sources*, vol. 172, pp. 209–214, 2007.
- [116] A. A. Shah, T. R. Ralph, and F. C. Walsh, “Modeling and simulation of the degradation of perfluorinated ion-exchange membranes in PEM fuel cells,” *Journal of the Electrochemical Society*, vol. 156, no. 4, pp. B465–B484, 2009.
- [117] M. H. Wang, H. Guo, C. F. Ma, F. Ye, J. Yu, X. Liu, Y. Wang, and C. Y. Wang, “Temperature measurement technologies and their application in the research of fuel cells,” in *Proceedings of the 1st International Conference on Fuel Cell Science, Engineering and Technology*, 2003, pp. 95–100.
- [118] J. Lebak, S. T. Ali, P. Møller, C. Mathiasen, L. P. Nielsen, and S. K. Kær, “Quantification of *in situ* temperature measurements on a PBI-based high temperature PEMFC unit cell,” *International Journal of Hydrogen Energy*, vol. 35, pp. 9943–9953, 2010.
- [119] Multiple, *Sensor technology handbook*, J. Wilson, Ed. Elsevier, 2005.
- [120] M. M. Mench, D. J. Bufford, and T. W. Davis, “*In situ* temperature distribution measurement in an operating polymer electrolyte fuel cell,” in *Proceedings of the IMECE'03 2003 ASME International Mechanical Engineering Congress & Exposition*. Washington DC, (USA): ASME, November 16-21 2003, p. 14 pp.
- [121] M. Wilkinson, M. Blanco, E. Gu, J. J. Martin, D. P. Wilkinson, J. J. Zhang, and H. Wang, “*In situ* experimental technique for measurement of temperature and current

distribution in proton exchange membrane fuel cells,” *Electrochemical and Solid-State Letters*, vol. 9, pp. A507–A511, 2006.

[122] G. Zhang, L. Guo, L. Ma, and H. Liu, “Simultaneous measurement of current and temperature distributions in a proton exchange membrane fuel cell,” *Journal of Power Sources*, vol. 195, pp. 3597–3604, 2010.

[123] S. He, M. M. Mench, and S. Tadigadapa, “Thin film temperature sensor for real-time measurement of electrolyte temperature in a polymer electrolyte fuel cell,” *Sensors and Actuators A Physical*, vol. 125, pp. 170–177, 2006.

[124] C.-Y. Lee, S.-J. Lee, and C.-L. Hsieh, “Application of micro sensor on diagnosis of micro fuel cells,” in *Proceedings of the 2nd IEEE international conference on Nano/Micro Engineered Molecular Systems*. IEEE, January 16-19, 2007 2007, pp. 434–437.

[125] C.-Y. Lee, G.-W. Wu, and C.-L. Hsieh, “In situ diagnosis of micrometallic proton exchange membrane fuel cells using microsensors,” *Journal of Power Sources*, vol. 172, pp. 363–367, 2007.

[126] C.-Y. Lee, S.-J. Lee, R.-D. Huang, and C.-W. Chuang, “Integration of the micro thermal sensor and porous silicon as the gas diffusion layer for micro fuel cell,” in *Proceedings of the 7th IEEE International Conference on Nanotechnology*, Hong Kong (CN), 2-5 August 2007 2007.

[127] C. Y. Lee, S. J. Lee, and G. W. Wu, “*in situ* measuring of temperature and humidity within the membrane electrode assembly by micro-sensors,” in *Proceedings of the 35th International MATADOR Conference*, S. Hinduja and K.-C. Fan, Eds., 2007, pp. 377–380.

[128] C.-Y. Lee, W.-J. Hsieh, and G.-W. Wu, “Embedded flexible micro-sensors in MEA for measuring temperature and humidity in a micro-fuel cell,” *Journal of Power Sources*, vol. 181, pp. 237–243, 2008.

[129] C.-Y. Lee and C.-H. Lin, “A novel integration approach for combining the micro thermal sensor and stainless steel foil as gas diffusion layer in micro fuel cell,” *Renewable Energy*, vol. 35, pp. 759–762, 2010.

- [130] C.-Y. Lee, C. Chang, P.-C. Chan, R.-D. Huang, and M.-S. Tong, "Fabrication of Micro-sensors based on a parylene thin-film substrate for monitoring proton exchange membrane fuel cells," in *Proceedings of the 2010 5th IEEE International Conference on Nano/Micro Engineered and Molecular Systems*. Xiamen (CN): IEEE, 20-23 January 2010 2010, pp. 102–105.
- [131] C.-Y. Lee, C. Chang, W.-J. Hsieh, W.-Y. Fan, C.-Y. Huang, and C.-Y. Chao, "Flexible micro-sensors on stainless steel foil for monitoring proton exchange membrane fuel cells," in *Proceedings of the 2010 5th IEEE International Conference on Nano/Micro Engineered and Molecular Systems*, 2010, pp. 106–109.
- [132] C. Lee, F. Weng, C. Cheng, H. Shiu, S.-P. Jung, W.-C. Chang, P.-C. Chan, W.-T. Chen, and C.-J. Lee, "Use of flexible micro-temperature sensor to determine temperature *in situ* and to simulate a proton exchange membrane fuel cell," *Journal of Power Sources*, vol. 196, pp. 228–234, 2011.
- [133] K. Inman and X. Wang, "In-Situ Temperature Measurement on Cathode GDL in a PEMFC Using an Optical Fiber Temperature Sensor," *Journal of The Electrochemical Society*, vol. 160, no. 6, pp. F496–F500, 2013.
- [134] T. J. McIntyre, W. P. Partridge, S. W. Allison, L. C. Maxey, M. R. Cates, C. L. Britton, R. Lenarduzzi, T. J. Toops, and T. K. Plant, "Fiber optic temperature sensors for PEM fuel cells," Presentation Department of Energy Hydrogen, Fuel cells, and Infrastructure program review meeting, 2005. [Online]. Available: http://www.hydrogen.energy.gov/pdfs/progress04/ivh4_mcintyre.pdf
- [135] K. Inman, X. Wang, and B. Sangeorzan, "Design of an optical thermal sensor for proton exchange membrane fuel cell temperature measurement using phosphor thermometry," *Journal of Power Sources*, vol. 195, pp. 4753–4757, 2010.
- [136] S. Tao, J. C. Fanguy, X. Hu, and Q. Yan, "Fiber optic sensors for *in situ* real-time monitoring PEM fuel cell operation," in *Proceedings of FUELCELL2005 Third*

International Conference on Fuel Cell Science, Engineering and Technology. Ypsilanti, Michigan (US): ASME, 23-25 May 2005 2005, pp. 231–234.

[137] N. A. David, P. M. Wild, J. Hu, and N. Djilali, “In-fibre Bragg grating sensors for distributed temperature measurement in a polymer electrolyte membrane fuel cell,” *Journal of Power Sources*, vol. 192, pp. 376–380, 2009.

[138] N. A. David, P. M. Wild, J. Jensen, T. Navessin, and N. Djilali, “Simultaneous in situ measurement of temperature and relative humidity in a PEMFC using optical fiber sensors,” *Journal of The Electrochemical Society*, vol. 157, no. 8, pp. B1173–B1179, 2010.

[139] S. Basu, H. Xu, M. W. Renfro, and B. M. Cetegen, “*In situ* optical diagnostics for measurements of water vapor partial pressure in PEM fuel cell,” *Journal of Fuel Cell Science and Technology*, vol. 3, pp. 1–7, 2006.

[140] S. Basu, M. W. Renfro, H. Gorgun, and B. M. Cetegen, “*In situ* simultaneous measurements of temperature and water partial pressure in a PEM fuel cell under steady state and dynamic cycling,” *Journal of Power Sources*, vol. 159, pp. 987–994, 2006.

[141] S. Basu, M. Renfro, and B. Cetegen, “Spatially resolved optical measurements of water partial pressure and temperature in a PEM fuel cell under dynamic operating conditions,” *Journal of Power Sources*, vol. 162, pp. 286–293, 2006.

[142] B. M. Cetegen, M. W. Renfro, and S. Basu, “Fiber optic based in-situ diagnostics for PEM fuel cells,” U.S. Patent US 2008/0118783 A1, 2008.

[143] R. Sur, T. J. Boucher, M. W. Renfro, and B. M. Cetegen, “In situ measurements of water vapor partial pressure and temperature dynamics in a PEM fuel cell,” *Journal of The Electrochemical Society*, vol. 157, no. 1, pp. B45–B53, 2010.

[144] G. Hinds, M. Stevens, J. Wilkinson, M. de Podesta, and S. Bell, “Novel *in situ* measurements of relative humidity in a polymer electrolyte membrane fuel cell,” *Journal of Power Sources*, vol. 186, pp. 52–57, 2009.

[145] J. Burns, “Resistive thermometers,” in *Measurements, Instrumentation, and Sensors Handbook*, J. G. Webster, Ed. CRC Press LLC, 1999, ch. 32.2.

- [146] K. T. V. Grattan and B. T. Meggitt, Eds., *Optical Fiber Sensor Technology - Advanced Applications – Bragg Gratings and Distributed Sensors*. Kluwer Academic Publishers, 2000.
- [147] A. H. Khalid and K. Kontis, “Thermographic phosphors for high temperature measurements: Principles, current state of the art and recent applications,” *Sensors*, vol. 8, pp. 5673–5744, 2008.
- [148] S. Tao and A. Jayaprakash, “A fiber optic temperature sensor with an epoxy-glue membrane as a temperature indicator,” *Sensors and Actuators B Chemical*, vol. 119, no. 2, pp. 615 – 620, 2006.
- [149] Y.-J. Rao, “In-fibre Bragg grating sensors,” *Measurement Science and Technology*, vol. 8, no. 4, pp. 355–375, 1997.
- [150] R. Kashyap, “Principles of optical fiber grating sensors,” in *Fiber Bragg Gratings*, 2nd ed. Burlington, MA: Academic Press, 2009, ch. 10, pp. 441–502.
- [151] R. Frank, “Semiconductor junction thermometers,” in *Measurements, Instrumentation, and Sensors Handbook*. CRC Press LLC, 1999, ch. 32.5.
- [152] S. Bell, G. Hinds, M. Podesta, M. Stevens, and J. Wilkinson, “EnglishHumidity, Pressure, and Temperature Measurements in an Interdigitated-Flow PEM Hydrogen Fuel Cell,” *EnglishInternational Journal of Thermophysics*, vol. 33, no. 8-9, pp. 1583–1594, 2012. [Online]. Available: <http://dx.doi.org/10.1007/s10765-011-1095-7>
- [153] A. Bazylak, “Liquid water visualization in PEM fuel cells: A review,” *International Journal of Hydrogen Energy*, vol. 34, pp. 3845–3857, 2009.
- [154] M. M. Mench, Q. L. Dong, and C. Y. Wang, “In situ water distribution measurements in a polymer electrolyte fuel cell,” *Journal of Power Sources*, vol. 124, pp. 90–98, 2003.
- [155] Y. P. Patil, T. A. P. Seery, M. T. Shaw, and R. S. Parnas, “In Situ Water Sensing in a Nafion Membrane by Fluorescence Spectroscopy,” *Industrial & Engineering Chemistry Research*, vol. 44, no. 16, pp. 6141–6147, 2005.

- [156] R. S. Parnas and Y. P. Patil, "Optical fiber based fluorescence sensor for in-situ measurement and control of fuel cells," U.S. Patent US 7,695,970 B2, 2010.
- [157] H. Nishikawa, R. Kurihara, S. Sukemori, T. Sugawara, H. Kobayasi, S. Abe, T. Aoki, Y. Ogami, and A. Matsunaga, "Measurements of humidity and current distribution in a PEFC," *Journal of Power Sources*, vol. 155, no. 2, pp. 213 – 218, 2006.
- [158] Vaisala, "Operating Manual HMI41 Indicator and HMP42 Probe," Online, 1998. [Online]. Available: http://www.vaisala.com/Vaisala%20Documents/-User%20Guides%20and%20Quick%20Ref%20Guides/-HMI41_and_HMP42_User_Guide_in_English.pdf
- [159] Sensirion, "Datasheet SHT7x (SHT71, SHT75) Humidity and Temperature Sensor," Online, 2010. [Online]. Available: http://www.sensirion.com/en/pdf/-product_information/Datasheet-humidity-sensor-SHT7x.pdf
- [160] J. Wu, X. Z. Yuan, H. Wang, M. Blanco, J. J. Martin, and J. Zhang, "Diagnostic tools in PEM fuel cell research: Part II Physical/chemical methods," *International Journal of Hydrogen Energy*, vol. 33, pp. 1747–1757, 2008.
- [161] J. Stumper, S. A. Campbell, D. P. Wilkinson, M. C. Johnson, and M. Davis, "In-situ methods for the determination of current distributions in PEM fuel cells," *Electrochimica Acta*, vol. 43, no. 24, pp. 3778–3783, 1998.
- [162] P. Ghosh, T. Wüster, H. Dohle, N. Kimiaie, J. Mergel, and D. Stolten, "In situ approach for current distribution measurement in fuel cells," *Journal of Power Sources*, vol. 154, pp. 184–191, 2006.
- [163] S. J. C. Cleghorn, C. R. Derouin, M. S. Wilson, and S. Gottesfeld, "A printed circuit board approach to measuring current distribution in a fuel cell," *Journal of Applied Electrochemistry*, vol. 28, pp. 663–672, 1998.
- [164] C. Wieser, A. Helmbold, and E. Gülzow, "A new technique for two-dimensional current distribution measurements in electrochemical cells," *Journal of Applied Electrochemistry*, vol. 30, pp. 803–807, 2000.

- [165] M. Noponen, T. Mennola, M. Mikkola, T. Hottinen, and P. Lund, "Measurement of current distribution in a free-breathing PEMFC," *Journal of Power Sources*, vol. 106, no. 1-2, pp. 304 – 312, 2002.
- [166] G. Bender, M. S. Wilson, and T. A. Zawodzinski, "Further refinements in the segmented cell approach to diagnosing performance in polymer electrolyte fuel cells," *Journal of Power Sources*, vol. 123, no. 2, pp. 163 – 171, 2003.
- [167] M. M. Mench and C. Y. Yang, "An *in situ* method for determination of current distribution in PEM fuel cells applied to a Direct Methanol fuel cell," *Journal of The Electrochemical Society*, vol. 150, pp. A79–A85, 2003, nice comments on DMFC water management.
- [168] M. M. Mench, C. Y. Wang, and M. Ishikawa, "*In situ* current distribution measurements in polymer electrolyte fuel cells," *Journal of The Electrochemical Society*, vol. 150, pp. A1052–A1059, 2003.
- [169] A. B. Geiger, R. Eckl, A. Wokaun, and G. G. Scherer, "An approach to measuring locally resolved currents in polymer electrolyte fuel cells," *Journal of The Electrochemical Society*, vol. 151, pp. A394–A398, 2004.
- [170] A. Hakenjos, H. Muentner, U. Wittstadt, and C. Hebling, "A PEM fuel cell for combined measurement of current and temperature distribution, and flow field flooding," *Journal of Power Sources*, vol. 131, pp. 213–216, 2004.
- [171] D. G. Strickland, S. Litster, and J. G. Santiago, "Current distribution in polymer electrolyte membrane fuel cell with active water management," *Journal of Power Sources*, vol. 174, pp. 272–281, 2007.
- [172] J. J. Hwnag, W. R. Chang, R. G. Peng, P. Y. Chen, and A. Su, "Experimental and numerical studies of local current mapping on a PEM fuel cell," *International Journal of Hydrogen Energy*, vol. 33, pp. 5718–5727, 2008.

- [173] D. J. L. Brett, S. Atkins, N. P. Brandon, V. Vesovic, N. Vasileiadis, and A. R. Kucernak, "Measurement of the current distribution along a single flow channel of a solid polymer fuel cell," *Electrochemistry Communications*, vol. 3, no. 11, pp. 628 – 632, 2001.
- [174] M. Noponen, J. Itonen, A. Lundblad, and G. Lindbergh, "Current distribution measurements in a PEFC with net flow geometry," *Journal of Applied Electrochemistry*, vol. 34, no. 3, pp. 255–262, 2004.
- [175] H. Sun, G. Zhang, L.-J. Guo, and H. Liu, "A novel technique for measuring current distributions in PEM fuel cells," *Journal of Power Sources*, vol. 158, pp. 326–332, 2006.
- [176] S. A. Freunberger, M. Reum, J. Evertz, A. Wokaun, and F. N. Büchi, "Measuring the current distribution in PEFCs with sub-millimeter resolution," *Journal of The Electrochemical Society*, vol. 153, no. 11, pp. A2158–A2165, 2006.
- [177] D. Webb and S. Møller-Holst, "Measuring individual cell voltages in fuel cell stacks," *Journal of Power Sources*, vol. 103, pp. 54–60, 2001.
- [178] B. Wells, "Fuel cell anomaly detection method and apparatus," U.S. Patent US 6,953,630 B2, 2005.
- [179] G. W. Skala and R. S. Foley, "Optical fuel cell stack cell voltage monitoring," U.S. Patent US 7,687,174 B2, 2010.
- [180] J.-N. Han, G.-G. Park, Y.-G. Yoon, T.-H. Yang, W.-Y. Lee, and C.-S. Kim, "A new evaluation method of anode/cathode used for polymer electrolyte membrane fuel cell," *International Journal of Hydrogen Energy*, vol. 28, no. 6, pp. 609 – 613, 2003.
- [181] O. Herrera, W. Mérida, and D. P. Wilkinson, "Sensing electrodes for failures diagnostics in fuel cells," *Journal of Power Sources*, vol. 190, pp. 103–109, 2009.
- [182] F. N. Büchi, A. Marek, and G. G. Scherer, "*In situ* membrane resistance measurements in polymer electrolyte fuel cells by fast auxiliary current pulses," *Journal of The Electrochemical Society*, vol. 142, pp. 1895–1901, 1995.

- [183] K. R. Cooper and M. Smith, "Electrical test methods for on-line fuel cell ohmic resistance measurement," *Journal of Power Sources*, vol. 160, pp. 1088–1095, 2006.
- [184] www.microworld.eu, "Four point probe theory," <http://www.four-point-probe.eu/>.
- [185] T. Mennola, M. Mikkola, M. Noponen, T. Hottinen, and P. Lund, "Measurement of ohmic voltage losses in individual cells of a PEMFC stack," *Journal of Power Sources*, vol. 112, pp. 261–272, 2002.
- [186] J. Stumper, H. Haas, and A. Granados, "In situ determination of MEA resistance and electrode diffusivity of a fuel cell," *Journal of The Electrochemical Society*, vol. 152, pp. A837–A844, 2005.
- [187] S. Srinivasan, E. Ticianelli, C. Derouin, and A. Redondo, "Advances in solid polymer electrolyte fuel cell technology with low platinum loading electrodes," *Journal of Power Sources*, vol. 22, no. 3-4, pp. 359 – 375, 1988, proceedings of the Space Electrochemical Research and Technology Conference.
- [188] P. Zhou, C. Wu, and G. Ma, "Contact resistance prediction and structure optimization of bipolar plates," *Journal of Power Sources*, vol. 159, no. 2, pp. 1115 – 1122, 2006.
- [189] Y. Zhou, G. Lin, A. Shih, and S. Hu, "A micro-scale model for predicting contact resistance between bipolar plate and gas diffusion layer in PEM fuel cells," *Journal of Power Sources*, vol. 163, no. 2, pp. 777 – 783, 2007, selected Papers presented at the FUEL PROCESSING FOR HYDROGEN PRODUCTION SYMPOSIUM at the 230th American Chemical Society National Meeting Washington, DC, USA, 28 August - 1 September 2005.
- [190] X. Lai, D. Liu, L. Peng, and J. Ni, "A mechanical-electrical finite element method model for predicting contact resistance between bipolar plate and gas diffusion layer in PEM fuel cells," *Journal of Power Sources*, vol. 182, no. 1, pp. 153 – 159, 2008.
- [191] Z. Wu, Y. Zhou, G. Lin, S. Wang, and S. J. Hu, "An improved model for predicting electrical contact resistance between bipolar plate and gas diffusion layer in proton

exchange membrane fuel cells,” *Journal of Power Sources*, vol. 182, no. 1, pp. 265 – 269, 2008.

[192] D. P. Davies, P. I. Adcock, M. Turpin, and S. J. Rowen, “Bipolar plate materials for solid polymer fuel cells,” *Journal of Applied Electrochemistry*, vol. 30, pp. 101–105, 2000.

[193] V. Mishra, F. Yang, and R. Pitchumani, “Measurement and Prediction of Electrical Contact Resistance Between Gas Diffusion Layers and Bipolar Plate for Applications to PEM Fuel Cells,” *Journal of Fuel Cell Science and Technology*, vol. 1, no. 1, pp. 2–9, 2004.

[194] Y. Fu, M. Hou, D. liang, X. Yan, Y. Fu, Z. Shao, Z. Hou, P. Ming, and B. Yi, “The electrical resistance of flexible graphite as flowfield plate in proton exchange membrane fuel cells,” *Carbon*, vol. 46, no. 1, pp. 19 – 23, 2008.

[195] E. Okel, B. Schaar, and O. Kanoun, “Simultaneous measurement of bulk and contact resistance of conductive materials for fuel cells,” in *Instrumentation and Measurement Technology Conference Proceedings, 2008. IMTC 2008. IEEE*, Victoria, BC (CA), May 2008, pp. 1462 –1465.

[196] R. C. Makkus, A. H. Janssen, F. A. de Bruijn, and R. K. Mallant, “Use of stainless steel for cost competitive bipolar plates in the SPFC,” *Journal of Power Sources*, vol. 86, pp. 274–282, 2000.

[197] J. Ihonen, F. Jaouen, G. Lindbergh, and G. Sundholm, “A novel polymer electrolyte fuel cell for laboratory investigations and *in-situ* contact resistance measurements,” *Electrochimica Acta*, vol. 46, pp. 2899–2911, 2001.

[198] T. Gu, W.-K. Lee, J. W. van Zee, and M. Murthy, “Effect of reformat components on PEMFC performance. Dilution and reverse water gas shift reaction,” *Journal of The Electrochemical Society*, vol. 151, pp. A2100–A2105, 2004.

[199] C. T. Holt, A. M. Azad, S. L. Swartz, R. R. Rao, and P. K. Dutta, “Carbon monoxide sensor for PEM fuel cell systems,” *Sensors and Actuators B Chemical*, vol. 87, pp. 414–420, 2002.

- [200] C. Pijolat, G. Tournier, and J. P. Viricelle, "Detection of CO in H₂-rich gases with a samarium doped ceria (SDC) sensor for fuel cell applications," *Sensors and Actuators B Chemical*, vol. 141, pp. 7–12, 2009.
- [201] A. Hashimoto, T. Hibino, and M. Sano, "A fuel-cell-type sensor for detection of carbon monoxide in reformed gases," *Electrochemical and Solid-State Letters*, vol. 5, no. 2, pp. H1–H3, 2002.
- [202] K. W. Kirby, A. C. Chu, and K. C. Fuller, "Detection of low level carbon monoxide in hydrogen-rich gas streams," *Sensors and Actuators B Chemical*, vol. 95, no. 1-3, pp. 224 – 231, 2003, selected papers from Eurosensors XVI.
- [203] W. G. Planje, G. J. M. Janssen, and M. P. de Heer, "A two-electrode sensor cell for CO detection in a H₂-rich gas," *Sensors and Actuators B Chemical*, vol. 99, no. 2-3, pp. 544 – 555, 2004.
- [204] R. Mukundan, E. L. Brosha, and F. H. Garz3, "A low temperature sensor for the detection of carbon monoxide in hydrogen," *Solid State Ionics*, vol. 175, pp. 497–501, 2004.
- [205] K. S. Bhambare, S. Gupta, M. M. Mench, and A. Ray, "A carbon monoxide sensor in polymer electrolyte fuel cells based on symbolic dynamic filtering," *Sensors and Actuators B Chemical*, vol. 134, pp. 803–815, 2008.
- [206] F. A. de Bruijn, V. A. T. Dam, and G. J. M. Janssen, "Review: Durability and degradation issues of PEM fuel cell components," *Fuel Cells*, vol. 08, pp. 3–22, 2008.
- [207] R. Mohtadi, W. k. Lee, S. Cowan, J. W. V. Zee, and M. Murthy, "Effects of Hydrogen Sulfide on the Performance of a PEMFC," *Electrochemical and Solid-State Letters*, vol. 6, no. 12, pp. A272–A274, 2003.
- [208] F. A. Uribe, S. Gottesfeld, and J. Thomas A. Zawodzinski, "Effect of Ammonia as Potential Fuel Impurity on Proton Exchange Membrane Fuel Cell Performance," *Journal of The Electrochemical Society*, vol. 149, no. 3, pp. A293–A296, 2002.

- [209] N. Rajalakshmi, T. Jayanth, and K. Dhathathreyan, "Effect of Carbon Dioxide and Ammonia on Polymer Electrolyte Membrane Fuel Cell Stack Performance," *Fuel Cells*, vol. 3, no. 4, pp. 177–180, 2003.
- [210] H. J. Soto, W. Kum Lee, J. W. V. Zee, and M. Murthy, "Effect of Transient Ammonia Concentrations on PEMFC Performance," *Electrochemical and Solid-State Letters*, vol. 6, no. 7, pp. A133–A135, 2003.
- [211] R. Halseid, P. J. Vie, and R. Tunold, "Effect of ammonia on the performance of polymer electrolyte membrane fuel cells," *Journal of Power Sources*, vol. 154, no. 2, pp. 343–350, 2006, selected papers from the Ninth Ulm Electrochemical Days.
- [212] L. Lindén, J. Rabek, H. Kaczmarek, A. Kaminska, and M. Scoconi, "Photooxidative degradation of polymers by HO and HO₂ radicals generated during the photolysis of H₂O₂, FeCl₃, and Fenton reagents," *Coordination Chemistry Reviews*, vol. 125, no. 1-2, pp. 195 – 217, 1993.
- [213] X. Hu and S. Tao, "An optical fiber H₂O₂-sensing probe using a titanium(IV) oxyacetylacetonate immobilized Nafion coating on a bent optical fiber probe," *IEEE Sensors Journal*, vol. 11, pp. 2032–2036, 2011.
- [214] H. A. Khorami, J. F. Botero-Cadavid, P. Wild, and N. Djilali, "Spectroscopic detection of hydrogen peroxide with an optical fiber probe using chemically deposited Prussian blue," *Electrochimica Acta*, vol. 115, pp. 416–424, 2014. [Online]. Available: <http://www.sciencedirect.com/science/article/pii/S0013468613021580>
- [215] B. C. Larisch and S. J. Duff, "Effect of H₂O₂ on characteristics and biological treatment of TCF bleached pulp mill effluent," *Water Research*, vol. 31, no. 7, pp. 1694–1700, Jul. 1997.
- [216] I. L. de Mattos, K. A. Shiraishi, A. D. Braz, and J. R. Fernandes, "Peróxido de hidrogênio: Importância e determinação," *Química Nova*, vol. 26, no. 3, pp. 373–380, 2003.

- [217] N. Adányi, T. Barna, T. Emri, M. Miskei, and I. Pócsi, “Hydrogen peroxide producing and decomposing enzymes: Their use in biosensors and other applications,” in *Industrial Enzymes*, J. Polaina and A. P. MacCabe, Eds. Springer Netherlands, 2007, ch. 25, pp. 441–459.
- [218] S. A. Kharitonov and P. J. Barnes, “Biomarkers of some pulmonary diseases in exhaled breath,” *Biomarkers*, vol. 7, no. 1, pp. 1–32, 2002.
- [219] M. Lee, B. C. Noone, D. O’Sullivan, and B. G. Heikes, “Method for the collection and HPLC analysis of hydrogen peroxide and C₁ and C₂ hydroperoxides in the atmosphere,” *Journal of Atmospheric and Oceanic Technology*, vol. 12, pp. 1060–1070, 1995.
- [220] A. Hickling and W. H. Wilson, “The anodic decomposition of hydrogen peroxide,” *Journal of The Electrochemical Society*, vol. 98, no. 11, pp. 425–433, 1951.
- [221] S. F. Burlatsky, V. Atrazhev, N. E. Cipollini, D. A. Condit, and N. Erikhman, “Aspects of PEMFC degradation,” *ECS Transactions*, vol. 1, no. 8, pp. 239–246, 2006.
- [222] V. O. Mittal, H. R. Kunz, and J. M. Fenton, “Membrane degradation mechanisms in PEMFCs,” *Journal of The Electrochemical Society*, vol. 154, no. 7, pp. B652–B656, 2007.
- [223] V. V. Atrazhev, E. N. Timokhina, S. F. Burlatsky, V. I. Sultanov, T. H. Madden, and M. Gummalla, “Direct mechanism of OH radicals formation in PEM fuel cells,” *ECS Transactions*, vol. 6, no. 25, pp. 69–74, 2008.
- [224] V. O. Mittal, H. R. Kunz, and J. M. Fenton, “Effect of catalyst properties on membrane degradation rate and the underlying degradation mechanism in PEMFCs,” *Journal of The Electrochemical Society*, vol. 153, no. 9, pp. A1755–A1759, 2006.
- [225] J. Qiao, M. Saito, K. Hayamizu, and T. Okada, “Degradation of perfluorinated ionomer membranes for PEM fuel cells during processing with H₂O₂,” *Journal of The Electrochemical Society*, vol. 153, no. 6, pp. A967–A974, 2006.

- [226] A. Ohma, S. Yamamoto, and K. Shinohara, "Membrane degradation mechanism during open-circuit voltage hold test," *Journal of Power Sources*, vol. 182, no. 1, pp. 39 – 47, 2008.
- [227] E. A. Khudaish, "The electrochemical oxidation of hydrogen peroxide on platinum electrodes at phosphate buffer solutions," Ph.D. dissertation, Massey University, Palmerston North, New Zealand, 1999.
- [228] A. A. Karyakin, "Prussian blue and its analogues: Electrochemistry and analytical applications," *Electroanalysis*, vol. 13, no. 10, pp. 813–819, 2001.
- [229] M. Aizawa, Y. Ikariyama, and H. Kuno, "Photovoltaic determination of hydrogen peroxide with a biophotodiode," *Analytical Letters*, vol. 17, no. B7, pp. 555–564, 1984.
- [230] L. J. Blum, S. M. Gautier, and P. R. Couler, "Luminescence fiber-optic biosensor," *Analytical Letters*, vol. 21, no. 5, pp. 717–726, 1988.
- [231] A. S. Keston and R. Brandt, "The fluorometric analysis of ultramicro quantities of hydrogen peroxide," *Analytical Biochemistry*, vol. 11, pp. 1–5, 1965.
- [232] E. W. Miller, O. Tulyanthan, E. Y. Isacoff, and C. J. Chang, "Molecular imaging of hydrogen peroxide produced for cell signaling," *Nature Chemical Biology*, vol. 3, no. 5, pp. 263–267, 2007.
- [233] D. Li and L. Wang, "Fluorescence hydrogen peroxide probe based on a microstructured polymer optical fiber modified with a Titanium dioxide film," *Applied Spectroscopy*, vol. 64, no. 5, pp. 514–519, 2010.
- [234] J. W. McCargar and V. D. Neff, "Thermodynamics of mixed-valence intercalation reactions: The electrochemical reduction of prussian blue," *Journal of Physical Chemistry*, vol. 92, pp. 3598–3604, 1988.
- [235] R. Koncki, T. Lenarczuk, and S. Gab, "Optical sensing schemes for Prussian blue/Prussian white film system," *Analytica Chimica Acta*, vol. 424, pp. 27–35, 2000.

- [236] X. Arys and A. L. and. A. M. Jonas, "Ordered polyelectrolyte "Multilayers". 1. Mechanisms of growth and structure formation: A comparison with classical fuzzy "multilayers"," *Macromolecules*, vol. 34, no. 10, pp. 3318–3330, 2001.
- [237] M. Kolasinska, R. Krastev, and T. G. adn Piotr Warszynski, "Layer-by-layer deposition of polyelectrolytes. Dipping versus spraying," *Langmuir*, vol. 25, pp. 1224–1232, 2009.
- [238] A. J. Chung and M. F. Rubner, "Methods of loading and releasing low molecular weigth cationic molecules in weak polyelectrolyte multilayer films," *Langmuir*, vol. 18, pp. 1176–1183, 2002.
- [239] A. A. Antipov, G. B. Sukhorukov, and H. Möhwald, "Influence of the ionic strength on the polyelectrolyte multilayers' permeability," *Langmuir*, vol. 19, pp. 2444–2448, 2003.
- [240] D. E. Curtin, R. D. Lousenberg, T. J. Henry, P. C. Tangeman, and M. E. Tisack, "Advanced materials for improved PEMFC performance and life," *Journal of Power Sources*, vol. 131, pp. 41–48, 2004.
- [241] M. Aoki, H. Uchida, and M. Watanabe, "Novel evaluation method for degradation rate of polymer electrolytes in fuel cells," *Electrochemistry Communications*, vol. 7, no. 12, pp. 1434 – 1438, 2005.
- [242] T. Madden, D. Weiss, N. Cipollini, D. Condit, M. Gummalla, S. Burlatsky, and V. Atrazhev, "Degradation of polymer-electrolyte membranes in fuel cells I. Experimental," *Journal of The Electrochemical Society*, vol. 156, pp. B657–B662, 2009.
- [243] A. Pozio, R. F. Silva, M. D. Francesco, and L. Giorgi, "Nafion degradation in PEFCs from end plate iron contamination," *Electrochimica Acta*, vol. 48, no. 11, pp. 1543 – 1549, 2003.
- [244] J. F. Botero-Cadavid, A. G. Brolo, P. Wild, and N. Djilali, "Detection of hydrogen peroxide using an optical fiber-based sensing probe," *Sensors and Actuators B: Chemical*,

vol. 185, pp. 166–173, Aug 2013. [Online]. Available: <http://dx.doi.org/10.1016/j.snb.2013.04.068>

[245] A. Rosidian, Y. Liu, and R. O. Claus, “Ionic self-assembly of ultrahard ZrO₂/polymer nanocomposite thin films,” *Advanced Materials*, vol. 10, no. 14, pp. 1087–1091, 1998.

[246] K. Castro, M. Pérez-Alonso, M. D. Rodríguez-Laso, L. A. Fernández, and J. M. Madariaga, “On-line FT-Raman and dispersive Raman spectra database of artists’ materials (e-VISART database),” *Analytical and Bioanalytical Chemistry*, vol. 382, pp. 248–258, 2005.

[247] L. Samain, B. Gilbert, F. Grandjean, G. J. Long, and D. Strivay, “Redox reactions in Prussian blue containing paint layers as a result of light exposure,” *Journal of Analytical Atomic Spectrometry*, vol. 28, pp. 524–535, 2013. [Online]. Available: <http://dx.doi.org/10.1039/C3JA30359D>

[248] B. Elemental, “Periodic table of elements and X-ray energies,” Online, 2011. [Online]. Available: http://www.bruker.com/fileadmin/user_upload/8-PDF-Docs/X-rayDiffraction_ElementalAnalysis/HH-XRF/Misc/Periodic_Table_and_X-ray_Energies.pdf

[249] C. Aparicio, L. Machala, and Z. Marusak, “Thermal decomposition of Prussian blue under inert atmosphere,” *Journal of Thermal Analysis and Calorimetry*, vol. 110, pp. 661–669, 2012.

[250] M. Ruiz-Bermejo, C. Rogero, C. Menor-Salván, S. Osuna-Esteban, J. Á. Martín-Gago, and S. Veintemillas-Verdaguer, “Thermal wet decomposition of Prussian blue: Implications for prebiotic chemistry,” *Chemistry & Biodiversity*, vol. 6, pp. 1309–1322, 2009.

[251] J.-P. Yuan and F. Chen, “Degradation of ascorbic acid in aqueous solution,” *Journal of Agricultural and Food Chemistry*, vol. 46, pp. 5078–5082, 1998.

- [252] R. L. Frost, A. W. Musumeci, J. Bouzaid, M. O. Adebajo, W. N. Martens, and J. T. Kloprogge, "Intercalation of hydrotalcites with hexacyanoferrate(II) and (III)—a thermoRaman spectroscopic study," *Journal of Solid State Chemistry*, vol. 178, no. 6, pp. 1940 – 1948, 2005. [Online]. Available: <http://www.sciencedirect.com/science/article/pii/S0022459605001374>
- [253] X. Shu, Y. Chen, H. Yuan, S. Gao, and D. Xiao, "H₂O₂ sensor based on the room-temperature phosphorescence of nano TiO₂/SiO₂ composite," *Analytical Chemistry*, vol. 79, pp. 3695–3702, 2007.
- [254] A. Navas Díaz, F. García Sanchez, and J. A. González García, "Hydrogen peroxide assay by using enhanced chemiluminescence of the luminol-H₂O₂–horseradish peroxidase system: Comparative studies," *Analytica Chimica Acta*, vol. 327, pp. 161–165, 1996.
- [255] A. Berger Collaudin and L. J. Blum, "Enhanced luminescent response of a fibre-optic sensor for H₂O₂ by a high-salt-concentration medium," *Sensors and Actuators B Chemical*, vol. 38-39, pp. 189–194, 1997.
- [256] C. N. Satterfield, G. M. Kavanagh, and H. Resnick, "Explosive characteristics of hydrogen peroxide vapor," *Industrial and Engineering Chemistry*, vol. 43, no. 11, pp. 2507–2514, 1951.
- [257] R. Schulte-Ladbeck, P. Kolla, and U. Karst, "Trace analysis of peroxide-based explosives," *Analytical Chemistry*, vol. 75, pp. 731–735, 2003.
- [258] Q. Jöbssis, H. C. Raatgeep, P. W. M. Hermans, and J. C. de Jongste, "Hydrogen peroxide in exhaled air is increased in stable asthmatic children," *European Respiratory Journal*, vol. 10, pp. 519–521, 1997.
- [259] R. Stolarek, P. Bialasiewicz, M. Krol, and D. Nowak, "Breath analysis of hydrogen peroxide as a diagnostic tool," *Clinica Chimica Acta*, vol. 411, pp. 1849–1861, 2010.
- [260] *Hydrogen peroxide in workplace atmospheres*, Online, Occupational Safety & Health Administration Std. [Online]. Available: www.osha.gov/dts/sltc/methods/inorganic/id006/hydrogen_peroxide.htm

- [261] *Hydrogen peroxide in workplace atmospheres*, Online, Occupational Safety & Health Administration Std. [Online]. Available: <http://www.osha.gov/dts/sltc/methods/-partial/t-id126sg-pv-01-0201-m/t-id126sg-pv-01-0201-m.html>
- [262] S. Radl, S. Ortner, R. Sungkorn, and J. G. Khinast, "The engineering of hydrogen peroxide decontamination systems," *Journal of Pharmaceutical Innovations*, vol. 4, pp. 51–62, 2009.
- [263] D. R. Gaskell, *Introduction to the Thermodynamics of Materials*, 4th ed. Taylor & Francis, 2009.
- [264] S. L. Mannat and M. R. R. Mannat, "On the analysis of mixture vapor pressure data: The hydrogen peroxide/ water system and its excess thermodynamic functions," *Chemistry: A European Journal*, vol. 10, pp. 6540–6557, 2004.
- [265] S. L. Manatt and M. R. R. Manatt, "On the analysis of mixture vapor pressure data: The hydrogen peroxide/ water system and its excess thermodynamic functions- Corrigendum," *Chemistry: A European Journal*, vol. 12, p. 3695, 2006.
- [266] D. S. A. . Co., "Dräger-Tubes & CMS-Handbook. 16th edition. Soil, Water, and Air Investigations as well as Technical Gas Analysis," Tech. Rep., 2011.
- [267] V. A. Sethuraman, J. W. Weidner, A. T. Haug, M. Pemberton, and L. V. Protsailo, "Importance of catalyst stability *vis-à-vis* hydrogen peroxide formation rates in PEM fuel cell electrodes," *Electrochimica Acta*, vol. 54, pp. 5571–5582, 2009.

Appendix A: Summary of *in situ* sensing techniques in PEMFCs

Table A-1: Summary of the *in situ* techniques for measuring temperature in PEMFCs

	Spatial resolution	Temporal resolution	Best accuracy	Cost	Merits	Drawbacks
Thermocouples	0.25 mm [121]	Good	± 0.19 °C	Low	Well-known technology. Widespread.	Difficult insertion on stack. Two wires per sensor. Trade-off robustness-size. May be affected by e. m. noise.
RTDs	110 μ m [124]	Good	± 0.3 °C [132]	Medium	Small size. Easy to mass produce. Easy placement in fuel cell.	2 wires per sensor. Substrate masks active area.
Optical fibers	700 μ m (phosph). [136] 10 mm (FBG) [137]	Good	± 0.2 °C [138]	High (interrogation system)	Multiple sensors on a fiber (FBG). Immune to e.m. noise. Chemically inert.	Brittle. May disturb gas flow. Difficult insertion.
Laser Absorption Spectroscopy	Low (average over channel length)	4 s [141]	$\pm 2\%$ in 80-100 °C [141]	High	Allows species detection. Does not disturb fuel cell operation.	Cannot be used if water condensates. Complex optical alignment and signal processing. Requires straight line-of-sight. Average temperatures
Others	Low (average over diverted channel)	8 s [144]	± 1.2 °C [144]	Low	Commercial. Easy to instrument.	Requires machining big pockets on flow-field plates. Mainstream gases do not flow through diverted channels.

Table A-2: Summary of the *in situ* techniques for measuring humidity in PEMFCs

	Spatial resolution	Temporal resolution	Best accuracy	Cost	Merits	Drawbacks
Capacitive	100 μ m [124]		0.25 %RH [124]	Medium	Small size. Easy to mass produce. Easy placement inside the fuel cell	2 wires per sensor. Substrate masks active area. May be affected by e.m. noise
Optical fibers	10 mm (length of FBG) [138]	10 s (90% full height) [138]	± 2 %RH [138]	High (interrogation system)	Small size. Multiple sensors on a fiber. Immune to e.m. noise. Chemically inert.	Brittle. May disturb gas flow. Difficult insertion.
Laser Absorption Spectroscopy	Low (average over channel length)	4 s [141]	± 2.5 %RH [143]	Medium	Does not interfere with PEMFC operation	Cannot be used if water condensates. Complex optical alignment and signal processing. Requires straight line-of-sight. Average temperatures. Limited range (40-90 %RH)
Commercial devices and instruments	Medium (limited by proximity of extraction ports)	90 s [157]	± 1.8 %RH [144]	Medium	Commercial. Easy to instrument.	Requires altering graphite plates. Not feasible for stacks.
Fluorescent dyes	Medium (limited by placement of optical fiber)			Low	Only technique that measures water content in membrane	Requires custom membrane. Membrane thicker than commercial membranes.

Table A-3 : Merits and drawbacks of the *in situ* techniques for measuring current in PEMFC

Technique	Merits	Drawbacks	Remarkable approaches
Partial catalyst	Spatial resolution customizable according to the catalyzed area.	Requires special MEA fabrication process	Stumper et al. [161]
Subcells	Performance isolated from main cell. Good for localized information.	Complex alignment during assembly. Requires special MEA fabrication process	Stumper et al. [161]
Segment current collector	Medium spatial resolution. Can be improved reducing size of segments.	Complex manufacture. MEA placed in the spacers between segments is not covered.	Bender et al. [166]
Segment GDL	Medium spatial resolution. Can be improved reducing size of segments.	Complex manufacture. Incomplete MEA utilization.	Hakenjos et al. [170]
Segment catalyst layer	Increased spatial resolution.	Complex manufacture.	Bender et al. [166]
Flow field lands as current collector	Reduced contact resistance. Customizable design.	Complex manufacture.	Mench and Yang [167]
Resistor network	Low alterations to fuel cell components. It could be integrated into a stack. Low cost. Spatial resolution dependent on number of segments.	It has not been tested in a stack yet.	Ghosh et al. [162]
Current collector embedded in polymeric flow field	Flow field easily machined. Multiple geometries of flow field can be studied.	Matching thermal expansion of material is required. Complex manufacturing.	Bender et al. [166] Hakenjos et al. [170]
Printed circuit board (PCB)	Easy to mass produce. Well-known technique	May increase contact resistance. It is not a complete <i>in situ</i> measurement	Sun et al. [175]
Theoretical approaches	Current can be determined by measuring another parameter. Good spatial resolution.	Based in adiabatic assumptions.	Freunberger et al. [176]
Insertion of commercial sensor	Off the shell application	Highly intrusive.	Nishikawa et al. [157]

Appendix B: Review on spectroscopic techniques for detection of hydrogen peroxide in small concentrations

Table B-1. Spectroscopic techniques based on Absorbance –colorimetric techniques–

Mechanisms	Reagents involved	Detection limit	Range	Remarkable comments about the technique	Refs
Phenol red is oxidized by H ₂ O ₂ in a reaction mediated by HRP	Phenol red (Phenolsulfonphthalein) Horseradish peroxidase (HRP)	1×10 ⁻⁶ M	1–60×10 ⁻⁶ M	The absorbance of the phenol red increases at 610 nm with the concentration of H ₂ O ₂ It works in both acid and basic environments	[33]
Trinder reagent, TOOS and H ₂ O ₂ form a colored quinine catalyzed by the presence of a peroxidase such as HRP	<i>N</i> -Ethyl- <i>N</i> -(2-hydroxy-3-sulfo-3-propyl)-3-methylaniline sodium salt (TOOS) Trinder reagent (4-aminoantipyrin) Horseradish peroxidase (HRP)	1×10 ⁻⁶ M	5–25 ×10 ⁻⁶ M	Maximum change in absorbance at 750 nm It has been only proved under physiological conditions (pH 7.0 and 37 °C)	[35]
PDV reacts with H ₂ O ₂ in acidic medium creating an stable red colored complex OPDV=oxo-peroxo-pyridine-2,6-dicarboxylato-vanadate(V)	Pyridine-2,6-dicarboxylic acid and vanadate (PDV)	0.29×10 ⁻⁶ M	1.47×10 ⁻⁶ – 1.47×10 ⁻³ M	Maximum change in absorption at 432 nm Complex formation occurs only under acid conditions (pH<1)	[34]
Fenton reaction (Fe ²⁺ +H ₂ O ₂ → Fe ³⁺ +OH ⁻ +HO), takes place when Fe ²⁺ ions are present in the presence of H ₂ O ₂ . The produced Fe ³⁺ reacts with the Xylenol orange forming a compound that changes absorbance	Xylenol Orange [<i>o</i> -cresosulfonphthalein-3,3-bis(sodium methyliminodiacetate)] Sorbitol	10 ⁻⁹ M	0–10×10 ⁻⁶ M	Maximum change in absorbance at 560 nm Fenton reaction generates OH ⁻ radicals, which can accelerate membrane degradation in fuel cells	[36]
Changes in the absorbance of Meldola's-blue due to oxidation by H ₂ O ₂ , reaction catalyzed by the enzyme hemin	Meldola's blue Tetramethylorthosilicate (TMOS)	10 ⁻⁸ M	10 ⁻⁸ –10 ⁻¹ M	Maximum change in absorbance at 720 nm Different sol–gel chemistry proved but only TMOS exhibited good response Requires recovery of the sensor in Sodium Metabisulfite (Na ₂ S ₂ O ₅)	[37]
Changes in the absorbance of Meldola's-blue	Meldola's blue	10 ⁻⁷ M	10 ⁻⁷ –10 ⁻¹ M	Maximum change in absorbance at 720 nm	[29,

due to oxidation by H ₂ O ₂ , reaction catalyzed by the enzyme hemin	Hemin Polyanion PAA ⁻ (Poly acrylic acid) Polycation PAH ⁺ (Poly(allylamine hydrochloride))			It has been successfully proved in optical fibres It saturates at high concentration Immobilization of Meldola's blue and hemin using layer-by-layer electrostatic self-assembly Light source, LED at 850 nm and Photodetector at 850 nm Recovery of the sensor after saturation is achieved by immersion in reductive agent Sodium Metabisulfite (Na ₂ S ₂ O ₅)	[39]
The first step involves the reduction of Prussian blue to Prussian white in ascorbic acid. The detection occurs when H ₂ O ₂ oxidizes Prussian White back to the Blue form changing its absorbance	Prussian Blue Polyanion PAA ⁻ (Poly acrylic acid) Polycation PAH ⁺ (Poly(allylamine hydrochloride)) Abscorbic acid	5×10 ⁻⁶ M	5×10 ⁻⁶ – 0.1×10 ⁻³ M	Maximum absorbance at 720 nm It has been successfully proved in optical fibres Response time is exponential with concentration of H ₂ O ₂ Immobilization of Prussian blue using layer-by-layer electrostatic self-assembly Shows better response applying multilayers with low pH and capping with multilayers at high pH Recovery of the sensor is required reducing the Prussian blue to Prussian white prior a new detection	[38]
TiO(ACAC) ₂ complex immobilized in Nafion [®] coating changes its absorbance when H ₂ O ₂ creates a new complex by ligand exchange	Titanium(IV) oxyacetylacetonate (TiO(ACAC) ₂) Nafion 5% in low aliphatic alcohol mixture with 45% water	74×10 ⁻⁹ M	8.8×10 ⁻⁶ – 1.8×10 ⁻³ M	Maximum absorbance change at 360 nm (UV) It has been successfully proved in optical fibre Nafion [®] coating provides protection against acidic environment in PEMFC	[213]

Table B-2. Spectroscopic techniques based on Fluorescence

Mechanisms	Reagents	Detection limit	Range	Remarkable comments about the technique	Refs.
Scopoletin is oxidized by H ₂ O ₂ in a reaction mediated by HRP.	Scopoletin (7-OH-6-methoxycoumarin)	0.2×10 ⁻⁶ M	0.2–1.6×10 ⁻⁶ M	Maximum absorbance at 350 nm (UV); Maximum emission at 460 nm (Blue)	[43]
The oxidation of scopoletin quenches the original fluorescence of this compound	Horseradish peroxidase (HRP)			The presence of H ₂ O ₂ quenches the fluorescence It requires replenishment of scopoletin after exhaustion	
The oxidation of HVA by H ₂ O ₂ in a reaction mediated by HRP, produces a highly fluorescent dimer (2,2'-dihydroxy-3,3'-dimethoxydiphenyl-5,5'-diacetic acid)	Homovanillic acid (4-hydroxy-3-methoxy-phenyl acetic acid) (HVA) Horseradish Peroxidase (HRP)	44 ×10 ⁻⁹ M	44×10 ⁻⁹ –4.4×10 ⁻⁶ M	Maximum absorbance at 312 nm (UV); Maximum emission at 405 nm (Violet) pH dependent, with low fluorescence under pH 6. Therefore, it would not be suitable for PEMFCs' environment	[44]
H ₂ O ₂ oxidizes DCFH as Dichlorofluorescein, a fluorescent compound in the presence of HRP	2',7'-Dichlorofluorescein (DCFH) Horseradish peroxidase (HRP)	10×10 ⁻⁶ M	0–120×10 ⁻⁶ M	Maximum absorbance at 510 nm (Cyan-Green) ; Maximum emission at 530 nm (Green) pH dependent and suffer cross-sensitivity with other Reactive Oxygen Species (ROS)	[45]
Oxidation of the non-fluorescent acetaminophen to a fluorescent compound by H ₂ O ₂ in acidic medium	Acetaminophen Sulphuric acid (H ₂ SO ₄)	15×10 ⁻⁹ M	5×10 ⁻⁸ –24×10 ⁻⁶ M	Maximum absorbance at 298 nm; Maximum emission at 333 nm (Both in the UV)	[47]
The produced compound is suspected to be <i>p</i> -benzoquinone, which fluoresces under UV light				The oxidation occurs in acidic medium, which can favour its use in PEMFC Optimal conditions were reached with heating of the solution up to 100 °C The technique is simple and inexpensive	
HRP is immobilized in a dialysis membrane, which is attached to the tip of an optical fibre.	Homovanillic acid (4-hydroxy-3-methoxy-phenyl acetic acid) (HVA)	50×10 ⁻⁹ M	5×10 ⁻⁸ –5×10 ⁻⁵ M	Maximum absorbance at 315 nm (UV); Maximum emission at 425 nm (Violet–Blue)	[46]
The oxidation of HVA by H ₂ O ₂ in a reaction mediated by HRP, produces a highly fluorescent dimer	Horseradish Peroxidase (HRP)			Completion of the reaction is slow, detecting 1×10 ⁻⁶ M takes ≈ 4 min Light source: Xenon lamp 450 Watts, adapted with a monochromator at 315 nm. A fluorometer is used to measure the spectrum Maximum response under pH 8.5 – 9.0, with low fluorescen	
H ₂ O ₂ oxidizes Amplex red turning it into a fluorescent compound called resorufin in a reaction catalyzed by	Amplex red (<i>N</i> -Acetyl-3,7-dihydroxy-phenonazin)	50 ×10 ⁻⁹ M	Up to 20×10 ⁻⁶ M	Maximum absorbance at 563 nm (Green); Maximum emission at 587 nm (Green–Yellow)	[42]
				Oxidase-catalyzed assay with amplex red results in increase in fluorescence on oxidation	

HRP	Horseradish peroxidase (HRP)			rather than in decrease as in scopoletin assay Reaction buffer pH 7.4, which is high in comparison with the one found in a PEMFC	
The compound loses the pentafluorobenzene part due to perhydrolysis becoming into a fluorescein.	Pentafluorobenzenesulfonyl fluoresceins	1.4×10^{-6} M	1.4×10^{-6} – 0.6×10^{-3} M	Maximum excitation at 492 nm (Cyan); Maximum emission at 530 nm (Green) The test is not enzymatically driven and the reaction is non oxidative High dependence on the pH, the fluorescent intensity is reached at pH 7.4, and decreases to 20% of maximum when pH is 6.6	[48]
The compound loses the disulfonate part due to perhydrolysis becoming into naphthofluorescein	Naphthofluorescein disulfonate	81.5×10^{-12} M	6×10^{-9} – 4×10^{-6} M	Maximum excitation at 595 nm (Yellow); Maximum emission at 660 nm (Red) The test is not enzymatically driven and the reaction is non oxidative Big Stokes' shift	[51]
PF1 turns into green fluorescein	Peroxifluor-1 (PF1)	10×10^{-6} M	10 – 100×10^{-6} M	PF1 has a maximum excitation at 450 nm; maximum emission at 515 nm	[49,
PR1 turns into red	Peroxyresorufin-1 (PR1)			PR1 has a maximum excitation at 530 nm ; Maximum emission at 585 nm	50,
PX1 turns into blue	Peroxyxanthone-1 (PX1)			PX1 has a maximum excitation at 350 nm (UV); Maximum emission at 445 nm The test requires up to 30 min	52]
TiO ₂ /SiO ₂ composite prepared by sol–gel route which phosphorescence is quenched by H ₂ O ₂	Tetraethoxysilane Tetrabutyl Titanium	4×10^{-6} M	7×10^{-6} – 7×10^{-2} M	Phosphorescence at excitation of 403 nm; emission at broadband visible 450–650 nm Recovery of the phosphorescence after immersion in hydroxylamine hydrochloride solution	[253]
Rh6G-TiO ₂ doped film covers the inner walls of microstructured optical fibre and acts as a waveguide of the light The fibre is immersed in a KI solution with H ₂ SO ₄ . H ₂ O ₂ oxidation reduces I ⁻ to I ₂ causing the fluorescence quenching of Rh6G	Rhodamine 6G (Rh6G) Potassium Iodide (KI) Sulphuric acid (H ₂ SO ₄) Tetrabutyl titanate	1.6×10^{-7} M	1.6×10^{-7} – 9.6×10^{-5} M	Maximum absorbance at 532 nm; Maximum emission at 573 nm Probe only responds to H ₂ O ₂ at a certain concentration of KI in solution quenching the fluorescence of Rh6G Only has an adequate response in acidic medium; the acidity is adjusted using H ₂ SO ₄	[233]

Table B-3. Spectroscopic techniques based on Chemiluminescence

Mechanisms	Reagents	Detection limit	Range	Remarkable comments about the technique	Refs.
Luminol oxidation by H ₂ O ₂ in presence of HRP produces chemiluminescence HRP is immobilized in a polyacrylamide gel on the tip of an optical fibre	Luminol Horseradish Peroxidase (HRP)	1×10 ⁻⁶ M	10 ⁻⁶ –10 ⁻⁴ M	Maximum emission at 430 nm Luminol in solution in excess so that the intensity of the chemiluminescence indicates the amount of H ₂ O ₂ Diameter of the optical fibre 0.125 in pH dependent with maximum response at pH 9.0	[56]
Luminol oxidation by H ₂ O ₂ in presence of HRP produces chemiluminescence In this reference different enhancers of the chemiluminescence of the	Horseradish Peroxidase (HRP) Luminol <u>Enhancers</u> <i>p</i> -coumaric acid (4-hydroxycinnamic acid) <i>p</i> -iodophenol aniline phenol	(All in ×10 ⁻⁶ M) <i>p</i> -coumaric (0.08) <i>p</i> -iodophenol (0.12) Aniline (0.13) No enhancer (0.18) Phenol (0.19)	0–7×10 ⁻⁶ M	Maximum emission at 425 nm pH dependent with maximum response at pH 8.4	[254]
Luminol oxidation by H ₂ O ₂ in presence of HRP produces chemiluminescence HRP is covalently immobilized onto a polyamide membrane attached to the tip of an optical fibre bundle	Luminol Firefly Luciferin (enhancer of the chemiluminescence) Horseradish Peroxidase (HRP)	29×10 ⁻⁹ M	48×10 ⁻⁹ – 0.2×10 ⁻³ M	Maximum emission at 430 nm Peak of chemiluminescence after 2 sec of starting the reaction (Instead of 10 sec without enhancer) pH dependent with maximum response at pH 8.5	[255]
Luminol oxidation by H ₂ O ₂ in presence of HRP produces chemiluminescence	Tetramethylorthosilicate (TMOS) Horseradish Peroxidase (HRP)	6.7×10 ⁻⁴ M	0.1–3.0×10 ⁻³ M	Maximum Emission at 425 nm Entrapment in sol-gel matrix is independent of proteins functionality	[57]

HRP is microencapsulated in sol-gel matrix	Luminol			Sol-gel water content maintain aqueous conditions pH dependent with maximum response at pH 8.5	
Luminol oxidation by H ₂ O ₂ in presence of HRP produces chemiluminescence	Tetraethyl orthosilicate (TEOS)	8 × 10 ⁻⁶ M	0– 2 × 10 ⁻³ M	Maximum Emission at 430 nm	[58]
HRP is immobilized in a sol-gel membrane under conditions that allow to obtain crack-free coatings	Luminol Horseradish Peroxidase (HRP)			Exhibits maximum of chemiluminescence within 30 sec, returns to baseline within 60 sec Long lasting 1000 times in 2 months pH dependent with maximum response at pH 9.1	
Luminol oxidation by H ₂ O ₂ in presence of HRP produces chemiluminescence	Tetraethyl orthosilicate (TEOS)	2.8 x 10 ⁻⁷ M	8x10 ⁻⁷ – 1x10 ⁻⁴ M	Reusable 500 times up to 50 hours	[59]
HRP is immobilized in sol-gel in a flow cell	Horseradish Peroxidase (HRP)			Flow cell with all components immobilized.	
Luminol is immobilized in an anion exchange resin	Luminol			pH dependent with maximum response at pH 9.0	
Chemiluminescence is produced as a reaction between H ₂ O ₂ , a peroxalate ester, and the fluorescent dye	Peroxalate polymer (Synthesized in the researcher's lab)	250 × 10 ⁻⁹ M	0-10 × 10 ⁻⁶ M	Maximum emissions: Perylene (460 nm), Rubrene (560 nm), Pentacene (630 nm)	[60]
The dye is encapsulated in peroxalate nanoparticles	Fluorescent dyes (Perylene, Rubrene, Pentacene)			Peroxalate chemiluminescence requires the generation of a four-membered dioxetanedione intermediate, only formed by H ₂ O ₂ and not by other reactive oxygen species Chemiluminescence half life of 25 minutes in the presence of 10 × 10 ⁻⁶ M of H ₂ O ₂ Tested in physiological conditions to detect H ₂ O ₂ from macrophages in mice	
Chemiluminescence is produced as a reaction between H ₂ O ₂ , a peroxalate ester, and the fluorescent dye	Peroxalate micelles	50 × 10 ⁻⁹ M	0–1 × 10 ⁻⁶ M	Maximum emission at 560 nm	[61]
Dyes are immobilized in copolymeric micelles	Rubrene dye (5,6,11,12-tetraphenylnaphthacene)			Half life chemiluminescence 1.5 min Micelles are 33 nm in diameter with a polyethylene glycol coat to avoid phagocytosis (their main application is monitoring <i>in-vivo</i> cell cultures)	

Appendix C: Practical considerations for the immobilization of Prussian blue on the tip of multimode optical fibers

Several considerations were followed to obtain an adequate immobilization of soluble Prussian blue (Sigma-Aldrich, Oakville, ON, Canada, product No. 03899) onto the tip of multi-mode optical fibers SFS105/125Y and SFS200/225Y (Thorlabs, Newton, NJ), where the core and cladding diameters in micrometers are indicated in the reference of each fiber.

As a safety precaution, the use of nitrile or latex disposable gloves, as well as the proper eye protection is required at all stages of the reagent's immobilization on the tip of the optical fiber. In addition, solutions and solid waste must be properly disposed according to local regulations.

C.1 Fiber cleaving

The first step to obtain the proper immobilization of the reagent onto the fiber surface is the careful cleaving and cleansing of the distal end of the optical fiber. The cleaving process starts with the acrylate coating removal using a Micro-strip[®] mechanical stripping tool (Micro Electronics Inc., Seekonk, MA) with a .006 inch or .010 inch blade, according to the diameter of the fiber cladding to expose (125 μm or 225 μm , respectively). Approximately 50 mm of the acrylate coating need to be removed to provide an adequate grip to the fiber holder of the cleaving machine. After the coating removal, a solvent like isopropanol or ethanol is used to remove dust particles and coating residues from the exposed cladding.

The fiber is placed in the grooves of the fiber holder of an EFC11 fiber cleaver apparatus (Ericsson Network Technologies, Sweden) and held in place using the low-torsion clamps. Constant tension is applied by pushing down the tension lever. The cleaving initiates by pushing down the lever that releases the blade. This action makes the diamond cutting blade to move perpendicularly towards the fiber applying an ultrasonic vibration that scores and cleaves the optical fiber.

In the eventuality that the fiber is not cleaved after the blade scored it, the adjustment of the tension on the cleaving machine or the tuning in the blade position may be required.

C.2 Fiber chemical cleansing

Once the fiber is cleaved, the next step involves a thorough cleaning process of any organic residue from the cleaved end. The recommended procedure consists of the immersion of the optical fiber in a 3:1 solution of highly concentrated (> 98 wt%) sulfuric acid (H_2SO_4) and 30 wt% hydrogen peroxide (H_2O_2). This solution is commonly known as “piranha solution”, and does not only removes the organic impurities, it also hydroxylizes the surface of the optical fiber adding OH^- groups, which makes the surface of the fiber negatively charged.

To facilitate the handling of the optical fiber, and to avoid the direct contact of the cleaved end with the walls of the container with the cleansing solution, a stirring glass rod is used. The optical fiber is held parallel to the glass rod leaving the cleaved end a few millimeters off the end of the rod, and PTFE tape is wrapped around both. A few turns of PTFE tape wound close to the end of the glass rod also creates a slight bending of the cleaved end of the optical fiber so that the surfaces stay out of contact (Figure C-1).

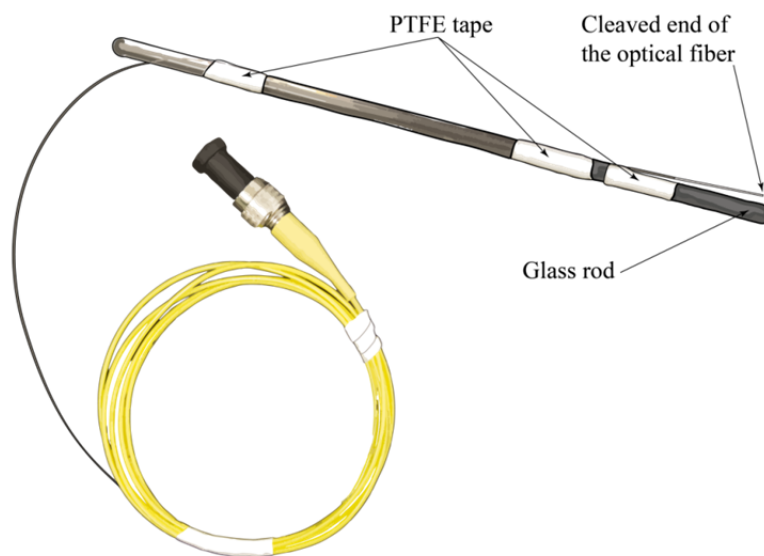


Figure C-1: Optical fiber immobilized for the cleansing and coating processes.

After the immersion of the optical fiber in piranha solution for 30 minutes, rinsing with distilled water and annealing at 80 °C for 60 minutes is recommended [93, 245].

C.3 Polyelectrolyte solutions preparation

The polyelectrolyte solutions for the multilayer deposition are prepared using acetate buffer solution at pH 4.0 as solvent. This buffer solution is prepared with a lower ionic strength to produce a more tightly packed structure of polyelectrolyte layers [96], using distilled water (18.2 M Ω ·cm), with 82.2 mg L⁻¹ of Sodium acetate (C₂H₃NaO₂), and 193.8 μ L L⁻¹ of Glacial acetic acid (CH₃COOH), which produce acetate buffer solution (ABS) with 10 \times 10⁻³ mole L⁻¹ of ionic strength buffer at pH 4.0**.

The polycation solution containing Prussian blue is prepared using 2.0 mg mL⁻¹ of poly(allylamine hydrochloride) (PAH⁺, Sigma-Aldrich, M_w \approx 15,000, product No. 283215) and 2.5 mg mL⁻¹ of Prussian blue soluble (PB, Sigma-Aldrich, product No. 03899). The solution of ABS with PAH⁺ and PB is sonicated for 10 minutes to ensure homogeneity in the dispersed colloids (Note that in spite of its “soluble” name, Prussian blue soluble has a low solubility and stays as a dispersion of colloids [71]).

The polyanion solution is prepared using 2.0 mg mL⁻¹ poly(acrylic acid) (PAA⁻, Sigma-Aldrich, M_w \approx 100,000, product No. 523925). PAA⁻ is distributed at a concentration of 35 wt% in water at a density of 1.14 g mL⁻¹. These parameters must be considered to prepare the correct concentration of the polyanion solution. Also, due to its high viscosity, it is necessary to keep the tip of the micropipette immersed in the PAA⁻ stock solution for at least 1 minute to ensure the volume taken by the micropipette has the right volume.

Using aliquots of aqueous solutions of 0.1 mole L⁻¹ hydrochloric acid (HCl), and 0.1 mole L⁻¹ sodium hydroxide (NaOH), it is possible to adjust the pH to the required values. For the regular layers, the pH used is 4.0, and for the capping bilayers the pH used is 5.5 [38].

** Online Acetate buffer calculation tool, (Dec 04 2013) www.egr.msu.edu/biofuelcell/tools/acetate/acetate.html

C.4 Coating process (deposition of the multilayer coating)

The coating of the multilayer structure follows the procedure described by Decher [95]. Since the optical fiber tips are at this point cleaved, cleansed, and already possess a negatively charged surface (as a result of the immersion in piranha solution), the first coating will proceed by immersing them in the polycationic solution of PAH^+ and PB.

The adsorption process requires at least 10 minutes ensuring the deposition of a homogeneous film [94]. A good practice, but not mandatory, is to use the light source and the spectrometer in the configuration presented in the experimental setup (Figure 2, Chapter 4:) to monitor the intensity of the light reflected from the tip of the fiber as the deposition of the layer proceeds. For this purpose, the SpectraSuite software (OceanOptics, Dunedin, FL) can be used^{††}.

After the immersion in the polycation solution, the fibers are rinsed by immersing three times in fresh distilled water for 2, 1, and 1 minutes, respectively. This rinsing process removes the non-adsorbed excess material and preserves the integrity of the deposited film. It is not advised to stir the rinsing solutions or to use a squirt bottle to rinse the fibers since the adsorbed films are very delicate at this point. Following the rinsing stage, the fibers are immersed in the polyanionic solution of PAA^- . After which a new rinsing stage is performed. This completes the deposition of an immobilizing bilayer on the tip of the optical fibers. A schematic of the whole process is shown in Figure C-2.

Del Villar et al. [38] reported that a total of 17 bilayers provide enough response since they immobilize an adequate amount of PB without threaten the mechanical stability of the multilayered structure deposited.

^{††} In the processes of coating optical fibers with the multilayered structure to immobilize PB performed in the experimental work of this dissertation, the monitoring the reflected intensity the immersion in the polycation solutions showed that around 15 to 20 minutes were required for the reflected light to plateau, whereas around 10 minutes were required for the intensity of the reflected light to plateau in the polyanion immersion.

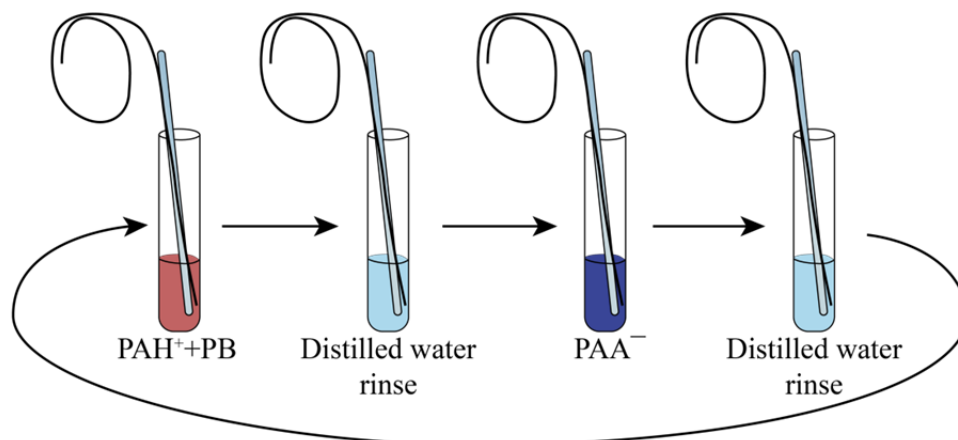


Figure C-2: Schematic of the deposition of immobilizing bilayers on the tip of an optical fiber by the electrostatic self-assembly (ESA) of polyelectrolytes (Adapted from Ref. [95])

During the coating process it is advisable to refresh the solutions used every three or four deposited layers. Also, a quick sonication of the stock solutions before the replenishment of the coating solutions (about 30 seconds) ensures homogeneity.

The coating of the fiber tips ends by applying two capping bilayers with solutions at the same concentrations of polyions but without adding PB. The pH of these capping solutions is also higher than the one used in the immobilizing layers (pH 5.5) to minimize the leaching of immobilized PB [40].

C.5 Annealing and aging processes

After the coating, the fibers are placed inside an oven at 100 °C for 2 hours to evaporate the excess of water within the multilayered structure and to improve the mechanical stability of the deposited film [93]. After which an aging stage for one week is performed.

If the immobilization technique is successfully performed, the coated optical fibers will exhibit a pale dark blue color in the coated area, as observed in Figure C-3.

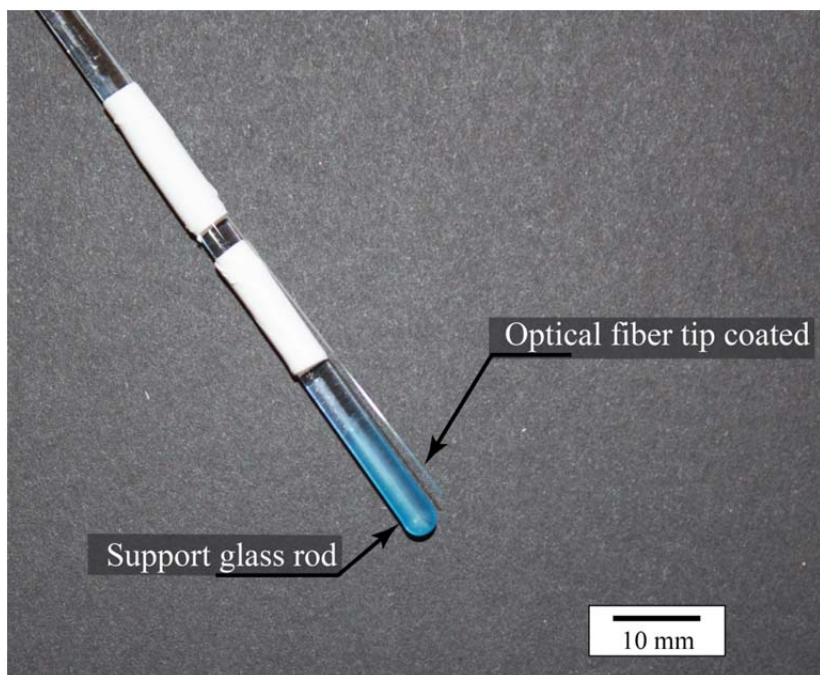


Figure C-3: Coated optical fiber.

Appendix D: Detection of hydrogen peroxide in vapor phase

D.1 Introduction

The optical fiber sensor developed in this dissertation proved to be able to determine the presence and concentration of hydrogen peroxide in liquid solutions; however, there are multiple applications where the detection of hydrogen peroxide in vapor phase is crucial.

In the target application of this dissertation, polymer electrolyte membrane fuel cells (PEMFCs), it is still matter of debate whether or not hydrogen peroxide is produced as a liquid or in a vapor phase. One of the arguments towards the assumption of liquid formation is that at the operating temperatures and pressures of PEMFCs (60-90 °C and 1-3 atm), H_2O_2 will be in liquid state [14, 15]. Thus, while the water produced stays in vapor phase at the normal operation temperatures of the PEMFC, H_2O_2 could remain in liquid phase.

Another factor to take into consideration is that hydrogen peroxide has a low stability at high temperatures and decomposes into water and oxygen [16] or into radicals that, due to their high reactivity, interact with other components in the MEA and are not detected. For this reason, not all the H_2O_2 produced in the PEMFC remains unaltered and can be easily detected.

Other applications where a sensor of hydrogen peroxide in gaseous phase would be pertinent include: homeland security and defense, since hydrogen peroxide at high concentrations can be used as a precursor of explosives and the vapor of hydrogen peroxide itself is explosive [79, 256, 257]; the biomedical field, where the detection of hydrogen peroxide vapor in exhaled breath can be used as a biomarker indicator of the presence of illnesses such as asthma and chronic obstructive pulmonary disease (COPD) [218, 258, 259]; and finally, in the industrial health and safety monitoring, since prolonged exposure to H_2O_2 vapors can affect mucous tissues like eyes and respiratory tract. According to the Occupational Health and Safety Administration from the Department of Labor of the US (OHSA), the maximum limit of exposure for workers to atmospheres with hydrogen peroxide vapor is of 1 ppm (part per million) [260, 261].

D.2 Concentration of hydrogen peroxide vapor in a solution of H₂O-H₂O₂

The equilibrium of the vapor-liquid between a hydrogen peroxide in an aqueous medium and its vapor follows a non-ideal liquid mixtures behavior [262]. One possible approach to calculate the non-ideal liquid mixture is to formulate the situation for ideal mixtures and apply the activity coefficient, which is function of the temperature and the species interaction.

The *molar fraction*, χ_i , of a the species i in a solution is the ratio of number of moles of i in the system to the total number of moles of all components of the system. From Raoult's Law, the vapor pressure of the gas over an ideal solution can be stated as: $P_i = \chi_i P_i^{sat}$, where P_i is the vapor pressure of the species i in solution and, P_i^{sat} is the vapor pressure of the pure species i at the given temperature [263]. From this point, the vapor pressure for water and hydrogen peroxide can be calculated following the expression [262]:

$$P_i = P_i^{sat} \cdot \gamma_i \cdot \chi_i \quad (\text{D.1})$$

where, γ_i , indicates the activity coefficient of the species i (water or hydrogen peroxide).

The calculation of the partial pressure P_i^{sat} of each species can be found in diverse sources in the literature. Manatt and Manatt [264, 265] presented the expressions for determining these partial pressures in mmHg. In the case of water, the equation is valid for temperatures, T , in a range from 273.15 to 433.15 K; (0 – 160 °C):

$$\log_{10} P_{\text{H}_2\text{O}}^{sat} = 19.389127 - \frac{2861.9133}{T} - 3.2418662 \cdot \log_{10} T - 1.0799994 \times 10^{-4} \cdot T - 7.9189289 \times 10^{-6} \cdot T^2 + 1.5411774 \times 10^{-8} \cdot T^3 - 8.1926991 \times 10^{-12} \cdot T^4 \quad (\text{D.2})$$

For hydrogen peroxide, the vapor pressure has two expressions depending on the temperature [264, 265]:

273.15 < T < 363.15 K; (0 – 90 °C):

$$\log_{10} P_{\text{H}_2\text{O}_2}^{\text{sat}} = 24.8436 - \frac{3511.54}{T} - 4.61453 \cdot \log_{10} T - 3.60245 \times 10^{-3} \cdot T - 7.73423 \times 10^{-6} \cdot T^2 + 1.78355 \times 10^{-8} \cdot T^3 - 2.27008 \times 10^{-13} \cdot T^4 \quad (\text{D.3})$$

$363.15 < T < 433.15$ K; (90–160 °C):

$$\log_{10} P_{\text{H}_2\text{O}_2}^{\text{sat}} = 38.8572 - \frac{3627.72}{T} - 11.2133 \cdot \log_{10} T + 4.74132 \times 10^{-3} \cdot T \quad (\text{D.4})$$

Assuming that the hydrogen peroxide solution in water is prepared for an *ex situ* measurement, the molar fraction of the species can be determined by controlling the amount of hydrogen peroxide stock solution that is added to the distilled water. Commonly, hydrogen peroxide is commercially available in 3 wt% and 30 wt% solution in water. Therefore, the maximum concentration attainable diluting these solutions is 30 wt%.

To prepare a solution of a desired wt% of hydrogen peroxide, $\text{wt}\%_{\text{prepared}}$, it is necessary to know the density of the stock solution, $\rho_{\text{H}_2\text{O}_2 \text{ stock}}$, which is provided by the manufacturer of the hydrogen peroxide. Considering a stock solution of 30 wt% H_2O_2 , according to the manufacturer (Caledon Labs, Georgetown, ON), the density of this solution of H_2O_2 is $\rho_{30 \text{ wt}\% \text{ H}_2\text{O}_2 \text{ stock}} = 1.1078 \text{ g mL}^{-1}$.

Some expressions that help calculating the volume of stock solution to add to certain volume of distilled water to prepare a desired concentration are:

$$\text{wt}\%_{\text{desired}} = \frac{m_{\text{H}_2\text{O}_2}}{m_{\text{H}_2\text{O}_2} + m_{\text{H}_2\text{O}}} \times 100 \quad (\text{D.5})$$

$$m_{\text{H}_2\text{O}_2} = 0.3 \times m_{30 \text{ wt}\% \text{ stock added}} \quad (\text{D.6})$$

$$m_{30 \text{ wt}\% \text{ stock added}} = v_{30 \text{ wt}\% \text{ stock added}} \times \rho_{30 \text{ wt}\% \text{ H}_2\text{O}_2 \text{ stock}} \quad (\text{D.7})$$

$$m_{\text{H}_2\text{O}} = m_{\text{H}_2\text{O in 30wt}\% \text{ stock added}} + m_{\text{Distilled H}_2\text{O added}} \quad (\text{D.8})$$

$$m_{\text{H}_2\text{O}} = 0.7 \times m_{30\text{wt}\% \text{ stock added}} + \rho_{\text{H}_2\text{O}} \times v_{\text{Distilled H}_2\text{O added}} \quad (\text{D.9})$$

$$v_{\text{total solution}} = v_{30 \text{ wt}\% \text{ stock added}} + v_{\text{Distilled H}_2\text{O added}} \quad (\text{D.10})$$

here, m , v , and ρ , indicate the mass, volume, and density of the substances specified by the subindices.

Combining Equations (D.5) to (D.10) it is possible to establish a system of equations and solve it for the volumes of stock solution and distilled water to add and obtain a solution of the desired wt%:

$$\begin{bmatrix} \rho_{30 \text{ wt}\% \text{ H}_2\text{O}_2 \text{ stock}} (wt\%_{\text{desired}} - 0.3 \times 100) & \rho_{\text{H}_2\text{O}} \cdot wt\%_{\text{desired}} \\ 1 & 1 \end{bmatrix} \begin{bmatrix} v_{30 \text{ wt}\% \text{ stock added}} \\ v_{\text{Distilled H}_2\text{O added}} \end{bmatrix} = \begin{bmatrix} 0 \\ v_{\text{total solution}} \end{bmatrix} \quad (\text{D.11})$$

The water density as a function of the temperature can be determined from known expressions in the literature [264]:

$$\rho_{\text{H}_2\text{O}} = 1.000 + C_1 \cdot T + C_2 \cdot T^2 + \frac{C_3}{T} + \frac{C_4}{T^2} \quad (\text{D.12})$$

$273.15 < T < 328.15$ K; (0–55 °C):

$$\begin{cases} C_1 = -3.171838 \times 10^{-3} \\ C_2 = 4.279879 \times 10^{-6} \\ C_3 = 367.0906 \\ C_4 = -59471.27 \end{cases}$$

$328.15 < T < 433.15$ K; (55–160 °C):

$$\begin{cases} C_1 = 4.718129 \times 10^{-4} \\ C_2 = -1.709110 \times 10^{-6} \\ C_3 = 27.28696 \\ C_4 = -7352.166 \end{cases}$$

The masses of each species in the solution and the molecular weights of water and hydrogen peroxide, $M_{W \text{ H}_2\text{O}} = 18.01528 \text{ g mol}^{-1}$ and $M_{W \text{ H}_2\text{O}_2} = 34.0147 \text{ g mol}^{-1}$.

Thus, in the prepared solution of $\text{wt}\%_{\text{desired}}$, the number of moles of water, $n_{\text{H}_2\text{O}}$:

$$m_{\text{H}_2\text{O}} = (1 - \text{wt}\%) \cdot v_{30 \text{ wt}\% \text{ stock added}} \cdot \rho_{30 \text{ wt}\% \text{ H}_2\text{O}_2 \text{ stock}} + v_{\text{Distilled H}_2\text{O added}} \cdot \rho_{\text{H}_2\text{O}}$$

$$n_{\text{H}_2\text{O}} = \frac{m_{\text{H}_2\text{O}}}{M_{W \text{ H}_2\text{O}}} \quad (\text{D.13})$$

and the number of moles of hydrogen peroxide, $n_{\text{H}_2\text{O}_2}$:

$$m_{\text{H}_2\text{O}_2} = \text{wt}\% \cdot v_{30 \text{ wt}\% \text{ stock added}} \cdot \rho_{30 \text{ wt}\% \text{ H}_2\text{O}_2 \text{ stock}}$$

$$n_{\text{H}_2\text{O}_2} = \frac{m_{\text{H}_2\text{O}_2}}{M_{W \text{ H}_2\text{O}_2}} \quad (\text{D.14})$$

The molar fraction of each species is calculated from the number of moles in solution:

$$\chi_{\text{H}_2\text{O}} = \frac{n_{\text{H}_2\text{O}}}{n_{\text{H}_2\text{O}} + n_{\text{H}_2\text{O}_2}} \quad (\text{D.15})$$

$$\chi_{\text{H}_2\text{O}_2} = \frac{n_{\text{H}_2\text{O}_2}}{n_{\text{H}_2\text{O}} + n_{\text{H}_2\text{O}_2}} \quad (\text{D.16})$$

The final parameters required for determining the vapor pressure of the water and the hydrogen peroxide in solution are the activity coefficients from each species [262]:

$$\ln(\gamma_{\text{H}_2\text{O}}) = \frac{(1 - \chi_{\text{H}_2\text{O}})^2}{R \cdot T} \cdot \left(B_0 + B_1 \cdot (1 - 4 \cdot \chi_{\text{H}_2\text{O}}) + B_2 \cdot (1 - 2 \cdot \chi_{\text{H}_2\text{O}}) \cdot (1 - 6 \cdot \chi_{\text{H}_2\text{O}}) \right. \\ \left. + B_3 \cdot (1 - 2 \cdot \chi_{\text{H}_2\text{O}})^2 \cdot (1 - 8 \cdot \chi_{\text{H}_2\text{O}}) \right) \quad (\text{D.17})$$

$$\ln(\gamma_{\text{H}_2\text{O}_2}) = \frac{\chi_{\text{H}_2\text{O}_2}^2}{R \cdot T} \cdot \left(B_0 + B_1 \cdot (3 - 4 \cdot \chi_{\text{H}_2\text{O}_2}) + B_2 \cdot (1 - 2 \cdot \chi_{\text{H}_2\text{O}_2}) \cdot (5 - 6 \cdot \chi_{\text{H}_2\text{O}_2}) \right. \\ \left. + B_3 \cdot (1 - 2 \cdot \chi_{\text{H}_2\text{O}_2})^2 \cdot (7 - 8 \cdot \chi_{\text{H}_2\text{O}_2}) \right) \quad (\text{D.18})$$

The parameters B_0 to B_3 are the coefficients in a Redlich-Kister analysis of the excess Gibbs energy for the mixture; they are temperature dependent and can be determined for different temperature intervals [264, 265]:

B_0 is calculated as a piecewise function of the temperature:

$273.15 < T < 317.636$ K; (0 – 44.486 °C); Lorentzian type function:

$$B_0 = C_{00} + \frac{(C_{10} \cdot C_{20})}{\pi \cdot (C_{20}^2 + (T - C_{30})^2)} \quad (\text{D.19})$$

$$\begin{cases} C_{00} = -666.8830; & C_{20} = 8.261924 \\ C_{10} = -2499.584; & C_{30} = 327.4487 \end{cases}$$

$317.636 < T < 348.222$ K; (44.486 – 75.072 °C); Average between Lorentzian type function and 2nd order polynomial:

$$B_0 = \frac{1}{2} \left(C_{00} + \frac{(C_{01} \cdot C_{02})}{\pi \cdot (C_{02}^2 + (T - C_{03})^2)} + P_{10} + P_{11} \cdot T + P_{12} \cdot T^2 \right) \quad (\text{D.20})$$

$$\begin{cases} C_{00} = -666.8830; & C_{02} = 8.261924; & P_{10} = 17418.34; & P_{12} = 0.1663847 \\ C_{01} = -2499.584; & C_{03} = 327.4487; & P_{11} = -109.9125; & \end{cases}$$

$348.222 < T < 391.463$ K; (75.072 – 118.313 °C); 2nd order polynomial function:

$$B_0 = P_{20} + P_{21} \cdot T + P_{22} \cdot T^2 \quad (\text{D.21})$$

$$\{P_{20} = -6110.401; \quad P_{21} = 28.08669; \quad P_{22} = -0.03587408$$

$391.463 < T < 433.15$ K; (118.313–160 °C); constant:

$$B_0 = -612.9613 \quad (\text{D.22})$$

A plot of B_0 as function of the temperature is presented in Figure D-1:

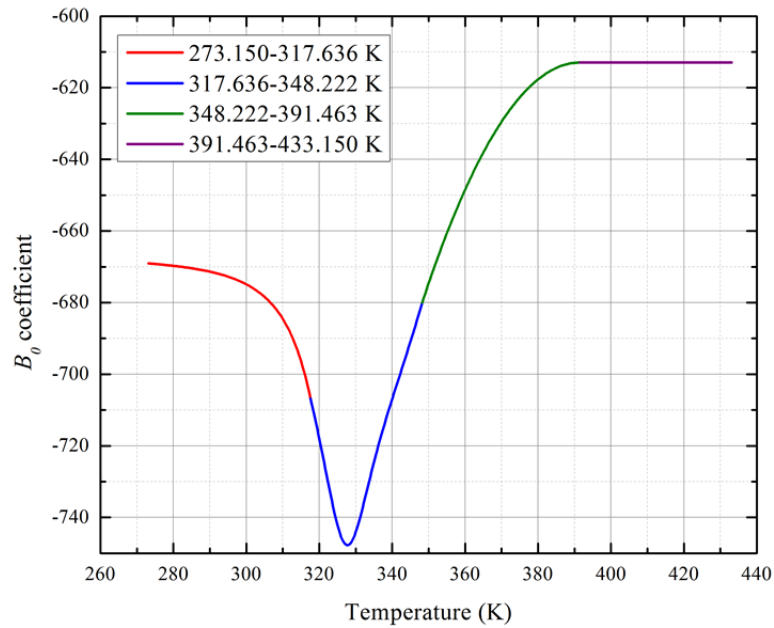


Figure D-1: Piecewise B_0 function

B_1 coefficient is a Lorentzian function in the entire temperature range (273.15–433.15 K):

$$B_1 = C_{01} + \frac{(C_{11} \cdot C_{21})}{\pi \cdot (C_{21}^2 + (T - C_{31})^2)} \quad (\text{D.23})$$

$$\begin{cases} C_{01} = 126.7385; & C_{21} = 12.33364 \\ C_{11} = -2558.776; & C_{31} = 343.1050 \end{cases}$$

B_2 coefficient is a sigmoidal function in the entire temperature range (273.15–433.15 K):

$$B_2 = \frac{C_{02} + C_{12}}{\{1 + \exp[C_{22} \cdot (T - C_{32})]\}} \quad (\text{D.24})$$

$$\begin{cases} C_{02} = 63.18354; & C_{22} = 0.4745954 \\ C_{12} = -149.9278; & C_{32} = 348.1642 \end{cases}$$

B_3 coefficient is a sigmoidal function in the entire temperature range (273.15–433.15 K):

$$B_3 = \frac{C_{03} + C_{13}}{\{1 + \exp[C_{23} \cdot (T - C_{33})]\}} \quad (\text{D.25})$$

$$\begin{cases} C_{03} = 59.42228; & C_{23} = 0.8321514 \\ C_{13} = -199.2644; & C_{33} = 346.2121 \end{cases}$$

This completes the calculation of the water and hydrogen peroxide activity coefficients, $\gamma_{\text{H}_2\text{O}}$, and $\gamma_{\text{H}_2\text{O}_2}$, and allows Eq. (D.1) to be solved for these two species.

Having the vapor pressure for each species calculated, the molar fraction of the species in gas phase can be calculated from Dalton's law [262]:

$$y_i = \frac{P_i}{P_{\text{total}}} \quad (\text{D.26})$$

being, P_{total} , the total ambient pressure, usually taken as 101,325 Pa.

Using the ideal gas law, the concentration of species i in mg L^{-1} can be obtained as:

$$c_i = \frac{P_i \cdot M_{w_i}}{R \cdot T} \quad (\text{D.27})$$

where, P_i is the vapor pressure (which needs to be converted to Pa since Eqs.(D.2) to (D.4) give the pressures in mmHg), M_{w_i} is the molecular weight of the substance (in g mol^{-1}), R is the molar gas constant ($8.31451 \text{ J mol}^{-1} \text{ K}^{-1}$), and T is the absolute temperature in K.

To obtain the vapor concentration in ppm (parts per million), it is required to determine the molar volume of the gas ($\text{m}^3 \text{ mol}^{-1}$). Assuming the vapor of the species i as ideal gases:

$$P \cdot V = n \cdot R \cdot T$$

$$MV_i = \frac{V}{n} = \frac{R \cdot T}{P_i} \quad (\text{D.28})$$

the concentration in ppm is given by [266]:

$$c_i \text{ [ppm]} = \frac{c_i \text{ [mg L}^{-1}\text{]} \cdot MV_i \cdot 10^6}{M_{W_i}} \quad (\text{D.29})$$

where M_{W_i} , the molar weight of the species i .

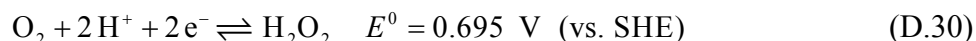
D.3 Concentration of hydrogen peroxide in vapor phase produced in an operating PEMFC

The concentration in vapor phase of the hydrogen peroxide produced during operation of a PEMFC could be estimated by two possible approaches; one considering as valid the rates of production of H_2O_2 obtained via an electrochemical approach by Sethuraman et al. [18, 267], using an electrochemical cell with rotating ring-disc electrode, where it was found that peroxide formation occurs mostly on the cathode side and it is strongly influenced by temperature and relative humidity, as well as, that it is dependent on the type of catalyst. The second approach, also obtained using the electrochemical technique of cyclic voltammetry with Pt wire electrodes, comes from Liu and Zuckerbrod [23], where H_2O_2 was detected *in situ* in an operating PEMFC.

D.3.1 Approach using rotating ring-disc electrode experiments

Sethuraman et al. [18, 267] reported the maximum rate of hydrogen peroxide formation in PEMFCs under different conditions. Their experiments were based on the use of an electrochemical cell with a rotating disc-ring electrode. As an attempt to set the upper limit of detection that *in situ* sensors for hydrogen peroxide would require to be effective in an operating PEMFC these rates of H_2O_2 would be consider as .

The formation of hydrogen peroxide on the catalyst surface occurs via a 2-electron reduction of molecular oxygen, as presented in Section 1.3.1:



Rotating ring-disc electrode, technique #1

The disc, made of glassy carbon, was coated with a film of Pt/Vulcan catalyst and Nafion[®], the effective load of catalyst $\approx 14.1 \mu\text{g Pt cm}^{-2}$. The ring was made of Pt, and a solution of Perchloric acid (HClO_4) was used as the electrolyte in the electrochemical cell. The test consisted of performing a sweep voltammetry on the rotating disc from 0 to 1.2 V (vs. SHE) while the ring was held at a constant potential of 1.2 V (vs. SHE).

The experimental setup produces H_2O_2 in the rotating disc as an effect of an oxygen reduction reaction (ORR) with 2-electron. Oxygen is fed into the electrolyte, and the dissolved oxygen is the one that takes part in the ORR on the rotating disc. Since the products of the ORR on the disc surface are transported to the ring, H_2O_2 is collected here and oxidized back according to the opposite reaction described in Eq. (D.30), which produces oxygen, protons, and electrons which produce a current that is proportional to the amount of H_2O_2 produced and captured.

The rate of production of H_2O_2 in the cathode was estimated from a combination of different parameters such as: the temperature of the electrochemical cell, the concentration of oxygen, the concentration of protons in the electrolyte (which was related to the water activity and hence to the relative humidity), and the parameters obtained from the rotating ring-disc electrode setup.

Assuming the results obtained in this experiment were accurate, and the reported formation rates effectively correspond to those observed in an operating PEMFC, it would be found that in the cathode the maximum rate of formation occurs at conditions of low relative humidity (0 %RH) and high temperatures (95 °C). Under these circumstances, the rate of

formation of H_2O_2 predicted is $\approx 0.7 \times 10^{-6} \text{ mol cm}^{-2} \text{ s}^{-1}$. A reproduction of the Figure 9 from Ref. [18] indicating these results is shown in Figure D-2.

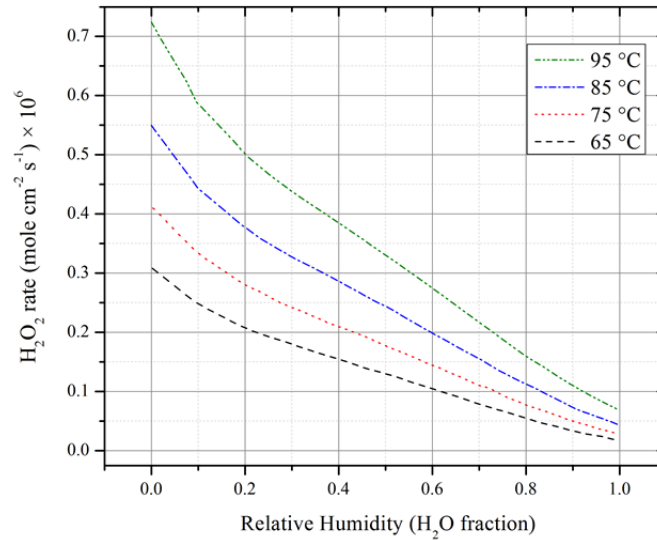


Figure D-2: Rates of H_2O_2 formation in the cathode side of the PEMFC as function of relative humidity and temperature. Local potential $\sim 0.6 \text{ V}$, which translates as an overpotential of 0.095 V in the H_2O_2 formation (Adapted from Ref.[18])

Considering the fact that the rates of formation for H_2O_2 were calculated at cathode potentials of $\sim 0.6 \text{ V}$, and assuming a typical polarization curve for a PEMFC, where the current density is near 1.0 Amp cm^{-2} , it is possible to perform an estimation of the water molar rate using the Faraday law [2]:

$$\frac{\dot{n}_{\text{H}_2\text{O}}}{A} = \frac{j}{nF} \quad (\text{D.31})$$

where: $\frac{\dot{n}_{\text{H}_2\text{O}}}{A}$, is the water molar rate per unit of area A ($\text{mol cm}^{-2} \text{ s}^{-1}$); n , the number of equivalent electrons involved in the electrochemical whole cell reaction for a hydrogen fuel cell (2 equivalent electrons); j , is the current density (assumed 1.0 Amp cm^{-2}); and F , the Faraday constant ($96,485 \text{ C eq.electron}^{-1} \text{ mol}^{-1}$). Performing this calculation,

$$\frac{\dot{n}_{\text{H}_2\text{O}}}{A} = 5.1822 \times 10^{-6} \text{ mol cm}^{-2} \text{ s}^{-1}.$$

Based on this result, the hydrogen peroxide molar fraction rate per unit of area, expressed as the ratio between the moles of H_2O_2 produced and the total amount of moles of H_2O_2 and H_2O produced per cm^2 each second:

$$\frac{\dot{\chi}_{\text{H}_2\text{O}_2}}{A} = \frac{1}{A} \cdot \left(\frac{\dot{n}_{\text{H}_2\text{O}_2}}{\dot{n}_{\text{H}_2\text{O}} + \dot{n}_{\text{H}_2\text{O}_2}} \right) = \frac{0.7 \times 10^{-6}}{0.7 \times 10^{-6} + 5.1822 \times 10^{-6}} \left[\frac{\text{mol}}{\text{cm}^2 \text{ s}} \right] = 0.119 \quad (\text{D.32})$$

This result would indicate that near 11.9% of the produced moles in the PEMFC correspond to H_2O_2 .

Considering the molecular weight of each species, M_{w_i} , it is possible to determine the mass fraction rate of H_2O_2 :

$$\frac{\dot{n}_{\text{H}_2\text{O}_2} \cdot M_{w_{\text{H}_2\text{O}_2}}}{\dot{n}_{\text{H}_2\text{O}} \cdot M_{w_{\text{H}_2\text{O}}} + \dot{n}_{\text{H}_2\text{O}_2} \cdot M_{w_{\text{H}_2\text{O}_2}}} = \quad (\text{D.33})$$

$$\frac{0.7 \times 10^{-6} \left[\frac{\text{mol}}{\text{cm}^2 \text{ s}} \right] \cdot 34.0147 \left[\frac{\text{g}}{\text{mol}} \right]}{5.1822 \times 10^{-6} \left[\frac{\text{mol}}{\text{cm}^2 \text{ s}} \right] \cdot 18.01528 \left[\frac{\text{g}}{\text{mol}} \right] + 0.7 \times 10^{-6} \left[\frac{\text{mol}}{\text{cm}^2 \text{ s}} \right] \cdot 34.0147 \left[\frac{\text{g}}{\text{mol}} \right]} = 0.2032$$

This result indicates that the produced H_2O_2 in the PEMFC operating at those extreme conditions (0 %RH, 95 °C), would equal the amount of a H_2O_2 solution of 20.3 wt%.

In spite of the astonishing amount of hydrogen peroxide that would be produced in an operating PEMFC if the values of the production rates presented by Sethuraman et al. [18] are correct, it could be possible to evaluate the possible concentration of the H_2O_2 in vapor phase. For this, following the procedure presented in Section D.2, assuming that the temperature is 95 °C, and that the concentration of the desired solution, $\text{wt}\%_{\text{desired}}$, is that one obtained from solving Eq. (D.33).

Following this procedure, the concentration of H_2O_2 in vapor phase is 14.19 mg L^{-1} or 12,600 ppm. This value is very high and unrealistic.

Rotating ring-disc electrode, technique #2

A second manuscript later published by Sethuraman et al. [267] revealed that the type of catalyst film impacts greatly the rate of formation of H_2O_2 . In this case, different catalysts were applied to the rotating disc. Pt, PtCo, and PtIrCo were three of the catalysts employed, all supported in Ketjen black carbon. A reproduction from figure 7 in this manuscript [267], that shows the observed formation rates for H_2O_2 using these catalysts is presented in Figure D-3.

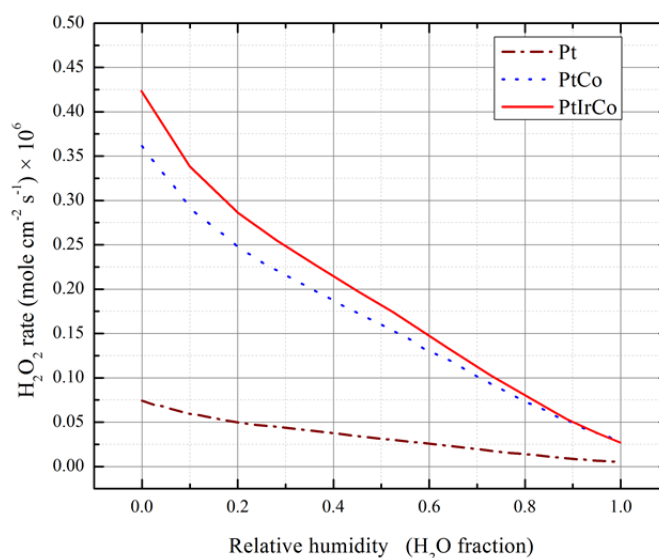


Figure D-3: Estimated rates of H_2O_2 formation in the cathode side of a PEMFC with different catalysts as a function of relative humidity at 75 °C. Local potential ~ 0.6 V, (overpotential of 0.095 V in the H_2O_2 formation) (Adapted from Ref. [267])

One of the first details to notice is that for the case of Pt as catalyst in the PEMFC, Figure D-2 presents a maximum estimated rate of formation at 75 °C (slightly over 0.4×10^{-6} mol cm^{-2} s^{-1}), whereas in Figure D- it merely reaches 0.07×10^{-6} mol cm^{-2} s^{-1} . This result indicates that possibly the values presented in the former manuscript were somehow overestimated.

Another consideration is that according to what is reported in Table 1 of Ref. [267] for rates of H_2O_2 formation in operating conditions of PEMFCs (94 %RH, 75 °C, 1 atm). The production of H_2O_2 in the cathode would be 0.007×10^{-6} mol cm^{-2} s^{-1} and 0.004×10^{-6} mol

$\text{cm}^{-2} \text{ s}^{-1}$ for Pt supported in Ketjen black carbon and Pt supported in Vulcan XC-72R, respectively.

Under the latter formation rates, the *wt%* of H_2O_2 in solution would reach 0.25 wt% and 0.15 wt% for Pt on Ketjen black carbon and Pt on Vulcan, respectively. Also, the maximum concentration observed at 75 °C, for 0 %RH would be 2.5 wt%.

In vapor phase, the concentrations of H_2O_2 in ppm would be 29.8, 52.1, and 522.7 in the three conditions previously described. These values are considerably more reasonable and could serve better as a target for the development of a vapor phase sensor for H_2O_2 in PEMFCs.

D.3.2 Approach considering experimental detected values of *in situ* H_2O_2 in an operating PEMFC

Liu and Zuckerbrod presented in their manuscript [23] a technique to detect the presence of H_2O_2 *in situ* in an operating PEMFC. Considering that H_2O_2 once it gets formed in the fuel cell can be quickly decomposed either into radicals or into water and oxygen, it can occur that the detectable H_2O_2 be considerably less than that formed in the operating PEMFC.

From their experimental technique, Liu and Zuckerbrod determined that the concentration of the H_2O_2 present was a function of the membrane thickness [23]. This supports the idea that it is the crossover of molecular oxygen from the cathode the main originating of H_2O_2 . When O_2 reaches regions inside the membrane of lower potential can be electrochemically reduced to H_2O_2 in the presence of dissolved Pt particles. This effect is more prone to occur in thinner membranes [11, 22].

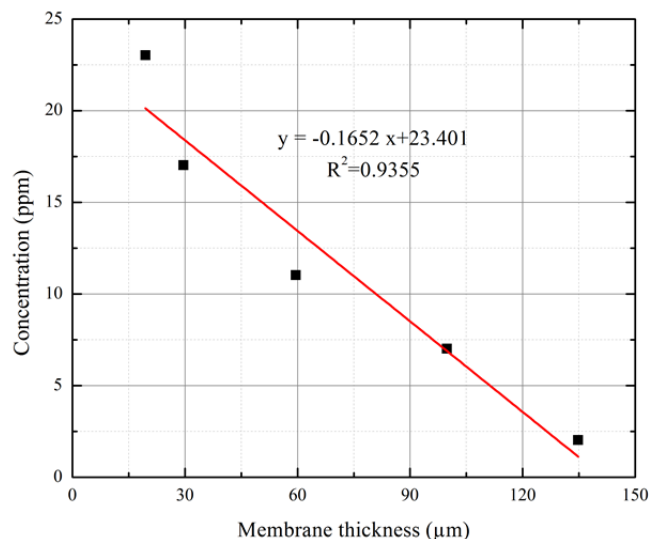


Figure D-4: Estimation of H_2O_2 concentration in fuel cells with different membrane thickness. (Adapted from Ref. [23])

Figure D-4 shows the estimated concentrations of H_2O_2 obtained from the electrochemical *in situ* measurements from Liu and Zuckerbrod [23]. It is observed that the maximum concentration at the thinnest membrane is below 25 ppm. The study compared the observed peak currents for the electrochemical sensor at known *ex situ* concentrations of H_2O_2 - H_2O solutions, and the ones observed from each different tested membrane.

If the concentration of H_2O_2 in solution equals 25 ppm, and considering that the molar weight of hydrogen peroxide, $M_{\text{H}_2\text{O}_2} = 34.0147 \text{ g mol}^{-1}$, it is possible to determine that a solution with a concentration of $1 \text{ mol L}^{-1} \text{ H}_2\text{O}_2$ will have 34014.7 ppm. Therefore, 25 ppm would be $735 \times 10^{-6} \text{ mol L}^{-1}$; which, as a matter of fact, is within the range of detection of the optical fiber sensor developed in this dissertation for detection of H_2O_2 in solution [244], but also would be 0.0025 wt%. Such quantity of H_2O_2 in solution at a temperature of $75 \text{ }^\circ\text{C}$ would produce 0.51 ppm of H_2O_2 in vapor phase.

D.4 Materials and Methods

Optical fiber sensors were fabricated following the procedure described in Appendix C. The operating principle of these sensors is described in detail in Section 2.2 of this dissertation. Hydrogen peroxide solutions to generate the vapor phase of hydrogen

peroxide and water were prepared using Hydrogen peroxide 30 wt% (Caledon Labs, Georgetown, ON) in distilled water ($18.2 \text{ M}\Omega \cdot \text{cm}$). Acetate buffer solution, prepared following the procedure described in Section C.3, was used as solvent in hydrogen peroxide solutions at concentrations of $100 \text{ }\mu\text{mol L}^{-1}$ and $200 \text{ }\mu\text{mol L}^{-1}$. These liquid solutions were used to evaluate the initial response of some of the tested the sensor prior to the vapor phase determination. Similarly, a pH 4.0 solution with a concentration of 0.04 mol L^{-1} of *L*-Ascorbic acid (Sigma-Aldrich, product No. 25,556-4) was prepared using ABS, and employed to perform the reduction stage in liquid.

The experiment for determining the concentration of H_2O_2 in vapor phase consisted of first preparing 50 mL of solutions of water and hydrogen peroxide in an Erlenmeyer flask with a capacity of 500 mL, by mixing the adequate volumes of each substance to obtain the desired *wt%* in liquid phase. The mixtures were slightly agitated and de-aerated by blowing N_2 in the flask during 60 seconds. The flasks were immediately covered with 2 sheets of Parafilm[®] M tightly sealing their mouths to avoid the vapor to escape or dilution of the inside by incoming air. These solutions prepared stayed still during at least 30 minutes before the measurement with the sensor while reaching equilibrium.

Each optical fiber sensor was placed inside a piece of 5 cm length PTFE tubing which distal end was cut diagonally in the shape of a hypodermic needle, the proximal end of this tubing was sealed with silicone. For the test the sensor was held vertically, and the proximal end of the fiber was connected to the common arm of a bifurcated optical fiber. The arm #1 of this bifurcated fiber bringing the light from a white light source (HL-2000-FHSA, OceanOptics, Dunedin, FL), while the arm #2 carries the reflected light from the sensor coating to an optical fiber spectrometer (USB200, OceanOptics). The intensity of the light was recorded in the SpectraSuite software (OceanOptics) at a rate of 1 Hz collecting the spectrum after an integration time of 500 ms. An illustration of this experimental setup is shown in Figure D-5.

The experiment for detection of H_2O_2 vapor then proceeds with the initial reduction of the sensing film from Prussian blue (PB) to the Prussian white (PW) form, by immersing the

sensor in a container with 0.04 M ascorbic acid. This chemical reduction takes about 10 min. to exhibit a stable reading in the reflected intensity. After this, in some of the experiments the sensors were subjected to two initial redox tests with a liquid solutions of 100 and 200 μM H_2O_2 , each followed by a reducing stage. These two redox tests allowed the proper operation of the sensor to be evaluated; after which, the tests in vapor phase were performed.

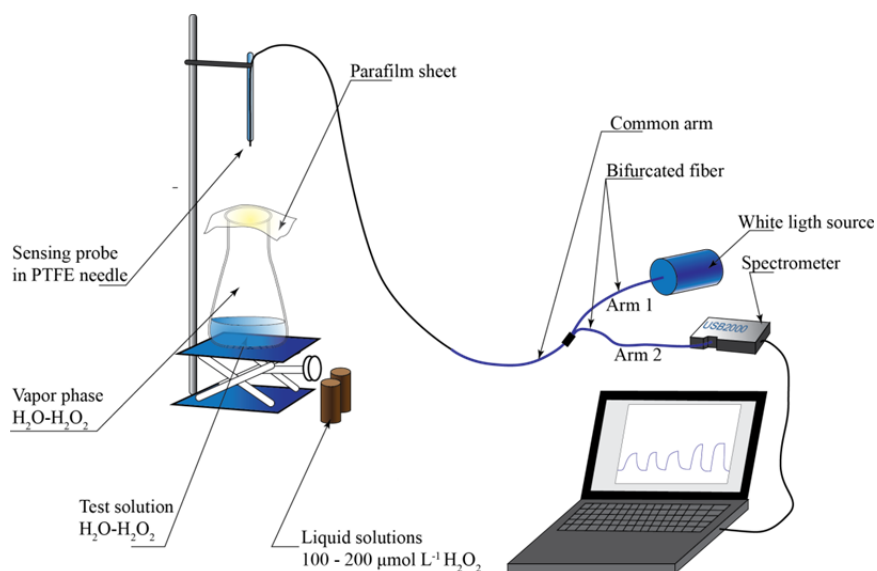


Figure D-5: Schematic of the experimental setup for the detection of H_2O_2 in vapor phase

The tests in vapor phase were performed by placing an Erlenmeyer flask containing the prepared solution on the platform of a lab scissor jack located under the sensor in the PTFE needle, and raising the platform of the jack until the needle pierced the Parafilm[®] M protective sheet. In this way the sensing coating enters in contact with the vapor phase entrapped in the Erlenmeyer flask.

The H_2O_2 vapor presents in the interior of the Erlenmeyer flask, causes the oxidation of the sensing film, transforming the PW in PB, increasing the intensity of the reflected light. After reaching the saturation during the oxidation stage, the sensor was immersed in the solution of ascorbic acid to complete the redox test.

Each experiment generally involved several redox tests, and in some of the performed experiments it involved stages where the sensor was left exposed to ambient air, or placed in either distilled water or in a sealed Erlenmeyer containing 50 mL of distilled water or 50 g of silica gel desiccant. The later allowing the response of the sensor to be evaluated for pure water vapor and dry N₂, respectively.

D.5 Results

Using a first fiber sensor, the first experiment consisted of subjecting the sensor to vapor phases from solutions at 30, 25, 20, 15, and 10 wt% H₂O₂. The reflected intensity during this experiment is shown in Figure D-6. Since the temperature influences the vapor phase concentration, it is reported for each case.

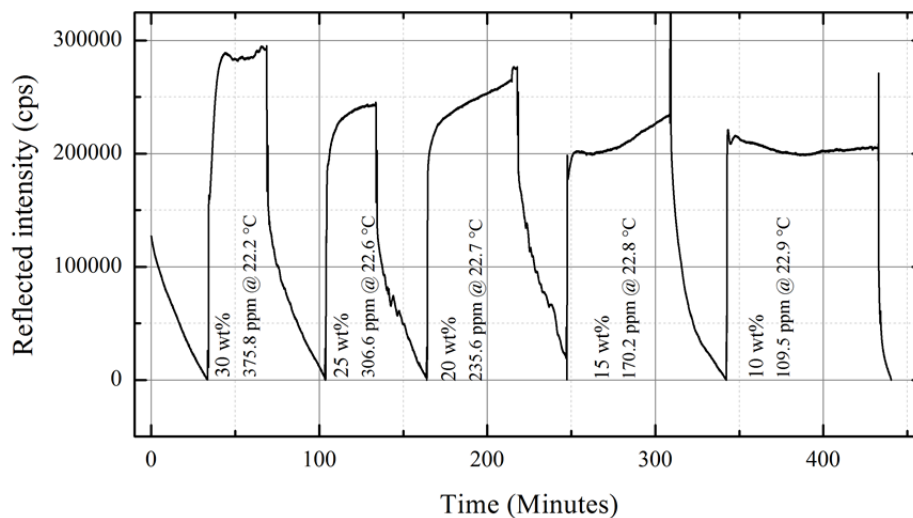


Figure D-6: Reflected intensity of the sensor to H₂O₂ in vapor phase from liquid solutions at 30, 25, 20, 15, 10 wt%

A rise time analysis, the time required for the signal to go from 10% to 90% of its maximum intensity, was performed to the response peak of each test. A plot of the result times versus the concentration in ppm of the vapor phase is presented in Figure D-7.

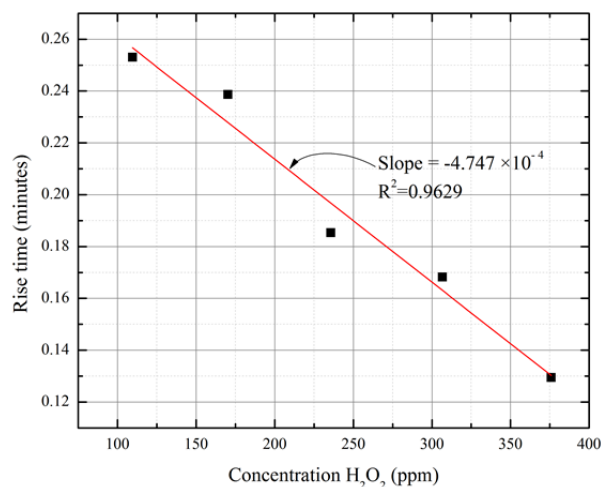


Figure D-7: Rise time vs. Concentration for a sensor in vapor phase. Liquid solutions at 30, 25, 20, 15, and 10 wt% H₂O₂

In a second experiment, the same sensor was subjected to tests increasing the concentration of the liquid solution generating the vapor phase. Table D-1 presents the corresponding concentrations in liquid solution, temperatures, and concentrations in vapor phase.

Table D-1: Concentrations in liquid and gas phase for sensing experiment 2

Concentration in liquid phase (H ₂ O ₂ wt%)	Temperature (°C)	Concentration in vapor phase (H ₂ O ₂ ppm)
Dry N ₂	22.3	0
0.0 (Distilled water)	22.5	0
1.0	22.3	9.8
2.0	22.3	19.8
3.0	22.3	29.9
4.0	22.2	40.1
5.0	--	50.6
10.0	--	105.2
15.0	--	164.6
20.0	--	229.5
25.0	--	300.7
30.0	--	379.0

Note: From 5.0 to 30.0 wt% the temperature was estimated as the average of temperatures in the previously recorded tests

The results for the second experiment are presented in Figure D-8.

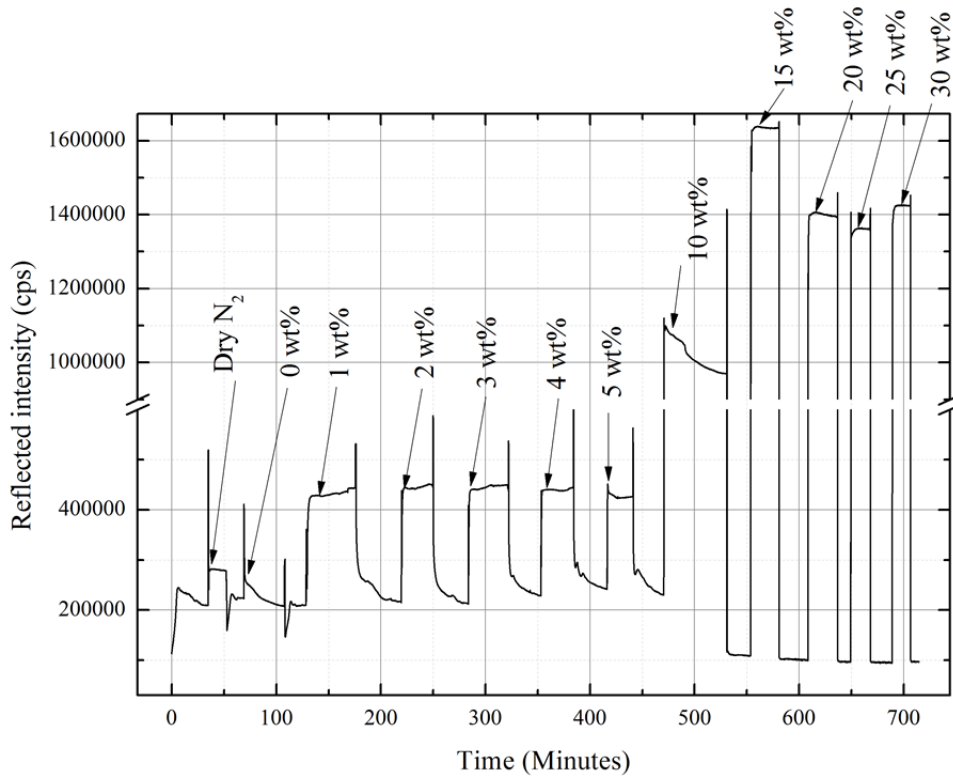


Figure D-8: Reflected intensity of the sensor to dry N₂ and H₂O₂ vapor from liquid solutions with 0, 1, 2, 3, 4, 5, 10, 15, 20, 25, and 30 H₂O₂ wt%

The results of a similar analysis to the one previously reported showing the 10-90% risetime versus the concentration of H₂O₂ in vapor phase is plotted in Figure D-9.

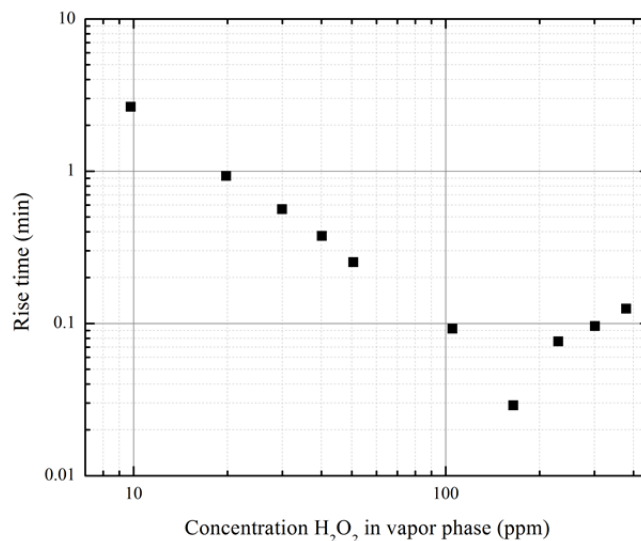


Figure D-9: Rise time versus concentration for a sensor in vapor phase. Liquid solutions at 1, 2, 3, 4, 5, 10, 15, 20, 25, and 30 wt% H₂O₂

The results observed in Figure D-9 are partially in agreement with those observed in Figure D-7. To start, the rise time diminishes with the concentration, but not in the complete range of the studied concentrations, only from 9.8 to 164 ppm; after which the rise time started to increase. Also, it is noticed that the test at 10 wt% H₂O₂ (105 ppm) showed an unexpected decreasing behavior, which could have been caused by the sudden rise in the concentration, but as well as effect of a damage to the sensor.

A second observation is that, while the experiment showed in Figure D-7 has a rise time linearly decreasing with the concentration in a linear scale; the second experiment was decreasing linearly with the concentration and time in a log-log scale. This later case is similar to the one observed as response of the sensor in liquid phase at low concentrations.

It was noted that the sensor did not exhibit a reliable response after this experiment.

A second fiber tested under more diverse set of experiments showed for one of these experiments the response presented in Figure D-10. The first two immersions in liquid solutions present inverse exponential behaviors similar to those observed in the sensor presented in Chapter 4: of this dissertation, but the sensor response observed when it was exposed to vapor phase environments was not always showing a consistent trending.

What can be noticed is that the response to H_2O_2 in vapor phase shows a faster increase of the reflected intensity than the observed for the water vapor case, as noticed by comparison of Figure D-10(b) and (c).

The response to different concentrations of H_2O_2 in vapor phase was extracted from other performed experiments using the same second optical fiber sensor. The intensity of these responses was normalized and it is displayed in Figure D-11.

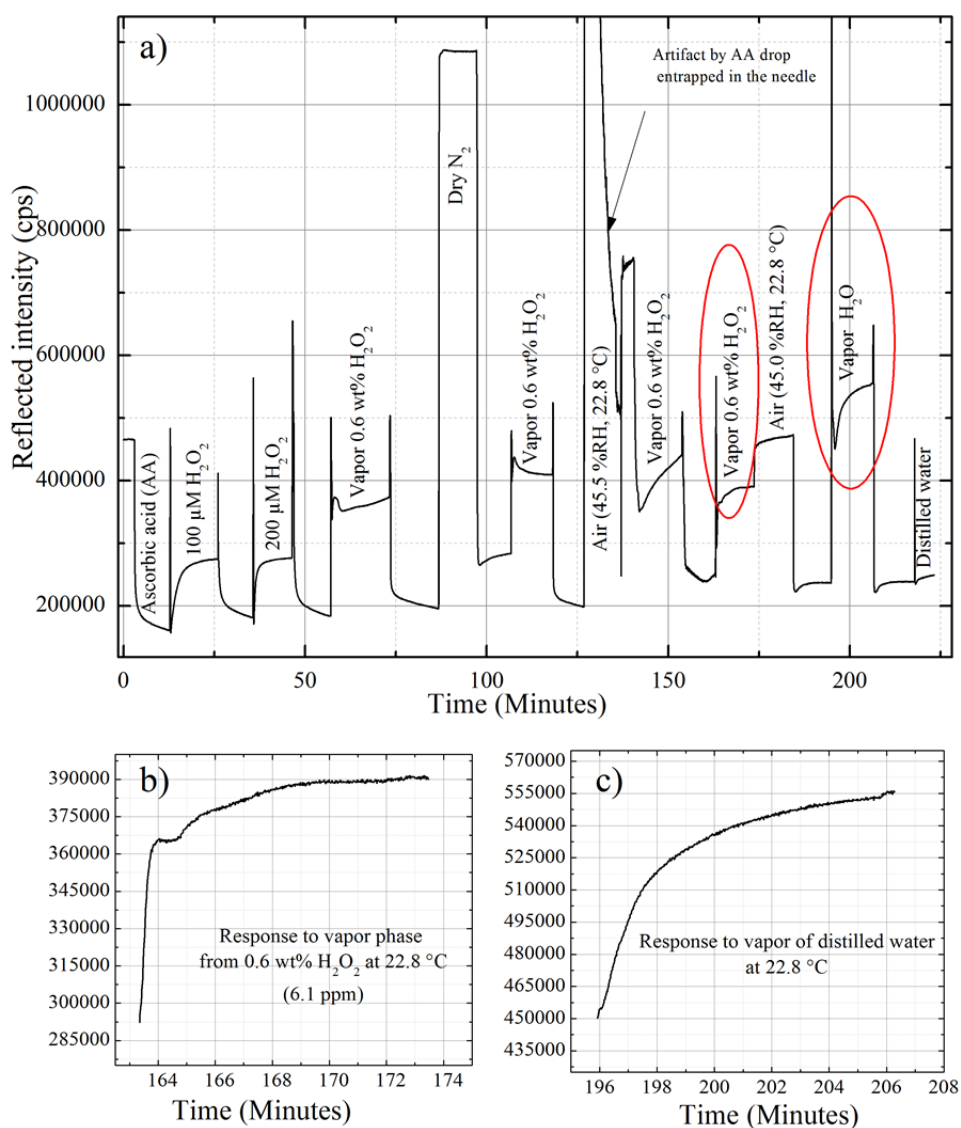


Figure D-10: a) Intensity vs. time response observed during a complete experiment in vapor phase; b) Response of the sensor to vapor at 6.1 ppm H_2O_2 ; c) Response of the sensor to water vapor.

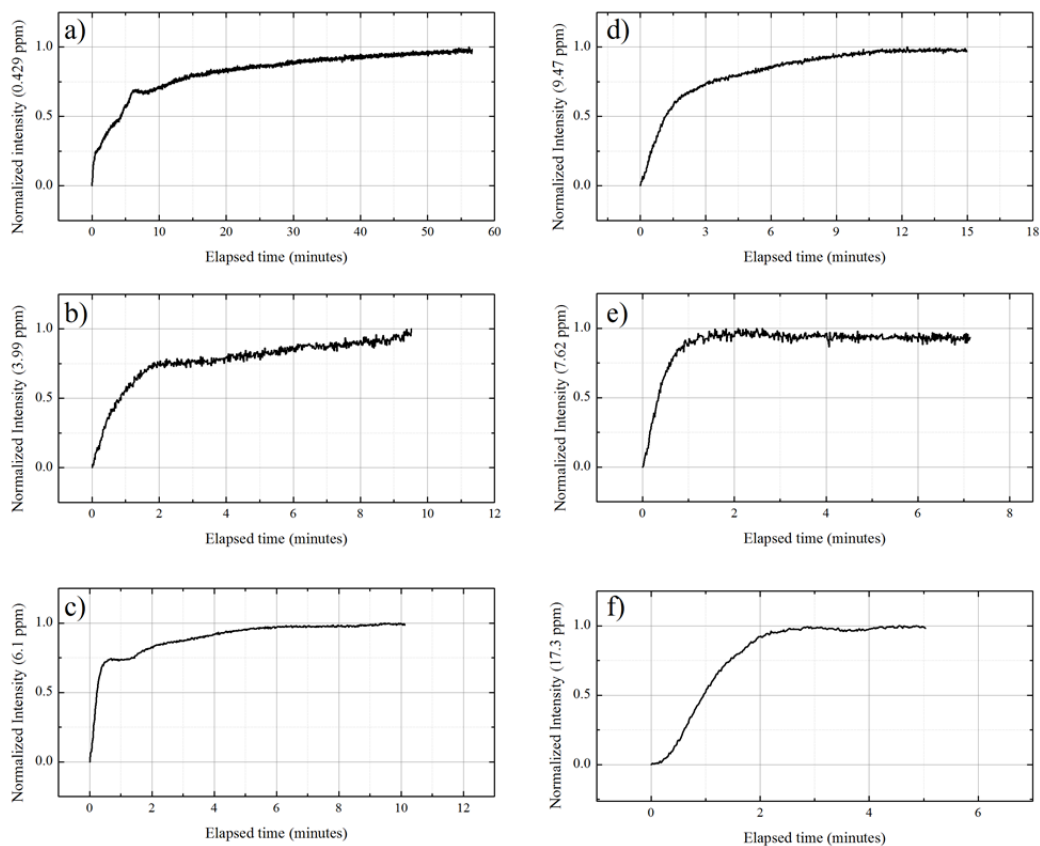


Figure D-11: Response of the optical fiber sensor to various concentrations of H_2O_2 in vapor phase: a) 0.429 ppm; b) 3.99 ppm; c) 6.10 ppm; d) 9.47 ppm; e) 7.62 ppm; and f) 17.3 ppm

Once again, the temporal response of the reflected intensity showed some dependence on the concentration, this is presented in Figure D-12. However, since there was no consistent response, the results are presented without further analysis.

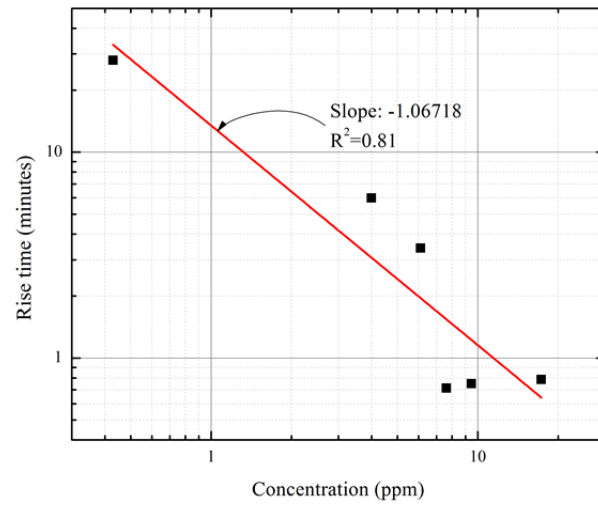


Figure D-12: Rise time versus concentration for a sensor in vapor phase for tests showed in Figure D-11